



**One Chaperone to Rule Them All:
Deciphering How Chromatin
is Assembled During
DNA Replication**

Clément Rouillon

One Chaperone to Rule Them All: Deciphering How Chromatin is Assembled During DNA Replication

Clément Rouillon

One Chaperone to Rule Them All: Deciphering How Chromatin is Assembled During DNA Replication

ISBN/EAN: 978-90-393-7686-7

doi:10.33540/2277

Copyright © 2024 Clément André Philippe Rouillon

All rights reserved. No part of this thesis may be reproduced, stored or transmitted in any way or by any means without the prior permission of the author, or when applicable, of the publishers of the scientific papers.

Print production by TOSAM Studio

The title page illustrations for Chapters 1, 2, 3, 5, 6, and the Addendums were created using DALL-E. The images featured on the cover and the title page of Chapter 4 were generated with Blender using PDB: 1AOI and the AlphaFold-Multimer prediction presented in Chapter 4, respectively.

One Chaperone to Rule Them All: Deciphering How Chromatin is Assembled During DNA Replication

Une Chaperone Pour les Gouverner Toutes : Comprendre Comment la Chromatine Est Assemblée Pendant la Réplication de l'ADN

(avec un résumé en Français)

In de Ban van de Chaperone: Ontrafelen Hoe Chromatine Wordt Samengesteld Gedurende DNA Replicatie

(met een samenvatting in het Nederlands)

Proefschrift

ter verkrijging van de graad van doctor aan de
Universiteit Utrecht
op gezag van de
rector magnificus, prof. dr. H.R.B.M. Kummeling,
ingevolge het besluit van het College voor Promoties
in het openbaar te verdedigen op

donderdag 4 juli 2024 des middags te 2.15 uur

door

Clément André Philippe Rouillon

geboren op 14 maart 1994
te EPINAL, Frankrijk

Promotor:

Prof. dr. G.J.P.L. Kops

Copromotor:

Dr. F. Mattioli

Beoordelingscommissie:

Prof. dr. ir. J.P.W.M. Bakkers (voorzitter)

Prof. dr. P. Knipscheer

Prof. dr. S.M.A. Lens

Prof. dr. A. Perrakis

Prof. dr. M. Tanenbaum

Table of contents

- 6 Chapter 1
General introduction
- 38 Chapter 2
CAF-1 deposits newly synthesized histones during DNA replication using distinct mechanisms on the leading and lagging strands
- 90 Chapter 3
Enabling PCNA labeling to probe PCNA interactions on DNA using single molecule experiments
- 108 Chapter 4
CAF-1 uses an extended binding interface on PCNA for its recruitment on newly synthesized DNA
- 132 Chapter 5
Reconstitution of nucleosome assembly by human CAF-1 reveals plasticity in histone and PCNA binding
- 154 Chapter 6
General Discussion
- 164 Chapter 7
Addendums



1

Introduction

Abstract

Genomic DNA, the blueprint of cellular life, is intricately packaged into chromatin within each cell. Chromatin is a complex of DNA and histone proteins that together form the iconic “beads on a string” structure, providing a structural scaffold to the genome. Furthermore, through the use of Post Translational Modifications (PTMs) and histone variants, chromatin provides a sophisticated regulatory layer known as epigenetics. Epigenetic information plays a pivotal role in modulating genomic mechanisms and it defines the transcriptionally active “open” euchromatin from the transcriptionally silenced “closed” heterochromatin.

During cell division, preserving epigenetic information is paramount for maintaining chromatin structures and cellular identity. This occurs through chromatin replication, a process intricately linked to DNA replication, which in turn ensures the faithful inheritance of epigenetic marks. Due to the highly charged nature of histones, the specialized family of the histone chaperones dynamically controls the deposition of histones during this process. Among the vast and growing family of histone chaperones, Chromatin Assembly Factor 1 (CAF-1) emerges as a central player with critical roles in cell differentiation, homeostasis, and cancer development. CAF-1 deposits histone onto newly synthesized DNA, contributing to the genomic packaging following DNA replication. Its recruitment to DNA replication forks is orchestrated by Proliferating Cell Nuclear Antigen (PCNA), a versatile protein central to numerous cellular functions. Despite the recognized crucial significance of the CAF-1-PCNA pathway in health and disease, the precise coordination of their activities remains elusive. Here, we review the intricate components of chromatin and its regulations in the context of epigenetic inheritance, with a specific focus on deciphering the role of the CAF-1-PCNA pathway.

Chromatin structure and dynamics

Chromatin organization

Chromatin serves as the primary structure for the storage and compaction of genetic information within eukaryotic cells. It comprises genomic DNA intricately associated with histone proteins, forming fundamental units referred to as nucleosomes (1) (Figure 1A). A nucleosome is composed of an octamer of histones wrapped by approximately 147 base pairs (bp) of DNA (2) (Figure 1B). The four major histone types involved in nucleosome formation are H3, H4, H2A, and H2B, with H3 and H4 forming a heterodimer, and similarly, H2A pairs with H2B (2). The nucleosome assembly process initiates with the association of two H3-H4 dimers to form a $(\text{H3-H4})_2$ tetramer, which is deposited onto DNA, marking the formation of a tetrasome, the pivotal first step in nucleosome assembly (Figure 1C). Following this, two H2A-H2B dimers are incorporated, completing the octameric structure, which is then wrapped by DNA (Figures 1B and 1C) (2). This intricate assembly is facilitated by the electrostatic compatibility between the positively charged histone core and the negatively charged DNA. Notably, nucleosomes exhibit a preference for assembling onto negatively supercoiled DNA (3, 4), which is the predominant conformation of DNA within the cell nucleus (5).

Chromatin exists in diverse states that govern the accessibility of the underlying DNA, and these states vary across different chromosomal regions. Two primary states exist: open chromatin, or euchromatin, which allows easy access to DNA and contains active genes as well as promoters and replication origins (6), and closed chromatin, known as heterochromatin, which exhibits limited access to the underlying DNA and is associated with silenced genes and non-coding DNA (6). Heterochromatin is notably concentrated at specific regions in the genome, including centromeres, pericentromeric regions and telomeres (6). Historically, we distinguish two types of heterochromatin in human cells: facultative heterochromatin, whose location varies by cell type, and constitutive heterochromatin, which is conserved in all cell types (7). To achieve limited access to DNA within heterochromatin, nucleosomes are tightly stacked, a process mediated by specific proteins such as linker histone H1 and Heterochromatin Protein 1 (HP1) (8). These proteins facilitate tight associations between neighboring nucleosomes (8).

In addition to these structural features, cells have evolved further regulatory layers by modulating the state of histones within nucleosomes, contributing to the dynamic control and organization of chromatin. Further discussed below.

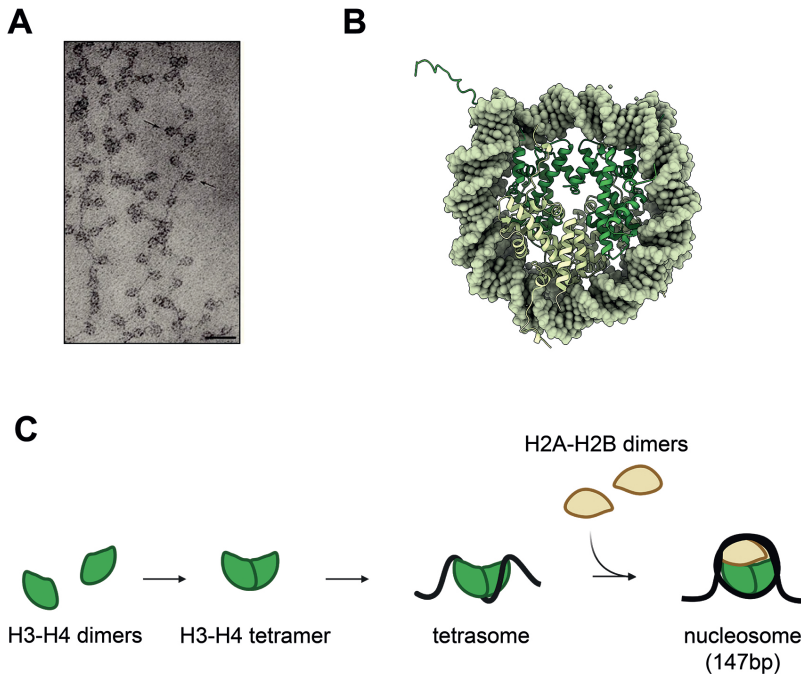


Figure 1: (A) Electron microscopy picture of chromatin in low ionic strength, displaying the so-called “beads on a string” pattern (1). The beads represent nucleosomes that are connected by genomic DNA. (B) Crystal structure of the nucleosome (PDB: 1A0I), composed of 147bp of DNA wrapped around a histone octamer (2). Histone dimers H3-H4 and H2A-H2B are respectively colored in green and beige. (C) Stepwise assembly of histones proteins into a nucleosome. Two H3-H4 dimers associate into a $(\text{H3-H4})_2$ tetramer. It is then deposited on DNA to form the tetrasome, the core structure of the final nucleosome. Two H2A-H2B dimers are then incorporated, and 147bp of DNA wrap the entire histone octamer. This image was created with BioRender.com.

Chromatin regulates gene expression and genome accessibility using histone PTMs and variants

Chromatin compaction is crucial in the regulation of DNA accessibility, defining the boundaries between euchromatin and heterochromatin. Cells have evolved regulated mechanisms for fine-tuning these dynamic chromatin structures. These mechanisms encompass DNA modifications (9), the use of histone variants (10), and the deposition of post-translational modifications (PTMs) on histone tails (Figure 2A). Collectively, these mechanisms create a complex, multi-layered network of regulation that lies at the core of nearly all vital cellular processes. These processes include transcription, DNA replication, DNA repair and chromatin organization, among others (11).

Histone PTMs, predominantly located on lysine residues of histone tails, serve as pivotal regulators of chromatin organization (11) (Figure 2A). Major histone PTMs include methylation (mono, di, or tri), acetylation, phosphorylation, ubiquitination, and SUMOylation (11). Of note, distinct PTMs are associated with heterochromatin and euchromatin, contributing to the organization of chromatin within the nucleus. In facultative heterochromatin, Polycomb Repressive Complexes (PRC) PRC1 and PRC2 catalyze H2AK119 monoubiquitination and H3K27 trimethylation

respectively, leading to transcription silencing (12). In contrast, constitutive heterochromatin is characterized by H3K9 di- and tri-methylation, with several enzymes facilitating the establishment of these marks in mammals (13). These include the methyltransferases SUV39H1, SUV39H2, SETDB1, SETDB2, and G9A (also known as EHMT2) (reviewed in (13)). The intricate interplay between these various methyltransferases remains a subject of ongoing research.

Euchromatin also harbors specific histone PTMs that promote recruitment of transcription factors and gene expression (14). H3K27ac is found at enhancers while H3K4me3 localizes to promoters and transcription start sites, and directly impacts the activity of RNA polymerase II (15). On the other hand, H3K36me3, another euchromatin-specific mark, is predominantly enriched within gene bodies and is thought to directly regulate transcription elongation, and mRNA splicing (16).

In addition to PTMs, histone variants serve as a powerful tool to modulate chromatin structures. Histone H3 and histone H2A exhibit a remarkable diversity of variants, in contrast to the relatively fewer variants known for histones H4 and H2B (10). These variants add another layer of regulation for chromatin structure and they govern essential cellular processes such as transcription and DNA repair (10).

Histone H3 variants have been extensively characterized, and three primary variants are distinguished. The DNA replication-dependent variants H3.1/H3.2 are specifically deposited genome-wide during DNA synthesis on the nascent sister chromatids (Figure 2B) (17). H3.1 is also deposited following DNA repair and is frequently enriched in heterochromatin (Figure 2B) (17). Concurrently, the H3.3 variant is deposited independently of DNA replication, primarily during transcription (17), although it is also found in specific heterochromatic regions, such as telomeres (Figure 2B) (18). CENP-A is the most divergent of H3 variants and it is exclusively located at centromeres (Figure 2B) where it plays a particularly important role during mitosis (19, 20).

Much like H3 variants, H2A variants have a significant influence on chromatin organization, although our understanding of their functions remains limited. For instance, H2A.Z originally found to be enriched in active genes, play essential roles in the regulation of a wide range of nuclear processes with diverse and contrasting functions such as activation and repression of transcription (21). This has made its characterization more complex, despite very active research. On the other hand, H2A.X is specifically important at sites of DNA damage and is pivotal in regulating DNA repair processes (22). Lastly, macroH2A is the most divergent histone variant, and is particularly enriched on the inactive X chromosome (23). However, the precise function of the macroH2A variant remains poorly understood (24). Importantly, these histone variants can undergo various PTMs, and multiple isoforms exist for several of them. This intricate and extensive regulation of chromatin underscores the need for further in-depth research to fully elucidate the exact roles of each variant and their PTMs.

Histone chaperones control chromatin dynamics

So far, we have highlighted the complex organization of chromatin and the several layers of regulation that modulate its structure and function. These intricate mechanisms require precise control over histone proteins throughout the cell cycle and across all chromatin structures. Histone chaperones effectively control histone dynamics within the cell, preventing unintended interactions arising from the highly basic nature of histones (isoelectric point > 10) (25, 26). These chaperones oversee the trafficking of histones within the cell and govern their deposition onto or

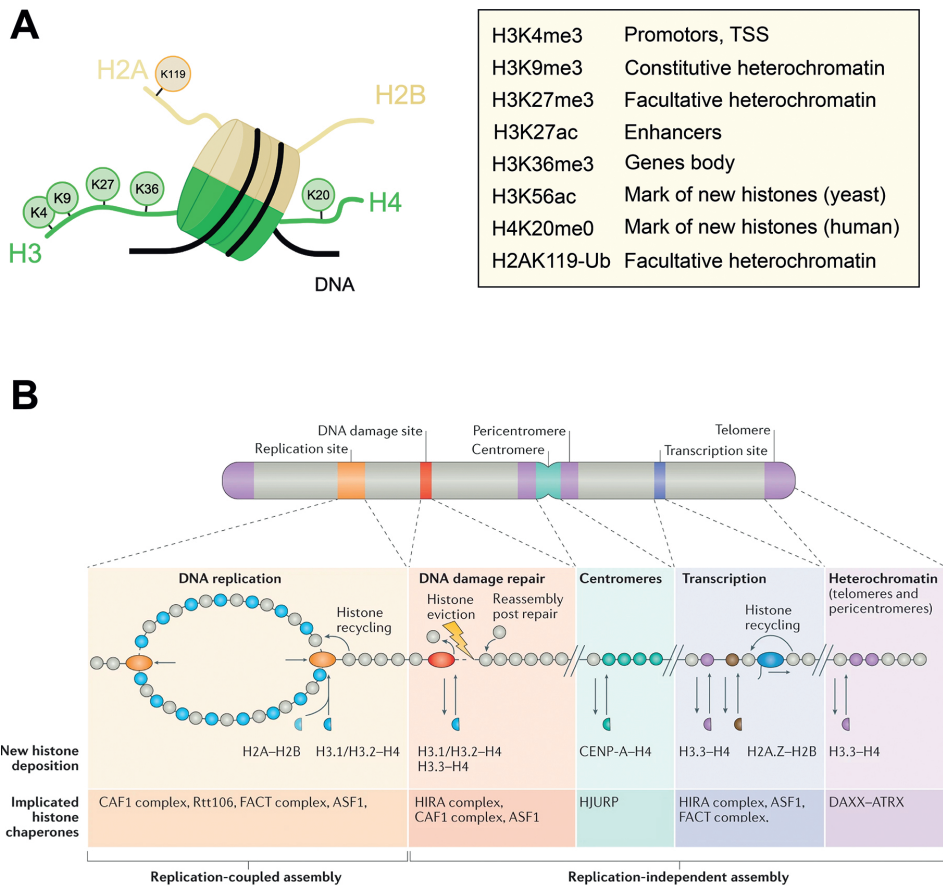


Figure 2: (A) Left panel: Nucleosome cartoon highlighting the sites of important PTMs on the tails of H3, H4 and H2A. Right panel: Details of the genomic functions related to the PTMs highlighted in the left panel (TSS: Transcription Start Site). This image was created with BioRender.com. **(B)** Overview of H3 variants dynamics along the chromosome, and the histone chaperone involved (copied from (26) with permission granted from springer nature).

removal from the chromatin on a genome-wide scale. Notably, histone chaperones are characterized by intrinsically disordered and negatively charged acidic domains, making them well-suited for histone binding (25, 26). Furthermore, they perform their functions in a non-catalytic manner (in an ATP-independent manner,) setting them apart from other histone-binding proteins such as chromatin remodelers (25). While some histone chaperones facilitate the transfer of histones to other chaperones, others can deposit histone on DNA to form *bona fide* nucleosomes (25). Distinct types of histone chaperones exist, including those specific to H3-H4 (Figure 2B), some with promiscuity for both H3-H4 and H2A-H2B, and others that chaperone entire histone octamers (26, 27).

H3-H4 chaperones are the most widely studied since the identification of the first histone chaperone in *Xenopus oocytes*, 45 years ago (28). Subsequently, a multitude of other H3-H4 chaperones have been identified, each playing roles in numerous vital cellular processes (25, 29). These H3-H4 chaperones can be categorized into different groups (Figure 2B): DNA

replication-dependent chaperones, which manage and deposit H3.1-H4 onto DNA during DNA synthesis, DNA replication-independent chaperones, which promote the exchange of H3.1 with H3.3 in specific genomic loci, and chaperones involved in histones trafficking and nuclear import (25, 26, 29, 30).

Following their synthesis in the cytoplasm, histones are rapidly chaperoned to form H3-H4 and H2A-H2B heterodimers by the NASP/HSC70/HSP90 and IPO9/NAP1 complexes, respectively (29). These heterodimers are subsequently imported into the nucleus, where distinct chaperoning pathways regulate their dynamics.

Once inside the nucleus, the histone chaperone ASF1 binds to H3-H4 and governs its distribution within the nucleoplasm (29). Structural studies have shown that ASF1 binding to H3-H4 is not compatible with H3-H4 tetramerization (31). Therefore, ASF1 is presumed to act as a regulator of H3-H4 availability and distribution within the nucleus. Notably, there are two isoforms of ASF1 in humans, namely ASF1A and ASF1B (32). The current model suggests that ASF1B provides H3.1-H4 to the histone chaperone Chromatin Assembly Factor 1 (CAF-1) during DNA replication (33), whereas ASF1A supplies H3.3-H4 to the chaperone HIRA and DAXX in DNA replication-independent pathways (33, 34). However, this model remains speculative as cell-based experiments have shown that both ASF1 isoforms are promiscuous towards H3.1 and H3.3 (35) and other studies found that CAF-1 binds both ASF1A and ASF1B (36). Therefore, further studies need to decipher the precise pathways regulating the distribution of H3.1 and H3.3 to their respective chaperones.

The DNA replication-independent pathway is characterized by different chaperones that regulate H3-H4 incorporation along the chromosome. HIRA deposits H3.3-H4 dimers at active regulatory elements such as enhancers, and promoters, as well as within gene bodies (37) (Figure 2B). While its function is essential for development in mice (38) and the enrichment of H3.3 across the genome (39), the regulation and precise mechanism of action of HIRA remains largely unknown. Future studies are required to elucidate the precise role of this chaperone and its contribution to cellular homeostasis. During transcription, the chaperones FACT and SPT6 facilitate transcription, where they cooperate with the chromatin remodelers CHD1 to disrupt chromatin ahead of the transcription machinery and promote histones recycling following the passage of RNA polymerase II (Figure 2B) (40–43). In certain heterochromatic regions, specialized histone chaperones have evolved to promote the deposition of H3.3. DAXX associates with the chromatin remodeler ATRX and deposits H3.3 at telomeres (Figure 2B) (18), which is thought to be important for proper development of mammalian gametes (44). Centromeres, on the other hand, are heterochromatic regions with unique chromatin content. Here, the chaperone HJURP deposits the H3 variant CENP-A (Figure 2B), which is essential for kinetochore assembly during mitosis (45). While H3.1 and H3.3 are better characterized, there is limited knowledge about the trafficking of CENP-A within the cell and its incorporation into nucleosomes. Further studies are needed to determine the precise mechanisms governing its deposition on DNA and to identify other chaperones involved upstream of HJURP.

As of today, H2A-H2B are less extensively characterized, and rarely exhibit the same level of specificity as observed for H3-H4 in DNA replication-independent and -dependent pathways. Instead, they often share histone chaperones with H3-H4 such as FACT and NAP1 that control their incorporation without distinctions between transcription, DNA replication or other cellular programs (41, 46–50).

In budding yeast, the Chz1 chaperone was found to specifically interact with the H2A.Z variant (51). In mammals ANP32E removes H2A.Z from chromatin (52), while YL1 is thought to deposit this variant (53). Interestingly, all H2A.Z chaperones are thought to cooperate with the chromatin remodelers SRCAP or p400/TIP60 to efficiently mediate H2A.Z deposition on chromatin (52–54). This collaboration is reminiscent of the observed partnership between DAXX and the chromatin remodeler ATRX for the deposition of H3.3 at telomeres (18). Future studies will need to explore the interplay between histone chaperones and chromatin remodelers during chromatin dynamics.

APLF and recently ANP32B have been proposed to chaperone the macroH2A variants (55, 56), albeit the precise mechanisms used by these chaperones to control macroH2A incorporation is still unknown. Notably, APLF has also been shown to chaperone the entire histone octamer (57). To date, this is the only histone chaperone known to handle an entire octamer.

Chromatin replication

Eukaryotic genomes are packaged into chromatin, a structural framework that governs fundamental cellular processes such as DNA replication, gene expression, or DNA repair. Maintaining the integrity of chromatin through mitosis is critical to safeguard transcriptional programs that define homeostasis and cellular identity. Consequently, prior to cell division, chromatin information is accurately reestablished on the newly synthesized sister chromatids

mirroring that of the mother cell. Safeguarding this process preserves the cellular identity and overall functionality of the future daughter cells. Complex mechanisms have evolved to safeguard chromatin information throughout cell division, occurring concurrently with DNA replication during the S phase of the cell cycle.

DNA replication

General principles

Chromatin replication is intricately linked to the process of DNA replication itself. When cells divide in mitosis, their genome must first be faithfully duplicated to provide a copy of the “manual” for the future daughter cells. This critical process, known as DNA replication, involves the faithful duplication of a DNA molecule (the parental DNA) into two identical DNA strands (the daughter strands or sister chromatids) (Figure 3A) (reviewed in (58)).

DNA replication begins during the G1 phase with the licensing of replication origins (59). Multiple origins exist within each chromosome to facilitate the rapid and efficient duplication of the genome. In budding yeast, a well-defined consensus sequence governs this process, while in metazoans, origins are less intrinsically defined, and epigenetic factors are thought to play a significant role (60). The replication machinery assembles in the multiple step process that begins with origin licensing. There, several proteins, including the Origin Recognition Complex (ORC) assemble at replication origins, facilitating the loading of two Mini Chromosome Maintenance (MCM2-7) helicases in a head-to-head configuration, with each helicase encircling the DNA (61, 62). Then, a subset of these licensed origins enters the next phase known as origin firing, which activates the helicases for DNA unwinding and subsequent synthesis. This step is tightly regulated by CDK and DDK kinases as the cell transitions from G1 to S phase (59). Following origin firing,

each helicase encircles one of the two DNA strands, and the exposed single-stranded DNA (ssDNA) is subsequently protected by Replication Protein A (RPA) (Figure 3A). Accessory factors GINS and Cdc45 combine with MCM2-7 to form the active CMG helicase (Cdc45-MCM2-7-GINS) (63, 64). They are followed by DNA polymerase epsilon (Pol ϵ) that forms a tight association with the CMG, marking the future site of DNA synthesis for the leading strand (65, 66) (Figure 3A). This newly formed structure induces the recruitment of several factors, including DNA polymerase alpha (Pol α), which initiates DNA synthesis on both the leading and lagging strands by synthesizing a short RNA that primes DNA synthesis for the replicative DNA polymerases (Figure 3A) (67). Two distinct DNA polymerases function on the two daughter strands: as mentioned earlier, Pol ϵ acts on the leading strand, while DNA polymerase delta (Pol δ) operates on the lagging strand (67) (Figure 3A). Notably, the initial unwinding of the replication origin results in short under-replicated regions on the leading strand, and it is thought that Pol δ is responsible for filling these gaps, highlighting its unique role on the leading strand during DNA replication initiation (68–70).

Both Pol ϵ and Pol δ exhibit limited intrinsic activity for DNA synthesis. Biochemical reconstitutions revealed that Pol δ has no intrinsic processivity, while Pol ϵ shows minimal activity (71) that is further increased by its interaction with the CMG (72). To circumvent this inherent lack of processivity, both polymerases utilize a DNA replication processivity factor called Proliferating Cell Nuclear Antigen (PCNA) that tethers the polymerases onto the DNA, enabling rapid and efficient DNA synthesis (Figure 3A) (73). PCNA is a homotrimeric protein that encircles double-stranded DNA at replication forks (74) and directly interacts with the polymerases, anchoring and stabilizing them on the template DNA (Figure 3A). Biochemical studies found that while PCNA has a high binding affinity for Pol δ , the interaction with Pol ϵ is 30-fold weaker (75), emphasizing the importance of the Pol ϵ -CMG interaction for the full processivity of the leading strand polymerase (76). While little is known on the interaction between PCNA and Pol ϵ , the structure of a PCNA-Pol δ complex has revealed that a single anchor point between PCNA and Pol δ is mediating their interaction (77, 78), leaving the other two PCNA monomers available for recruiting additional factors.

Following origin firing, DNA replication transitions to the elongation phase, where the two assembled DNA replication machineries (also known as replisomes) move in opposite directions, creating two replication forks. Within each replisome, DNA polymerases ϵ and δ synthesize DNA in the 5'-3' direction on each strand. However, due to the antiparallel orientation of the DNA double helix, the two native strands are synthesized in opposite directions, leading to two distinct mechanisms of DNA synthesis. On the leading strand, Pol ϵ directly interacts with the CMG and synthesizes DNA in a continuous manner, following the translocation of the CMG on parental DNA (Figure 3A). However, on the lagging strand, Pol δ synthesizes DNA in a discontinuous manner in short DNA fragments (~200 bp) called Okazaki fragments (Figure 3A) (79). Each of these fragments are primed by Pol α and subsequently extended by Pol δ . They are later processed and ligated together during Okazaki fragments maturation, a process orchestrated by PCNA (Figure 3A) (80). Indeed, PCNA recruits the endonuclease FEN1 which removes the RNA primer (previously synthesized by Pol α), and the ligase LIG1/Cdc9 that joins Okazaki fragments together (Figure 3A) (80). Replication elongation then proceeds along the chromosome until two replisomes converge, leading to DNA replication termination (reviewed in (81)).

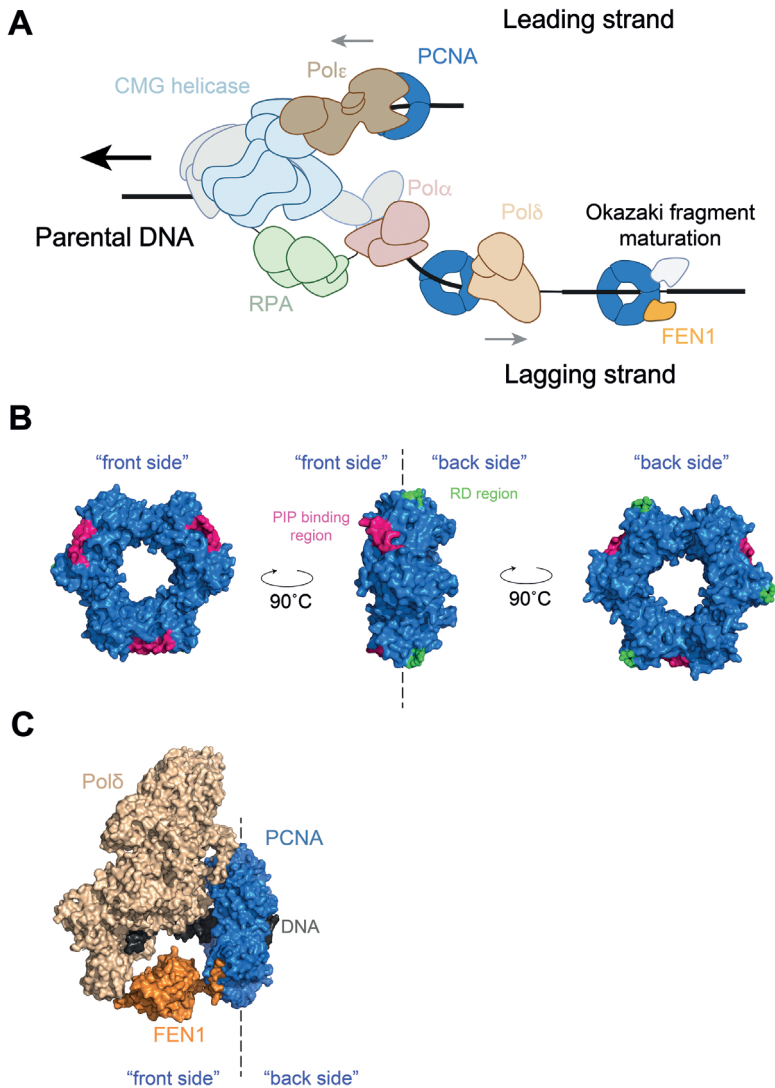


Figure 3: (A) Schematic of the eukaryotic replication machinery. The CMG helicase (Cdc45, MCM2-7, GINS) translocates on the leading strand template and unwinds the parental DNA. The exposed ssDNA in the process is protected by RPA. Pol α primes DNA synthesis by synthesizing a short RNA primer. On the leading strand, Pole directly binds the CMG and synthesizes DNA following the translocation of the CMG. On the lagging strand, Pol δ synthesizes DNA in the opposite direction and produces short discontinuous Okazaki fragments. Both polymerases are stabilized on DNA by the ring-shaped homotrimer PCNA. PCNA also mediates Okazaki fragments maturation by recruiting the endonuclease FEN1 and a ligase. This image was created with BioRender.com. **(B)** PCNA structure (PDB: 1PLQ) (74). Right panel: Front face of PCNA that harbors the PIP binding regions on each monomer (magenta). The RD regions, an additional interface known to be important for PCNA function in yeast, is colored in purple (88). **(C)** CryoEM structure of a human PCNA homotrimer simultaneously bound to Pol δ and FEN1 (PDB: 6TNZ) (78). Both the polymerase and FEN1 engage a single PCNA monomer, leaving the third one available for additional interactions. This structure highlights the ability of PCNA to mediate several functions at the same time.

PCNA is a master regulator of DNA replication forks

As previously mentioned, PCNA is central to DNA replication by providing processivity to DNA polymerases and by coordinating Okazaki fragment maturation on the lagging strand. PCNA was originally identified as an essential protein for DNA replication in the SV40 system (82), and as an auxiliary protein for Pol δ (83) and Pol ϵ (76) during DNA synthesis. Since then, it has been shown that PCNA is involved in several key cellular processes such as, DNA repair, chromatin assembly, epigenetic inheritance, sister chromatid cohesion and cell cycle regulation (73).

As a ring-shaped homotrimer (Figure 3B) (74) belonging to the sliding clamp family, PCNA encircles double-stranded DNA, sliding bidirectionally in an ATP-independent manner (84). The inner surface of the ring is enriched in positively charged amino acids, providing a suitable surface for sliding on DNA (85). The front side of the PCNA ring, facing DNA synthesis and binding polymerases, features the Inter Domain Connected Loop (IDCL), defining the PCNA Interacting Peptide (PIP) binding pocket on each monomer (Figure 3B) (73). This region is highly conserved and serves as the primary interaction site for binding partners carrying PIPs, a conserved domain found in PCNA interactors, with the consensus sequence Q-x-x- Ψ -x-x- θ - θ , in which Ψ is a small amino acid with an aliphatic chain (L, V, or I), θ is an aromatic residue (Y or F), and x is any residue (86). Yet, recent studies revealed that many proteins that bind PCNA via the PIP binding pocket use degenerate PIP motifs not strictly following the consensus sequence (87). Moreover, while the PIP binding pocket mediates numerous crucial interactions, PCNA also employs additional surfaces to bind proteins. This is notably the case of the RD region on the back side of PCNA (Figure 3B). Indeed, mutations on the PCNA surface, outside the PIP binding pocket, significantly impact PCNA functions, emphasizing a complex interaction network throughout its diverse functions (Figure 3B) (88). Due to its homotrimeric configuration, PCNA harbors three distinct binding sites for PIPs, allowing multiple interactions simultaneously. A recent structural analysis of a complex involving PCNA on DNA, binding Pol δ and FEN1 simultaneously (Figure 3C) (78) confirmed that PCNA uses a so-called toolbelt mechanism during Okazaki fragment maturation (73).

PCNA abundance on DNA is tightly regulated by clamp loaders, enzymatic complexes whose activity relies on ATP hydrolysis (89). Two distinct types of clamp loaders are recognized based on their capacity to either load or unload PCNA. The RFC1-5 pentamer is the consensus clamp loader that loads PCNA at single-stranded/double-stranded DNA junctions (more specifically at free 3'OH termini) (90, 91). Other clamp loaders are referred to as RFC-like clamp loaders (RLC) as they all share the RFC2-5 subunits, with RFC1 being the differing subunit (89). For instance, heptameric clamp loader CTF18-RFC directly binds Pole on the leading strand during DNA replication, where it is thought to specifically load PCNA (92–95). While CTF18-RFC plays an important role during unperturbed DNA synthesis (92, 93) and sister chromatid cohesion (96), it is plausible that it further regulates PCNA-mediated function on the leading strand. In contrast, the only PCNA unloader known is ATAD5-RFC (Elg1 in yeast) that removes PCNA from DNA, following DNA replication (97, 98). This enzyme is pivotal, as it tightly controls PCNA-mediated processes on DNA. It is worth noting that most biochemical studies on PCNA have employed reconstitutions that lack the DNA loading component, leaving a significant gap in understanding how PCNA-mediated reactions occur on DNA.

As previously mentioned, PCNA plays various roles beyond DNA replication. This comprises DNA repair where it recruits repair factors during Translesion Synthesis (TLS), Nucleotide Excision Repair (NER), Base Excision Repair (BER) and Mismatch Repair (MMR) (73, 86).

PCNA also controls cell cycle progression, notably by binding to p21 that negatively regulates cell cycle entry in S phase. (99). Furthermore, PCNA is at the heart of chromatin control and epigenetics inheritance where it promotes DNA and histones methylation in heterochromatin (100, 101), sister chromatids cohesion following DNA replication (102) and where it recruits the chromatin remodelers SMARCAD1 (103). Importantly, PCNA controls chromatin assembly on newly-synthesized DNA, by recruiting the histone chaperone CAF-1 to replication forks, where nucleosomes are subsequently assembled (further discussed below) (88, 104). In essence, PCNA stands out as an exceptionally multifaceted protein, engaging with dozens of proteins that collectively govern multiple essential cellular processes (86). Consequently, mechanisms are in place to regulate these interactions and prevent uncontrolled processes. Indeed, PCNA is subject to several modifications that modulate its ability to interact with certain proteins (reviewed in (86)). A few examples are the ubiquitination of K164 that leads to recruitment of low fidelity polymerases during TLS, while its SUMOylation inhibit homologous recombination (73) and favor interaction with CAF-1 during transcription-DNA replication conflict in human cells (105). Despite intense research efforts, the full extent of the regulation of PCNA function throughout the cell cycle remains poorly understood. This is due to the overlap and complexity of the various pathways converging to PCNA. Although several PCNA inhibitors are already used as cancer treatments (73), a better understanding of the regulation of its activity is promising for more targeted therapies.

Recycling of epigenetic information

DNA replication occurs in the context of chromatin in cells and the passage of the replisome is a disruptive process for chromatin (Figure 4A) (106–108). Indeed, the histones on parental DNA (parental histones) are evicted by histone chaperones, an essential process for replisome passage. However, these parental histones carry vital PTMs that dictate chromatin organization and function, including methylation marks such as H4K20me2 or H3K27me3 (106, 107). Consequently, histones with their PTMs are recycled and redeposited onto each daughter strand (109), ensuring that the chromatin organization on sister chromatids mirrors that of the parental chromatin (Figure 4A).

As previously mentioned, histone dynamics are controlled by histone chaperones. When the replisome encounters a nucleosome, the chaperone FACT initiates its disassembly (110) (Figure 4B). Subsequently, recycled H2A-H2B dimers remain intact, and the remaining H3-H4 tetramer is extracted from chromatin and recycled without dissociation, preserving its tetrameric structure (111). Using genomic-based methods in yeast and mouse embryonic stem cells, two distinct H3-H4 recycling pathways were identified (112–114).

In the first pathway, H3-H4 recycling towards the leading strand is facilitated by the Pole chaperone (Figure 4B) (114). Pole is made out of four subunits: Pol2, Dpb2, Dpb3 and Dpb4 in yeast (POLE1, POLE2, POLE3 and POLE4 in human respectively). Notably, Dpb3-Dpb4 harbors a long acidic domain and a histone fold that resembles H2A-H2B, providing an ideal docking site for H3-H4 (115). Whether Pole directly redeposits H3-H4 onto the newly synthesized DNA or involves another chaperone remains unknown. In the second pathway, parental H3-H4 are recycled toward the lagging strand, involving multiple chaperones such as MCM2, Pol α , and RPA, which are all part of the replisome (Figure 4B) (113, 116–119). Similarly to the leading strand, we ignore whether

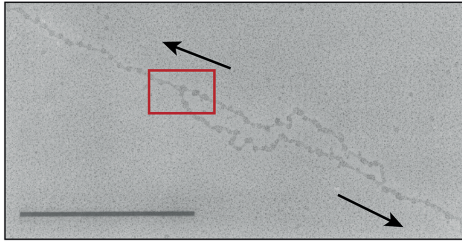
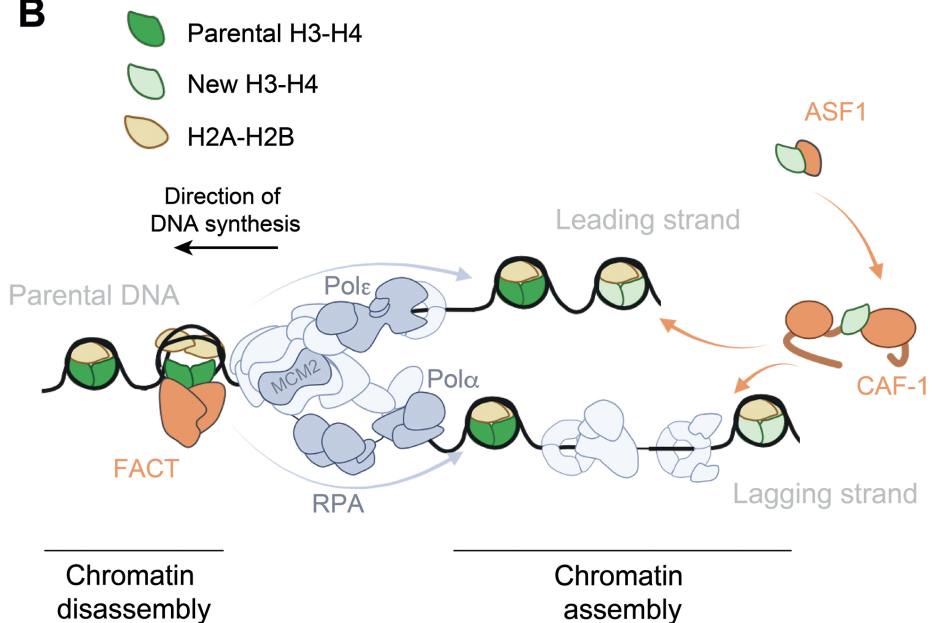
A**B**

Figure 4: (A) Electron microscopy picture of a “replication bubble” in the context of chromatin (171). The red rectangle indicates a replication fork progressing through chromatin. (B) Schematic of chromatin replication dynamics at replication forks, as happening in the red rectangle in panel A (reviewed in (106, 107)). Histone chaperones that are part of the replisome are highlighted in light purple, while external chaperones are colored in orange. FACT disassembles nucleosomes upstream of the replisome. Pole promotes recycling of H3-H4 towards the leading strand. MCM2, Pol α , and RPA facilitate H3-H4 recycling towards the lagging strand. Pol α also contributes to H2A-H2B recycling towards the lagging strand. CAF-1 directly assembles nucleosomes on newly replicated DNA, using new H3-H4 handed over by ASF1. This image was created with BioRender.com.

these chaperones are simply handling the histones towards the lagging strand or if some may be able to redeposit them onto the newly-synthesized DNA. Importantly, both pathways are simultaneous and allow to recycle H3-H4 in a symmetrical manner, ensuring that each chromatid receives about 50% of parental histones (Figure 4B) (119). In addition to histone chaperones that are part of the replisome, FACT is known to contribute to H3-H4 recycling towards both the leading and lagging strands (120). Furthermore, multiple interactions between FACT and

other chaperones embedded in the replisome have been identified (117, 118, 121, 122) and FACT is known to deposit histones on DNA to form nucleosomes (123–125). Therefore, FACT is a prominent candidate as the chaperone that coordinates parental histone recycling with their reassembly on newly synthesized DNA.

A recent study suggests that the recycling of parental H3-H4 specifically occurs on heterochromatin, while histones carrying active PTMs on euchromatin inefficiently recycle (126). Yet, other studies showed that active marks such as H3K4me3 and H3K36me3 are efficiently and symmetrically recycled at replication forks (109, 127, 128). Despite these discrepancies, all studies converge to the idea that in euchromatin, the inheritance of chromatin marks also depends on epigenetic components, such as transcription factors and transcription itself, that in turn, promote the re-establishment of active chromatin marks.

H2A-H2B recycling is a less explored and poorly understood aspect of chromatin dynamics. Yet, it has been shown that the proper recycling of H2A-H2B is crucial for maintaining heterochromatin domains (129). Recent findings indicate that, similarly to H3-H4, H2A-H2B is recycled symmetrically between leading and lagging strands (129). To date, Pola is the sole replisome component known to chaperone H2A-H2B towards the lagging strand, while no chaperone has been identified for recycling towards the leading strand (129, 130). While other chaperones such as FACT are hypothesized to contribute to H2A-H2B recycling during DNA replication (42, 48), comprehensive testing and further investigations are required to establish the complete network of histone chaperones regulating H2A-H2B recycling at replication forks.

***De novo* histone deposition**

Newly synthesized histone supply

During DNA replication, parental histones are recycled towards the two sister chromatids, resulting in a 2-fold dilution of histone abundance on DNA (106). In order to maintain chromatin density on both sister chromatids, new histones must be deposited (Figure 4B) (106). Therefore, a burst in the production of new H3.1-H4 dimers as well as H2A-H2B occurs during the G1/S transition of the cell cycle (17). These histones are marked by hyperacetylation and the absence of methylation marks typical of parental histones (e.g. H4K20me0, H3K9me0) (131). Following synthesis and nuclear import of H3.1-H4 dimers, the ASF1 chaperone regulates their intranuclear dispatch, with the ASF1B isoform specifically handling H3.1-H4 (33). Subsequently, the histone dimers are handed over from ASF1 to CAF-1, the histone chaperone responsible for depositing new histones on newly replicated DNA (Figure 4B) (132). Once loaded with histones, CAF-1 is guided to sites of ongoing DNA synthesis, where it directly deposits H3.1-H3 on the newly replicated DNA (Figure 4B) (104). Importantly, this process is mediated through a direct interaction between CAF-1 and the DNA polymerase processivity factor PCNA, enriched at the back of the replisome (Figure 4B) (88, 104).

The function of CAF-1 during DNA replication impacts several fundamental processes, playing a crucial role in cellular differentiation and preserving cell identity (133, 134). Additionally, CAF-1 is involved in DNA repair pathways such as homologous recombination (HR) (135), non-homologous end joining (NHEJ) (136), and transcription replication conflict (105), and its genetic depletion is lethal in metazoans (137–141). Therefore, due to its crucial role in S phase, CAF-1 plays a significant part in maintaining homeostasis in cycling cells, especially in highly proliferative cells

like cancer cells. For this reason CAF-1 has become a potential therapeutic target in the past decade (142, 143).

CAF-1 architecture

CAF-1 is a heterotrimer consisting of large (Cac1/p150), middle (Cac2/p60), and small (Cac3/p48) subunits in yeast and human respectively (Figure 5A) (144–146). Due to a high degree of disorder in the large subunit, it has been historically difficult to characterize the structure of CAF-1 (147–149). However, a recent study succeeded to solve the structure of a human CAF-1 subcomplex (lacking the N and C termini of p150) bound to the histones H3-H4 (150). Their results align with several biochemical studies, indicating that both the middle and small subunits have a similar globular fold with WD40 repeats (147–149). The large subunit binds the other two subunits with independent interfaces. The small and middle subunits do not interact with each other (Figure 5A). The N terminus of the large subunit contains two PIP domains (PIP1 and PIP2) and a DNA binding “KER” domain, while the acidic domain lies between the binding interfaces for the middle and small subunits (Figure 5A) (147, 151–154). Interestingly, a small globular Winged Helix Domain (WHD), crucial for chromatin assembly and the association of two CAF-1 on DNA, engages in an intramolecular interaction with the acidic domain (147, 151, 155) (Figure 5A). This interaction is relieved when histones bind to the acidic domain, making the WHD available for DNA interactions (Figure 5A) (155).

In humans, the large subunit of CAF-1 (p150) exhibits additional domains not identified in yeast. Specifically, it directly interacts with the heterochromatin protein HP1 through a conserved domain in its N-terminus (PxVxL) (156, 157). While CAF-1 is functionally linked to heterochromatin maintenance (158), the role and regulatory mechanisms of the interaction with HP1 are not fully understood. Furthermore, the p150 subunit also features a SUMO interacting motif (SIM), believed to facilitate the SUMOylation of binding partners such as PCNA (105, 159). Interestingly, it has been suggested that CAF-1 also functions with ubiquitin moieties, particularly during unperturbed DNA synthesis (160) and translesion synthesis (161). However, the role and impact of these moieties on human CAF-1 remain elusive, requiring further investigation for a comprehensive understanding of their function.

Mechanism of CAF-1-mediated chromatin assembly

CAF-1 plays a crucial role in depositing histones on newly replicated DNA. In yeast, this process depends on the acetylation of H3K56 by Rtt109 (162), a step that promotes the transfer of H3-H4 from ASF1 to CAF-1. Although the details of this handover mechanism are not well-characterized, it is known to occur through an interaction between ASF1 and the C-terminus of the Cac2/p60 subunit (163) resulting in a H3-H4 dimer being chaperoned by CAF-1. The acidic domain, located in the large subunit, neutralizes positive charges along the H3-H4 dimer, particularly on the side where DNA binds in a nucleosome (150). The middle subunit also contributes to H3-H4 chaperoning, although to a lesser extent, and its precise contribution to chromatin assembly remains unclear. On the other hand, the small subunit forms contacts with the N-terminus tail of H3 (sites of vital PTMs such as H3K4 and H3K9). This is particularly interesting in light of CAF-1 function in the establishment of heterochromatin domains bearing H3K9me3 (158).

The mechanism of CAF-1-mediated nucleosome assembly is only partially understood, primarily because it was studied in absence of other factors (Figure 5B). Upon receiving an H3-H4

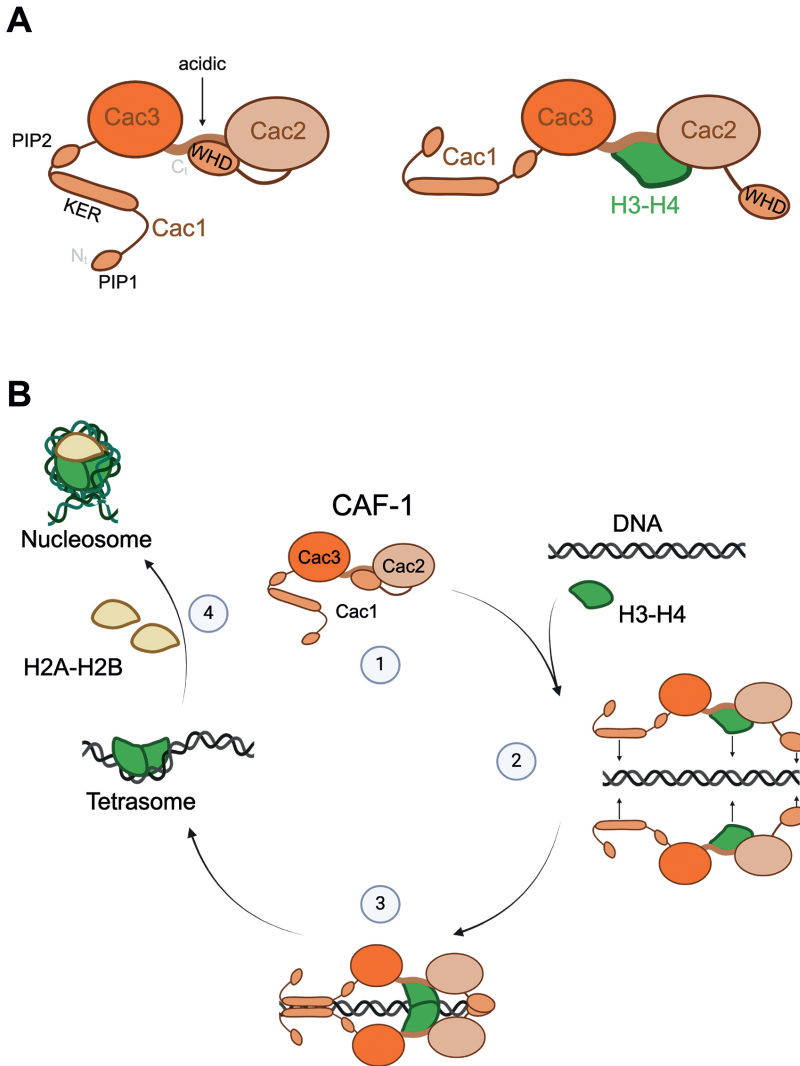


Figure 5: (A) Left panel: Overall architecture of the CAF-1 heterotrimer (the nomenclature refers to *S.cerevisiae*). Cac2 and Cac3 are globular subunits, while Cac1 is highly disordered. Cac1 harbors two PIPs in its N terminus (namely PIP1 and PIP2), interspaced by a KER DNA binding domain. At the C terminus, a WHD DNA binding domain engages in an intramolecular interaction with an acidic domain located in the middle of Cac1. This acidic domain and the Cac2 subunit are the primary binding sites for H3-H4 dimers. Right panel: H3-H4 binding to the acidic domain destabilizes its own interaction with the WHD, which becomes exposed and available for DNA binding. This image was created with BioRender.com. **(B)** Mechanism of nucleosome assembly by CAF-1 in absence of other factors (reviewed in (172)). **1.** Free CAF-1 is in an auto-inhibitory configuration, where the WHD domain engages with the acidic domain of Cac1. **2.** H3-H4 binding to the acidic domain destabilizes the WHD interaction. The WHD is then available for DNA interaction. Two CAF-1-H3-H4 complexes associate on DNA via their WHD. **3.** The association of two CAF-1-H3-H4 on DNA promotes the formation of a (H3-H4)₂ tetramer. **4.** The (H3-H4)₂ tetramer is wrapped by 80nt of DNA, forming the tetrasome. Two H2A-H2B dimers are then incorporated, forming the full histone octamer. The DNA further wraps itself (147 bp) around the histone complex to form a nucleosome. This image was created with BioRender.com.

dimer from ASF1, CAF-1 chaperones it with its acidic domain. CAF-1 binding to the H3-H4 dimer exposes the tetramerization interface on H3, allowing the formation of a (H3-H4)₂ tetramer later (Figure 5B). This was recently confirmed by the first Cryo-EM structure of the core CAF-1 complex with H3-H4 (150). The binding of H3-H4 to the acidic domain destabilizes the intramolecular interaction with the WHD, which becomes available for DNA interaction (Figure 5B). Finally, two CAF-1-H3-H4 complexes associate on DNA, in a step that is promoted by the WHD (Figure 5B). The histone tetramer is then enveloped by 80 bp of DNA through electrostatic interactions, resulting in tetrasome assembly (Figure 5B) (144, 152).

While informative, this mechanism does not consider the PCNA requirement observed in cells (88, 152), and more sophisticated reconstitutions are being developed to study the effect of PCNA. Early studies revealed that CAF-1 is recruited to replication forks by the DNA replication factor PCNA through the PIP domains in the large subunit (88). PIP2 was shown to have a prominent role in nucleosome assembly, whereas the role of PIP1 remains unclear and unexplored (151, 152). Furthermore, at replication forks, PCNA is engaged in interaction with DNA polymerases or Okazaki fragment maturation machineries. How CAF-1 positions itself in these PCNA moieties is unclear. Therefore, the actual mechanism employed by CAF-1 and PCNA in replication-coupled chromatin assembly remains largely unknown.

Chromatin maturation

In the wake of DNA replication, sister chromatids carry a mixture of newly-synthesized and recycled parental histones (106, 107). Recycled parental histones, enriched with essential PTMs and variants, contrast with the “naïve” new histones deposited by CAF-1, which lack pertinent epigenetic information. Therefore, a process known as chromatin maturation occurs to maintain the pre-replicative epigenetic landscape on all nucleosomes (106, 107). Because chromatin maturation occurs differently across diverse chromatin domains as well as between different species, it has been particularly difficult to study (13, 106)

Research on chromatin maturation has primarily focused on heterochromatin domains, which remains a very active field of research. Following replisome passage, key facultative heterochromatin marks such as H2A-K119 ubiquitination (Ub) and H3K27me₃ are uniformly distributed on both leading and lagging strands (127, 129). H2A-K119Ub and H3K27me₃ engage in a positive feedback loop with PRC1 and PRC2 respectively, facilitating their propagation in cis, to neighboring naïve histones (129).

In constitutive heterochromatin, the re-establishment of H3K9me₃ on nascent DNA involves an intricate network of histone methyltransferases (13). Recent discoveries suggest that the histone chaperone DAXX recruits histone methyltransferases to facilitate H3.3K9me₃ deposition on chromatin suggesting that chromatin assembly and maturation may happen concurrently (164). Interestingly, in mouse cells, while H3K9me₂ is symmetrically distributed at DNA replication forks, H3K9me₃ is only recycled towards the leading strand, raising questions as to how this mark is re-established on lagging strand (165). This evidence suggests that chromatin maturation may also occur in trans between sister chromatids. Future work needs to decipher the complexity of H3K9me₃ establishment on nascent DNA amid the high redundancy of methyltransferases regulating this pathway.

Maturation in euchromatin domains is relatively understudied. It is thought that the recycling of H3K4me₃ and H3K36me₃ during DNA replication facilitates re-entry of RNA polymerase II

and the binding of transcription factors (128). Therefore, active transcription may subsequently lead to the maturation of native histones with active marks. Further investigations are essential to elucidate the precise mechanisms governing the restoration of active marks in euchromatin and the precise role of transcription in this pathway.

Aim and Outline of the thesis.

In the last decade, the histone chaperone CAF-1 has emerged as a new marker of several cancers and tumor proliferation (142, 143, 166–168). Yet, we do not understand how CAF-1 exerts its primary function in our cells, leaving a gap in our knowledge of its role in health and disease. Early studies identified CAF-1 as a chromatin assembly factor that collaborates with the DNA replication factor PCNA to achieve chromatinization of naked DNA during S phase (88, 104, 145). However, the mechanism used by CAF-1 and PCNA to propagate epigenetic information through cell division remains unknown. Investigating the precise molecular mechanisms employed by CAF-1 and PCNA during chromatin assembly would greatly advance our understanding of chromatin replication. In this thesis, we present an in-depth study of this mechanism. In **Chapter 2**, we combined biochemical reconstitutions with genomic approaches to describe the mechanism of CAF-1-mediated new histone deposition in S phase. Our work highlighted the complex interplay between DNA synthesis and chromatin assembly revealing the physical uncoupling of *de novo* histone deposition pathway from the replisome. This work has prompted further questions into the assembly of the CAF-1-PCNA complex, leading us to develop single-molecule-based assays due to the limitations of conventional in-bulk methods (**Chapter 3**). Given the notorious challenges associated with studying PCNA-mediated reactions on DNA, most previous single-molecule studies of PCNA excluded DNA from their reconstitutions. In **Chapter 3**, we extensively troubleshooted the fluorescent labeling of PCNA to obtain a suitable method that does not affect the stability of the protein on DNA. Our collaboration with Pr. Nynke Dekker (TU Delft) resulted in the establishment of a novel setup that enables the observation of PCNA reactions on DNA at the single-molecule level. Our lab will now use this tool to gain insights into the assembly of CAF-1-PCNA complexes and the kinetics of chromatin assembly in this context.

While CAF-1 is emerging as a promising therapeutic target (143), we still lack high resolution structural information of the CAF-1-PCNA complex. Solving the structure of this complex would pave the way for the development of inhibitors aimed at targeting CAF-1 function in diseases. In **Chapter 4**, we combine AlphaFold and biochemical reconstitutions to gain insights into the assembly of CAF-1-PCNA complexes at DNA replication forks. Our work highlights a complex and extensive interaction between CAF-1 and PCNA. Notably, we identify a novel binding interface between these proteins that we believe to be unique among the various interactions mediated by PCNA. This discovery holds promise for the development of therapies focused on CAF-1, as this newly identified interaction may offer means to selectively target CAF-1 function with PCNA without interfering with the numerous other essential processes mediated by PCNA.

Our work in Chapters 2, 3 and 4 using yeast proteins brought tremendous insights in the CAF-1-PCNA-mediated chromatin assembly mechanism. However, in order to translate this knowledge into potential health improvement, it is imperative to validate these findings using human proteins. Importantly, these mechanisms in humans are regulated by PTMs and protein

variants (35, 169, 170) and these differences may well regulate CAF-1 activity in cells. In **Chapter 5**, we set up biochemical reconstitutions with human proteins and demonstrated that the mechanism of chromatin assembly on PCNA is conserved. Furthermore, our research indicates that CAF-1 exhibits relatively low specificity in its interactions with binding partners, particularly concerning certain PTMs and histone variants. Our work sheds lights on how cells regulate the function of CAF-1 at DNA replication forks.

References

1. D. E. Olins, A. L. Olins, Chromatin history: our view from the bridge. *Nat. Rev. Mol. Cell Biol.* **4**, 809–814 (2003).
2. K. Luger, A. W. Mäder, R. K. Richmond, D. F. Sargent, T. J. Richmond, Crystal structure of the nucleosome core particle at 2.8 Å resolution. *Nature* **389**, 251–260 (1997).
3. P. Pfaffle, V. Jackson, Studies on rates of nucleosome formation with DNA under stress. *J. Biol. Chem.* **265**, 16821–16829 (1990).
4. D. J. Clark, G. Felsenfeld, Formation of nucleosomes on positively supercoiled DNA. *EMBO J.* **10**, 387–395 (1991).
5. S. Corless, N. Gilbert, Investigating DNA supercoiling in eukaryotic genomes. *Brief. Funct. Genomics* **16**, 379–389 (2017).
6. C. D. Allis, T. Jenuwein, The molecular hallmarks of epigenetic control. *Nat. Rev. Genet.* **17**, 487–500 (2016).
7. O. Bell, A. Burton, C. Dean, S. M. Gasser, M.-E. Torres-Padilla, Heterochromatin definition and function. *Nat. Rev. Mol. Cell Biol.* **24**, 691–694 (2023).
8. R. C. Allshire, H. D. Madhani, Ten principles of heterochromatin formation and function. *Nat. Rev. Mol. Cell Biol.* **19**, 229–244 (2018).
9. V. R. B. Liyanage, J. S. Jarmasz, N. Murugesan, M. R. Del Bigio, M. Rastegar, J. R. Davie, DNA Modifications: Function and Applications in Normal and Disease States. *Biology* **3**, 670–723 (2014).
10. S. Martire, L. A. Banaszynski, The roles of histone variants in fine-tuning chromatin organization and function. *Nat. Rev. Mol. Cell Biol.* **21**, 522–541 (2020).
11. A. J. Bannister, T. Kouzarides, Regulation of chromatin by histone modifications. *Cell Res.* **21**, 381–395 (2011).
12. P.-O. Angrand, Structure and Function of the Polycomb Repressive Complexes PRC1 and PRC2. *Int. J. Mol. Sci.* **23**, 5971 (2022).
13. J. Padeken, S. P. Methot, S. M. Gasser, Establishment of H3K9-methylated heterochromatin and its functions in tissue differentiation and maintenance. *Nat. Rev. Mol. Cell Biol.* **23**, 623–640 (2022).
14. O. Morrison, J. Thakur, Molecular Complexes at Euchromatin, Heterochromatin and Centromeric Chromatin. *Int. J. Mol. Sci.* **22**, 6922 (2021).
15. T. H. Beacon, G. P. Delcuve, C. López, G. Nardocci, I. Kovalchuk, A. J. van Wijnen, J. R. Davie, The dynamic broad epigenetic (H3K4me3, H3K27ac) domain as a mark of essential genes. *Clin. Epigenetics* **13**, 138 (2021).

16. Z. Sun, Y. Zhang, J. Jia, Y. Fang, Y. Tang, H. Wu, D. Fang, H3K36me3, message from chromatin to DNA damage repair. *Cell Biosci.* **10**, 9 (2020).
17. K. Delaney, N. Weiss, G. Almouzni, The cell-cycle choreography of H3 variants shapes the genome. *Mol. Cell* **0** (2023).
18. P. W. Lewis, S. J. Elsaesser, K.-M. Noh, S. C. Stadler, C. D. Allis, Daxx is an H3.3-specific histone chaperone and cooperates with ATRX in replication-independent chromatin assembly at telomeres. *Proc. Natl. Acad. Sci. U. S. A.* **107**, 14075–14080 (2010).
19. A. Guse, C. W. Carroll, B. Moree, C. J. Fuller, A. F. Straight, In vitro centromere and kinetochore assembly on defined chromatin templates. *Nature* **477**, 354–358 (2011).
20. V. De Rop, A. Padeganeh, P. S. Maddox, CENP-A: the key player behind centromere identity, propagation, and kinetochore assembly. *Chromosoma* **121**, 527–538 (2012).
21. Y. Colino-Sanguino, S. J. Clark, F. Valdes-Mora, The H2A.Z-nucleosome code in mammals: emerging functions. *Trends Genet.* **38**, 273–289 (2022).
22. M. Podhorecka, A. Skladanowski, P. Bozko, H2AX Phosphorylation: Its Role in DNA Damage Response and Cancer Therapy. *J. Nucleic Acids* **2010**, 920161 (2010).
23. B. P. Chadwick, H. F. Willard, Histone H2A variants and the inactive X chromosome: identification of a second macroH2A variant. *Hum. Mol. Genet.* **10**, 1101–1113 (2001).
24. P. Oberdoerffer, K. M. Miller, Histone H2A variants: Diversifying chromatin to ensure genome integrity. *Semin. Cell Dev. Biol.* **135**, 59–72 (2023).
25. C. Warren, D. Shechter, Fly Fishing for Histones: Catch and Release by Histone Chaperone Intrinsically Disordered Regions and Acidic Stretches. *J. Mol. Biol.* **429**, 2401–2426 (2017).
26. C. M. Hammond, C. B. Strømme, H. Huang, D. J. Patel, A. Groth, Histone chaperone networks shaping chromatin function. *Nat. Rev. Mol. Cell Biol.* **18**, 141–158 (2017).
27. I. Corbeski, X. Guo, B. V. Eckhardt, D. Fasci, W. Wiegant, M. A. Graewert, K. Vreeken, H. Wienk, D. I. Svergun, A. J. R. Heck, H. van Attikum, R. Boelens, T. K. Sixma, F. Mattioli, H. van Ingen, Chaperoning of the histone octamer by the acidic domain of DNA repair factor APLF. *Sci. Adv.* **8**, eabo0517 (2022).
28. R. A. Laskey, B. M. Honda, A. D. Mills, J. T. Finch, Nucleosomes are assembled by an acidic protein which binds histones and transfers them to DNA. *Nature* **275**, 416–420 (1978).
29. A. J. Pardal, F. Fernandes-Duarte, A. J. Bowman, The histone chaperoning pathway: from ribosome to nucleosome. *Essays Biochem.* **63**, 29–43 (2019).
30. F. Mattioli, S. D'Arcy, K. Luger, The right place at the right time: chaperoning core histone variants. *EMBO Rep.* **16**, 1454–1466 (2015).
31. C. M. English, M. W. Adkins, J. J. Carson, M. E. A. Churchill, J. K. Tyler, Structural basis for the histone chaperone activity of Asf1. *Cell* **127**, 495–508 (2006).
32. H. H. W. Silljé, E. A. Nigg, Identification of human Asf1 chromatin assembly factors as substrates of Tousled-like kinases. *Curr. Biol.* **11**, 1068–1073 (2001).

- 33.** F. Abascal, A. Corpet, Z. A. Gurard-Levin, D. Juan, F. Ochsenbein, D. Rico, A. Valencia, G. Almouzni, Subfunctionalization via Adaptive Evolution Influenced by Genomic Context: The Case of Histone Chaperones ASF1a and ASF1b. *Mol. Biol. Evol.* **30**, 1853–1866 (2013).
- 34.** C. Fromental-Ramain, P. Ramain, A. Hamiche, The Drosophila DAXX-Like Protein (DLP) Cooperates with ASF1 for H3.3 Deposition and Heterochromatin Formation. *Mol. Cell. Biol.* **37**, e00597-16 (2017).
- 35.** H. Tagami, D. Ray-Gallet, G. Almouzni, Y. Nakatani, Histone H3.1 and H3.3 Complexes Mediate Nucleosome Assembly Pathways Dependent or Independent of DNA Synthesis. *Cell* **116**, 51–61 (2004).
- 36.** J. A. Mello, H. H. W. Silljé, D. M. J. Roche, D. B. Kirschner, E. A. Nigg, G. Almouzni, Human Asf1 and CAF-1 interact and synergize in a repair-coupled nucleosome assembly pathway. *EMBO Rep.* **3**, 329–334 (2002).
- 37.** C. Xiong, Z. Wen, J. Yu, J. Chen, C.-P. Liu, X. Zhang, P. Chen, R.-M. Xu, G. Li, UBN1/2 of HIRA complex is responsible for recognition and deposition of H3.3 at cis-regulatory elements of genes in mouse ES cells. *BMC Biol.* **16**, 110 (2018).
- 38.** C. Roberts, H. F. Sutherland, H. Farmer, W. Kimber, S. Halford, A. Carey, J. M. Brickman, A. Wynshaw-Boris, P. J. Scambler, Targeted Mutagenesis of the Hira Gene Results in Gastrulation Defects and Patterning Abnormalities of Mesoendodermal Derivatives Prior to Early Embryonic Lethality. *Mol. Cell. Biol.* **22**, 2318–2328 (2002).
- 39.** A. D. Goldberg, L. A. Banaszynski, K.-M. Noh, P. W. Lewis, S. J. Elsaesser, S. Stadler, S. Dewell, M. Law, X. Guo, X. Li, D. Wen, A. Chagier, R. C. DeKever, J. C. Miller, Y.-L. Lee, E. A. Boydston, M. C. Holmes, P. D. Gregory, J. M. Grealley, S. Rafii, C. Yang, P. J. Scambler, D. Garrick, R. J. Gibbons, D. R. Higgs, I. M. Cristea, F. D. Urnov, D. Zheng, C. D. Allis, Distinct Factors Control Histone Variant H3.3 Localization at Specific Genomic Regions. *Cell* **140**, 678–691 (2010).
- 40.** G. Orphanides, G. LeRoy, C. H. Chang, D. S. Luse, D. Reinberg, FACT, a factor that facilitates transcript elongation through nucleosomes. *Cell* **92**, 105–116 (1998).
- 41.** C. Jeronimo, F. Robert, The histone chaperone FACT: a guardian of chromatin structure integrity. *Transcription* **13**, 16–38 (2022).
- 42.** R. Belotserkovskaya, S. Oh, V. A. Bondarenko, G. Orphanides, V. M. Studitsky, D. Reinberg, FACT Facilitates Transcription-Dependent Nucleosome Alteration. *Science* **301**, 1090–1093 (2003).
- 43.** F. Robert, C. Jeronimo, Transcription-coupled nucleosome assembly. *Trends Biochem. Sci.* **48**, 978–992 (2023).
- 44.** I. Bogolyubova, D. Bogolyubov, DAXX Is a Crucial Factor for Proper Development of Mammalian Oocytes and Early Embryos. *Int. J. Mol. Sci.* **22**, 1313 (2021).
- 45.** M. C. Barnhart, P. H. J. L. Kuich, M. E. Stellfox, J. A. Ward, E. A. Bassett, B. E. Black, D. R. Foltz, HJURP is a CENP-A chromatin assembly factor sufficient to form a functional de novo kinetochore. *J. Cell Biol.* **194**, 229–243 (2011).

- 46.** C. Aguilar-Gurreri, A. Larabi, V. Vinayachandran, N. A. Patel, K. Yen, R. Reja, I. Ebong, G. Schoehn, C. V. Robinson, B. F. Pugh, D. Panne, Structural evidence for Nap1-dependent H2A–H2B deposition and nucleosome assembly. *EMBO J.* **35**, 1465–1482 (2016).
- 47.** S. J. McBryant, Y.-J. Park, S. M. Abernathy, P. J. Laybourn, J. K. Nyborg, K. Luger, Preferential binding of the histone (H3-H4)₂ tetramer by NAP1 is mediated by the amino-terminal histone tails. *J. Biol. Chem.* **278**, 44574–44583 (2003).
- 48.** M. Hondele, T. Stuwe, M. Hassler, F. Halbach, A. Bowman, E. T. Zhang, B. Nijmeijer, C. Kotthoff, V. Rybin, S. Amlacher, E. Hurt, A. G. Ladurner, Structural basis of histone H2A–H2B recognition by the essential chaperone FACT. *Nature* **499**, 111–114 (2013).
- 49.** D. J. Kemble, L. L. McCullough, F. G. Whitby, T. Formosa, C. P. Hill, FACT Disrupts Nucleosome Structure by Binding H2A-H2B with Conserved Peptide Motifs. *Mol. Cell* **60**, 294–306 (2015).
- 50.** T. Stuwe, M. Hothorn, E. Lejeune, V. Rybin, M. Bortfeld, K. Scheffzek, A. G. Ladurner, The FACT Spt16 “peptidase” domain is a histone H3–H4 binding module. *Proc. Natl. Acad. Sci.* **105**, 8884–8889 (2008).
- 51.** E. Luk, N.-D. Vu, K. Patteson, G. Mizuguchi, W.-H. Wu, A. Ranjan, J. Backus, S. Sen, M. Lewis, Y. Bai, C. Wu, Chz1, a nuclear chaperone for histone H2AZ. *Mol. Cell* **25**, 357–368 (2007).
- 52.** A. Obri, K. Ouararhni, C. Papin, M.-L. Diebold, K. Padmanabhan, M. Marek, I. Stoll, L. Roy, P. T. Reilly, T. W. Mak, S. Dimitrov, C. Romier, A. Hamiche, ANP32E is a histone chaperone that removes H2A.Z from chromatin. *Nature* **505**, 648–653 (2014).
- 53.** Y. Cai, J. Jin, L. Florens, S. K. Swanson, T. Kusch, B. Li, J. L. Workman, M. P. Washburn, R. C. Conaway, J. W. Conaway, The Mammalian YL1 Protein Is a Shared Subunit of the TRRAP/TIP60 Histone Acetyltransferase and SRCAP Complexes *. *J. Biol. Chem.* **280**, 13665–13670 (2005).
- 54.** R. Dronamraju, S. Ramachandran, D. K. Jha, A. T. Adams, J. V. DiFiore, M. A. Parra, N. V. Dokholyan, B. D. Strahl, Redundant Functions for Nap1 and Chz1 in H2A.Z Deposition. *Sci. Rep.* **7**, 10791 (2017).
- 55.** I. K. Mandemaker, E. Fessler, D. Corujo, C. Kotthoff, A. Wegerer, C. Rouillon, M. Buschbeck, L. T. Jae, F. Mattioli, A. G. Ladurner, The histone chaperone ANP32B regulates chromatin incorporation of the atypical human histone variant macroH2A. *Cell Rep.* **42**, 113300 (2023).
- 56.** P. V. Mehrotra, D. Ahel, D. P. Ryan, R. Weston, N. Wiechens, R. Kraehenbuehl, T. Owen-Hughes, I. Ahel, DNA Repair Factor APLF Is a Histone Chaperone. *Mol. Cell* **41**, 46–55 (2011).
- 57.** Chaperoning of the histone octamer by the acidic domain of DNA repair factor APLF | Science Advances. <https://www-science-org.proxy.library.uu.nl/doi/10.1126/sciadv.abo0517>.
- 58.** P. M. J. Burgers, T. A. Kunkel, Eukaryotic DNA Replication Fork. *Annu. Rev. Biochem.* **86**, 417–438 (2017).
- 59.** S. P. Bell, K. Labib, Chromosome Duplication in *Saccharomyces cerevisiae*. *Genetics* **203**, 1027–1067 (2016).
- 60.** B. Ekundayo, F. Bleichert, Origins of DNA replication. *PLoS Genet.* **15**, e1008320 (2019).

- 61.** Z. Yuan, A. Riera, L. Bai, J. Sun, S. Nandi, C. Spanos, Z. A. Chen, M. Barbon, J. Rappsilber, B. Stillman, C. Speck, H. Li, Structural basis of MCM2-7 replicative helicase loading by ORC-Cdc6 and Cdt1. *Nat. Struct. Mol. Biol.* **24**, 316 (2017).
- 62.** T. C. R. Miller, J. Locke, J. F. Greiwe, J. F. X. Diffley, A. Costa, Mechanism of head-to-head MCM double-hexamers formation revealed by cryo-EM. *Nature* **575**, 704–710 (2019).
- 63.** A. Costa, I. Ilves, N. Tamberg, T. Petojevic, E. Nogales, M. R. Botchan, J. M. Berger, The structural basis for MCM2-7 helicase activation by GINS and Cdc45. *Nat. Struct. Mol. Biol.* **18**, 471–477 (2011).
- 64.** S. E. Moyer, P. W. Lewis, M. R. Botchan, Isolation of the Cdc45/Mcm2-7/GINS (CMG) complex, a candidate for the eukaryotic DNA replication fork helicase. *Proc. Natl. Acad. Sci. U. S. A.* **103**, 10236–10241 (2006).
- 65.** P. Goswami, F. Abid Ali, M. E. Douglas, J. Locke, A. Purkiss, A. Janska, P. Eickhoff, A. Early, A. Nans, A. M. C. Cheung, J. F. X. Diffley, A. Costa, Structure of DNA-CMG-Pol epsilon elucidates the roles of the non-catalytic polymerase modules in the eukaryotic replisome. *Nat. Commun.* **9**, 5061 (2018).
- 66.** S. Muramatsu, K. Hirai, Y.-S. Tak, Y. Kamimura, H. Araki, CDK-dependent complex formation between replication proteins Dpb11, Sld2, Pol (epsilon), and GINS in budding yeast. *Genes Dev.* **24**, 602–612 (2010).
- 67.** T. A. Guillian, J. T. P. Yeeles, An updated perspective on the polymerase division of labor during eukaryotic DNA replication. *Crit. Rev. Biochem. Mol. Biol.* **55**, 469–481 (2020).
- 68.** Y. Daigaku, A. Keszthelyi, C. A. Müller, I. Miyabe, T. Brooks, R. Retkute, M. Hubank, C. A. Nieduszynski, A. M. Carr, A global profile of replicative polymerase usage. *Nat. Struct. Mol. Biol.* **22**, 192–198 (2015).
- 69.** J. T. P. Yeeles, A. Janska, A. Early, J. F. X. Diffley, How the Eukaryotic Replisome Achieves Rapid and Efficient DNA Replication. *Mol. Cell* **65**, 105–116 (2017).
- 70.** V. Aria, J. T. P. Yeeles, Mechanism of Bidirectional Leading-Strand Synthesis Establishment at Eukaryotic DNA Replication Origins. *Mol. Cell* **73**, 199–211.e10 (2018).
- 71.** O. Chilkova, P. Stenlund, I. Isoz, C. M. Stith, P. Grabowski, E.-B. Lundström, P. M. Burgers, E. Johansson, The eukaryotic leading and lagging strand DNA polymerases are loaded onto primer-ends via separate mechanisms but have comparable processivity in the presence of PCNA. *Nucleic Acids Res.* **35**, 6588–6597 (2007).
- 72.** R. E. Georgescu, L. Langston, N. Y. Yao, O. Yurieva, D. Zhang, J. Finkelstein, T. Agarwal, M. E. O'Donnell, Mechanism of asymmetric polymerase assembly at the eukaryotic replication fork. *Nat. Struct. Mol. Biol.* **21**, 664–670 (2014).
- 73.** K. N. Choe, G.-L. Moldovan, Forging Ahead through Darkness: PCNA, Still the Principal Conductor at the Replication Fork. *Mol. Cell* **65**, 380–392 (2017).
- 74.** T. S. R. Krishna, X.-P. Kong, S. Gary, P. M. Burgers, J. Kuriyan, Crystal structure of the eukaryotic DNA polymerase processivity factor PCNA. *Cell* **79**, 1233–1243 (1994).

- 75.** G. D. Schauer, M. E. O'Donnell, Quality control mechanisms exclude incorrect polymerases from the eukaryotic replication fork. *Proc. Natl. Acad. Sci.* **114**, 675–680 (2017).
- 76.** S. H. Lee, Z. Q. Pan, A. D. Kwong, P. M. Burgers, J. Hurwitz, Synthesis of DNA by DNA polymerase epsilon in vitro. *J. Biol. Chem.* **266**, 22707–22717 (1991).
- 77.** F. Zheng, R. E. Georgescu, H. Li, M. E. O'Donnell, Structure of eukaryotic DNA polymerase δ bound to the PCNA clamp while encircling DNA. *Proc. Natl. Acad. Sci.* **117**, 30344–30353 (2020).
- 78.** C. Lancey, M. Tehseen, V.-S. Raducanu, F. Rashid, N. Merino, T. J. Ragan, C. G. Savva, M. S. Zaher, A. Shirbini, F. J. Blanco, S. M. Hamdan, A. De Biasio, Structure of the processive human Pol δ holoenzyme. *Nat. Commun.* **11**, 1109 (2020).
- 79.** R. Okazaki, T. Okazaki, K. Sakabe, K. Sugimoto, A. Sugino, Mechanism of DNA chain growth. I. Possible discontinuity and unusual secondary structure of newly synthesized chains. *Proc. Natl. Acad. Sci. U. S. A.* **59**, 598–605 (1968).
- 80.** H. Sun, L. Ma, Y.-F. Tsai, T. Abeywardana, B. Shen, L. Zheng, Okazaki fragment maturation: DNA flap dynamics for cell proliferation and survival. *Trends Cell Biol.* **33**, 221–234 (2023).
- 81.** J. M. Dewar, J. C. Walter, Mechanisms of DNA replication termination. *Nat. Rev. Mol. Cell Biol.* **18**, 507–516 (2017).
- 82.** G. Prelich, M. Kostura, D. R. Marshak, M. B. Mathews, B. Stillman, The cell-cycle regulated proliferating cell nuclear antigen is required for SV40 DNA replication in vitro. *Nature* **326**, 471–475 (1987).
- 83.** G. Prelich, C.-K. Tan, M. Kostura, M. B. Mathews, A. G. So, K. M. Downey, B. Stillman, Functional identity of proliferating cell nuclear antigen and a DNA polymerase- δ auxiliary protein. *Nature* **326**, 517–520 (1987).
- 84.** A. B. Kochaniak, S. Habuchi, J. J. Loparo, D. J. Chang, K. A. Cimprich, J. C. Walter, A. M. van Oijen, Proliferating Cell Nuclear Antigen Uses Two Distinct Modes to Move along DNA. *J. Biol. Chem.* **284**, 17700–17710 (2009).
- 85.** M. De March, N. Merino, S. Barrera-Vilarmau, R. Crehuet, S. Onesti, F. J. Blanco, A. De Biasio, Structural basis of human PCNA sliding on DNA. *Nat. Commun.* **8**, 13935 (2017).
- 86.** G.-L. Moldovan, B. Pfander, S. Jentsch, PCNA, the Maestro of the Replication Fork. *Cell* **129**, 665–679 (2007).
- 87.** E. M. Boehm, M. T. Washington, R.I.P. to the PIP: PCNA-binding motif no longer considered specific: PIP motifs and other related sequences are not distinct entities and can bind multiple proteins involved in genome maintenance. *BioEssays News Rev. Mol. Cell. Dev. Biol.* **38**, 1117–1122 (2016).
- 88.** Z. Zhang, K. Shibahara, B. Stillman, PCNA connects DNA replication to epigenetic inheritance in yeast. **408**, 5 (2000).
- 89.** K. Lee, S. H. Park, Eukaryotic clamp loaders and unloaders in the maintenance of genome stability. *Exp. Mol. Med.* **52**, 1948–1958 (2020).
- 90.** T. Tsurimoto, B. Stillman, Purification of a cellular replication factor, RF-C, that is required for coordinated synthesis of leading and lagging strands during simian virus 40 DNA replication in vitro. *Mol. Cell. Biol.* **9**, 609–619 (1989).

- 91.** G. D. Bowman, M. O'Donnell, J. Kuriyan, Structural analysis of a eukaryotic sliding DNA clamp-clamp loader complex. *Nature* **429**, 724–730 (2004).
- 92.** Y. Baris, M. R. G. Taylor, V. Aria, J. T. P. Yeeles, Fast and efficient DNA replication with purified human proteins. *Nature* **606**, 204–210 (2022).
- 93.** K. Stokes, A. Winczura, B. Song, G. De Piccoli, D. B. Grabarczyk, Ctf18-RFC and DNA Pol ϵ form a stable leading strand polymerase/clamp loader complex required for normal and perturbed DNA replication. *Nucleic Acids Res.* **48**, 8128–8145 (2020).
- 94.** V. P. Bermudez, Y. Maniwa, I. Tappin, K. Ozato, K. Yokomori, J. Hurwitz, The alternative Ctf18-Dcc1-Ctf8-replication factor C complex required for sister chromatid cohesion loads proliferating cell nuclear antigen onto DNA. *Proc. Natl. Acad. Sci. U. S. A.* **100**, 10237–10242 (2003).
- 95.** H. W. Liu, C. Bouchoux, M. Panarotto, Y. Kakui, H. Patel, F. Uhlmann, Division of Labor between PCNA Loaders in DNA Replication and Sister Chromatid Cohesion Establishment. *Mol. Cell* **78**, 725-738.e4 (2020).
- 96.** J. S. Hanna, E. S. Kroll, V. Lundblad, F. A. Spencer, *Saccharomyces cerevisiae* CTF18 and CTF4 are required for sister chromatid cohesion. *Mol. Cell. Biol.* **21**, 3144–3158 (2001).
- 97.** T. Kubota, K. Nishimura, M. T. Kanemaki, A. D. Donaldson, The Elg1 Replication Factor C-like Complex Functions in PCNA Unloading during DNA Replication. *Mol. Cell* **50**, 273–280 (2013).
- 98.** M.-S. Kang, E. Ryu, S.-W. Lee, J. Park, N. Y. Ha, J. S. Ra, Y. J. Kim, J. Kim, M. Abdel-Rahman, S. H. Park, K. Lee, H. Kim, S. Kang, K. Myung, Regulation of PCNA cycling on replicating DNA by RFC and RFC-like complexes. *Nat. Commun.* **10**, 2420 (2019).
- 99.** S. Waga, G. J. Hannon, D. Beach, B. Stillman, The p21 inhibitor of cyclin-dependent kinases controls DNA replication by interaction with PCNA. *Nature* **369**, 574–578 (1994).
- 100.** L. Schermelleh, A. Haemmer, F. Spada, N. Rösing, D. Meilinger, U. Rothbauer, M. C. Cardoso, H. Leonhardt, Dynamics of Dnmt1 interaction with the replication machinery and its role in postreplicative maintenance of DNA methylation. *Nucleic Acids Res.* **35**, 4301–4312 (2007).
- 101.** P.-O. Estève, H. G. Chin, A. Smallwood, G. R. Feehery, O. Gangisetty, A. R. Karpf, M. F. Carey, S. Pradhan, Direct interaction between DNMT1 and G9a coordinates DNA and histone methylation during replication. *Genes Dev.* **20**, 3089–3103 (2006).
- 102.** G.-L. Moldovan, B. Pfander, S. Jentsch, PCNA controls establishment of sister chromatid cohesion during S phase. *Mol. Cell* **23**, 723–732 (2006).
- 103.** S. P. Rowbotham, L. Barki, A. Neves-Costa, F. Santos, W. Dean, N. Hawkes, P. Choudhary, W. R. Will, J. Webster, D. Oxley, C. M. Green, P. Varga-Weisz, J. E. Mermoud, Maintenance of silent chromatin through replication requires SWI/SNF-like chromatin remodeler SMARCAD1. *Mol. Cell* **42**, 285–296 (2011).
- 104.** K. Shibahara, B. Stillman, Replication-dependent marking of DNA by PCNA facilitates CAF-1-coupled inheritance of chromatin. *Cell* **96**, 575–585 (1999).

- 105.** M. Li, X. Xu, C.-W. Chang, L. Zheng, B. Shen, Y. Liu, SUMO2 conjugation of PCNA facilitates chromatin remodeling to resolve transcription-replication conflicts. *Nat. Commun.* **9**, 2706 (2018).
- 106.** K. R. Stewart-Morgan, N. Petryk, A. Groth, Chromatin replication and epigenetic cell memory. *Nat. Cell Biol.* **22**, 361–371 (2020).
- 107.** T. M. Escobar, A. Loyola, D. Reinberg, Parental nucleosome segregation and the inheritance of cellular identity. *Nat. Rev. Genet.* **22**, 379–392 (2021).
- 108.** V. Jackson, In vivo studies on the dynamics of histone-DNA interaction: evidence for nucleosome dissolution during replication and transcription and a low level of dissolution independent of both. *Biochemistry* **29**, 719–731 (1990).
- 109.** N. Reverón-Gómez, C. González-Aguilera, K. R. Stewart-Morgan, N. Petryk, V. Flury, S. Graziano, J. V. Johansen, J. S. Jakobsen, C. Alabert, A. Groth, Accurate Recycling of Parental Histones Reproduces the Histone Modification Landscape during DNA Replication. *Mol. Cell* **72**, 239–249.e5 (2018).
- 110.** C. F. Kurat, J. T. P. Yeeles, H. Patel, A. Early, J. F. X. Diffley, Chromatin Controls DNA Replication Origin Selection, Lagging-Strand Synthesis, and Replication Fork Rates. *Mol. Cell* **65**, 117–130 (2017).
- 111.** M. Xu, C. Long, X. Chen, C. Huang, S. Chen, B. Zhu, Partitioning of histone H3-H4 tetramers during DNA replication-dependent chromatin assembly. *Science* **328**, 94–98 (2010).
- 112.** N. Petryk, M. Dalby, A. Wenger, C. B. Stromme, A. Strandsby, R. Andersson, A. Groth, MCM2 promotes symmetric inheritance of modified histones during DNA replication. *Science* **361**, 1389–1392 (2018).
- 113.** H. Gan, A. Serra-Cardona, X. Hua, H. Zhou, K. Labib, C. Yu, Z. Zhang, The Mcm2-Ctf4-Pola Axis Facilitates Parental Histone H3-H4 Transfer to Lagging Strands. *Mol. Cell* **72**, 140–151.e3 (2018).
- 114.** C. Yu, H. Gan, A. Serra-Cardona, L. Zhang, S. Gan, S. Sharma, E. Johansson, A. Chabes, R.-M. Xu, Z. Zhang, A mechanism for preventing asymmetric histone segregation onto replicating DNA strands. *Science* **361**, 1386–1389 (2018).
- 115.** H. He, Y. Li, Q. Dong, A.-Y. Chang, F. Gao, Z. Chi, M. Su, F. Zhang, H. Ban, R. Martienssen, Y. Chen, F. Li, Coordinated regulation of heterochromatin inheritance by Dpb3–Dpb4 complex. *Proc. Natl. Acad. Sci. U. S. A.* **114**, 12524–12529 (2017).
- 116.** H. Huang, C. B. Strømme, G. Saredi, M. Hödl, A. Strandsby, C. González-Aguilera, S. Chen, A. Groth, D. J. Patel, A unique binding mode enables MCM2 to chaperone histones H3-H4 at replication forks. *Nat. Struct. Mol. Biol.* **22**, 618–626 (2015).
- 117.** B. Safaric, E. Chacin, M. J. Scherr, L. Rajappa, C. Gebhardt, C. F. Kurat, T. Cordes, K. E. Duderstadt, The fork protection complex recruits FACT to reorganize nucleosomes during replication. *Nucleic Acids Res.* **50**, 1317–1334 (2022).

- 118.** S. Liu, Z. Xu, H. Leng, P. Zheng, J. Yang, K. Chen, J. Feng, Q. Li, RPA binds histone H3-H4 and functions in DNA replication-coupled nucleosome assembly. *Science* **355**, 415–420 (2017).
- 119.** Z. Li, X. Hua, A. Serra-Cardona, X. Xu, S. Gan, H. Zhou, W.-S. Yang, C.-L. Chen, R.-M. Xu, Z. Zhang, DNA polymerase α interacts with H3-H4 and facilitates the transfer of parental histones to lagging strands. *Sci. Adv.* **6**, eabb5820 (2020).
- 120.** K. Gurova, H.-W. Chang, M. E. Valieva, P. Sandlesh, V. M. Studitsky, Structure and function of the histone chaperone FACT – Resolving FACTual issues. *Biochim. Biophys. Acta BBA - Gene Regul. Mech.* **1861**, 892–904 (2018).
- 121.** X. Wang, Y. Tang, J. Xu, H. Leng, G. Shi, Z. Hu, J. Wu, Y. Xiu, J. Feng, Q. Li, The N-terminus of Spt16 anchors FACT to MCM2–7 for parental histone recycling. *Nucleic Acids Res.*, gkad846 (2023).
- 122.** J. Wittmeyer, L. Joss, T. Formosa, Spt16 and Pob3 of *Saccharomyces cerevisiae* form an essential, abundant heterodimer that is nuclear, chromatin-associated, and copurifies with DNA polymerase α . *Biochemistry* **38**, 8961–8971 (1999).
- 123.** T. Wang, Y. Liu, G. Edwards, D. Krzizike, H. Scherman, K. Luger, The histone chaperone FACT modulates nucleosome structure by tethering its components. *Life Sci. Alliance* **1**, e201800107 (2018).
- 124.** F.-K. Hsieh, O. I. Kulaeva, S. S. Patel, P. N. Dyer, K. Luger, D. Reinberg, V. M. Studitsky, Histone chaperone FACT action during transcription through chromatin by RNA polymerase II. *Proc. Natl. Acad. Sci. U. S. A.* **110**, 7654–7659 (2013).
- 125.** Y. Liu, K. Zhou, N. Zhang, H. Wei, Y. Z. Tan, Z. Zhang, B. Carragher, C. S. Potter, S. D'Arcy, K. Luger, FACT caught in the act of manipulating the nucleosome. *Nature* **577**, 426–431 (2020).
- 126.** T. M. Escobar, O. Oksuz, R. Saldaña-Meyer, N. Descostes, R. Bonasio, D. Reinberg, Active and Repressed Chromatin Domains Exhibit Distinct Nucleosome Segregation during DNA Replication. *Cell* **179**, 953–963.e11 (2019).
- 127.** A. Wenger, A. Biran, N. Alcaraz, A. Redó-Riveiro, A. C. Sell, R. Krautz, V. Flury, N. Reverón-Gómez, V. Solis-Mezarino, M. Völker-Albert, A. Imhof, R. Andersson, J. M. Brickman, A. Groth, Symmetric inheritance of parental histones governs epigenome maintenance and embryonic stem cell identity. *Nat. Genet.* **55**, 1567–1578 (2023).
- 128.** K. R. Stewart-Morgan, N. Reverón-Gómez, A. Groth, Transcription Restart Establishes Chromatin Accessibility after DNA Replication. *Mol. Cell* **75**, 284–297.e6 (2019).
- 129.** V. Flury, N. Reverón-Gómez, N. Alcaraz, K. R. Stewart-Morgan, A. Wenger, R. J. Klose, A. Groth, Recycling of modified H2A-H2B provides short-term memory of chromatin states. *Cell* **186**, 1050–1065.e19 (2023).
- 130.** C. Evrin, J. D. Maman, A. Diamante, L. Pellegrini, K. Labib, Histone H2A-H2B binding by Pol α in the eukaryotic replisome contributes to the maintenance of repressive chromatin. *EMBO J.* **37**, e99021 (2018).

- 131.** G. Saredi, H. Huang, C. M. Hammond, C. Alabert, S. Bekker-Jensen, I. Forne, N. Reverón-Gómez, B. M. Foster, L. Mlejnkova, T. Bartke, P. Cejka, N. Mailand, A. Imhof, D. J. Patel, A. Groth, H4K20me0 marks post-replicative chromatin and recruits the TONSL–MMS22L DNA repair complex. *Nature* **534**, 714–718 (2016).
- 132.** J. K. Tyler, C. R. Adams, S. R. Chen, R. Kobayashi, R. T. Kamakaka, J. T. Kadonaga, The RCAF complex mediates chromatin assembly during DNA replication and repair. *Nature* **402**, 555–560 (1999).
- 133.** S. Cheloufi, U. Elling, B. Hopfgartner, Y. L. Jung, J. Murn, M. Ninova, M. Hubmann, A. I. Badeaux, C. Euong Ang, D. Tenen, D. J. Wesche, N. Abazova, M. Hogue, N. Tasdemir, J. Brumbaugh, P. Rathert, J. Jude, F. Ferrari, A. Blanco, M. Fellner, D. Wenzel, M. Zinner, S. E. Vidal, O. Bell, M. Stadtfeld, H. Y. Chang, G. Almouzni, S. W. Lowe, J. Rinn, M. Wernig, A. Aravin, Y. Shi, P. J. Park, J. M. Penninger, J. Zuber, K. Hochedlinger, The histone chaperone CAF-1 safeguards somatic cell identity. *Nature* **528**, 218–224 (2015).
- 134.** L. Cheng, X. Zhang, Y. Wang, H. Gan, X. Xu, X. Lv, X. Hua, J. Que, T. Ordog, Z. Zhang, Chromatin Assembly Factor 1 (CAF-1) facilitates the establishment of facultative heterochromatin during pluripotency exit. *Nucleic Acids Res.* **47**, 11114–11131 (2019).
- 135.** T.-H. Huang, F. Fowler, C.-C. Chen, Z.-J. Shen, B. Sleckman, J. K. Tyler, The Histone Chaperones ASF1 and CAF-1 Promote MMS22L-TONSL-Mediated Rad51 Loading onto ssDNA during Homologous Recombination in Human Cells. *Mol. Cell* **69**, 879–892.e5 (2018).
- 136.** M. Hoek, M. P. Myers, B. Stillman, An analysis of CAF-1-interacting proteins reveals dynamic and direct interactions with the KU complex and 14-3-3 proteins. *J. Biol. Chem.* **286**, 10876–10887 (2011).
- 137.** M. Clémot, A. Molla-Herman, J. Mathieu, J.-R. Huynh, N. Dostatni, The replicative histone chaperone CAF1 is essential for the maintenance of identity and genome integrity in adult stem cells. *Development* **145**, dev161190 (2018).
- 138.** S. Fischer, S. Prykhozhij, M. J. Rau, C. J. Neumann, Mutation of zebrafish *caf-1b* results in S phase arrest, defective differentiation, and p53-mediated apoptosis during organogenesis. *Cell Cycle Georget. Tex* **6**, 2962–2969 (2007).
- 139.** M. Houliard, S. Berlivet, A. V. Probst, J.-P. Quivy, P. Héry, G. Almouzni, M. Gérard, CAF-1 Is Essential for Heterochromatin Organization in Pluripotent Embryonic Cells. *PLOS Genet.* **2**, e181 (2006).
- 140.** M. Hoek, B. Stillman, Chromatin assembly factor 1 is essential and couples chromatin assembly to DNA replication in vivo. *Proc. Natl. Acad. Sci.* **100**, 12183–12188 (2003).
- 141.** Y. Song, F. He, G. Xie, X. Guo, Y. Xu, Y. Chen, X. Liang, I. Stagljar, D. Egli, J. Ma, R. Jiao, CAF-1 is essential for Drosophila development and involved in the maintenance of epigenetic memory. *Dev. Biol.* **311**, 213–222 (2007).
- 142.** M. Mascolo, G. Ilardi, F. Merolla, D. Russo, M. L. Vecchione, G. De Rosa, S. Staibano, Tissue Microarray-Based Evaluation of Chromatin Assembly Factor-1 (CAF-1)/p60 as Tumour Prognostic Marker. *Int. J. Mol. Sci.* **13**, 11044–11062 (2012).

- 143.** A. G. Sykaras, A. Pergaris, S. Theocharis, Challenging, Accurate and Feasible: CAF-1 as a Tumour Proliferation Marker of Diagnostic and Prognostic Value. *Cancers* **13**, 2575 (2021).
- 144.** P. D. Kaufman, R. Kobayashi, B. Stillman, Ultraviolet radiation sensitivity and reduction of telomeric silencing in *Saccharomyces cerevisiae* cells lacking chromatin assembly factor-I. *Genes Dev.* **11**, 345–357 (1997).
- 145.** S. Smith, B. Stillman, Purification and characterization of CAF-I, a human cell factor required for chromatin assembly during DNA replication in vitro. *Cell* **58**, 15–25 (1989).
- 146.** B. Stillman, Chromatin assembly during SV40 DNA replication in vitro. *Cell* **45**, 555–565 (1986).
- 147.** P. V. Sauer, J. Timm, D. Liu, D. Sitbon, E. Boeri-Erba, C. Velours, N. Mücke, J. Langowski, F. Ochsenbein, G. Almouzni, D. Panne, Insights into the molecular architecture and histone H3-H4 deposition mechanism of yeast Chromatin assembly factor 1. *eLife* **6**, e23474 (2017).
- 148.** D. Kim, D. Setiaputra, T. Jung, J. Chung, A. Leitner, J. Yoon, R. Aebersold, H. Hebert, C. K. Yip, J.-J. Song, Molecular Architecture of Yeast Chromatin Assembly Factor 1. *Sci. Rep.* **6** (2016).
- 149.** F. Mattioli, Y. Gu, J. L. Balsbaugh, N. G. Ahn, K. Luger, The Cac2 subunit is essential for productive histone binding and nucleosome assembly in CAF-1. *Sci. Rep.* **7**, 46274 (2017).
- 150.** C.-P. Liu, Z. Yu, J. Xiong, J. Hu, A. Song, D. Ding, C. Yu, N. Yang, M. Wang, J. Yu, P. Hou, K. Zeng, Z. Li, Z. Zhang, X. Zhang, W. Li, Z. Zhang, B. Zhu, G. Li, R.-M. Xu, Structural insights into histone binding and nucleosome assembly by chromatin assembly factor-1. *Science* **381**, eadd8673 (2023).
- 151.** K. Zhang, Y. Gao, J. Li, R. Burgess, J. Han, H. Liang, Z. Zhang, Y. Liu, A DNA binding winged helix domain in CAF-1 functions with PCNA to stabilize CAF-1 at replication forks. *Nucleic Acids Res.* **44**, 5083–5094 (2016).
- 152.** T. R. Ben-Shahar, A. G. Castillo, M. J. Osborne, K. L. B. Borden, J. Kornblatt, A. Verreault, Two Fundamentally Distinct PCNA Interaction Peptides Contribute to Chromatin Assembly Factor 1 Function. *Mol. Cell. Biol.* **29**, 6353–6365 (2009).
- 153.** R. Rosas, R. R. Aguilar, N. Arslanovic, A. Seck, D. J. Smith, J. K. Tyler, M. E. Churchill, A novel single alpha-helix DNA-binding domain in CAF-1 promotes gene silencing and DNA damage survival through tetrasome-length DNA selectivity and spacer function. *eLife* **12**, e83538 (2023).
- 154.** P. D. Kaufman, R. Kobayashi, N. Kessler, B. Stillman, The p150 and p60 Subunits of Chromatin Assembly Factor I: A Molecular Link between Newly Synthesized Histones and DNA Replication.
- 155.** F. Mattioli, Y. Gu, T. Yadav, J. L. Balsbaugh, M. R. Harris, E. S. Findlay, Y. Liu, C. A. Radebaugh, L. A. Stargell, N. G. Ahn, I. Whitehouse, K. Luger, DNA-mediated association of two histone-bound complexes of yeast Chromatin Assembly Factor-1 (CAF-1) drives tetrasome assembly in the wake of DNA replication. *eLife* **6** (2017).
- 156.** N. Murzina, A. Verreault, E. Laue, B. Stillman, Heterochromatin Dynamics in Mouse Cells: Interaction between Chromatin Assembly Factor 1 and HP1 Proteins. *Mol. Cell* **4**, 529–540 (1999).

- 157.** A. Thiru, D. Nietlispach, H. R. Mott, M. Okuwaki, D. Lyon, P. R. Nielsen, M. Hirshberg, A. Verreault, N. V. Murzina, E. D. Laue, Structural basis of HP1/PXVXL motif peptide interactions and HP1 localisation to heterochromatin. *EMBO J.* **23**, 489–499 (2004).
- 158.** A. Loyola, H. Tagami, T. Bonaldi, D. Roche, J. P. Quivy, A. Imhof, Y. Nakatani, S. Y. R. Dent, G. Almouzni, The HP1 α -CAF1-SetDB1-containing complex provides H3K9me1 for Suv39-mediated K9me3 in pericentric heterochromatin. *EMBO Rep.* **10**, 769–775 (2009).
- 159.** J. Uwada, N. Tanaka, Y. Yamaguchi, Y. Uchimura, K. Shibahara, M. Nakao, H. Saitoh, The p150 subunit of CAF-1 causes association of SUMO2/3 with the DNA replication foci. *Biochem. Biophys. Res. Commun.* **391**, 407–413 (2010).
- 160.** Y. Daigaku, T. J. Etheridge, Y. Nakazawa, M. Nakayama, A. T. Watson, I. Miyabe, T. Ogi, M. A. Osborne, A. M. Carr, PCNA ubiquitylation ensures timely completion of unperturbed DNA replication in fission yeast. *PLOS Genet.* **13**, e1006789 (2017).
- 161.** B. Wen, H.-X. Zheng, D.-X. Deng, Z.-D. Zhang, J.-H. Heng, L.-D. Liao, L.-Y. Xu, E.-M. Li, CHAF1A promotes the translesion DNA synthesis pathway in response to DNA replication stress. bioRxiv [Preprint] (2023). <https://doi.org/10.1101/2023.04.21.537900>.
- 162.** L. Zhang, A. Serra-Cardona, H. Zhou, M. Wang, N. Yang, Z. Zhang, R.-M. Xu, Multisite Substrate Recognition in Asf1-Dependent Acetylation of Histone H3 K56 by Rtt109. *Cell* **174**, 818–830.e11 (2018).
- 163.** J. K. Tyler, K. A. Collins, J. Prasad-Sinha, E. Amiott, M. Bulger, P. J. Harte, R. Kobayashi, J. T. Kadonaga, Interaction between the Drosophila CAF-1 and ASF1 chromatin assembly factors. *Mol. Cell. Biol.* **21**, 6574–6584 (2001).
- 164.** M. Carraro, I. A. Hendriks, C. M. Hammond, V. Solis-Mezarino, M. Völker-Albert, J. D. Elsborg, M. B. Weisser, C. Spanos, G. Montoya, J. Rappsilber, A. Imhof, M. L. Nielsen, A. Groth, DAXX adds a de novo H3.3K9me3 deposition pathway to the histone chaperone network. *Mol. Cell* **83**, 1075-1092.e9 (2023).
- 165.** Z. Li, S. Duan, X. Hua, X. Xu, Y. Li, D. Menolfi, H. Zhou, C. Lu, S. Zha, S. P. Goff, Z. Zhang, Asymmetric distribution of parental H3K9me3 in S phase silences L1 elements. *Nature* **623**, 643–651 (2023).
- 166.** S. Staibano, M. Mascolo, F. P. Mancini, A. Kisslinger, G. Salvatore, M. Di Benedetto, P. Chieffi, V. Altieri, D. Prezioso, G. Ilardi, G. De Rosa, D. Tramontano, Overexpression of chromatin assembly factor-1 (CAF-1) p60 is predictive of adverse behaviour of prostatic cancer. *Histopathology* **54**, 580–589 (2009).
- 167.** S. E. Polo, S. E. Theocharis, L. Grandin, L. Gambotti, G. Antoni, A. Savignoni, B. Asselain, E. Patsouris, G. Almouzni, Clinical significance and prognostic value of chromatin assembly factor-1 overexpression in human solid tumours. *Histopathology* **57**, 716–724 (2010).
- 168.** A. Volk, J. D. Crispino, The role of the chromatin assembly complex (CAF-1) and its p60 subunit (CHAF1b) in homeostasis and disease. *Biochim. Biophys. Acta BBA - Gene Regul. Mech.* **1849**, 979–986 (2015).

- 169.** T. Thakar, W. Leung, C. M. Nicolae, K. E. Clements, B. Shen, A.-K. Bielinsky, G.-L. Moldovan, Ubiquitinated-PCNA protects replication forks from DNA2-mediated degradation by regulating Okazaki fragment maturation and chromatin assembly. *Nat. Commun.* **11**, 2147 (2020).
- 170.** A. Gérard, S. Koundrioukoff, V. Ramillon, J.-C. Sergère, N. Mailand, J.-P. Quivy, G. Almouzni, The replication kinase Cdc7-Dbf4 promotes the interaction of the p150 subunit of chromatin assembly factor 1 with proliferating cell nuclear antigen. *EMBO Rep.* **7**, 817–823 (2006).
- 171.** S. L. McKnight, O. L. Miller, Electron microscopic analysis of chromatin replication in the cellular blastoderm drosophila melanogaster embryo. *Cell* **12**, 795–804 (1977).
- 172.** P. V. Sauer, Y. Gu, W. H. Liu, F. Mattioli, D. Panne, K. Luger, M. E. Churchill, Mechanistic insights into histone deposition and nucleosome assembly by the chromatin assembly factor-1. *Nucleic Acids Res.* **46**, 9907–9917 (2018).



2

CAF-1 deposits newly synthesized histones during DNA replication using distinct mechanisms on the leading and lagging strands

Clément Rouillon^{1,8}, Bruna V. Eckhardt^{1,8}, Leonie Kollenstart^{2,3,8}, Fabian Gruss¹, Alexander E.E. Verkennis¹, Inge Rondeel¹, Peter H.L. Krijger⁴, Giulia Ricci¹, Alva Biran^{2,3}, Theo van Laar⁵, Charlotte M. Delvaux de Fenffe¹, Georgiana Luppens¹, Pascal Albanese⁶, Koichi Sato⁴, Richard A. Scheltema⁶, Wouter de Laat⁴, Puck Knipscheer^{4,7}, Nynke H. Dekker⁵, Anja Groth^{2,3,*}, Francesca Mattioli^{1,*}

¹*Hubrecht Institute-KNAW & University Medical Center Utrecht, Utrecht, the Netherlands;*

²*Novo Nordisk Foundation Center for Protein Research (CPR), University of Copenhagen, Copenhagen, Denmark;*

³*Biotech Research and Innovation Center, University of Copenhagen, Copenhagen, Denmark.*

⁴*Onco Institute, Hubrecht Institute-KNAW and University Medical Center Utrecht, Utrecht, the Netherlands.* ⁵*Kavli Institute of Nanoscience Delft, TU Delft, The Netherlands;*

⁶*Utrecht Institute for Pharmaceutical Sciences, Utrecht University, the Netherlands*

⁷*Department of Human Genetics, Leiden University Medical Center, Leiden, The Netherlands*

⁸ These authors contributed equally to this work

*Correspondence: Francesca Mattioli: f.mattioli@hubrecht.eu,
Anja Groth: anja.groth@cpr.ku.dk

Nucleic Acid Research 2023, DOI: 10.1093/nar/gkad171

The author of this thesis, contributed to Figure 1, Figure 2, Figure 4, Figure 5, Figure S1, Figure S2, and Figure S4.

Abstract

During every cell cycle, both the genome and the associated chromatin must be accurately replicated. Chromatin Assembly Factor-1 (CAF-1) is a key regulator of chromatin replication, but how CAF-1 functions in relation to the DNA replication machinery is unknown. Here, we reveal that this crosstalk differs between the leading and lagging strand at replication forks. Using biochemical reconstitution, we show that DNA and histones promote CAF-1 recruitment to its binding partner PCNA and reveal that two CAF-1 complexes are required for efficient nucleosome assembly under these conditions. Remarkably, in the context of the replisome, CAF-1 competes with the leading strand DNA polymerase epsilon (Pol ϵ) for PCNA binding. However, CAF-1 does not affect the activity of the lagging strand DNA polymerase Delta (Pol δ). Yet, in cells, CAF-1 deposits newly synthesized histones equally on both daughter strands. Thus, on the leading strand, chromatin assembly by CAF-1 cannot occur simultaneously to DNA synthesis, while on the lagging strand these processes may be coupled. We propose that these differences may facilitate distinct parental histone recycling mechanisms and accommodate the inherent asymmetry of DNA replication.

Introduction

During every cell cycle, a new copy of the genome is made. At the same time, genomic chromatin organization must be replicated to ensure faithful transmission of the parental epigenetic state to both daughter cells after cell division. Therefore, genome and chromatin replication are tightly coupled and regulated by the concerted action of several dozens of proteins. Errors in both processes affect cell function; they can derail developmental programs or cause diseases, such as cancer (1–4).

DNA is replicated by the replisome, which is comprised of a core Cdc45-MCM-GINS (CMG) helicase complex, DNA polymerases and regulatory factors (5–9). Two distinct DNA polymerases function on the two daughter strands: DNA polymerase epsilon (Pol ϵ) acts on the leading strand, whereas DNA polymerase delta (Pol δ) acts on the lagging strand (10–14). Because both DNA polymerases synthesize DNA in the 5'-3' direction, the two strands are replicated via distinct mechanisms. Pol ϵ tightly binds the CMG and continuously extends the leading strand, while Pol δ discontinuously synthesizes short Okazaki fragments, which are later processed and ligated on the lagging strand (13–17). Despite their mechanistic differences, both DNA polymerases require the processivity factor Proliferating Cell Nuclear Antigen (PCNA) for their function. PCNA is an essential homotrimeric clamp that encircles newly synthesized double-stranded DNA, tethering the DNA polymerases to DNA. It is abundant at replication forks where, in addition to the DNA polymerases, it binds many other factors involved in genome replication, chromatin assembly and the response to stress and damage (18–20).

Chromatin replication requires proteins that function as histone chaperones, which include replisome components with histone binding properties (i.e. MCM2, Pole, Pol α and RPA) and *bona fide* histone chaperones that are recruited to the replisome (i.e. FACT, CAF-1 and ASF1) (4). These proteins coordinate the recycling of parental histones to spatially maintain the landscape of histone post-translational modifications. They also promote the incorporation of newly synthesized histones to preserve nucleosome density on the daughter DNA strands (2, 4). Replicated DNA is readily assembled into chromatin (21, 22), a process that constitutes the first critical step to the re-establishment of epigenetic modifications on histones genome-wide (2, 4, 23–27).

Chromatin Assembly Factor-1 (CAF-1) is a key regulator of chromatin assembly during DNA replication (28). CAF-1 deletion is lethal during vertebrate development (29–31), and transient CAF-1 depletion affects cell cycle progression and cell fate (26, 32–41). CAF-1 forms a heterotrimeric complex consisting of Cac1, Cac2 and Cac3 in yeast and p150, p60 and p48 in mammals. The complex chaperones newly synthesized histones H3-H4 and deposits them onto DNA at sites of DNA synthesis (42–47). CAF-1 activity at replication forks depends on its interaction with PCNA, which occurs via canonical PCNA Interacting Peptides (PIPs) present on the large CAF-1 subunit (48–52). While the function of CAF-1 has been studied in cells and in the SV40 systems, a detailed bottom-up biochemical reconstitution to address the molecular mechanism by which CAF-1 assembles chromatin during DNA replication and its interplays with the replisome is still lacking.

Here we developed biochemical systems to study the crosstalk between CAF-1 and key components of the DNA replication machinery, combining our previous CAF-1 histone chaperone assays (53, 54) with primer extension assays and the recent *in vitro* reconstitutions

of the eukaryotic replisome (8, 9). We find that CAF-1 recruitment to PCNA requires DNA and is modulated by histones. Two CAF-1 complexes bind PCNA and are necessary for PCNA-dependent nucleosome assembly. CAF-1 interaction with PCNA inhibits the activity of the leading-strand DNA polymerase Pole, but not of the lagging-strand polymerase Pol δ . Yet, in cells, we show that CAF-1 deposits histones equally on the leading and lagging strands during DNA replication. Thus, our work reveals an unexpected difference in the crosstalk between CAF-1, PCNA and the two replicative polymerases, suggesting different mechanisms for the coupling of nucleosome assembly to DNA synthesis on the two daughter strands.

Results

CAF-1 recruitment to PCNA requires DNA

We first set out to study the interaction between CAF-1 and PCNA in the context of DNA, as this is the context in which the CAF-1-PCNA interaction occurs during DNA replication. Therefore, we loaded PCNA onto nicked plasmids using the ATP-dependent clamp loader RFC1-5 (70), and separated DNA-loaded from free PCNA on a size exclusion column (SEC) (Supplementary Figure S1A) (71). When adding CAF-1, we observed that the three CAF-1 subunits co-eluted with DNA-loaded PCNA, suggesting the formation of a CAF-1-PCNA-plasmid complex (Figure 1A and Supplementary Figure S1B-C). As CAF-1 uses PIPs to bind PCNA in cells (38, 50–52), we introduced mutations in these domains to test their importance in our *in vitro* system (Supplementary Figure S1D). The mutant CAF-1_PIP** no longer bound to DNA-loaded PCNA (Figure 1B and Supplementary Figure S1C), confirming that our *in vitro* reconstitution recapitulates the physiological determinants of the CAF-1-PCNA interaction.

Next, we investigated how DNA contributes to the CAF-1-PCNA interaction. CAF-1 did not co-elute with PCNA in the absence of DNA (Supplementary Figure S1E) or when PCNA was not loaded onto DNA (i.e. by omission of ATP) (Figure 1C and Supplementary Figure S1C), suggesting that DNA is required for the CAF-1-PCNA interaction. To confirm that the interaction between CAF-1 and PCNA is DNA-dependent, we crosslinked CAF-1 to fluorescently labeled PCNA on nicked DNA plasmids using glutaraldehyde, followed by nuclease digestion and SDS-PAGE analysis to determine if more transient protein-protein complexes are formed in solution, which may be lost during the SEC purification. Again, we observed significant CAF-1-PCNA complexes only when PCNA was loaded onto DNA (Figure 1D). These results indicate that DNA is required for a stable interaction between CAF-1 and PCNA.

CAF-1 contains two DNA binding regions in its large Cac1 subunit: the Lys-Glu-Arg rich (or KER) region located at the N-terminus, which is flanked by the PIPs, and the winged-helix domain (WHD) at the C-terminus (Supplementary Figure S1D). Either domain is required for CAF-1 function in cells (46, 51, 72, 73), but their relative role in CAF-1 mechanism remains unclear, as both domains must be mutated simultaneously in order to disrupt CAF-1 activity *in vitro* in the absence of PCNA (53). We thus tested whether these domains contributed to the DNA-dependent interaction of CAF-1 to PCNA. Deletion of the KER domain or its mutation into a neutral unstructured sequence (CAF-1_ Δ KER and CAF-1_KER*, respectively) abrogated the interaction between CAF-1 and DNA-loaded PCNA, similarly to the effect of the CAF-1_PIP** mutant (Figure 1E and Supplementary Figure S1F). However, mutations in the WHD (CAF-1_WHD*) had no effect on binding to DNA-loaded PCNA (Figure 1F). These results indicate that

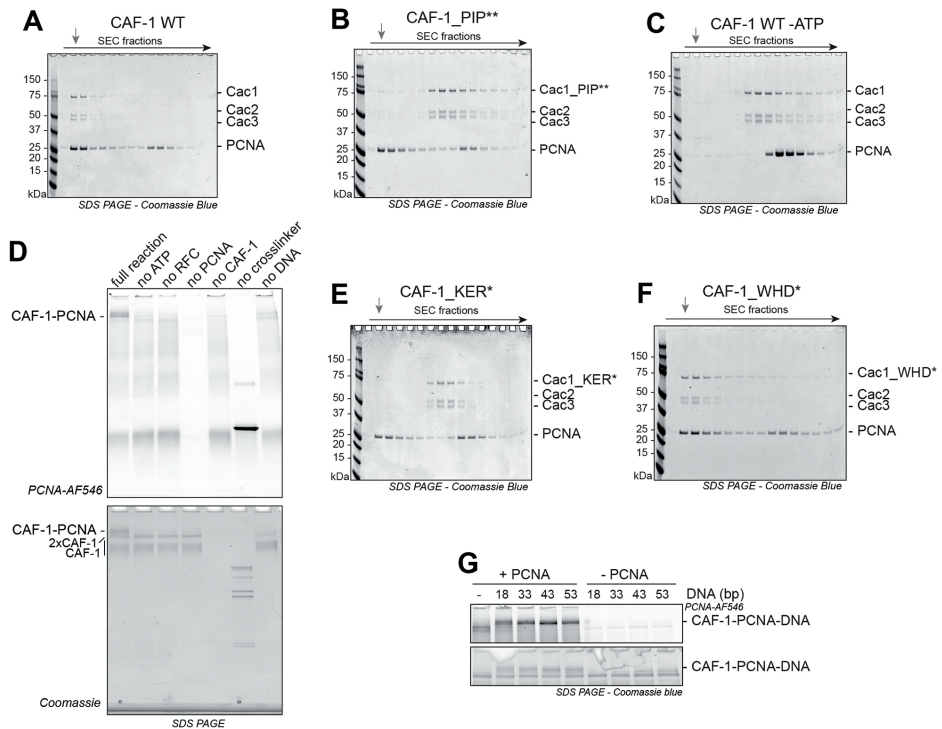


Figure 1: DNA and histones control CAF-1 recruitment to DNA-loaded PCNA.

A-C) SDS PAGE following separation on SEC of a CAF-1-PCNA binding reaction on DNA plasmids using WT CAF-1 (A), a CAF-1_PIP** mutant (B), or WT CAF-1 in absence of ATP (C). The grey arrow indicates the elution volume of the plasmid DNA. Chromatograms are shown in Supplementary Figure S1C. **D)** SDS PAGE of glutaraldehyde crosslinking reactions of fluorescent PCNA (3 μ M), CAF-1 (1.5 μ M), RFC (150 nM) and nicked pUC19 plasmid (300 nM) after nuclease digestion. Fluorescence scan for PCNA (546 nm) and Coomassie staining are shown. The CAF-1 and PCNA interaction is dependent on PCNA loading onto DNA. **E-F)** Coomassie-stained SDS PAGE following SEC of a CAF-1-PCNA binding reaction on DNA plasmids using CAF-1_KER* (E) and CAF-1_WHD* (F) mutants. **G)** Crosslinking experiment between CAF-1 (3 μ M) and labeled PCNA (4.5 μ M) on DNA fragments (1.5 μ M) of various sizes. RFC and ATP were not added to actively load PCNA and DNA was not digested in these reactions. Full gels re shown in Supplementary Figure S1I.

Having established that DNA is required for the CAF-1-PCNA interaction, we investigated whether there is a minimum DNA length required to promote this interaction. We first confirm that CAF-1 binds 10-fold more weakly to a 18 bp DNA ($K_d > 2 \mu$ M) than to a 33, 43 or 53 bp DNA ($K_d = 0,33, 0,23$ and $0,18 \mu$ M respectively) (Supplementary Figure S1G), in line with previous observations (74). Mutations in the KER domain strongly inhibit the CAF-1-DNA interaction, while WHD mutations have a minor effect (Supplementary Figure S1H). Complex formation was less efficient on the 18 bp DNA fragment, where PCNA can load in the absence of RFC, than on the longer 43 and 53 bp DNAs (Figure 1G and Supplementary Figure S1I). This suggests that a minimum of ± 30 bp need to be exposed for CAF-1 to stably bind PCNA on DNA. Notably, the AlphaFold model of the Cac1-KER domain (residues 128-226) predicts a long helical structure of $\sim 145 \text{ \AA}$, which is confirmed by a very recent crystal structure (75) and corresponds to the length of ~ 44 bp of duplex DNA (Supplementary

Figure S1J). This domain displays a positively charged surface along its helical arrangement, which may structurally explain the link we observe between DNA length and CAF-1 binding, assuming that this surface interacts with the negatively charged phosphate backbone of the DNA via electrostatic interactions. Overall, these observations suggest that the CAF-1-PCNA interaction on DNA is stabilized by DNA of at least ~30 bp via the KER domain in CAF-1.

Reconstitution of PCNA-dependent nucleosome assembly by CAF-1

In cells, PCNA directs CAF-1-mediated chromatin assembly (42, 48–50). However, we and others have recently shown that CAF-1 is able to assemble nucleosomes *in vitro* in the absence of other factors (53, 74, 76). To determine how the presence of PCNA affects the histone chaperone activity of CAF-1, we set out to develop a nucleosome assembly assay that recapitulates the PCNA dependency of CAF-1 activity observed *in vivo*. The challenge is to differentiate between PCNA-dependent and PCNA-independent (i.e. purely DNA driven (53)) activity of CAF-1. To overcome this challenge, we mixed a nicked plasmid where PCNA can be loaded, with a competitor negatively supercoiled plasmid where PCNA-independent CAF-1 activity takes place efficiently. Following a PCNA loading step, we added CAF-1-H3-H4 complexes to promote tetramer deposition followed by the addition of fluorescently labeled H2A-H2B, which associate with tetrasomes *in vitro* to form nucleosomes. To measure PCNA-dependent nucleosome assembly, we quantify the histones fluorescence signal on the nicked plasmid relative to the total histone signal on both plasmids in each lane. Micrococcal nuclease (MNase)-based analysis of nucleosome fragments (± 150 bp) are also used to assess nucleosome formation. We named this setup PCNA-NAQ assay, based on our previously established Nucleosome Assembly and Quantitation (NAQ) assay (53, 62).

We first established that the PCNA-NAQ assay measures PCNA-dependent and -independent CAF-1 activity. Efficient nucleosome assembly (monitored by an increase in H2B fluorescence) on the nicked plasmid was observed only when PCNA is loaded on DNA and CAF-1 is present (Figure 2A). When PCNA loading was blocked by the omission of ATP, PCNA or RFC (Figure 2A), the histone fluorescence signal shifted to the supercoiled plasmid, confirming that the signal on the nicked plasmid is largely dependent on PCNA. As expected, omission of CAF-1 led to a drastic reduction of histone deposition (Figure 2A and Supplementary Figure S2A), reinforcing that CAF-1 is the nucleosome assembly machinery on both plasmids in our reconstitution. No nucleosomes were formed upon omission of either histones H3-H4 or H2A-H2B (Supplementary Figure S2B). Moreover, using labeled H3-H4 instead of H2A-H2B did not affect these results (Supplementary Figure S2C), confirming that our signal is a *bona fide* measure of assembled nucleosomes. Quantification of the histone fluorescence signal on the nicked plasmid compared to total histone signal showed that roughly 50% of the nucleosomes are assembled in a PCNA-dependent manner, when PCNA is loaded (Figure 2B). This is reduced to roughly 20% when PCNA was not loaded onto DNA (Figure 2B). These observations were confirmed using next generation sequencing approaches of the MNase products, when we used plasmids with distinct DNA sequences which allowed us to map relative nucleosome assembly and positioning (Supplementary Figure S2D-G). Thus, we developed a new method to study the PCNA-dependent nucleosome assembly function of CAF-1, where we can distinguish and quantify the PCNA-dependent or PCNA-independent activities of this histone chaperone complex.

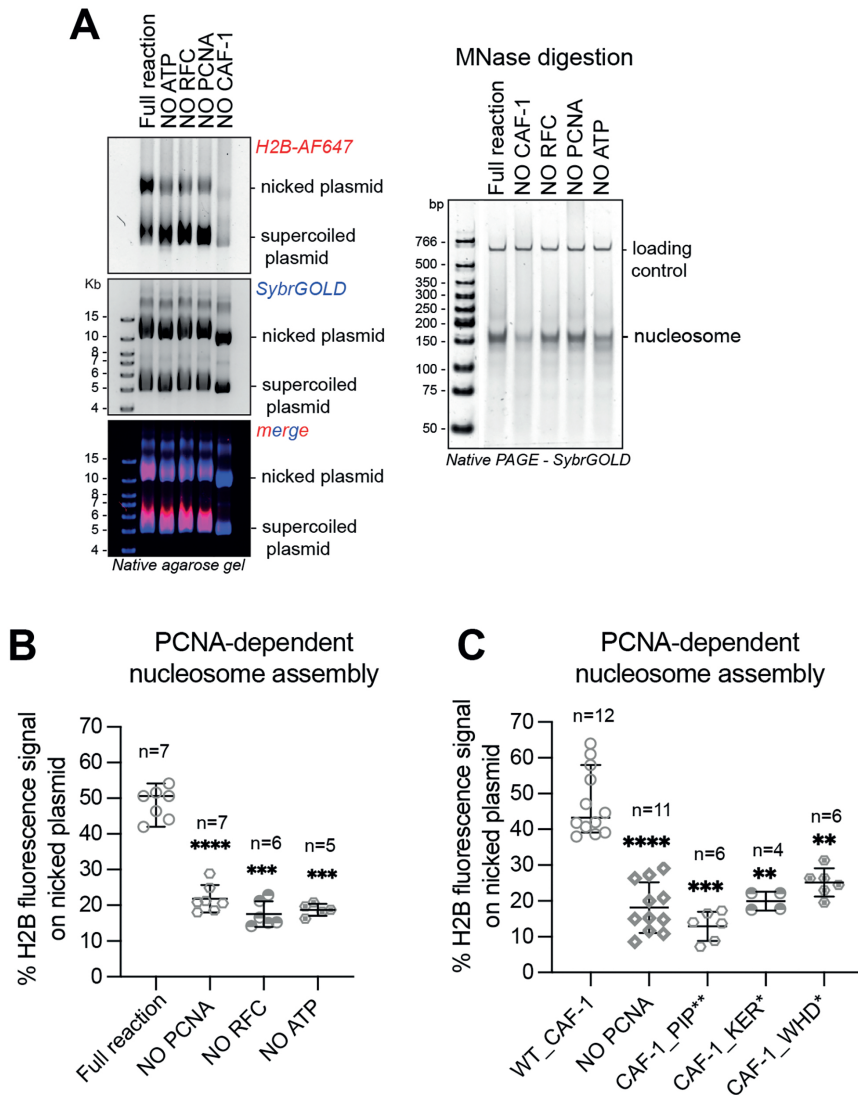


Figure 2: The WHD of CAF-1 controls PCNA-dependent nucleosome assembly.

A) (Left) Native agarose gel of PCNA-NAQ assay reactions. A reaction containing all components, and reactions where we removed either ATP, RFC, PCNA or CAF-1 are shown. Fluorescence signals for H2B-T112C labeled with AF647 (H2B-AF647) or DNA (SybrGOLD), and their overlay are shown. H2B fluorescence on the nicked plasmid (top panel) represents PCNA-dependent histone deposition. (Right) Native PAGE stained with SybrGOLD to detect protected DNA fragments following MNase digestion of samples in A. 150bp DNA fragments are characteristic of nucleosomal DNA, a 621bp loading control is used to monitor DNA retrieval during the purification procedure. Bands around 120bp represent hexasomes.

B) Quantification of the H2B fluorescence signal on the nicked plasmid relative to the total H2B signal in each lane in panel A as a measure of PCNA-dependent nucleosome assembly. **C)** Quantification of the PCNA-dependent nucleosome assembly activity for CAF-1_PIP**, CAF-1_KER* and CAF-1_WHD*. Means \pm SD is shown, * $p < 0.05$, ** $p < 0.01$, *** $p < 0.001$, **** $p < 0.0001$ (one-way ANOVA comparing WT CAF-1 to control conditions (B) or each mutant (C)). Gels are shown in Supplementary Figure S2H.

We then used this method to understand how CAF-1 assembles nucleosomes when bound to PCNA. We first tested if mutations in the KER domain or PIPs of Cac1, which are important for recruitment to DNA-loaded PCNA (Figure 1B, 1E), affected its PCNA-mediated activity. As expected, CAF-1_KER* and CAF-1_PIP** showed a reduction specifically in PCNA-dependent nucleosome assembly (Figure 2C and Supplementary Figure S2H), while the overall activity of the mutant complexes was not affected as seen by the consistent level of MNase-protected nucleosome fragments (Supplementary Figure S2H). This confirms that CAF-1 recruitment is necessary for PCNA-dependent nucleosome formation in our PCNA-NAQ assay, further validating the role of these domains in the CAF-1-PCNA interaction. Strikingly, the CAF-1_WHD* mutant also showed a decrease in PCNA-dependent nucleosome assembly activity (Figure 2C and Supplementary Figure S2H), despite being able to bind DNA-loaded PCNA (Figure 1F) and being fully active in nucleosome assembly in absence of PCNA as shown by the MNase digestion products (Supplementary Figure S2H). This demonstrates that the WHD domain is important for PCNA-dependent CAF-1 activity specifically. Our observations explain why WHD mutations affect chromatin assembly during DNA replication in yeast cells (51, 53, 73), and why previous *in vitro* reconstitutions that omitted PCNA were unable to recapitulate loss of function of this mutant (53, 74). In summary, we show that the WHD domain in CAF-1 is important for the PCNA-dependent nucleosome assembly function of the complex.

Two CAF-1 complexes bind PCNA to assemble nucleosomes

Two CAF-1 complexes are required to assemble one nucleosome in the absence of PCNA (53, 74). To understand how CAF-1 assembles nucleosomes when bound to PCNA, we therefore set out to study the stoichiometry of the CAF-1-PCNA complex on DNA. To this end, we used protein-protein crosslinking followed by nuclease digestion and SEC to analyze complexes in solution. These reaction products elute in two peaks of equal distribution (Figure 3A). We collected fractions from these peaks and analyzed them by mass photometry to determine their composition (77). We found that Peak1 (Figure 3A) contained CAF-1-PCNA complexes corresponding to predominantly two CAF-1 per PCNA trimer (~430 kDa), and a lower amount of three CAF-1 per PCNA trimer (~590 kDa) (Figure 3B), while Peak2 contained mostly free unbound CAF-1 (~190 kDa) and a small fraction of complexes containing one CAF-1 per PCNA trimer (~285 kDa) (Figure 3B). In line with RFC being present at substoichiometric concentrations in these samples, no RFC-containing complexes are detected in these experiments (RFC Δ N weights 220 kDa). These data indicate that the CAF-1-PCNA complex mainly assembles in a 2:1 (CAF-1 to PCNA trimer) stoichiometry on DNA, and to a lesser extent can form 3:1 or 1:1 assemblies.

To further evaluate the stoichiometry of CAF-1-PCNA-DNA complexes, we monitored complex formation using crosslinking at limiting concentrations of fluorescently labeled PCNA loaded onto DNA, which also allows us to estimate binding affinities. Without CAF-1, PCNA crosslinks with the clamp loader RFC. On gel, this complex runs at the same height as the 2xCAF-1-PCNA complex (Figure 3C and Supplementary Figure S3A). As we titrate CAF-1 above 100 nM, while maintaining RFC constant at 15 nM, this band increases in intensity (Figure 3C-D and Supplementary Figure S3A), indicating the formation of the CAF-1-PCNA complex. Interestingly, above 350 nM, we observed that 3xCAF-1-PCNA complexes formed while the 2xCAF-1-PCNA band became less pronounced (Figure 3C-D and Supplementary Figure S3A). We observed only a small fraction of 1xCAF-1-PCNA complexes (Figure 3C-D and Supplementary Figure S3A) in line with the mass

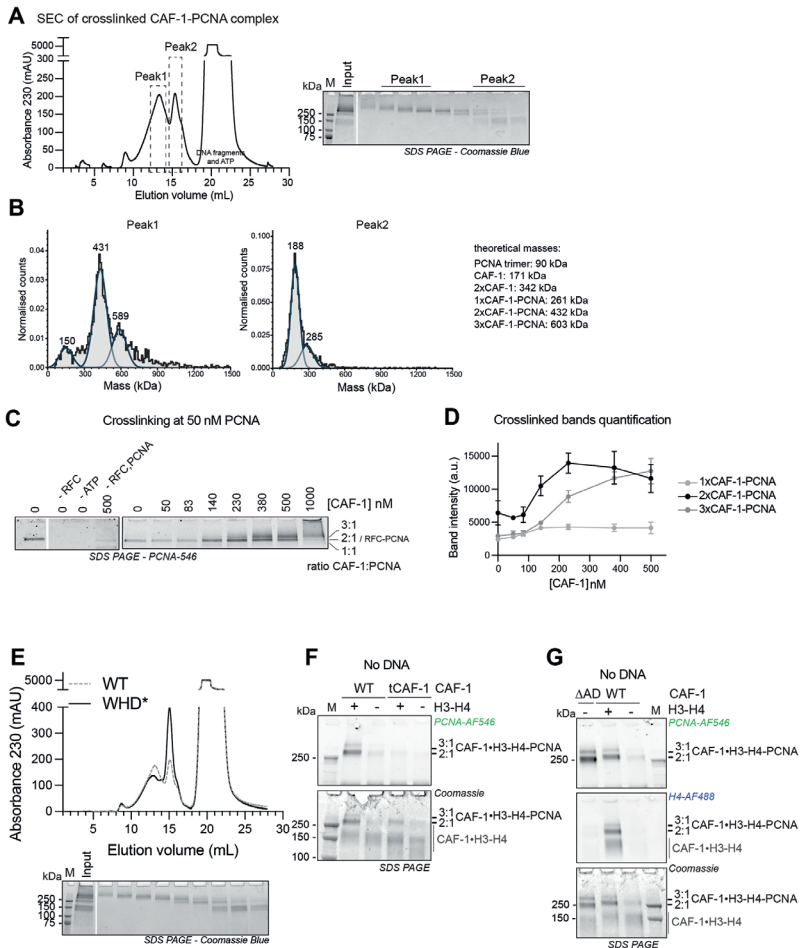


Figure 3: Two CAF-1 complexes bind to DNA-loaded PCNA and histones regulate this interaction.

A) (Left) SEC of crosslinked CAF-1-PCNA complexes after DNA digestion using 1 μM PCNA, 0.15 μM RFC, 1.5 μM WT CAF-1 and 0.3 μM nicked pUC19. After crosslinking with 0.2% glutaraldehyde and quenching, the samples were treated with nuclease to digest the DNA plasmid. (Right) Coomassie SDS-PAGE of the collected fraction. The fractions that were used to prepare mass photometry samples are shown as Peak1 and Peak2. **B)** Mass photometry data of pooled fractions of Peak1 (left) and Peak2 (right) from experiment in panel A. Theoretical masses are listed and calculated masses from the fitted data are shown in each graph. Normalized counts are shown. **C)** SDS PAGE of protein-protein crosslinking reactions after DNA digestion. These reactions contain 50 nM fluorescently labeled PCNA, 15 nM full-length RFC, 15 nM pUC19 and increasing CAF-1 concentrations. PCNA fluorescence signal is shown. Full gels are shown in Supplementary Figure S3A. **D)** Quantification of the fluorescence intensity of bands in C. Data are shown as mean \pm SD of three independent experiments. **E)** SEC and SDS-PAGE of crosslinked CAF-1-PCNA complexes after DNA digestion with CAF-1_WHD*, as in panel A. WT curve is shown in dashed gray line for comparison. **F)** SDS PAGE of crosslinking reactions containing fluorescent PCNA (5.5 μM) and H3-H4 (H4-E63C, 1.5 μM dimer concentration), CAF-1 or tCAF-1 (1.5 μM). DNA or RFC are not present in these reactions. **G)** SDS PAGE of crosslinking reactions containing fluorescent PCNA (5.5 μM) and H3-H4 (H4-E63C, 1.5 μM dimer concentration), CAF-1 or CAF-1_ΔΔAD (1.5 μM). DNA or RFC are not present in these reactions.

photometry results (Figure 3B). Together, these experiments demonstrate that CAF-1 prefers to bind PCNA on DNA with a 2:1 stoichiometry at concentrations around 100 nM. Above 350 nM, additional CAF-1 complexes can associate with DNA-loaded PCNA. Interestingly, only a very small fraction of CAF-1-PCNA complexes at a 1:1 stoichiometry is observed. This is in line with our previous observation that two CAF-1 complexes cooperatively associate on DNA (53, 74), and it shows that it also applies to PCNA-dependent CAF-1 chromatin assembly.

To ask if this assembly is important for CAF-1 histone chaperone function, we tested if mutations in the WHD domain affected the stoichiometry of CAF-1-PCNA complexes. Indeed, the WHD is important for the cooperative DNA binding of CAF-1 and for its function in cells (53), and mutations in the WHD affect the PCNA-dependent nucleosome assembly activity of CAF-1 in the PCNA-NAQ assay (Figure 2C). CAF-1_WHD* affected the composition of CAF-1-PCNA complexes, with a reduction in the formation of 2:1 or 3:1 CAF-1-PCNA complexes in solution (Figure 3E). This explains why this complex is inactive in PCNA-dependent nucleosome assembly (Figure 2C) and argues that two CAF-1 complexes are required for histone deposition also in the context of PCNA.

Histones further promote the CAF-1-PCNA interaction

Although histones are not strictly required for the formation of a CAF-1-PCNA complex on DNA (Figure 1), CAF-1 tightly binds H3-H4 during DNA replication. Thus, we set out to investigate if histones affect CAF-1 binding to PCNA. To this end, we investigated the role of histones on the CAF-1-PCNA interaction in the absence of DNA, because in DNA-containing reactions histones would be immediately deposited onto DNA, making it impossible to assess their effect on the CAF-1-PCNA interaction. As shown above, CAF-1 does not bind to PCNA when DNA is missing from the reaction (Supplementary Figure S1E). However, pre-incubation of CAF-1 with H3-H4 promotes the interaction between CAF-1 and PCNA in the absence of DNA in crosslinking experiments (Figure 3F). Deletion of the N-terminal region in Cac1, which contains the PIPs and KER domain (as in the truncated tCAF-1 construct, Supplementary Figure S1D), prevents the CAF-1-PCNA interaction (Figure 3F), confirming that this region is responsible for binding to PCNA within the complex. Interestingly, the interactions between CAF-1-H3-H4 and PCNA in the absence of DNA could not be observed from a SEC purification (Supplementary Figure S3B), suggesting that it is more dynamic than the interaction that is mediated by DNA.

Previous work has shown that H3-H4 binding to the CAF-1 acidic domain induces conformational changes at the PIPs, KER and WHD regions, that are important for CAF-1 histone chaperone function (53, 76). These conformational changes could be mimicked by deleting the acidic domain in CAF-1 (53), we thus generated a mutant carrying such deletion (CAF-1_ΔAD) to test if these conformational changes control the CAF-1-PCNA interaction. Strikingly, crosslinking between full-length CAF-1_ΔAD and PCNA shows efficient complex formation in absence of DNA and histones in crosslinking experiments (Figure 3G). Moreover, CAF-1_ΔAD efficiently forms complexes with PCNA on DNA at lower concentrations than WT CAF-1 (below 100 nM, Supplementary Figure S3C), suggesting an increase in binding affinity for this mutant to DNA-loaded PCNA. These data argue that changes that occur upon neutralization of the acidic domain (i.e. mimicking histone binding) in CAF-1 promote interactions with PCNA. Together these data suggest that histones are not required *per se* for PCNA binding on DNA, however they may

promote the CAF-1-PCNA interaction via conformational changes that involve the N-terminal region in Cac1.

CAF-1 inhibits DNA synthesis by Pol ϵ , but not Pol δ , via PCNA

At replication forks PCNA binds several proteins, most prominently the replicative DNA polymerases on both daughter strands. As replicated DNA is readily assembled into chromatin at replication forks (21, 22), we next asked how DNA polymerases and CAF-1 may share or compete for binding to PCNA.

To this end, we first investigated the effects of CAF-1 on PCNA-mediated DNA synthesis by the leading- and lagging-strand DNA polymerases Pol ϵ and Pol δ , in a primer extension assay. In this assay, the extension of a fluorescent DNA primer that is annealed to an RPA-coated single stranded plasmid is monitored over time. As previously shown, yeast Pol δ and Pol ϵ efficiently synthesized DNA in a PCNA-dependent fashion with distinct kinetics (Supplementary Figure S4A) (15–17, 78). We found that adding CAF-1 had minimal effects on DNA synthesis by Pol δ in this primer extension assay (Figure 4A). However, CAF-1 had a strong inhibitory effect on DNA synthesis by Pol ϵ , at concentrations of 150 nM where CAF-1 may bind PCNA with a 2:1 stoichiometry (Figure 4B, 3D). This effect was dose-dependent and indicative of competitive inhibition (Figure 4B and Supplementary Figure S4B). This suggests a dynamic and steric effect of CAF-1 on Pol ϵ -mediated DNA synthesis, and not on Pol δ . To test if the inhibition of Pol ϵ involved a crosstalk on PCNA, we used CAF-1 mutants that do not bind to DNA-loaded PCNA (i.e. CAF-1_PIP** and CAF-1_KER*). These mutants did not inhibit Pol ϵ activity (Figure 4C-D), demonstrating that the inhibitory effect of CAF-1 on Pol ϵ is exerted via PCNA. These data are consistent with CAF-1 and Pol ϵ competing for binding on PCNA.

Previous studies have shown that Pol δ has a higher binding affinity for PCNA ($K_{d_{app}}=13,7$ nM) than Pol ϵ ($K_{d_{app}}=326$ nM) (17). We found that CAF-1 binds PCNA on DNA with intermediate binding affinity (~100 nM) (Figure 3C-D). Therefore, we tested whether Pol δ might simply outcompete CAF-1 on PCNA, unlike Pol ϵ . To this end, we first used the CAF-1_ Δ AD mutant which shows tighter binding to DNA-loaded PCNA (estimated $K_d < 50$ nM, in the same range as Pol δ) (Supplementary Figure S3C). While inhibiting Pol ϵ even more strongly than WT CAF-1, this mutant had a minor effect on Pol δ activity when added at 300 nM (Supplementary Figure S4C). This suggests that interactions of CAF-1 with PCNA are possible during Pol δ -dependent synthesis, and Pol δ is largely unaffected by these CAF-1 interactions. In addition, we wanted to test if other PIP-containing proteins that bind PCNA with similar affinities could phenocopy the CAF-1 effects on the two polymerases. To this end, we used a catalytic-dead version of *Xenopus laevis* FEN1 D181A (FEN1_DA), which binds yeast PCNA as a monomer in a PIP-dependent manner and with affinities that are comparable to CAF-1 (Supplementary Figure S4D) (79). FEN1 did not inhibit Pol δ (80) or Pol ϵ in primer extension experiments (Figure 4E-F and Supplementary Figure S4E). This indicates that the observed CAF-1 effect cannot be generalized to other PIP-containing proteins and that simple PIP-binding competition does not explain the differential CAF-1 effect on the DNA polymerases. Therefore, we concluded that differences in PCNA binding affinities between the two polymerases do not solely explain the differences in their crosstalk to CAF-1, and we propose that additional (e.g. steric) effects by CAF-1 may play a role in the specific Pol ϵ inhibition. Together, these results support a model in which CAF-1 differentially affects DNA synthesis by the replicative polymerases on the two daughter strands.

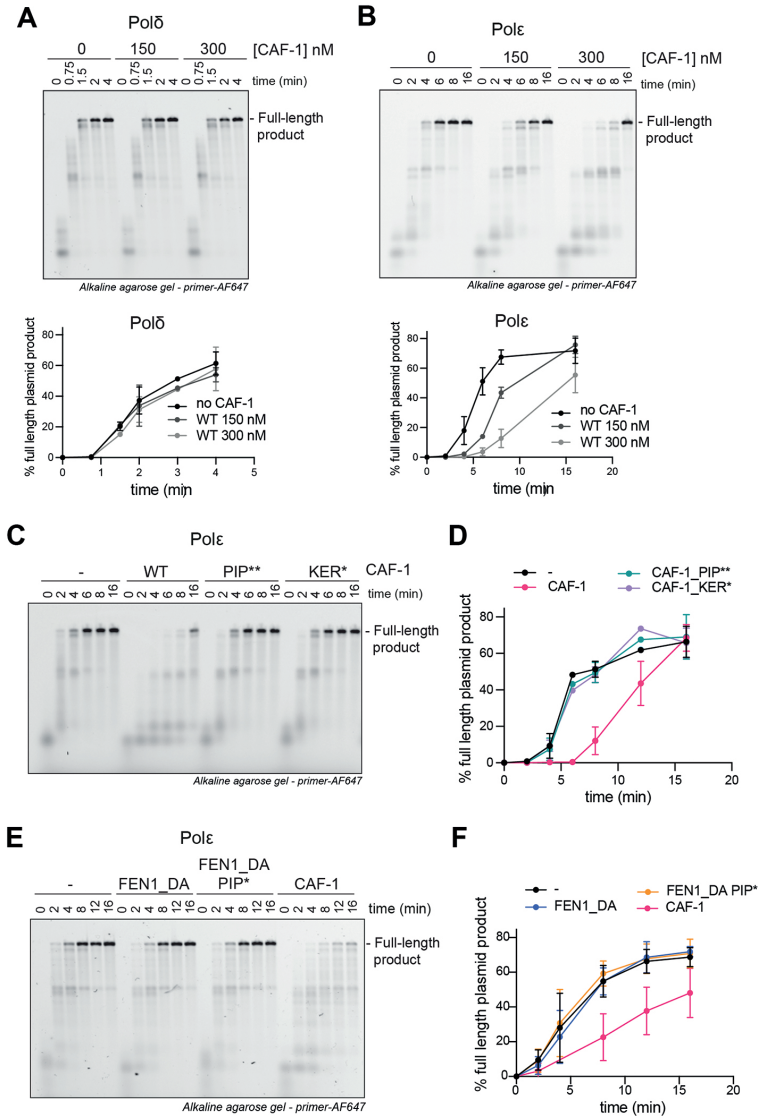


Figure 4: CAF-1 competes with Polε, not with Polδ, for PCNA binding.

A-B) (Top) Fluorescence scan of a denaturing alkaline agarose gel of primer extension reactions with Polδ (A) or Polε (B). The fluorescently labeled primer signal is shown. The polymerases were at 120 nM, PCNA 480 nM and CAF-1 concentrations as shown. (Bottom) Quantification of the full-length product band relative to the total fluorescence in each lane (expressed as percentages) from the top panels. Mean ±SD are shown for independent experiments (Polδ n=2 - Polε n=4). **C)** Fluorescence scan of denaturing alkaline agarose gel of primer extension reactions with Polε with CAF-1_PIP** and CAF-1_KER* mutants (300 nM). **D)** Quantification of primer extension by Polε in the presence of CAF-1 mutants. Mean ±SD are shown for three independent experiments. **E)** Fluorescence scan of denaturing alkaline agarose gel of primer extension reactions with Polε with FEN1_DA, FEN1_DA PIP* and CAF-1 (300 nM). **F)** Quantification of primer extension by Polε in the presence of FEN1_DA and its PIP* mutant version. Mean ±SD are shown for three independent experiments.

Pole function and interplay with CAF-1 are independent of histone binding

During DNA replication in cells, Pole and CAF-1 both bind H3-H4 (72, 81, 82). Thus, we set out to test whether histones regulate the crosstalk between CAF-1 and the DNA polymerases on PCNA.

First, we used fluorescence polarization assays to determine the binding affinity of Pole for H3-H4 and find that Pole binds H3-H4 with a K_d of 28 nM. This is a 25 times lower affinity than that of CAF-1 ($K_d=1,1$ nM) (Supplementary Figure S5A). Nevertheless, this would be sufficient to efficiently bind histones in our assay, where Pole is present at 120 nM. Pol δ has background binding to H3-H4 ($K_d\geq 300$ nM), similarly to RPA which is also present in the reactions ($K_d\geq 300$ nM) (Supplementary Figure S5A). These data show that Pole and CAF-1 efficiently bind H3-H4, while Pol δ and RPA do not bind histones in our assays.

To test the effect of histone binding in the crosstalk between CAF-1 and the DNA polymerases, we pre-incubated either the DNA polymerase or CAF-1 with H3-H4 and monitored how this affected DNA synthesis in primer extension assays. Pole activity was not affected by the addition of H3-H4 (Figure 5A) and the CAF-1-dependent inhibition of Pole was also largely unaffected by the presence of H3-H4 (Figure 5A). As expected, the addition of histones to reactions containing Pol δ had no effect on DNA synthesis or on its crosstalk with CAF-1 (Figure 5B). These data demonstrate that histones do not alter the differential effects that CAF-1 has on Pol δ and Pole via PCNA. This is in line with the limited role of histones in regulating the CAF-1-PCNA interaction on DNA (Figure 1, 3F and Supplementary Figure S3B), confirming that DNA is a dominant effector of the CAF-1-PCNA interaction and thus of the CAF-1 interplay with DNA synthesis. Together, this argues that the effects of CAF-1 on the DNA polymerases is relevant during chromatin assembly at replication forks when histones are bound to the histone chaperones.

Previous studies have shown that CAF-1, Pole and RPA can assemble chromatin during DNA replication (53, 81–83). As these proteins are all present in our assays, we set out to directly test which of these histone chaperones can assemble nucleosomes in these reconstitutions. To this end, we combined primer extension reactions with NAQ-based readouts to measure histone deposition (i.e. nucleosome assembly). Because in this assay the substrate is RPA-coated single-stranded DNA, nucleosome formation occurs only after DNA synthesis. In the absence of CAF-1, Pole containing reactions show background levels of nucleosome assembly (Figure 5C). These levels are even lower than the histone deposition that we observe with Pol δ , which we used as a negative control because it can synthesize DNA but does not bind histones (Figure 5C). Both reactions contain RPA, indicating that this complex also does not stimulate nucleosome assembly in these primer extension conditions. However, the addition of CAF-1 strongly increases nucleosome assembly in both conditions (Figure 5C). Similar results were observed when we measure nucleosome assembly on double-stranded DNA fragments using each histone chaperone complex in isolation (Supplementary Figure S5B), which shows that only CAF-1 can stimulate nucleosome assembly. Together, our data demonstrates that Pole and RPA are not intrinsically capable of nucleosome assembly in a replication-coupled manner, suggesting the main histone assembly factor in these reconstitutions is CAF-1.

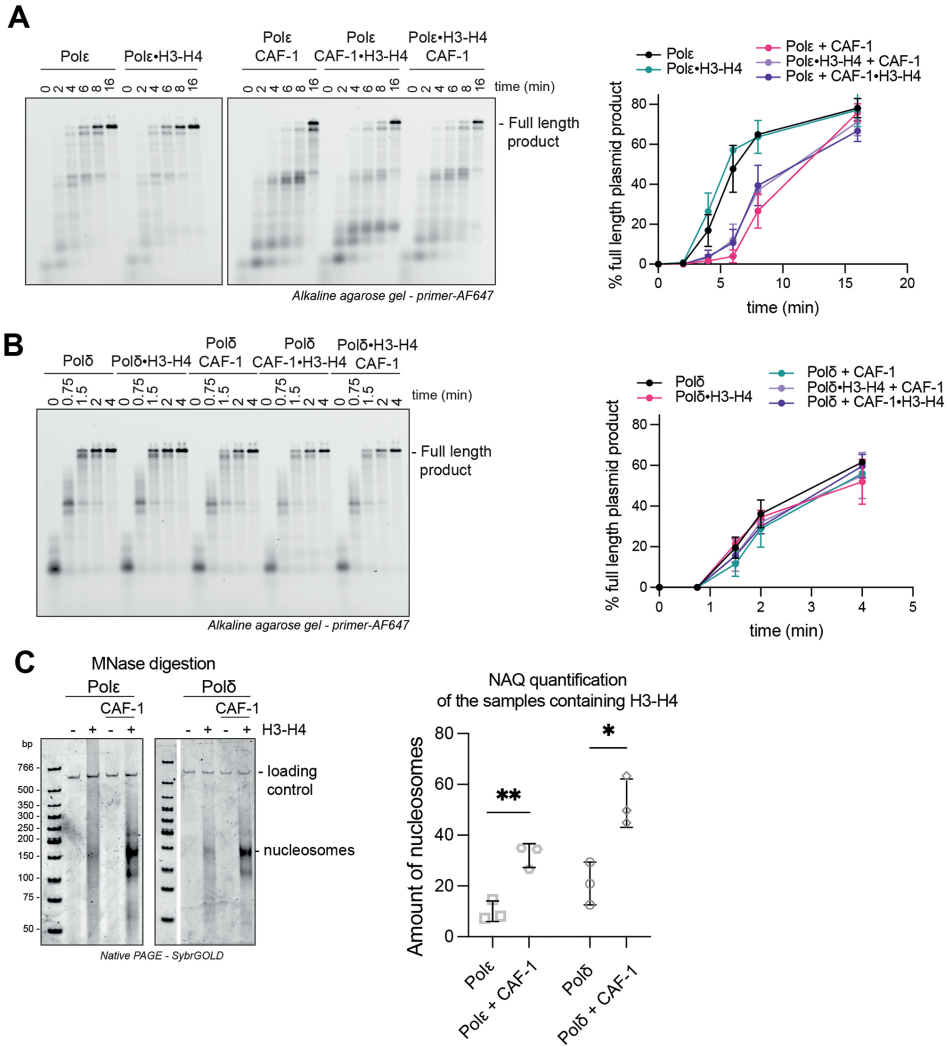


Figure 5: Polε function and interplay with CAF-1 are independent of histone binding

A-B) (Left) Fluorescence scan of denaturing alkaline agarose gel of primer extension reactions with Polε (A) or Polδ (B) in the presence of H3-H4. H3-H4 were either preincubated with the DNA polymerase or with CAF-1, as indicated by the •. The fluorescently labeled primer signal is shown. **(Right)** **(C)** (Left) Native PAGE stained with SybrGOLD to detect protected DNA fragments following MNase digestion during primer extension reactions with Polε or Polδ in presence of CAF-1. H3-H4 were co-incubated with the polymerase or with CAF-1 throughout the reaction, H2A-H2B were added at 16min and samples were immediately treated with 80 units MNase. (Right) Bioanalyzer-based quantification of protected nucleosomal fragments from samples on the left, relative to the loading control band in each lane. Mean ± SD is shown for three independent experiments. * p<0.05, ** p>0.01 (unpaired t-test comparing Polε or Polδ to the condition containing CAF-1).

CAF-1 deposits newly synthesized H3-H4 on both daughter strands in cells

We identified a differential crosstalk of CAF-1 with Pol ϵ and Pol δ , likely through their differential interaction with PCNA. As CAF-1 and Pol ϵ compete for binding on PCNA, we wondered whether CAF-1 is able to assemble nucleosomes on the leading strand. To address this question directly in cells, we used mouse embryonic stem cells (mESCs) and employed Sister Chromatid after Replication Sequencing (SCAR-seq) (67, 68). This is a genomic method that measures relative protein abundance on the two newly replicated daughter DNA strands, which allowed us to investigate whether depletion of CAF-1 results in a bias in deposition of new histones towards the leading strand.

We first generated a mESC line expressing a CAF-1 p150 subunit that is N-terminally tagged with FKBP12 (named dTAG-*Chaf1a*). dTAG-*Chaf1a* is targeted for proteasomal degradation in the presence of the degrader compound dTAG (84). In these cells, CAF-1 p150 is degraded within 1-2 hour of dTAG treatment (Supplementary Figure S6A), allowing acute depletion of CAF-1 during DNA replication to study its function with minimal pleiotropic effects. We observed that CAF-1 degradation led to a marked reduction of new histones, identified by H4 unmethylated at lysine 20 (H4K20me0), and DNA synthesis, recapitulating known effects of CAF-1 insufficiency (Supplementary Figure S6B-E) (35, 36, 85, 86).

Parental H3-H4 are recycled in a quasi-symmetrical fashion at replication forks, where each newly replicated DNA strand receives about 50% of these histones (67, 82). Simultaneously, newly synthesized histones are also symmetrically assembled on the two daughter strands to maintain nucleosome density on replicated DNA (67, 82). Control SCAR-seq experiments in untreated dTAG-*Chaf1a* mESCs confirmed these observations, using H3K27me3 as a marker of parental histones (23) and H4K20me0 to mark new histones (87, 88) (Figure 6A). Upon dTAG treatment, the total reads in the EdU inputs decreased, consistent with reduced DNA synthesis (Supplementary Figure S6F). Moreover, we observed a 2-fold reduction in reads for the H4K20me0 pulldown upon CAF-1 depletion (Figure 6B), with the H3K27me3-marked parental histones showing a comparable increase (Figure 6B). This could be due to increased MNase accessibility or to effects on parental histones dynamics. This demonstrates that CAF-1 is required for deposition of newly synthesized histones, while parental histone recycling occurs independently of CAF-1. Consistently, parental histones were distributed nearly symmetrically to both daughter strands in the absence of CAF-1 (Figure 6A). Moreover, depletion of CAF-1 did not result in an asymmetric distribution of the new histones that were deposited in this context. This argues that CAF-1 is active on both the leading and lagging strands of active replication forks in mESCs, as are backup systems such as HIRA-dependent gap filling (89).

Together, these data show that CAF-1 functions on both the leading and lagging strand of replication forks in mESCs, where it primarily deposits newly synthesized histones. CAF-1 removal affects the incorporation of these histones on both daughter strands equally without challenging parental histone recycling. This indicates that although CAF-1 and Pol ϵ compete for PCNA, both machineries efficiently function on the leading strand.

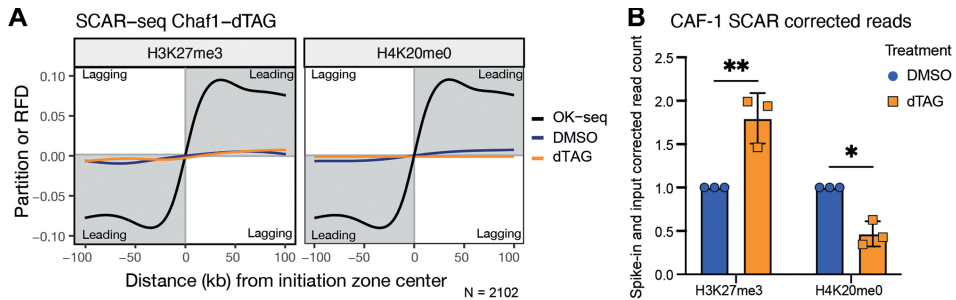


Figure 6: CAF-1 deposits newly synthesized H3-H4 on both leading and lagging strands.

A) Average SCAR-Seq profile of parental (H3K27me3) (left) or newly synthesized (H4K20me0) (right) histones across all replication initiation zones (N(IZ) = 2102) in control (DMSO) or dTAG treated samples. Partition is calculated as the proportion of forward (F) and reverse (R) read counts. Replication fork directionality (RFD) in WT cells measured by Okazaki fragment sequencing (OK-Seq) is shown for comparison. **B**) Spike-in normalized values for parental (H3K27me3) and new (H4K20me0) histone modification shows a significant reduction in H4K20me0 samples when CAF-1 is depleted. n=3 independent experiments. * p<0.05, ** p<0.01 (two-way ANOVA).

CAF-1 and Pol ϵ compete for PCNA within the replisome

As both CAF-1 and Pol ϵ function on the leading strand, we used biochemical reconstitutions to investigate the role of replisome proteins in the interplay between CAF-1 and Pol ϵ . Pol ϵ is an integral and essential component of the CMG complex at replication forks (10, 16, 17, 90, 91). We purified the yeast replisome components that were previously shown to recapitulate physiological DNA replication *in vitro* (8, 9) (Supplementary Figure S7A). Our preparations are active as they promote replication of ARS1-containing DNA plasmids in a manner that depends on the presence of the Dbf4-dependent kinase (DDK) (Supplementary Figure S7B) (9).

To focus on Pol ϵ activity, we used a pulse-chase setup in which we omitted Pol δ . This allowed us to quantify replication rates of the leading strand only (9), by monitoring replication rates (methods and Supplementary Figure S7B-C). In this assay, Pol ϵ is capable of DNA synthesis in the absence of PCNA with a rate of ~0.47 kb/min (Figure 7A-C) (9). The addition of PCNA and its loader RFC increases the rate to ~1.09 kb/min, recapitulating physiological speeds (Figure 7A-C) (9). Strikingly, the addition of CAF-1 led to a reduction in the rate to ~0.85 kb/min (Figure 7A-C), suggesting an inhibitory effect of CAF-1 towards Pol ϵ in the context of an active replisome. Consistently, the CAF-1_PIP** mutant did not reduce the speed of DNA replication (Figure 7A-C), confirming that this effect is PCNA-dependent. Moreover, a different PIP-containing protein (i.e. FEN1_DA) displayed no effect on Pol ϵ replication speed within the replisome (Figure 7D-F), suggesting that the observed PCNA-dependent effect of CAF-1 is not due to an unspecific effect on the availability of binding sites on PCNA.

Together, these data, combined with the observation that CAF-1 acts on both daughter strands (Figure 6A), support a competition between CAF-1 and Pol ϵ on PCNA may occur at physiological replication forks, with potential consequences for the control of replication speed of active CMG-Pol ϵ complexes.

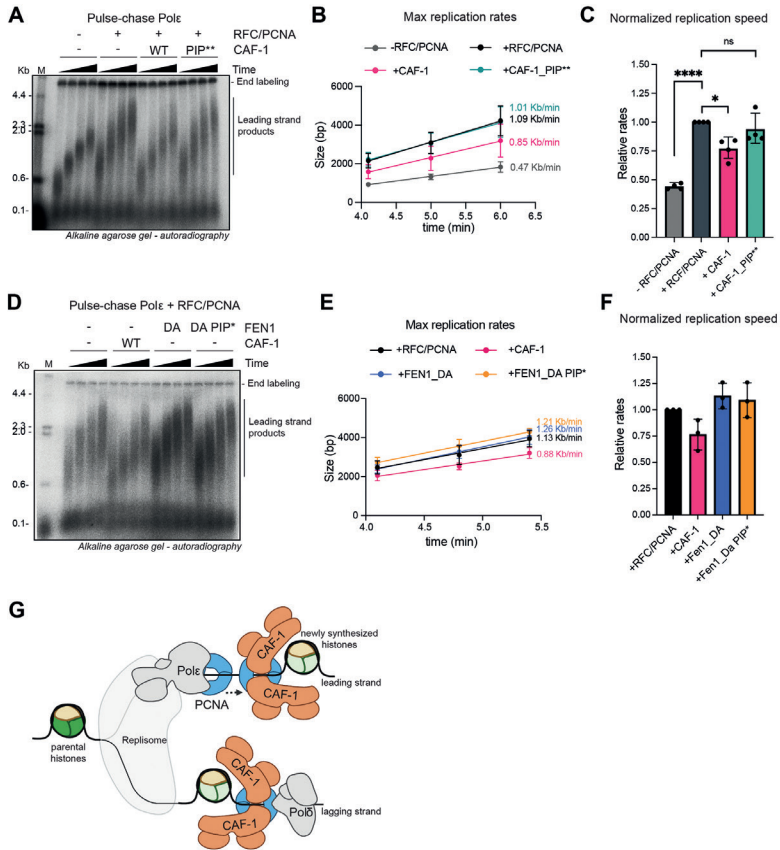


Figure 7: CAF-1 and Polε compete for PCNA binding within the replisome

A) Autoradiography scan of a denaturing agarose gel of DNA replication products from a pulse-chase experiment in presence of the yeast replisome (Pol δ and TopoII are omitted), to test the PCNA-dependent effect of CAF-1 on Pole. All proteins were present during the pulse step (3 minutes 20 seconds). After addition to the chase solution, reactions were stopped at the indicated time points (4, 5, 6 and 7 minutes). **B)** Quantification of the maximum replication fork rate for pulse-chase experiments in A. Data are shown as mean +/- SD of four independent experiments. **C)** Graph of normalized replication rates in relation to the +RFC/PCNA sample for each repeat. n=4 independent experiments. * p<0.05, **** p<0.0001, ns=not significant (one-way ANOVA). **D)** Autoradiography scan of a denaturing agarose gel of DNA replication products from a pulse-chase experiment in presence of the yeast replisome (Pol δ and TopoII are omitted), to test the PCNA-dependent effect of CAF-1 and FEN1_DA on Pole. All proteins were present during the pulse step (3 minutes 20 seconds). After addition to the chase solution, reactions were stopped at the indicated time points (4, 4.8 and 5.4 minutes). **E)** Quantification of the maximum replication fork rate for pulse-chase experiments in D. Data are shown as mean +/- SD of three independent experiments. **F)** Graph of normalized replication rates in relation to the +RFC/PCNA sample for each repeat. n=3 independent experiments. * p<0.05, ns=not significant (unpaired t-test). **G)** The crosstalk of CAF-1 mediated nucleosome assembly with the DNA replication machinery differs between the leading and lagging strand of replication forks. Two CAF-1 complexes associate with PCNA on DNA to assemble a nucleosome. CAF-1 competes with the leading strand DNA polymerase Pole for PCNA binding, but not with the lagging strand polymerase Pol δ . Nevertheless, CAF-1 deposits newly synthesized histones on both daughter strands. This means that on the leading strand, chromatin assembly by CAF-1 cannot occur on the same PCNA that is occupied by Pole. On the lagging strand, CAF-1 may share PCNA with Pol δ , but other scenarios could also be envisioned. A direct isolation of the CAF-1-PCNA-Pol δ complex is required to prove this hypothesis. The model was created with BioRender.com.

Discussion

Our work provides insights into how the essential histone chaperone CAF-1 functions during genome replication. We show that CAF-1 recruitment and its PCNA-dependent nucleosome assembly activity are regulated by a complex set of interactions between CAF-1 and PCNA, DNA and histones. Our results argue that several structural transitions regulate CAF-1, and we anticipate that these control the timing of CAF-1 arrival to, action on and departure from replication forks. This is linked with the interplay between CAF-1, PCNA and the DNA polymerases. CAF-1 competes with Pol ϵ for PCNA binding, while it has no effect on Pol δ . Yet, CAF-1 deposits newly synthesized histones equally on both strands in mESCs. Therefore, the competition between CAF-1 and Pol ϵ appears to be an integrated part of coordinating replication and nucleosome assembly and does not limit CAF-1 function. Our work suggest that different mechanisms are in place on the leading and lagging strand to couple DNA synthesis with CAF-1 mediated nucleosome assembly, in line with the inherent asymmetry of DNA replication and its chromatin assembly mechanisms.

CAF-1 effects on DNA synthesis on the two daughter strands

On the leading strand, we propose that CAF-1 and Pol ϵ either interact with distinct PCNA clamps or that they dynamically alternate in binding to PCNA, due to their competition (Figure 7G). The first model argues for a controlled spatial separation between DNA synthesis and chromatin assembly, raising questions on how this is enforced at replication forks where all these factors are enriched at the same site and nucleosomes are assembled almost immediately after DNA synthesis (92, 93). The second model instead evokes an attractive PCNA hand-off mechanism between Pol ϵ and CAF-1. In this mechanism, only when enough DNA has been synthesized by Pol ϵ (± 30 bp, Figure 1G), CAF-1 is recruited and its arrival destabilizes Pol ϵ from PCNA (Figure 4B) (15, 94). This allows CAF-1 to use PCNA for nucleosome assembly, and a new PCNA must be loaded for Pol ϵ to proceed with leading strand synthesis (19). This mechanism may enable continued PCNA loading on the leading strand during elongation (19), and the immediate coupling of chromatin assembly on newly replicated DNA (21, 22, 92, 93). It is also interesting to note that this molecular interplay could have direct effects on the speed of leading-strand DNA synthesis *in vivo*. Both models imply the need for regulatory steps in PCNA accessibility and loading on the leading strand, where the CTF18 clamp loader that binds Pol ϵ may well play a role (19, 95).

On the lagging strand, CAF-1 does not affect Pol δ activity (Figure 4A). Since Pol δ occupies only one of the PCNA monomers on the DNA-loaded clamp (96, 97) (Supplementary Figure S7D), and it allows binding of other PIP containing proteins (i.e. FEN1) (96), we speculate that CAF-1 and Pol δ may share the same PCNA clamp (Figure 7G). This is also consistent with cellular evidence that closely links Okazaki fragment size with nucleosome assembly by CAF-1 (53, 98). However, a direct isolation of the CAF-1-PCNA-Pol δ complex is required to conclusively prove this hypothesis. It will also be interesting to see if CAF-1 affects the Pol δ -dependent activities on the leading strand (9, 99).

De novo chromatin assembly during DNA replication

We show that CAF-1 primarily deposits newly synthesized histones H3-H4 equally on both daughter strands in cells (Figure 6). As Pol ϵ is a histone chaperone for parental H3-H4 (81, 82), the competition between CAF-1 and Pol ϵ on PCNA may further control the alternation of parental

and new histones incorporation on newly replicated leading strand DNA. Interestingly, we did not detect histone deposition activity by Pole in our assays, indicating that additional factors may be functioning on the leading strand to promote parental nucleosome assembly. On the lagging strand instead, as Pol δ does not have histone chaperone activity (Supplementary Figure S5A), CAF-1 may be required to be in close proximity to assemble chromatin. However, this activity needs to intercalate with parental histone deposition, for which the responsible histone chaperone still needs to be clearly defined. RPA is a good candidate (83) but we observe no activity for this complex in our primer extension assays. DNA polymerase alpha (Pol α) histone-binding is required for parental histone recycling to lagging strand (100–102), but it remains unclear how it could deposit histones in relation to PCNA loading and Pol δ function.

Interestingly, this and previous work highlight that CAF-1 does not strictly require PCNA for nucleosome assembly (Figure 2) (53, 74). This suggests that CAF-1 may use PIP-independent activities at replication forks after the initial PCNA-dependent recruitment, which should be considered when building models of chromatin assembly during DNA replication. To unravel these mechanisms, biochemical reconstitutions with integrated readouts for DNA synthesis and chromatin assembly at high spatial and time resolution, together with the use of CAF-1 separation-of-function mutants are required. Our work provides tools to build such complex reconstitutions, which will enable a complete understanding of how parental and new histone deposition pathways are integrated during ongoing DNA replication.

Material And Methods

Protein expression and purification

CAF-1 and PCNA mutants were made using standard mutagenesis procedures and purified following the wild-type purification protocols. We used yeast proteins, with the exception of *X.laevis* histones and FEN1. Several proteins used in our study were expressed and purified as previously described. This includes PCNA (55), Pol δ and Pol ϵ (8, 9), CAF-1 and its mutants (53). Lyophilized *Xenopus laevis* histones were purchased from the Histone Source at CSU, Fort Collins, CO, USA. These were labeled with maleimide dyes (when required) and refolded as in (56, 57). ORC, cdc6, Mcm2/7-cdt1, DDK, cdc45, Dpb11, GINS, S-CDK, Mcm10, RPA, Pola, Ctf4, Sld3/7, Sld2 and TopoII were purified as in (8). Csm3/Tof1, Topo I, RFC and PCNA were purified as described in (9). Mrc1 was expressed and purified following the procedure described in (58). PCNA-C4S-K164C from Zhihao Zhuang (59) does not contain a His-tag and it was purified with two HiTrapQ rounds of purification before gel filtration. All the concentrations for PCNA reported here refer to the monomer concentration. Additional purification protocols are:

RFC Δ N: Rosetta2 cells (Novagen) containing pBL481-RFC Δ N from Peter Burgers (60) were grown in 4 liters of Terrific Broth at 37°C to $A_{600}=1.6$. The temperature was shifted to 18°C and cells were incubated for 30 more minutes before adding 0.3 mM Isopropyl β -D-1-thiogalactopyranoside (IPTG). The expression was incubated for 16 hours and cells were harvested by centrifugation at 3200 x g for 15min. Cells were resuspended in 30 mM HEPES pH 7.5, 0,5 mM EDTA, 10% Glycerol, 200 mM NaCl, 1mM DTT, 0,5 mM p-methylphenyl-sulfonyl fluoride (PMSF) in presence of COMPLETE EDTA-free protease inhibitor (Roche). Cells were lyzed with sonication. DNA was precipitated with 0.5% of poly(ethyleneimine) (PEI) and the lysate was clarified by centrifugation

for 30 minutes at 21000xg. RFCΔN was precipitated with 0.28 g/ml of AmSO₄. The precipitates were collected by centrifugation at 12000xg for 45 minutes. Pellets were resuspended in 50ml of 30 mM HEPES pH 7.5, 0,5 mM EDTA, 10% Glycerol + 1mM DTT, 0.5mM PMSF in presence of COMPLETE EDTA-free protease inhibitor. The lysate was next dialyzed (using 12-14 MWCO membrane) against 2 liters of 30 mM HEPES pH 7.5, 0,5 mM EDTA, 10% glycerol + 100 mM NaCl, 1mM DTT for 2 hours. RFCΔN was injected on HiTrap SP HP 5ml column (Cytiva) equilibrated in buffer SP-A (30 mM HEPES pH 7.5, 10% Glycerol, 100 mM NaCl, 1mM TCEP). The column was washed with 25ml of SP-A buffer and eluted in a gradient of SP-B buffer (30 mM HEPES pH 7.5, 10% Glycerol, 800 mM NaCl, 1mM TCEP) along 60ml. Fractions containing RFCΔN were analyzed by SDS-PAGE and were pooled together. RFCΔN was then mixed with 3 ml of nickel beads equilibrated in His-A buffer (20mM HEPES 7.5, 200mM NaCl, 20 mM Imidazole, 10% Glycerol, 1 mM TCEP). Beads were washed with 100 ml of His-A buffer and RFCΔN was eluted with His-B buffer (20mM HEPES 7.5, 300mM NaCl, 300 mM Imidazole, 10% Glycerol, 0.05% ampholytes, 1 mM TCEP). Fractions containing RFC were concentrated and further purified on HiLoad 16/600 Superdex 200 (Cytiva) in 20mM HEPES 7.5, 200mM NaCl, 10% Glycerol, 1 mM TCEP, 0.05% ampholytes. RFCΔN was concentrated and stored at -80°C.

RPA from bacterial expression: Rosetta2 cells transformed with pRSF-Duet, RPA, a gift from Xiaodong Zhang (61), were grown in 2 liters of Terrific Broth at 37°C for 16 hours until A600=1.8. Cells were placed at 25°C and RPA expression was induced with 0.3 mM IPTG for 3 hours. Cells were harvested by centrifugation at 3200 x g for 15min and resuspended in lysis buffer (50 mM HEPES pH 7.5, 500 mM NaCl, 5% glycerol, 0.01% IGEPAL CA-630, 1mM TCEP) in presence of COMPLETE EDTA-free protease inhibitor (Roche). Cells were sonicated and the lysate was clarified by centrifugation at 50000xg for 50 minutes. The supernatant was recovered and injected on HiTrap HP 5ml column (Cytiva) equilibrated in lysis buffer. The column was washed with 50 ml of lysis buffer, 100 ml of His-A buffer (50 mM HEPES pH 7.5, 750 mM NaCl, 5% glycerol, 0.01% IGEPAL CA-630, 1mM TCEP, 30 mM Imidazole), and 25 ml of lysis buffer respectively. RPA was then eluted in a gradient of His-B buffer (50 mM HEPES pH 7.5, 150 mM NaCl, 5% glycerol, 0.01% IGEPAL CA-630, 1mM TCEP, 250 mM Imidazole) along 50ml. Fractions containing RPA were pooled and diluted in 50 mM HEPES pH 7.5, 5% glycerol, 0.01% IGEPAL CA-630, 1mM TCEP to bring the salt concentration to 150 mM NaCl. RPA was next injected on HiTrap Heparin HP 1ml (Cytiva) equilibrated in QA buffer (50 mM HEPES pH 7.5, 150 mM NaCl, 5% glycerol, 0.01% IGEPAL CA-630, 1mM TCEP). The column was washed with 20 ml of QA buffer and RPA was eluted in a gradient of QB buffer (50 mM HEPES pH 7.5, 1000 mM NaCl, 5% glycerol, 0.01% IGEPAL CA-630, 1mM TCEP) along 40ml. Fractions containing RPA were pooled together and injected on HiLoad 16/600 Superdex 200 (Cytiva) and eluted in 50 mM HEPES pH 7.5, 300 mM NaCl, 5% glycerol, 0.01% IGEPAL CA-630, 1mM TCEP. RPA was concentrated and stored at -80°C.

FEN1_DA from bacterial expression: The cDNA encoding the full-length *Xenopus laevis* FEN1 (S-form) D181A mutant was codon-optimized, synthesized (gBlocks Gene Fragments, Integrated DNA Technologies), and ligated into the BamHI-XhoI sites of the pGEX6P-1 vector. BL21 (DE3) RIL cells transformed with pGEX6P-1-xIFEN1.S_DA were grown in 2.4 liters of LB + Ampicillin at 30°C until A600=0.7. Cells were placed at 18°C and FEN1_DA expression was induced with 0.5 mM IPTG for overnight. Cells were harvested by centrifugation at 3200 x g for 15min and resuspended in 40 mL lysis buffer (50 mM TRIS-HCl pH 8, 500 mM NaCl, 10% glycerol, 1 mM EDTA, 1 mM PMSF, 0.1% IGEPAL CA-630, 2 mM DTT) in presence of COMPLETE EDTA-free protease inhibitor

(Roche). Cells were sonicated and the lysate was clarified by centrifugation at 26500xg for 20 minutes. The supernatant was recovered and added to Glutathione Sepharose 4B beads (Cytiva) equilibrated in lysis buffer. After incubation for 90 minutes, the beads were washed with 100 ml of wash buffer 1 (50 mM TRIS-HCl pH 8, 1 M NaCl, 10% glycerol, 1 mM EDTA, 1 mM PMSF, 0.1% IGEPAL CA-630, 2 mM DTT). Beads were then washed with 50 mL wash buffer 2 (50 mM TRIS-HCl pH 8, 300 mM NaCl, 10% glycerol, 0.1% IGEPAL CA-630, 2 mM DTT). Resuspended beads in 2 mL wash buffer 2 and cleaved protein from beads overnight at 4 °C using 100 U PreScission protease. Concentrated FEN1_DA was injected on Superose 6 Increase 10/300 GL (Cytiva) and eluted in Superose 6 buffer (20 mM HEPES-KOH pH 7.4, 300 mM NaCl, 10% glycerol, 2 mM DTT). Fractions were selected and FEN1_DA was concentrated and stored at -80°C.

Protein labeling with fluorescent dyes

Histones H2A-H2B (containing H2B-T112C) and H3-H4 (containing H4-E63C) were labeled with maleimide AlexaFluor-647 (AF647) or AlexaFluor-488 (AF488) respectively (56, 57), as indicated.

PCNA-C4S-K164C and PCNAK164C were labeled with Alexa Fluor 546. PCNA was diluted in labeling buffer (50 mM MOPS pH 7.0, 125 mM NaCl, 5 mM Sodium Acetate, 1 mM EDTA, 1 mM TCEP) to a final concentration of 1mg/ml. A 10-fold excess of TCEP was added to PCNA to ensure that all cysteines are effectively reduced. PCNA was then incubated with a 10-fold excess of AlexaFluor546. The reaction was incubated for 2 hours at room temperature, then quenched with 20 mM DTT final concentration for 30 minutes. labeled PCNA was then concentrated and injected on a Superdex 75 increase 10/300 column to remove free dye. PCNA was eluted in 20 mM HEPES pH 7.5, 125 mM NaCl, 1 mM TCEP. Fractions containing labeled PCNA were pooled and concentrated, and the protein was stored at -80°C.

Annealing of linear DNA fragments

Single-stranded DNA oligos of different lengths were purchased from IDT, either desalted (unlabeled oligos) or HPLC-purified (Alexa Fluor 647-conjugated oligos). For each length (18mer, 33mer, 43mer, 53mer) a forward oligo and a reverse oligo in reverse complement sequence were ordered. The 18mer and 33mer forward oligos included a 5' Alexa Fluor 647 label. Forward and corresponding reverse oligos were mixed in a 1:1 stoichiometric ratio at 20 µM each (18mer and 33mer) or 40 µM each (43mer and 53mer) with a final of 20 mM HEPES pH 7.5 and 25 mM NaCl. The mixed oligos were annealed by heating up to 95 C for 3 min, and then slowly cooled to room temperature over several hours. Annealed DNA was stored at -20 C.

EMSA

Native DNA-protein complexes were allowed to form in NA buffer: 25 mM TRIS pH 7.5, 150 mM NaCl, 1 mM EDTA, 0.02% Tween-20, 1 mM TCEP. Increasing amounts of CAF-1 (0 to 5 µM) were incubated in buffer for 10 min before addition of DNA (50 nM). Single stranded DNA oligos for 18bp, 33bp, 43 or 53 bp were purchased from IDT (labeled with AlexFluor647 at their 5' end, Supplementary Table S1) and annealed prior to the EMSA experiments. 10% final concentration of glycerol was added before loading the samples into a 6% PAGE. Gels were scanned for fluorescence and then stained with SybrGOLD before imaging with Amersham Image Quant 800. The data was analyzed and plotted using FIJI and GraphPad Prism. We quantified the fluorescent

signal of the unbound DNA band. We calculate the percentage of unbound DNA relative to the no CAF-1 condition. %bound DNA is then expressed as $100 - \text{percentage of unbound DNA}$. The K_d values were calculated using a one site binding curve with hill slope in GraphPad Prism. The 18bp data was fitted to a one site binding curve with a Hill coefficient constrained to 1.

PCNA-CAF-1 binding experiments on SEC

We used pUC19 plasmid as DNA template for PCNA loading. This plasmid was nicked using the restriction enzyme Nt.BspQI for 8 hours at 50°C, and was subsequently purified via phenol chloroform extraction. Reactions were performed in PCNA loading buffer 50mM HEPES pH 7.5, 200 mM NaCl, 0.01% IGEPAL CA-360, 1mM TCEP. PCNA (30 μM) was incubated for 5 minutes at 30°C with nicked pUC19 (0.3 μM) and RFCΔN (0.5 μM), in the presence of MgCl₂ (10 mM) and ATP (3 mM). Next, CAF-1 (5μM) was added to these reactions and incubated for 15 minutes at room temperature. Samples were next spun down for 5min at 17000xg before injection on Superose 6 increase 3.2-300 columns connected to an AKTA pure system fitted with PEEK I.D. 0.25 mm tubing. Fractions were analyzed on 4-12% gradient SDS-PAGE run in MES buffer.

PCNA-NAQ assay

We used pRC1765 (Addgene #141346, a gift from Rafael Fernández Leiro) as template for PCNA loading and nucleosome assembly. pRC1765 was nicked using the restriction enzyme Nt.BbvCI for 6 hours at 37°C, and was subsequently purified via phenol chloroform extraction. PCNA was loaded on DNA in PCNA loading buffer, in a final volume of 11μl: PCNA (10.9 μM) was added to an equimolar mixture of nicked and supercoiled pRC1765 (47.3 nM each), RFCΔN (1.1μM) in presence of MgCl₂ (8 mM) and ATP (10.9 mM). This reaction was incubated at 30°C for 5 minutes. First, samples were diluted with 25μl of NA buffer in order to decrease the high concentration of MgCl₂ which hinder proper nucleosome assembly, followed by addition of CAF-1•H3-H4 (0.1 μM final concentration for each – H3-H4 dimer concentration) to a final volume of 40 μl total. This tetrasome assembly step is incubated at room temperature for 15 minutes. Then, we added fluorescently labeled H2A-H2B dimers and incubated for 15 minutes at room temperature, to complete nucleosome formation (62). Samples were spin down for 5 minutes at 17000xg. 1μl of each reaction was mixed with 5μl of NA buffer and 5% sucrose final concentration for loading on 0.8% agarose gel and run for 90 minutes in 1X TAE (TRIS-Acetate EDTA) at 90 volts. 25μl of each reaction was digested with 80 units of MNase in a total volume of 100 μl (containing 50 mM TRIS pH 7.9, 5 mM CaCl₂) at 37°C for 10 minutes. MNase was inactivated by addition of EDTA. A 621bp DNA fragment was added as loading control and the DNA was further purified as in (62). MNase-digested samples were loaded on 6% PAGE and stained with SybrGOLD. The data was analyzed and plotted using FIJI, and GraphPad Prism. The PCNA-mediated activity of CAF-1 is quantified as the percentage of fluorescence on nicked plasmid relative to the total intensity (nicked + supercoiled) for each condition. The amount of MNase-protected fragments in each condition was quantified using Bioanalyzer (Agilent) on DNA High sensitivity chips. The bioanalyzer data was analyzed by normalizing the nucleosome band (140-160 bp) to the loading control at 621 bp within each lane, as in (62). Data was then plotted using GraphPad Prism.

MNase-seq of PCNA-NAQ assay

MNase-seq was used to quantify nucleosome assembly in the PCNA-NAQ assay. In order to distinguish nicked and supercoiled DNA, we used two plasmids with different sequences: pRS415 and pLox3 (Supplementary Table S2). After MNase inactivation a 207 bp DNA fragment was added as loading control in these experiments. Purified MNase-digested products (containing the loading control DNA) were used to prepare an Illumina sequencing library. First, samples were purified using the CleanNGS kit (GC biotech #CNGS-0008), according to the manufacturer's protocol. Next, the CleanNGS elute was adjusted to 25 μ l with 10 mM TRIS pH 7.5 and the ends of the digested DNA were repaired and phosphorylated at their 5' end using the End-It DNA End-repair kit (Lucigen #ER0720). DNA was purified using MinElute PCR Purification Kit (QIAGEN #28006). Next, 3'A overhangs were added to each fragment using the Klenow fragment (NEB #M0212M) and DNA was purified using MinElute PCR Purification Kit (QIAGEN #28006). Next, unique indexed DNA adapters (Supplementary Table S3) were ligated overnight at room temperature T4 DNA ligases (NEB # M0202L) to all fragments with A-overhangs and DNA was purified using MinElute PCR Purification Kit (QIAGEN #28006). Finally, all samples were amplified by a 8-cycle PCR-program using Phusion High-Fidelity DNA Polymerase (NEB #M0530L) using primers 5'- TCGTCGGCAGCGTCAGATGTGTATAAGAGACAGCTCGGCATTCCTGTGAACCGCTCTTCCGATCT-3' and 5'- GTCTCGTGGGCTCGGAGATGTGTATAAGAGACAGTACACTCTTTCCTACACGACGCTCTTCCGATCT-3', prior to a final clean up using the MinElute Purification Kit (QIAGEN #28006). Samples were pooled with a total concentration of 100 ng. The library was submitted for paired-end Illumina 150 bp PE sequencing at Macrogen (Amsterdam). fastq files are uploaded to OSF (https://osf.io/2vd4z/?view_only=5ffa1e0b749445da9b22a11577f3d47f). PCNA-NAQ-seq analysis was performed using custom scripts (<https://github.com/deLaatLab/PCNA-NAQ-seq>). The sequence data was demultiplexed by extracting reads that contained the ligated adapter index in both read ends and trimmed by removal of the 5' adapter sequence from the reads. Demultiplexed reads were mapped against the pLox3, pRS415 and loading control DNA sequences using BWA mem v0.7.17 and filtered using samtools with SAM flag 780 and mapping quality 60 and saved as bam files. The bam files were imported in R and fragments mapping to pLox3 and pRS415 with fragment lengths between 125 and 160 bp were selected for further analysis. The percentage of reads mapping to the nicked plasmid was calculated based on the total amount of reads found on both nicked and supercoiled plasmids. For coverage analysis pLox3 and pRS415 fragments were normalized for the total number of fragments mapping to the loading control sequence.

Primer extension assays

Experiments with Pol ϵ were performed in 25 mM HEPES-KOH pH 7.5, 150 mM potassium acetate, 8 mM magnesium acetate 1 mM TCEP, 1 mM ATP and 0.2 mg/ml BSA. Experiments with Pol δ were performed in 25 mM TRIS-HCl pH 7.5, 150 mM NaCl, 8 mM MgCl₂, 1 mM TCEP, 1 mM ATP and 0.2 mg/ml BSA. We used single stranded plasmid DNA as template for DNA synthesis, and it was produced as previously described (63). The concentrations reported here are for the final reaction that contains all components.

Single-strand pBluescript SK(-) (Supplementary Table S4) was incubated for 5 min at 80°C with a 5x excess of a 15 bp oligonucleotide and allowed to slowly cool down. The primer sequence is: G*G*G* T*T*C*GTGCACACA conjugated to an Alexa Fluor 647 dye at the 5' end (* indicates

nucleotides containing phosphorothioate bonds). The annealing reaction was coated with RPA (0.6-1.5 μM) for 5 minutes at 30°C. Next, PCNA (0.48 μM) was loaded in presence of RFC ΔN (0.12 μM) for 5 minutes at 30°C on DNA (12nM). Pol ϵ or Pol δ (0.12 μM) were primed onto the primer-template DNA in presence of dCTP, dGTP and dATP (75 μM of each) for 5 minutes at 30°C. Finally, dTTP (75 μM) was added to start the reaction. CAF-1 or FEN1 were also added at this step, at 300 nM unless stated otherwise in the figures. Reactions were quenched at various timepoints with 10 mM EDTA final concentration. Samples were mixed with 2% sucrose, 100 mM NaOH final concentrations and were loaded on denaturing alkaline 1.2% agarose gel. Gels were run for 16 hours at 40V, and imaged on a Typhoon. The data was analyzed and plotted using FIJI, and GraphPad Prism. DNA synthesis is quantified as the intensity of the full-length plasmid band relative to the total intensity in the entire lane.

For MNase analysis, 30 μL of primer extension reactions at the final time point (16 minutes for Pol ϵ and minutes for Pol δ) were mixed with 80 U of MNase in a total of 100 μL (containing 50 mM TRIS pH 7.9, 5 mM CaCl₂) at 37°C for 10 minutes. MNase was inactivated by addition of EDTA. A 621bp DNA fragment was added as loading control and the DNA was further purified as in (62). MNase-digested samples were loaded on 6% PAGE and stained with SybrGOLD and run on a Bioanalyzer (Agilent) using DNA High sensitivity chips. The bioanalyzer data was analyzed by normalizing the nucleosome band (140-150 bp) to the loading control at 621 bp within each lane, as in (62). Data was then plotted in excel and GraphPad Prism.

In-solution crosslinking experiments

CAF-1-PCNA on nicked plasmid: To buffer containing 20 mM HEPES pH 7.5, 200 mM NaCl, 1 mM TCEP, the following components were added in order at room temperature: 10 mM MgCl₂ (from 100 mM stock), 3 μM PCNA K164C, 0.15 μM RFC ΔN , 0.3 μM nicked (with Nt.BspQ1) pUC19 plasmid (from 1 μM stock), 1 mM ATP. This mixture was incubated at 30 °C for 5 min to increase the efficiency of PCNA loading onto DNA. Then, 1.5 μM CAF-1 was added and incubated for 10 min at room temperature. The total NaCl concentration during the loading reaction and after adding CAF-1, taking into account the contributions from each component, ranged between 100 and 110 mM. Samples were diluted 2-fold in buffer containing 20 mM HEPES pH 7.5, 100 mM NaCl, 1 mM TCEP, 0.02% IGEPAL CA-630, and incubated at room temperature for 10 min. Samples were subjected to chemical crosslinking by addition of a final concentration of 0.2% glutaraldehyde (from a 2.5% stock in water). The samples were incubated at room temperature for 20 min before quenching the crosslinker by addition of 100 mM TRIS pH 7.5 (from 1 M stock). To release the crosslinked complexes from the DNA, 10% of the sample volume Pierce universal nuclease, diluted 1:20 in buffer containing 20 mM HEPES pH 7.5, 100 mM NaCl, 5 mM MgCl₂, and 1 mM TCEP, was added. After incubation at room temperature for 10 min, 50 mM EDTA was added to quench the nuclease. Samples were spun down for 15 min at 13,000 xg at 4 °C and the supernatant was transferred to a new tube.

Complex formation of CAF-1 and PCNA on linear DNA: Linear DNA fragments with lengths of 18, 33, 43 or 53 bp were mixed with PCNA-C4S-K164C and CAF-1 in buffer containing 20 mM HEPES-KOH pH 7.6, 100 mM KCl, 0.01% IGEPAL CA-630 and 1 mM TCEP, and incubated on ice for 10 min. The final mixture contained 1.5 μM DNA, 4.5 μM Alexa Fluor 456 -labeled PCNA (concentration for a monomer), and 3 μM CAF-1. Samples were subjected to chemical crosslinking by diluting 3-fold in the same buffer and addition of a final concentration of 0.2%

glutaraldehyde (from a 2.5% stock in water). The samples were incubated at room temperature for 20 min before quenching the crosslinker by addition of 100 mM TRIS (from a 25x TAE stock containing 1 M TRIS). Samples were spun down for 5 min at 13,000 xg at 4°C and the supernatant was transferred to a new tube.

Complex formation of CAF-1-H3-H4 and PCNA without DNA: Histones H3-H4 (C110A, T71C) tetramers, labeled with AlexaFluor 488, were concentrated in 20 mM HEPES pH 7.5, 2 M NaCl, 1 mM EDTA, 1 mM TCEP to a final concentration of 79.4 μM using an Amicon Ultra-0.5 centrifugal concentrator with a molecular weight cut off of 10 kDa. CAF-1 WT or mutants were diluted to a concentration of 27.1 μM in 20 mM HEPES pH 7.5, 200 mM NaCl, 1 mM EDTA, 1 mM TCEP. CAF-1 was then mixed with the histones in a volumetric ratio of 3:1 to obtain samples with final concentrations of 20 μM CAF-1 and 10 μM H3-H4 tetramers. The NaCl concentration in these samples was around 650 mM. CAF-1-H3-H4 samples were mixed in order with buffer containing 20 mM HEPES pH 7.5, 60 mM NaCl, 1 mM TCEP and then PCNA-C4S-K164C (labeled with AlexaFluor 546, 185 μM stock) to obtain final concentrations of 1.5 μM CAF-1-H3-H4, 5.55 μM PCNA with a total of about 105 mM NaCl. Samples were diluted 2-fold in buffer containing 20 mM HEPES pH 7.5, 100 mM NaCl, 1 mM TCEP, 0.02% IGEPAL CA-630, and incubated at room temperature for 10 min. Samples were subjected to chemical crosslinking by addition of a final concentration of 0.2% glutaraldehyde (from a 2.5% stock in water). The samples were incubated at room temperature for 20 min before quenching the crosslinker by addition of 100 mM TRIS pH 7.5 (from 1 M stock). Samples were spun down for 15 min at 13,000 x g at 4 °C and the supernatant was transferred to a new tube.

Crosslinking of CAF-1-PCNA on DNA at limiting PCNA concentrations: AlexaFluor546-labeled PCNA K164C (50 nM) was loaded onto nicked (with Nt.BspQ1) pUC19 plasmids (15 nM) by RFC (15 nM). The reaction was conducted at 30 °C for 5 minutes in buffer containing 20 mM HEPES-KOH pH 7.6, 130 mM NaCl, 0.01% IGEPAL CA-630, 1 mM TCEP, 10 mM MgCl₂, 1 mM ATP. Then, CAF-1 or buffer control was titrated between 0-1 μM. The total NaCl concentration during the loading reaction and after addition of CAF-1, taking into account the contributions from each component, ranged between 100 and 110 mM. After 10 min at room temperature, the samples were diluted 4.5-fold by adding buffer containing 20 mM HEPES-KOH pH 7.6, 100 mM NaCl, 0.01% IGEPAL CA-630, 1 mM TCEP, before cross-linking with 0.2% glutaraldehyde. The cross-linking reaction took place at room temperature for 20 minutes, after which, it was quenched with a final concentration of 100 mM TRIS-HCl pH 7.5. DNA was digested using Pierce™ Universal Nuclease for Cell Lysis (Thermo Fisher Scientific) diluted to 1:20 in 20 mM HEPES-KOH pH 7.6, 100 mM NaCl, 5 mM MgCl₂, 1 mM TCEP and added to 10% of the crosslinking reaction volume. The digestion was quenched with 50 mM EDTA and immediately spun down for 5 minutes at 13,000 xg and 4°C to remove precipitates.

Crosslinking of FEN1-PCNA at limiting PCNA concentrations: AlexaFluor546-labeled PCNA K164C (50 nM) and FEN1_DA (0-0.6 mM) were mixed in buffer containing 20 mM HEPES-KOH pH 7.6, 100 mM NaCl, 0.01% IGEPAL CA-630, 1 mM TCEP. After 10 min at room temperature, the samples were diluted 4.5-fold by adding buffer containing 20 mM HEPES-KOH pH 7.6, 100 mM NaCl, 0.01% IGEPAL CA-630, 1 mM TCEP, before cross-linking with 0.2% glutaraldehyde. The crosslinking reaction took place at room temperature for 20 minutes, after which, it was quenched with a final concentration of 100 mM TRIS-HCl pH 7.5. Crosslinked samples were immediately spun down for 5 minutes at 13,000 g and 4°C to remove precipitates.

SDS-PAGE analysis of crosslinked samples: Crosslinked samples were mixed with 4x XT sample buffer and 20x XT reducing agent in appropriate volumetric ratios. These samples were loaded on 12% Criterion XT Bis-TRIS gels in XT MOPS buffer. Gels were run at 20 mA until the samples have completely entered the gel and then at 40 mA until the gel run was complete (typically between 2 and 3 hours). Gels were run at room temperature, and additionally in the dark if components contained fluorophores. Gels were scanned for histones H3-H4 and/or PCNA fluorescence (depending on the assay) on an AMERSHAM ImageQuant 800 imager (Cytiva). Band intensity was calculated using the ROI manager tool in Image J/Fiji and plotted using GraphPad Prism. Where applicable, gels were subsequently stained with Coomassie blue and scanned on AMERSHAM ImageQuant 800 imager (Cytiva).

Mass Photometry

Samples were prepared using crosslinking at stoichiometric conditions, the reactions (± 1.2 mL final volume after EDTA quenching) were concentrated to 500 μ L and loaded on a pre-equilibrated Superose 6 10/300 GL (Cytiva) column in buffer 20 mM HEPES-NaOH pH 7.5, 200 mM NaCl, 1 mM TCEP. Fractions were analyzed on SDS PAGE, the ones containing the complex of interest (Peak1 or Peak2) were pooled and concentrated to about 40 μ L (Abs280 close to 0.5). The samples were diluted 10 to 20-fold in 20 mM HEPES-NaOH pH 7.5, 100 mM NaCl, 1 mM TCEP right before measuring on a Refeyn OneMP instrument (Refeyn Ltd.). For each measurement, 13 μ L of this buffer was first placed into the CultureWell gaskets wells (Grace Biolabs) placed into the Microscope coverslips (24 mm \times 50 mm; Paul Marienfeld GmbH). After adjusting the focus, 2 μ L of sample was mixed in. Movies were recorded for 60 seconds at 100 frames per second. A calibration measurement under the same conditions was performed roughly every 15 measurements using an in-house prepared protein standard mixture: IgG4 Δ hinge-L368A (73 kDa), IgG1-Campath (149 kDa), apoferritin (479 kDa), and GroEL (800 kDa). Data was processed using DiscoverMP (Refeyn Ltd.) with bin width adjusted to 10, and each sample retrieved about 1500-3000 counts. Figures were prepared with the Refeyn instrument and edited in Illustrator.

Fluorescence polarization

Fluorescence Polarization assays were carried out in 25 mM TRIS pH 7.5, 300 mM NaCl, 5% glycerol, 1 mM EDTA, 0.01% NP-40 (added fresh), 0.01% CHAPS (added fresh), 1 mM DTT (added fresh). Binding reactions were prepared by mixing 10 nM of Alexa488-labeled H3-H4 (H3 C110A-H4 E63C) and increasing amounts of CAF-1, Pol ϵ , Pol δ or RPA in a final volume of 30 μ L in CORNING low flange 384 well black microplates (CLS3575). Binding data were measured using a CLARIOStar (BMG LabTech) plate reader. The data was analyzed and plotted using Microsoft Excel and GraphPad Prism. The binding affinity was determined using a One Site binding curve (not accounting for fluorescent label depletion) in GraphPad PRISM ($y = B_{max} * x / (K_d + x) + Background$, where B_{max} is the maximum specific binding, K_d is the equilibrium dissociation constant and Background is the measured binding with no added ligand). Fluorescence Polarization was measured three times over the course of 15 minutes for each sample, to ensure equilibration of the binding. Each experiment was performed in triplicate.

NAQ assay

This refers to Supplementary Figure S5B. The nucleosome assembly reaction was carried out at 200 nM of 207 bp DNA, 200 nM xenopus octamer maleimide AlexaFluor-647 (AF647) labeled on H2B T112C (containing H3 C110A mutant) and 500 nM CAF-1, Pol ϵ or RPA. After the assembly reaction, the samples were diluted to a DNA concentration of 50 nM in 100 μ l digestion reactions. 25U of MNase enzyme was added in a final buffer containing 50 mM TRIS pH 7.9, 5 mM CaCl $_2$. After incubation at 37°C for 10 min, the reactions were quenched with 10 μ l of 500 mM EDTA, pH 8. The DNA was then purified using a modified protocol of the MinElute kit from QIAGEN. 550 μ l of PB buffer and 10 μ l of 3 M sodium acetate were added to each sample and they were incubated at room temperature for 10 min. At this point, 50 ng of DNA loading control (or reference band, a 621 bp DNA fragment) was added to each tube. The samples were applied to the MinElute spin column and washed as prescribed by QIAGEN. The DNA was eluted with 10 μ l of water. 2.5 μ l were loaded on a 6% PAGE gel. The gel was run for 45 min at 200 V in 0.5x TBE buffer at room temperature. Gels were stained with SybrGOLD for DNA and imaged on an AMERSHAM ImageQuant 800 (Cytiva).

Cell culture, genome editing and western blot

Mouse ESCs used in this study were derived from the E14JU cell line with a 129/Ola background. For genome editing and next-generation sequencing experiments, ESCs were grown on gelatin-coated dishes (0.2 %) in serum+LIF conditions at 37 °C with 5 % CO $_2$. Media was prepared by supplying DMEM-GlutaMAX-pyruvate with fetal bovine serum (15 %), LIF (made in house), 1x non-essential amino acids (Gibco), 1x penicillin/streptomycin (Gibco) and 2-beta-ME (0.1 μ M). Cells were passaged using Trypsin-EDTA (Gibco) or TrypLE (Gibco). Cells were routinely tested for mycoplasma contamination. For genome editing *Chaf1a*-dTAG cells were generated by CRISPR-Cas9 using the SpCas9(BB)-2A-Puro (PX459) V2.0 plasmid (Addgene #62988) as described in (64) with sgRNA#1 (Supplementary Table S5), which targets the *Chaf1a* gene at the beginning of the ORF and a *Chaf1a*-linker-dTAG homology donor plasmid. Cells were transfected using Lipofectamine 3000 reagent (Invitrogen) using 0.5 μ g of sgRNA-plasmid and 2 μ g of donor plasmid. Cells were sparsely seeded on a 10 cm dish 24 hours post transfection and selected with Puromycin (2 μ g/mL) for 48 h. Thereafter, cells were expanded and genotyped with primers #1 and #2 (Supplementary Table S5). Positive clones were analyzed by Sanger sequencing with primers #3 and #4 (Integrated DNA Technologies, Supplementary Table S5) and degradation upon dTAG-13 (Tocris, 6605) treatment was confirmed by Western Blot by α -*Chaf1a* antibody (65). Fractionation cell extracts were prepared as in (66). Western Blotting was performed as described in (67).

Immunofluorescence

Cells treated with DMSO or dTAG-13 for 4 hours, were pulsed in EdU-containing media (10 μ M) for 10 min and immediately fixed for 15 min in 4% PFA at RT and stored in PBST (PBS with 0.3% Triton X-100). Primary antibody H4K20me0 was added at the concentration of 1:1000 in PBST with 5% donkey serum and incubated overnight. Incubation was followed by 3 washes in PBS and secondary antibody was then added in PBST. Samples were incubated with the secondary antibody in the dark at RT for 1h. After 3 washes, samples were stained with DAPI (1:10000) in PBST. Images were acquired with a ScanR high-content screening microscope (Olympus).

Automated and unbiased image analysis was carried out with the ScanR analysis software (version 2.8.1). Individual cells were identified based on DAPI staining and mean pixel intensity was measured for each channel. Data was exported and processed using Spotfire software (version 10.5.0; Tibco). Statistical analysis and visualization of results was done using R (v4.1.2) in RStudio (v2021.9.2.382).

SCAR-seq

A step-by-step protocol is available (68). Briefly, nascent SCAR-seq samples were prepared from *Chaf1a*-dTAG cells in three biological replicates for each histone PTM. Cells treated with DMSO or dTAG-13 for 2 hours, were pulsed in EdU-containing media (10 μ M) for 30 min and harvested immediately. For sample collection, media was aspirated, plates washed 2x with RT PBS and ice-cold PBS was added to the dishes. Cells were scraped in a cold room and collected by centrifugation, followed by nuclei isolation. Nuclei were aliquoted, snap-frozen and stored at -80° C until further use. For MNase digest, nuclei were counted manually using Kova Glasstic Slides and 2 U MNase (Worthington) were added per 1×10^6 nuclei. Digests were performed at 30° C for 20 minutes. For native ChIP, 30-50 μ g of chromatin was used per sample and incubated with antibodies in a total volume of 600 μ L overnight at 4° C with H3K27me3 antibody (Cell Signaling, 9733) or H4K20me0 antibody (Abcam, ab227804). Magnetic beads (anti-rabbit IgG Dynabeads, invitrogen) were added the next morning and samples were incubated for 2 hours. After three washes each with ice-cold RIPA buffer and RIPA 0.5M NaCl buffer, DNA was eluted and purified using the MinElute Reaction Cleanup kit (Qiagen). Mononucleosomal-sized fragments were isolated by double sided size selection with AMPure XP beads (Beckman Coulter). EdU-labeled DNA fragments were biotinylated using Click-iT chemistry as reported above but using Biotin-TEG-Azide (Berry & Associates) instead of Picolyl-azide-PEG4-Biotin. Libraries were prepared using the KAPA Hyper Prep Kit (Roche). Biotinylated fragments were captured using Dynabeads MyOne Streptavidin (Invitrogen) and EdU strands were purified by performing NaOH washes. Libraries were amplified in 9-11 PCR cycles. Libraries with mononucleosomal-sized inserts were isolated by double-sided size selection with AMPure XP beads (Beckman Coulter), followed by a second clean-up with 1.0x AMPure XP beads. Fragment distribution of libraries was checked on a Fragment Analyzer system (Agilent). Stranded input samples were prepared in parallel with SCAR-seq samples. Samples were sequenced single end (75bp) on a NextSeq500 instrument (Illumina).

Reads were processed, mapped and histone partition signal was computed as described previously (68). Briefly, for each strand the SCAR normalized signal (CPM) was computed in 1kb bins and smoothed in a uniform blur considering the neighboring 30 bins on each side. For each 1kb window, the signal from its corresponding SCAR input was subtracted and negative values were set to zero. Input corrected windows with CPM < 0.3 on both strands were filtered out and not considered for further analyzes. The final partition score for each 1kb window was calculated as: $\text{Partition} = (F - R)/(F + R)$ where F and R correspond to the number of normalized and input-corrected reads for the forward and reverse strand, respectively. The partition value relates to the ratio of histones with a specific modification being segregated to the nascent forward (Partition > 0) or nascent reverse (Partition < 0) strand within each window respectively. Okazaki-seq replication fork directionality (RFD) scores and filtered initiation zones (IZs) for mESC were taken from (67) and used to define replication via leading or lagging strand mechanism. The

RFD score in Okazaki-seq is calculated like SCAR-seq partition scores but subtracting the forward (F) strand signal from the reverse (R) strand signal instead: $RFD = (R - F)/(F + R)$.

The average partition signal from replicate 1 was used for visualization purposes in Partition line plots (Figure 6). To visualize the total reads in SCAR-seq, total mm10 mouse read counts were spike-in normalized to dm6 drosophila read counts as described in (69). By using the uniquely mapping, deduplicated reads in millions, the EdU-enriched Input samples ("ClickedInputs") was used as reference for relative spike-in abundance and EdU labeling efficiency. To visualize global signal in SCAR-seq, number of uniquely mapped, deduplicated mm10 reads of the SCAR sample (in million reads) were normalized to DMSO for each mark and replicate and plotted in replicates using R (v4.1.2) in RStudio (v2021.9.2.382).

End-point DNA replication with yeast replisome

These were carried out as in (9), all stock protein concentrations were determined by Bradford analysis. MCM was loaded onto 5.8 Kb ARS1 plasmid in 30 μ L reaction volumes, to final concentrations of 22.5 nM ORC, 100 nM Mcm2/7-cdt1, 45 nM Cdc6 and 4 nM plasmid DNA template, in buffer containing 25 mM HEPES-KOH pH 7.6, 100 mM potassium glutamate, 10 mM magnesium acetate, 0.02% IGEPAL CA-630, 5% glycerol, 5 mM ATP, 0.1 mg/mL BSA, 1 mM DTT. This reaction was incubated at 30°C for 20 minutes. After origin licensing, DDK was added to 25 nM and further incubated at 30°C for 30 minutes. The replication reaction was initiated by addition of FF500 buffer (50 mM HEPES-KOH pH 7.6, 500 mM potassium glutamate, 20 mM magnesium acetate, 0.02% IGEPAL CA-630, 2 mM DTT, 6 mM ATP, 0.2 mg/mL BSA, 0.4 mM CTP, GTP, UTP each, 0.16 mM dGTP, dATP, dTTP, dCTP and 40 nM α 32P-dCTP), followed by replication proteins in a master mix added to final reaction concentrations of 30 nM Dpb11, 40 nM cdc45, 210 nM GINS, 20 nM S-CDK, 5 nM Mcm10, 25 nM Sld3/7, 50 nM Sld2, 20 nM Pol ϵ , 100 nM RPA, 20 nM Pol α , 20 nM Ctf4, 20 nM TopoII, and another protein master mix added to final reaction concentrations of 20 nM Mrc1, 20 nM Csm3/Tof1, 10 nM TopoI, 20 nM RFC, 20 nM PCNA, 10 nM Pol δ . The replication reaction was conducted at 30 °C for 40 minutes. After this, the reaction was quenched by addition of 50 mM EDTA to 2x dilution. Samples were cleaned-up for unincorporated nucleotides using MicroSpin G-50 columns (Cytiva), after which they were denatured in 100 mM NaOH, 2% sucrose, bromocresol green as loading dye and 15 μ L samples were run on 0.7% alkaline agarose gels for 18 hours at 45 V. The next day, DNA was precipitated on gel by treatment with ice cold 5% TCA for 2 cycles of 15 minutes with TCA refreshment. The gel was dried in 2x chromatography Whatman paper and towel paper sandwich with a weight on top for 30 minutes, to remove excess moisture. After that, the Whatman paper gel sandwich was moved to a gel dryer for 2.5 hours at 55 °C. Gel was exposed to a phosphor screen for 2 days using Amersham Typhoon Biomolecular Image.

Pulse-chase experiments

These were carried out as in (9), all stock protein concentrations were determined by Bradford analysis. MCM was loaded onto 5.8 Kb ARS1 plasmid in 150-300 μ L reaction volumes, to final concentrations of 22.5 nM ORC, 100 nM Mcm2/7-cdt1, 45 nM Cdc6 and 4 nM plasmid DNA template, in buffer containing 25 mM HEPES-KOH pH 7.6, 100 mM potassium glutamate, 10 mM magnesium acetate, 0.01% IGEPAL CA-630, 5 mM ATP, 0.1 mg/mL BSA, 1 mM DTT. This reaction was incubated at 30°C for 30 minutes. After origin licensing, DDK was added to 25 nM

and further incubated at 30°C for 30 minutes. Replication proteins in a master mix were added to final pulse reaction concentrations of 30 nM Dpb11, 40 nM cdc45, 210 nM GINS, 20 nM S-CDK, 5 nM Mcm10, 25 nM Sld3/7, 50 nM Sld2, 20 nM Pol ϵ , 100 nM RPA, 40 nM PolA, 20 nM Ctf4, followed by another protein master mix added to final pulse reaction concentrations of 20 nM Mrc1, 20 nM Csm3/Tof1, 10 nM Topol. This reaction was then split into the pulse mixes containing 20 nM RFC, 20 nM PCNA, 180 nM CAF-1 or FEN1 (or corresponding storage buffers for control reactions), FF500 pulse buffer (50 mM HEPES-KOH pH 7.6, 500 mM potassium glutamate, 20 mM magnesium acetate, 0.02% IGEPAL CA-630, 2 mM DTT, 6 mM ATP, 0.2 mg/mL BSA, 0.4 mM CTP, GTP, UTP each, 0.16 mM dGTP, dATP, dTTP, 4 μ M dCTP and 66 nM α 32P-dCTP. Pulse reaction was conducted at 30 °C for 3 min 20 sec, when the chase (0.6 mM dCTP, dGTP, dATP, dTTP) was added. Time points were taken (15 μ L) at 4, 5, 6 and 7 min and replication reactions were quenched by addition to 2x dilution in 50 mM EDTA. Samples were cleaned-up for unincorporated nucleotides using MicroSpin G-50 columns (Cytiva), after which they were denatured in 10 mM NaOH, 2% sucrose, bromocresol green as loading dye and 14 μ L samples were run on 0.7% alkaline agarose gels for 18 hours at 45 V. The next day, DNA was precipitated on gel by treatment with ice cold 5% TCA for 2 cycles of 15 minutes with TCA refreshment. The gel was dried in 2x chromatography Whatman paper and towel paper sandwich with a weight on top for 30 minutes, to remove excess moisture. After that, the Whatman paper gel sandwich was moved to a gel dryer for 2.5 hours at 55°C. Gel was exposed to a phosphor screen for 2 days using Amersham Typhoon Biomolecular Image.

Max replication rate quantification

Data analysis was performed using the ImageQuant TL software. The raw data was analyzed using the 1D gel analysis option. Lanes were created manually with a 95% lane width. The background subtraction was done automatically using the minimum profile option. The peak of leading strand signal was selected manually under band detection in each lane. The upper boundary of the leading strand products, i.e. the front of the peak (created automatically by ImageQuant), was used as the max size of replicated products (example is shown in Supplementary Figure S7C). To convert mm to bp, a lane was created for the marker. The molecular size calibration was done using the standard ladder product sizes of Lambda DNA digested with HindIII. The conversion was computed automatically within the software using a log curve and Retardation factor (Rf) to propagate the values. The bp values calculated by ImageQuant for the earliest three time-points after addition of the chase were used in GraphPad prism to fit a linear regression, whose slope determined the max replication rates reported. To compare these rates independently on the variability of replication speed between experiments, we also normalized within each repeat the max replication rate of all conditions to the one of the +RFC/PCNA (no CAF-1) sample.

Availability

Fastaq files from MNase-seq are uploaded to OSF and can be accessed with the following link: https://osf.io/2vd4z/?view_only=5ffa1e0b749445da9b22a11577f3d47f

Supplementary Data

Supplementary Data are available at NAR online.

Authors Contributions

Conceptualization: C.R., B.V.E., L.K., A.G., F.M.

Data Curation: C.R., B.V.E., L.K., F.G., F.M.

Formal Analysis: C.R., B.V.E., L.K., F.G., A.E.E.V., I.R., P.H.L.K., F.M.

Funding acquisition: A.G., F.M.

Investigation: C.R., B.V.E., L.K., F.G., A.E.E.V., I.R., G.R., P.A., F.M.

Methodology: C.R., B.V.E., L.K., F.G., A.E.E.V., I.R., A.B., T.v.L., P.A., K.S., F.M.

Project administration: F.M.

Software: P.H.L.K.

Supervision: R.A.S., W.d.L., P.K., N.H.D., A.G., F.M.

Validation: C.D.v.F., G.L.

Visualization: C.R., B.V.E., L.K., F.G., F.M.

Writing – original draft: C.R., B.V.E., F.M.

Writing – Review & Editing: all authors

Acknowledgments

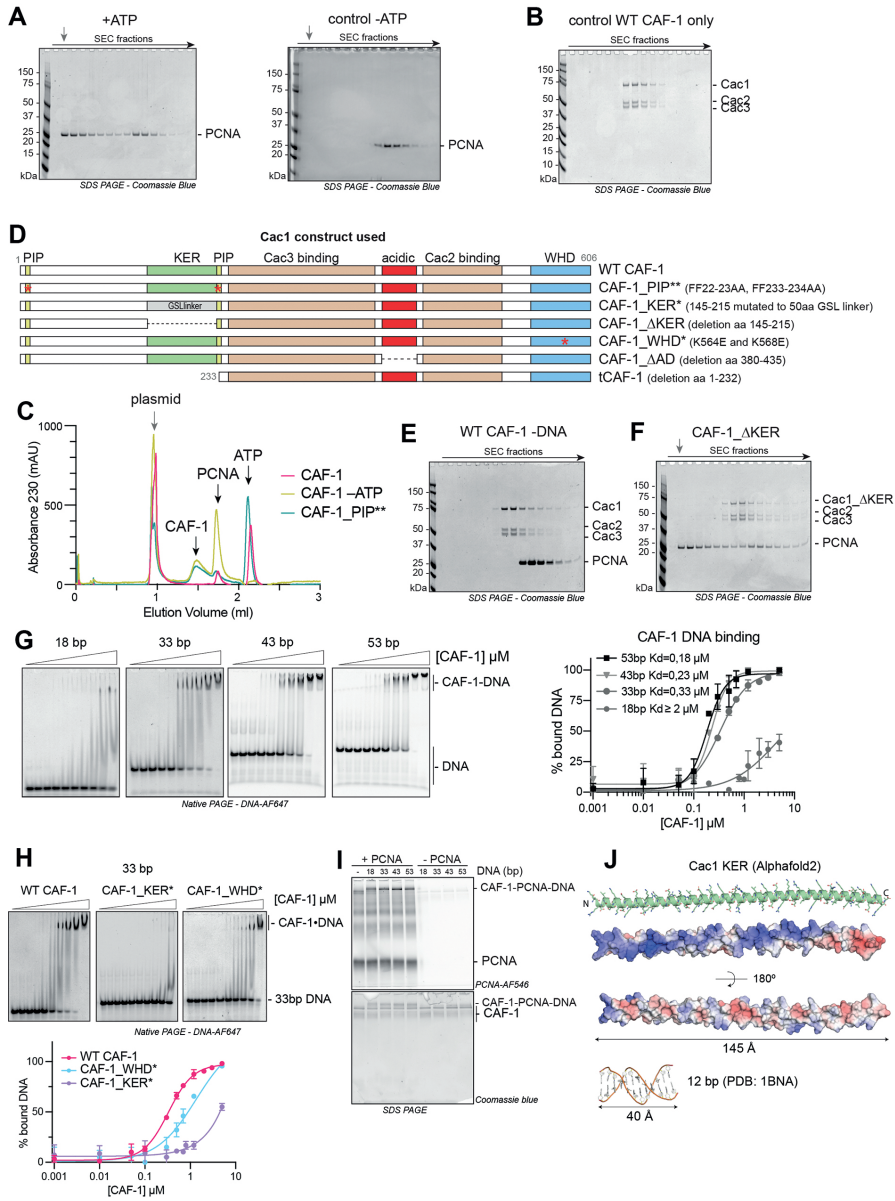
We thank John Diffley, Peter Burgers, Xiaodong Zhang, Rafael Fernández Leiro and Zhihao Zhuang for sharing reagents, Titia Sixma and Shreya Dharadhar for help with RFC Δ N purification, Juan Garaycochea for discussions and critical reading of the manuscript, Anke Sparmann at Life Science Editors for editing services (www.lifescienceeditors.com), Jamie Barnett for designing and sharing primers for NGS, Jan Dreyer for discussions on the PCNA-NAQ assay, The Histone Source at Colorado State University for lyophilized histones, and the CPR/ReNew Genomics platform.

Fundings

F.M. is funded by the Dutch Cancer Society (KWF 2014-6649) and the European Union (ERC-StG 851564). A.G. is supported by the European Research Council (ERC CoG 724436), the Lundbeck Foundation (R198-2015-269 and R313-2019-448), and the Independent Research Fund Denmark (7016-00042B) and the Novo Nordisk Foundation (NNF14OC0012839). Research at CPR is supported by the Novo Nordisk Foundation (NNF14CC0001). A.B. was supported by Marie Curie Individual Fellowship (841620). N.D. acknowledges funding from the Netherlands Organization for Scientific Research (NWO) through Top grant 714.017.002 and from the European Research Council through an Advanced Grant (REPLICHROMA; 789267). R.A.S. is funded through the European Union Horizon 2020 program INFRAIA project Epic-XS (Project 823839) and the research program NWO TA with project number 741.018.201, which is partly financed by NWO. P.K. was supported by the European Research Council (ERC) through an ERC Consolidator Grant (ERCCOG 101003210-XlinkRepair) and by the Onco Institute, which is partly financed by the Dutch Cancer Society (KWF). K.S. was supported by the Japanese Biochemical Society through the Osamu Hayaishi Memorial Scholarship for Study Abroad.

Conflict Of Interest

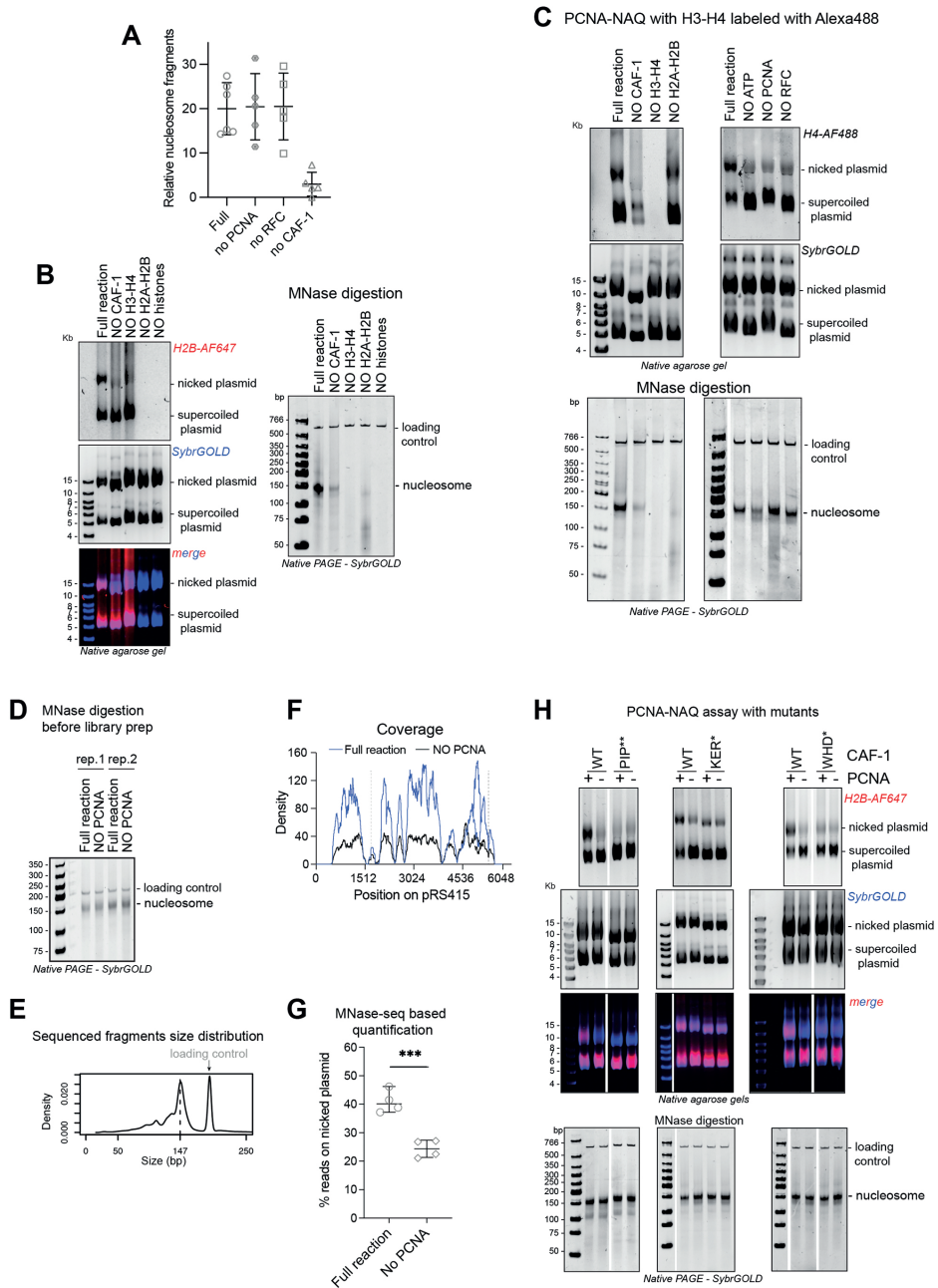
A.G. is cofounder and chief scientific officer (CSO) of Ankrin Therapeutics. The authors declare no competing interests.



Supplementary Figure S1 (Legend on next page)

Supplementary Figure S1

A) SDS PAGE following separation on SEC of a PCNA loading reaction on DNA plasmids (on the left) and the control omitting ATP (on the right). The grey arrow indicates the elution volume of the plasmid DNA. **B)** SDS PAGE following separation on SEC of WT CAF-1 only. **C)** Chromatogram (230 nm signal) of the Superose 6 runs whose SDS PAGE gels are shown in Figure 1A-C. The grey arrow indicates the elution volume of the plasmid DNA. Elution volume for CAF-1, PCNA and ATP are marked by black arrows. **D)** Cartoons of the Cac1 (large CAF-1 subunit) domains and the mutants used in this study. All complexes contain Cac2 and Cac3, in addition to the indicated Cac1 construct. **E)** SDS PAGE following separation on SEC of a control reaction where the DNA plasmid was omitted, from a CAF-1-PCNA binding experiment as in Figure 1A. **F)** SDS PAGE following separation on SEC of a CAF-1-PCNA binding reaction on nicked DNA plasmid using a CAF-1_ΔKER mutant. The grey arrow indicates the elution volume of the plasmid DNA. **G)** EMSA experiments and quantification of CAF-1 binding to double-stranded DNA fragments. Each 18-33-43-53 bp DNA fragment carries a AF647 fluorophore for detection and quantification. Disappearance of the unbound DNA band was used to calculate binding at different CAF-1 concentrations. Binding affinities K_d result from fitting the calculate data in GraphPad. 18 bp data is fitted with a One Site total binding curve, while the data with 33-43-53 bp DNA was fit accounting for cooperativity. The Hill coefficients obtained for these curves are 1.6, 2.7, 2.4 respectively. Means \pm SD is shown for each data point. At least three replicates were done for each experiment. **H)** EMSA experiments and quantification of binding to a 33-bp double-stranded DNA fragment of CAF-1_KER* and CAF-1_WHD* mutants. Disappearance of the unbound DNA band was used to calculate binding at different CAF-1 concentrations. Means \pm SD is shown for each data point. At least three replicates were done for each experiment. **I)** Crosslinking experiment between CAF-1 (3 mM) and labeled PCNA (4.5 mM) on DNA fragments (1.5 mM) of various sizes. DNA was not digested in these reactions. RFC and ATP were not added to actively load PCNA. These are the full gels of Figure 1G. **J)** Alphafold model of the KER domain in Cac1 (residues 128-226). Cartoon with sticks and electrostatics are shown. The electrostatics are calculated with the APBS plugin in Pymol. Blue is +5kEV and Red is -5kEV. A 12bp structure of B-DNA (PDB: 1BNA) is shown at the same scale of the KER domain for length comparison.



Supplementary Figure S2 (Legend on next page)

Supplementary Figure S2

A) Bioanalyzer-based quantification of nucleosome assembly (140-160 bp fragments) relative to the 621 bp loading control shows that CAF-1 is the main nucleosome assembly factor in our reactions.

B) Left panel: Native agarose gel of control PCNA-NAQ assay conditions. Fluorescence signal for H2B-T112C labeled with AF647 (H2B-AF647) or DNA (SybrGOLD), and their overlay are shown. H2B fluorescence on the nicked plasmid (top panel) represents PCNA-dependent histone deposition. Right panel: Native PAGE stained with SybrGOLD of protected DNA fragments following MNase digestion. 150bp DNA fragments are characteristic of nucleosomal DNA, a 621bp loading control is used to monitor DNA retrieval during the purification procedure.

C) Top panels: Native agarose gel of control PCNA-NAQ assay conditions where instead of fluorescently labeled H2A-H2B, we used labeled H3-H4. Fluorescence signal for H4-E63C labeled with AF488 (H4-AF488) is shown. Subsequently we stained with SybrGOLD to image DNA. H4 fluorescence on the nicked plasmid (top panel) represent PCNA-dependent histone deposition. Bottom panels: Native PAGE stained with SybrGOLD of protected DNA fragments following MNase digestion. 150bp DNA fragments are characteristic of nucleosomal DNA, a 621bp loading control is used to monitor DNA retrieval during the purification procedure.

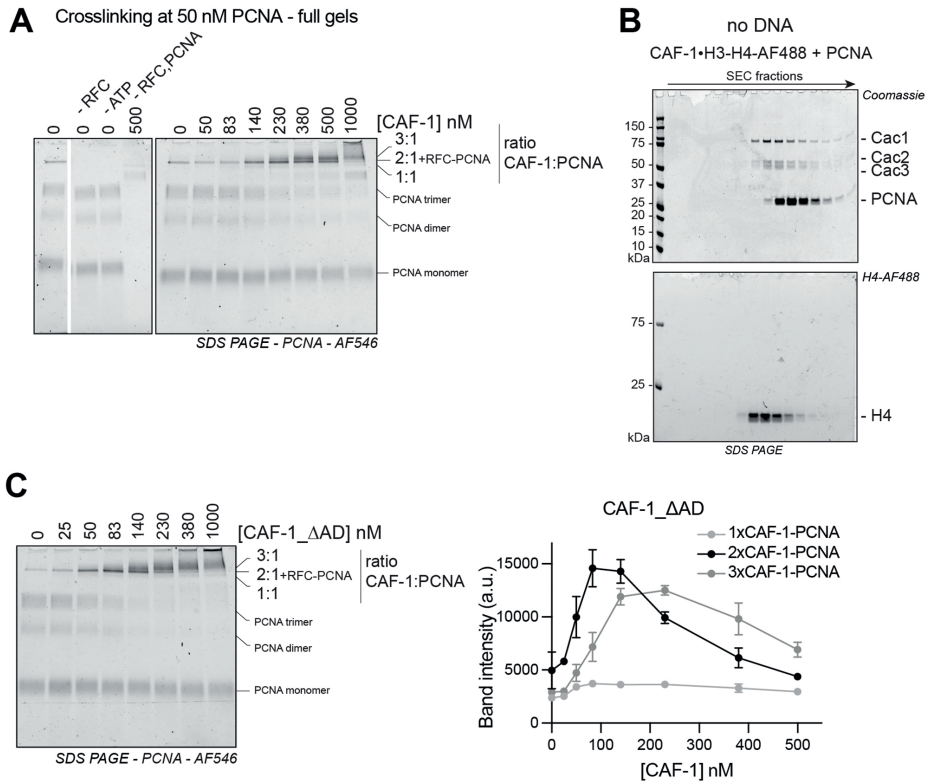
D) MNase digestion gel of PCNA-NAQ assay samples obtained for NGS analysis. These reactions contained a nicked and supercoiled plasmid with different sequences (pRS415 or pLox3). We used a 207 bp DNA loading control containing a 601-widom sequence.

E) Fragment size distribution of the sequenced reads confirms the dominance of a 150 bp size after MNase digestion and sequencing.

F) Example of reads coverage on the nicked plasmid when pRS415 was used in the full reaction or in a negative control reaction omitting PCNA. Dashed lines show the sites of nicking.

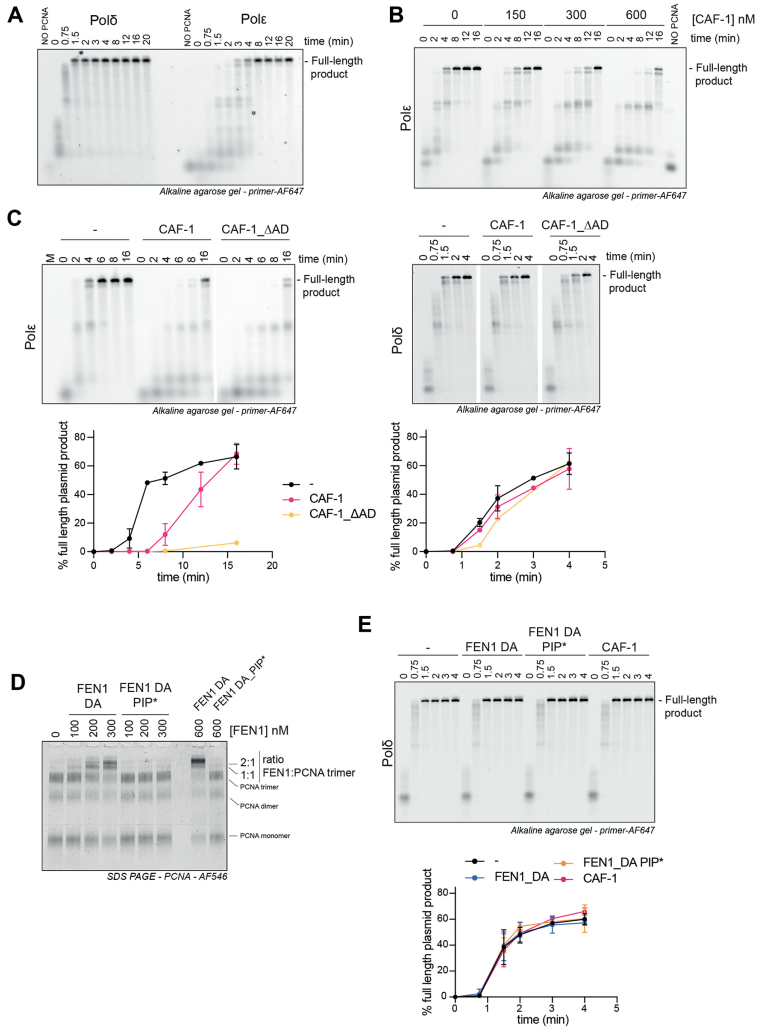
G) Quantification of the PCNA-dependent nucleosome assembly activity based on the NGS reads of WT CAF-1 and a no-PCNA control reaction. The percentage of reads on the nicked plasmid is shown over the total number of reads (for both plasmids). Means \pm SD is shown, and an unpaired t-test was applied to determine statistical significance, *** $p > 0,001$.

H) Native agarose gel (top) of control PCNA-NAQ assay conditions with CAF-1 mutants. Fluorescence signal for H2B-T112C labeled with AF647 (H2B-AF647) or DNA (SybrGOLD), and their overlay are shown. H2B fluorescence on the nicked plasmid (top panel) represents PCNA-dependent histone deposition. Bottom: Native PAGE stained with SybrGOLD of protected DNA fragments following MNase digestion. 150bp DNA fragments are characteristic of nucleosomal DNA, a 621bp loading control is used to monitor DNA retrieval during the purification procedure. Quantifications of H2B fluorescence are shown in Figure 2C.



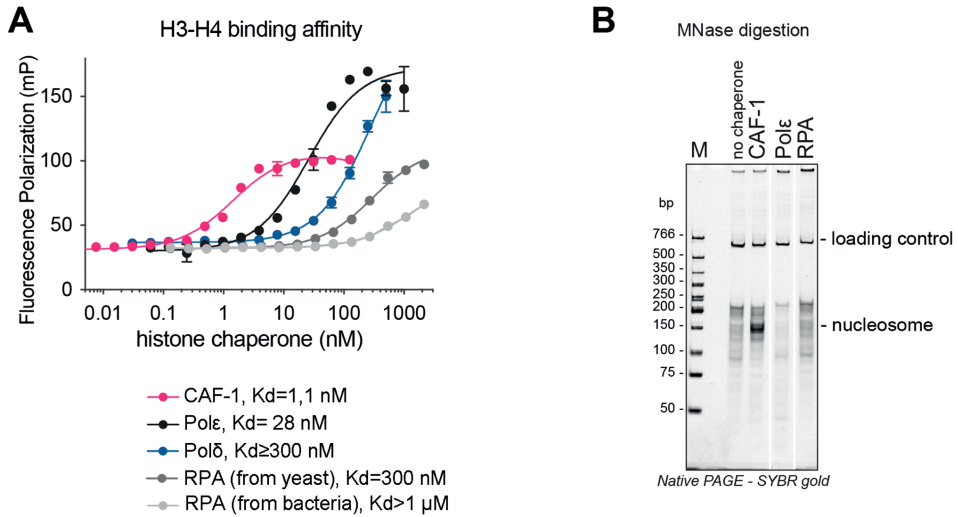
Supplementary Figure S3

A) Full gels of data in Figure 3C. PCNA fluorescence scan of SDS-PAGE of crosslinking experiment after DNA digestion, of reactions containing 50 nM PCNA, 15 nM RFC, 15 nM pUC19 and increasing CAF-1 concentrations. **B)** SDS PAGE after SEC of a reaction containing PCNA (30 M), and CAF-1 preloaded with labeled H3-H4 (5 M). No DNA or RFC is present in these reactions. After SDS PAGE run, we scan the gel for the H4-488 nm fluorescence (bottom), followed by staining with Coomassie (top). **C)** PCNA fluorescence scan of SDS-PAGE following protein-protein crosslinking after DNA digestion. These reactions contain 50 nM PCNA, 15 nM RFC, 15 nM pUC19 and increasing CAF-1 Δ AD concentrations. On the right: quantification of the CAF-1-PCNA bands. Mean \pm SD is shown of three replicates.



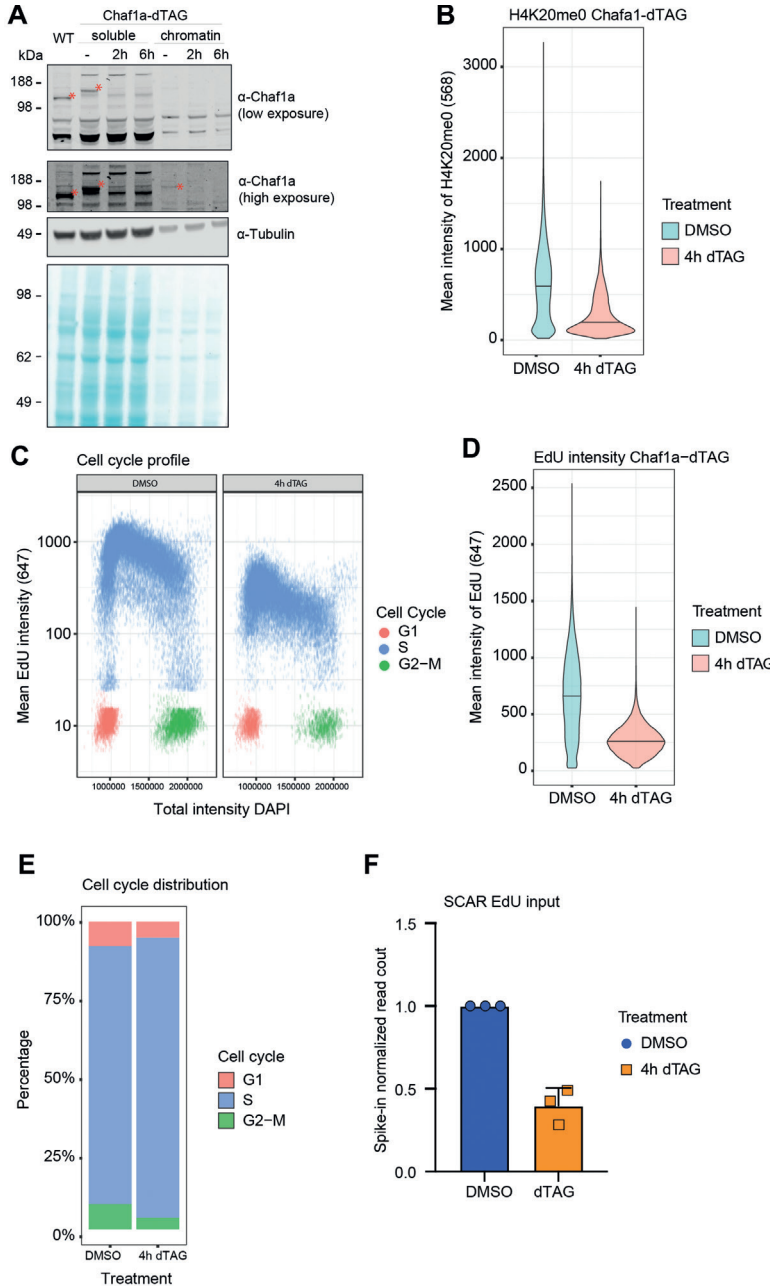
Supplementary Figure S4

A) Fluorescence (primer signal) scan of denaturing alkaline agarose gel of primer extension reactions with Polδ or Polε. The polymerases were at 120 nM, PCNA 480 nM. Both polymerases are active with different kinetics. Both polymerases depend on PCNA for activity. The NO-PCNA control lanes contain reactions that incubated for 20 minutes. **B)** Fluorescence (primer signal) scan of denaturing alkaline agarose gel of primer extension reactions with Pole in the presence of increasing amounts of WT CAF-1 (150-300-600 nM). **C)** Fluorescence (primer signal) scan of denaturing alkaline agarose gel of primer extension reactions with Pole (left) or Polδ (right) in the presence of CAF-1 WT or CAF-1_ΔAD (300 nM). Bottom: Quantification of the full-length product band relative to the total fluorescence in each lane (expressed as percentages). Mean ±SD are shown for three replicates. **D)** PCNA fluorescence scan of SDS-PAGE following protein-protein crosslinking. These reactions contain 50 nM PCNA and increasing FEN1_DA or FEN1_DA PIP* concentrations. **E)** Left panel: fluorescence (primer signal) scan of denaturing alkaline agarose gel of primer extension reactions with Polδ in the presence of WT CAF-1, FEN1_DA and FEN1_DA PIP* (all at 300 nM). Right panel: Quantification of the full-length product band relative to the total fluorescence in each lane (expressed as percentages). Mean ±SD are shown for three replicates.



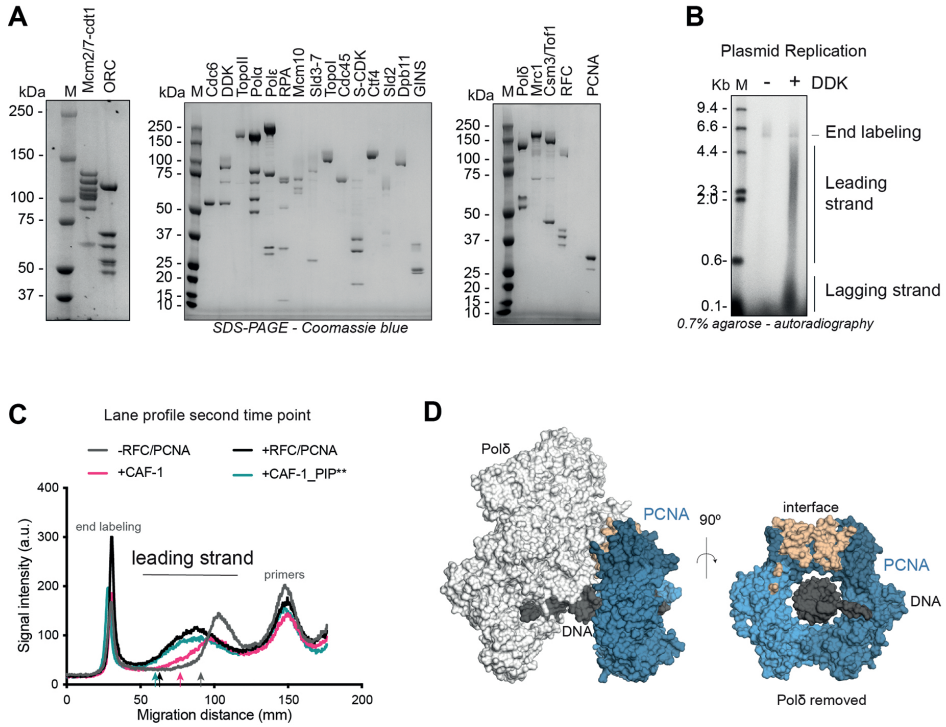
Supplementary Figure S5

A) Fluorescence polarization experiment to test binding to H3-H4 (where H4 is labeled at E63C using AF488). CAF-1, Pole, Pol δ , RPA expressed in yeast (used in Figure 7A) and RPA expressed in bacteria (used in Figure 4-5) were titrated to a solution containing 10 nM of labeled H3-H4. The data points were fit to a one site binding curve and the K_d were calculated in GraphPad. **B)** MNase digestion of a NAQ reaction where each histone chaperone was incubated with the histone octamer and subsequently with 207 bp DNA. Bands at 150 bp represent nucleosomes and these are observed only in the presence of CAF-1. RPA produced from yeast cells was used. A 621 bp loading control DNA is used to control for sample retrieval during the DNA purification step.



Supplementary Figure S6

A) Western blot analysis of soluble and chromatin fractions of mES cells treated with DMSO and dTAG for the indicated times. A WT cell line is shown as a control. **B)** Immunofluorescence results of mean H4K20me0 intensities in mESC upon CAF-1 depletion with dTAG shows a decrease in H4K20me0. **C)** Immunofluorescence results of mean EdU intensity vs total DAPI intensity. **D)** Mean EdU intensity in DMSO vs dTAG treated cells. **E)** Cell cycle distribution based on mean EdU intensity and total EdU intensity. Immunofluorescent data are represented from two replicates. **F)** Spike-in normalized input reads shows decreased EdU incorporation after depletion of CAF-1.



Supplementary Figure S7

A) SDS PAGE of protein preps that were used to reconstitute the yeast replisome. **B)** Autoradiography scan of denaturing agarose gel separation using DNA replication products, from an end-point plasmid replication experiment containing all yeast replisome components or, as control, omitting DDK. **C)** Example of lane profiles during pulse-chase experiment after 5 minutes of addition of the chase, as obtained by ImageQuant. The arrows indicate the front of the leading strand (created automatically by ImageQuant), used as the max size of replicated products to calculate the max replication rates. **D)** Surface visualization of yeast Polδ (in white) bound to PCNA (blue) on DNA (dark gray) from PDB 7KC0. In wheat we show the PCNA residues involved in the Pol interaction. On the right panel Polδ is not displayed.

Supplementary Information

Supplementary Table S1: Primers used for EMSA.

DNA primers	Reference
DNA oligo 18mer forward: GTCTACGAGCAATTGAGC	Mattioli et al., 2017
DNA oligo 18mer reverse: GCTCAATTGCTCGTAGAC	Mattioli et al., 2017
DNA oligo 33mer forward: GCTGTCTACGAGCAATTGAGCGCCTCGGCACC	Mattioli et al., 2017
DNA oligo 33mer reverse: GGTGCCGAGCCGCTCAATTGCTCGTAGACAGC	Mattioli et al., 2017
DNA oligo 43mer forward, 5' conjugated to AlexaFluor 647: CTAGAGCTGTCTACGAGCAATTGAGCGCCTCGGCACCGGGAT	This paper
DNA oligo 43mer reverse: ATCCCGGTGCCGAGCCGCTCAATTGCTCGTAGACAGCTCTAG	This paper
DNA oligo 53mer forward, 5' conjugated to AlexaFluor 647: CGGTGCTAGAGCTGTCTACGAGCAATTGAGCGCCTCGGCACCGGGATTCTGA	This paper
DNA oligo 53mer reverse: TCAGAAATCCCGGTGCCGAGCCGCTCAATTGCTCGTAGACAGCTCTAGCACCG	This paper

Supplementary Table S2, DNA sequences for plasmids and linear fragments used in MNase-seq

Name	DNA sequence
pLox3	AACGACCTACACCGAACTGAGATACCTACAGCGTGAGCTATGAGAAAGCGCCACGCTTCCCG AAGGGAGAAAGGCGGACAGGTATCCGGTAAGCGGCAGGGTCGGAACAGGAGAGCGCACGA GGGAGCTTCCAGGGGAAACGCCTGGTATCTTTATAGTCTGTGCGGTTTCGCCACCTCTGAC TTGAGCGTCGATTTTTGTGATGCTCGTCAGGGGGGCGGAGCCTATGAAAAACGCCAGCAAC GCGGCCCTTTTACGGTTCTGCGCCTTTTGCTGGCCTTTTGCTCACATGTCTTTCTGCGTTA TCCCTGATTGACTTGGGTCGCTCTTCTGTGGATGCCAGATGCCCTGCGTAAGCGGGTGTG GGCGGACAATAAAGTCTTAAACTGAACAAAATAGATCTAAACTATGACAATAAAGTCTTAAAC TAGACAGAATAGTTGTAAACTGAAATCAGTCCAGTTATGCTGTGAAAAAGCATACTGGACTTT TGTTATGGCTAAAGCAAACCTTCATTTTCTGAAGTGCAAATTCGCCGTCGTATTAAGAGGG GCGTGGCCAAGGGCATGTAAGACTATATTCGCGGCGTTGTGACAATTTACCGAACAACCTCCG CGGCCGGGAAGCCGATCTCGCCTTGAACGAATTGTTAGGTGGCGGTACTTGGGTCGATATCAA AGTGCATCACTTCTTCCCGTATGCCCAACTTTGTATAGAGAGCCACTGCGGGATCGTACCCTGA ATCTGCTTGACGCTAGATCACATAAGCACCAAGCGCGTTGGCCTCATGCTTGAGGAGATTGAT GAGCGCGGTGGCAATGCCCTGCCCTCCGGTCTCGCCGAGACTGCGAGATCATAGATATAGAT CTCACTACGCGGCTGCTCAAACCTGGGCAGAACGTAAGCCGCGAGAGCGCCAACAACCGCTT CTTGGTCGAAGGCAGCAAGCGCGATGAATGTCTTACTACGGAGCAAGTCCCGAGGTAATCGG AGTCCGGCTGATGTTGGGAGTAGGTGGCTACGTCTCCGAACCTCACGCCGAAAGATCAAGA GCAGCCCGCATGGATTTGACTTGGTCAGGGCCGAGCCTACATGTGCGAATGATGCCATACTT GAGCCACCTAACTTTGTTTTAGGGCGACTGCCCTGCTGCGTAACATCGTTGCTGCTGCGTAAC ATCGTTGCTGCTCCATAACATCAAACATCGACCCACGCGGTAACGCGCTTGCTGCTGGATGC CCGAGGCATAGACTGTACAAAAAACAGTCATAACAAGCCATGAAAACCGCCACTGCGCCGT TACCACCGCTGCGTTCCGTCAAGTCTTGGACCAGTTGCGTGAGCGATACGCTACTTGCATT ACAGTTTACGAACCGAACAGGCTTATGTCAAAGTGGTTTCGTGCCTTCATCCGTTTCCACGGTG TGCGTACCCCGCAACCTTGGGCAGCAGCGAAGTCGCCATAACTTCGTATAGCATAACATTATA CGAAGTTATCTGCCAGGCACATGGGTTTTACTAGTATCGATTTCGCGACCTACTCCGGAAATTA ATAGATCATGGAGATAATTAATAATGATAACCATCTCGAAATAAATAAGTATTTACTGTTTTTC GTAACAGTTTTGTAATAAAAAAACCTATAAATATCCGGATATTTCATACCGTCCCACCATCGG GCGCGGATCCCGACCATGCATCACCATCACCATCACCATAATCAGTGCCGGAAGGACGCGCG

Name	DNA sequence
	<p>GATCCCGACCATGCATCACCATCACCATCACCATAATCAGTGCGCGAAGGACATAACTCATGAA GCCTCCAGTATACCCATCGATTTCGAAGAAAGATACTCGCACTGGAAGAAAAACACTAAACTA CTTTATGATTACCTAAACACGAATCAACAAGTGGCCGCTCTTAACGTGCCAGTCTTTTCT GATTTAGATACCCTTCGGATGAGCATCGCATCTGTTATCCCTCATTTACATCTTCCCAAAAAC CTGAAGATGAGACCATATATATTAGCAAAAATATCCACGTTGGGTCAATAAAAATGGTCACTTT AAATAATTTGCACATGGACGAAATGGAATCAAACCGGAGAAGTTCGACAAGGTTTCCCTCCA AACACTTAGTAAATGACATCAGTATTTTCTTCCCAAACGGGGAATGCAATAGGGCAAGATATT TGCCTCAAAAATCCAGATATTATAGCCGGCCCTCTTCAGATGGTGAATCTACATATTCGATAG AACAAAACACGGCTCTACTAGAATAAGACAGTCCAAAATTCACATCCCTTTGAGACAAAAGCT GTTTGGTTACATGGTGTATTCAAGACGTGGAGGCAATGGATACTTCTTCGGCAGATATAAAT GAGGCGACTTCTTTAGCCTGGAAGTTCGAGCAGGAGGCCCTTTACTTTCTTCTCACTCCAAC GGCCAAGTTCAAGTTTGGGACATTAACAATATTCGCATGAGAACCCTATAATAGATTTACCC TTAGTGTCATAAACAGCGACGGAACAGCGGTGAATGATGTAACCTGGATGCCAACACACGAT TCCCTCTTTGCTGCTTGTACTGAAGGAAATGCGGTCTCCCTATTAGATCTGAGGACTAAGAAA GAGAAGTCCAGAGTAACCGTGAAAAACAGATGGTGGAGTAAACTCCTGTAGATTTAACTAT AAGAAGCTTTTAATTTAGCATCTGCAGATTCAAAATGGGAGGCTAAATTTATGGGATATTAGAA ACATGAACAAAAGCCCAATCGTACCATGGAGCACGGTACTTCCGTTTCAACTTTAGAATGGA GTCCAATTTTCGATACTGTATTGGCAACGGCTGGCCAAGAAGATGGGTAGTCAAGCTATGGG ATACCTCCTGCGAAGAACTATATTTACCATGGTGGTCAATGCTCGGTGTGAACGACATTTT GTGGGACGCTCATGACCCCTGGTTAATGTGCAGTGTGGCAAATGATAATTCAGTTACATATGG AAACCTGCAGGAAACCTTGTGGACATTCGTGAGCTTAGAGCTCGAGCTCGACAGCTTG TCGAGAAGTACTAGAGGATCATAATCAGCCATACCACATTTGTAGAGGTTTTACTTGCTTTAAA AAACCTCCCACACCTCCCCCTGAACCTGAAACATAAAATGAATGCAATGTTGTTGTTAACTT GTTTTATTGCAGCTTATAATGGTTACAAAATAAAGCAATAGCATCACAATTTACAAAATAAAGCA TTTTTTTCACTGCATTTAGTGTGGTTTTGTCCAAACTCATCAATGTATCTTATCATGTCTGGA TCTGATCACTGCTTGAGCCTAGAAGATCCGGCTGTAACAAAGCCGAAAGGAAGCTGAGTT GGCTGTGCCACCGCTGAGCAATAACTATCATAACCCCTAGGTGCCATTTTACCTACTTTCT CCGCACCCGACATAGATCTGGGCCAATTTTGGCGAAAATGAGACGTTGATCGGCACGTAAG AGGGTCCAACCTTACCATAATGAAATAAGATCACTACCGGGCTATTTTTGAGTTATCGAG ATTTTCAGGAGCTAAGGAAGCTAAAATGGAGAAAAAATCACTGGATATACCACCGTTGATAT ATCCCAATGGCATCGTAAAGAACATTTGAGGCATTTCACTGCAAGTGTCTCAATGTACCTATAAC CAGACCGTTCACTGAGTATTCAGGCTTTTTAAAGACCGTAAAGAAATAAGTACCAAGTTT TATCCGGCTTTATTCACATTTCTGCCCGCTGATGAATGCTCATCCGGAATTCGGTATGGCAA TGAAAGACGGTGAAGCTGGTATGGGATAGTGTACCCTTGTACACCGTTTTCCATGAGC AAACTGAAACGTTTTTCATCGCTCTGGAGTGAATACCACGACGATTTCCGGCAGTTTCTACACA TATATTCGAAGATGTGGCGTGTACGGTGAACACCTGGCCTATTTCCCTAAAGGGTTATTG AGAATATGTTTTCTGCTCAGCCAATCCCTGGGTGAGTTTCCACCTTTTGATTTAAACGGTGG CCAATAGACAACCTTCTTCGCCCCGTTTTACCATGGGCAAAATTTATAGCAAGCCGACACA AGGTGCTGATGCCGCTGGCGATTCAGGTTTCATCATGCCGTTTGTGATGGCTTCCATGTCGGCA GAATGCTTAATGAATTACAACAGTACTGCGATGAGTGGCAGGGCGGGCGTAATTTTTTAAG GCAGTTATTGGTGCCCTTAAACGCCTGGTTGCTACGCCTGAATAAGTGATAATAAGCGGATGA ATGGCAGAAATTCGAAAGCAAATTCGACCCGGTCTGCGTTTCCAGGGCAGGGTCTGTTAAATAG CCGCTTATGTCTATTGGTGTTTACC GGTTTATTGACTACCGGAAGCAAGTGTGACCGTGTGCTT CTCAAATGCCTGAGGCCAGTTTGTCTAGGCTCTCCCGTGGAGGTAATAATTGACGATATGAT CATTTATCTGCCTCCAGCTGACATTCATCCGGGTGAGCACCGTTTCTGCGGACTGGCTTT CTACGTGTTCCGCTTCTTTAGCAGCCCTTGCGCCCTGAGTGTCTGCGGCAGCGTGAAGCTAA TTCCCATGTCAGCGCTTAAGTGTCTGTGCTCACTCAAAAATGCTTTGAGAGGCTCTAAGGGC TTCTCAGTGCCTTACACTCCCTGGCTTGTGTCCACAACCGTTAAACCTTAAAGCTTAAAGCTTAAAG CCTTATATATCTTTTTTTCTTATAAAACTTAAACCTTAGAGCTATTTAAGTTGCTGATTTA TATTAATTTTATGTTCAAACATGAGAGCTTAGTACGTGAAACATGAGAGCTTAGTACGTTAGC CATGAGAGCTTAGTACGTTAGCCATGAGGGTTTAGTTCGTAAACATGAGAGCTTAGTACGTTA AACATGAGAGCTTAGTACGTGAAACATGAGAGCTTAGTACGTACTATCAACAGGTTGAACTGC TGATCAACAGATCCTCTACGCGGCCGCGGTACCATAACTTCGTATAGCATAACATATACGAAGT TATCTGTAACATAACGGTCTTAAGGTAGCGAGTTTAAACACTAGTATCGGATTCGCGACCTACT CCGGAATATTAATAGATCATGGAGATAATTAATGATAACCATCTCGCAATAAATAAGTATT TTACTGTTTTCGTAACAGTTTTGTAATAAAAAAACCTATAAATATCATAATCAGCCATACCACA TTTTGTAGAGGTTTTACTTGCTTTAAAAAACCTCCCACACCTCCCGTGAACCTGAAACATAAA</p>

Name	DNA sequence
	<p>ATGAATGCAATTGTTGTTAACTTGTTTATTGCAGCTTATAATGGTTACAAATAAAGCAA TAGCATCACAAATTCACAAATAAAGCATTTTTTTCACCTGCATTCTAGTTGTGGTTGTCC AAACTCATCAATGTATCTTATCATGTCTGGATCTGATCACTGCTTGAGCCTAGAAGATCCGG CTGCTAACAAAGCCCGAAAGGAAGCTGAGTGGCTGCTGCCACCCTGAGCAATAACTAT CATAACCCTAGGGTATACCCATCTAATTGGAACCCAGATAAGTGAAATCTAGTTCCAAACCTA TTTTGTCATTTTTAATTTTCGTATTAGCTTACGACGCTACACCCAGTCCCATCTATTTTGTG ACTCTTCCTAAATAATCCTTAAAACTCCATTTCCACCCCTCCAGTCCCAACTATTTTGT TCCGCCACAACCGGTTGACTTGGGTCAACTGTCAGACCAAGTTTACTCATATATACTTTAG ATTGATTTAAACTTCATTTTTAATTTAAAGGATCTAGGTGAAGATCCTTTTTGATAATCTC ATGACCAAAATCCCTTAAAGTGAGTTTTTCGTTCCACTGAGCGTCAGACCCCGTAGAAAAAGA TCAAAGGATCTTCTTGAGATCCTTTTTTCTGCGGTAATCTGCTGCTTGCAAACAAAAA ACCACCGCTACCAGCGGTGGTTTTGTTGCCGGATCAAGAGCTACCAACTCTTTTTCCGAAG GTAACGGCTTACGAGAGCGCAGATACAAATACTGTTCTTCTAGGTAGCCGTAGTTAGG CCACCCTTCAAGAACTCTGTAGCACCGCTACATACCTCGCTCTGCTAATCTGTTACCAG TGGCTGCTGCCAGTGGCGATAAGTCGTGCTTACCGGGTGGACTCAAGACGATAGTTACC GGATAAGCGCAGCGGTGCGGCTGAACGGGGGTTCTGTGCACACGCCAGCTTGGAGCG</p>
pRS415	<p>CGCTCCAAGCTGGGCTGTGTGCAGAACCCCGCTTTCAGCCGACCGCTGGCCTTATCCGGT AACTATCGTCTTGTAGTCCAACCCGGTAAGACACGACTTATCGCCACTGGCAGCAGCCACTGTA ACAGGATTAGCAGAGCGAGGTATGTAGGCGGTGCTACAGAGTCTTGAAGTGGTGGCCTAACTA CGGCTACACTAGAAGGACAGTATTTGGTATCTGCGCTCTGCTGAAGCCAGTTACCTTCGGAAAA AGAGTTGGTAGCTCTTGATCCGGCAAACAAACCACCGCTGGTAGCGGTGGTTTTTTGTTTGC AAGCAGCAGATACGCGCAGAAAAAAGGATCTCAAGAAGATCCTTTGATCTTTTCTACGGGG TCTGACGCTCAGTGGAAACGAAAAACTCACGTAAAGGATTTTGGTATGAGATATCAAAAAAGG ATCTTCACTAGATCCTTTTAAATTAAAAATGAAGTTTAAATCAATCTAAAGTATATATGAGTA AACTTGGTCTGACAGTTACCAATGCTTAATCAGTGAGGCACCTATCTCAGCGATCTGTCTATTC GTTTATCCATAGTTGCCCTGACTCCCCGTCGTGTAGATAACTACGATACGGGAGGGCTTACCATC TGGCCCCAGTGTGCAATGATACCGCGAGACCACGCTCACCAGCTCCAGATTTATCAGCAATA AACGACGACCGGGAAGGGCCGAGCGCAGAAGTGGTCTGCAACTTTATCCGCTCCATCCAG TCTATTAATTGTTGCCGGGAAGCTAGAGTAAGTAGTTCGCCAGTAAATAGTTTGCACAACGTTG TTGCCATTGCTACAGGCATCGTGGTGTACGCTCGTCTGTTGGTATGGCTCATTACAGCTCCGG TTCCCAACGATCAAGGCGAGTTACATGATCCCCATGTTGTGCAAAAAAGCGGTTAGCTCCTT CGGTCCTCCGATCGTTGTGAGAAGTAAGTTGGCCGAGTGTATCACTCATGGTTATGGCAGCA CTGCATAATCTCTTACTGTCTATGCCATCCGTAAGATGCTTTTCTGTGACTGGTGAGTACTCAAC CAAGTACTCTGAGAATAGTGTATGCGGGCACCAGTTGCTTGTGCCGCGCTGAATACGGGAT AATACCGCGCCACATAGCAGAACTTTAAAAGTGTCTATCATTGGAAAACGTTCTTCGGGGCGA AAACTCTCAAGGATCTTACCCTGTGAGATCCAGTTCGATGAACCCACTCGTGCACCCAACT GATCTTCAGCATCTTTACTTTACACAGCGTTTCTGGGTGAGCAAAAACAGGAAGGCAAAATG CCGCAAAAAAGGGAATAAGGGCGACACGGAAATGTTGAATACTCATCTTCTTTTTTCAAT ATTATTGAAGCATTATCAGGGTTATTGTCTCATGAGCGGATACATATTTGAATGTATTTAGAAA AATAACAAATAGGGGTTCCGCGCACATTTCCCGAAAAGTGCCACCTGGGTCCTTTTATCA CGTGCTATAAAAATAATTATAATTTAAATTTTTTAATATAAATATATAAATAAAAATAGAAAGT AAAAAAGAAATTAAGAAAAAATAGTTTTTGTGTTTCCGAAGATGTAAGAGACTCTAGGGGG ATCGCCAACAAATACTACCTTTTATCTTGCTTCTCTGCTCTCAGGTATTAATGCCGAATTGTT TCATCTGTCTGTGTAGAAGACCACACAGAAAATCCTGTGATTTTACATTTTACTTATCGTTA ATCGAATGTATATCTATTAACTGCTTTTTCTGTCTAATAATATATATGAAAGTACGCTTTT TGTTGAAATTTTTTAAACCTTTGTTTATTTTTTTTTTCTTCATTCCGTAACCTTCTACCTTCTT TATTTACTTTCTAAAATCCAAATACAAAACATAAAAAATAAATAAACACAGAGTAAATCCCAA ATTATCCATCATAAAAGATACGAGGCGCGTGAAGTTACAGGCAAGCGATCCGCTCTAAGA AACCATTATATCATGACATTAACCTATAAAAAATAGGCGTATCACGAGGCCCTTTCGCTCGCG CGTTTCGGTGATGAGCGTGAAACCTCTGACACATGCAGTCCCGGAGACGGTACAGCTTG TCTGTAAGCGGATGCCGGGAGCAGACAAGCCCGTCAGGGCGCTCAGCGGGTGTGGCGGG TGTGGGGCTGGCTTAACATGCGGCATCAGAGCAGATTGACTGAGAGTGCACCATATCGAC TACGTCGTTAAGGCCGTTTCTGACAGAGTAAATTTCTTGAGGGAACCTTACCATTATGGGAA ATGGTTCAAGAAGGATTTGACTTAACTCCATCAATGGTCAGGTCATTGAGTGTTTTTTATT TGTTGATTTTTTTTTTTTAGAGAAAATCCTCCAATATAAATTAGGAATCATAGTTTCAATG ATTTTCTGTTACACCTAACTTTTTTGTGTGGTGCCCTCCTCTTGTCAATATTAAGTTAAAGT</p>

Name	DNA sequence
	<p>CAATTCTTTTTCCTTATCACGTTGAGCCATTAGTATCAATTTGCTTACCTGTATTCCTTTACATCCT CCTTTTTCCTTCTTGATAAATGTATGTAGATTGCGTATATAGTTTCGTCTACCCTATGAACATATT CCATTTTGTAAATTCGTGTCGTTTCTATTATGAATTTCAATTTATAAAGTTTATGTACAAATATCATAA AAAAAGAGAATCTTTAAGCAAGGATTTCTTAACCTCTTCGGCGACAGCATCCCAGCATTCGG TGGTACTGTTGGAACCACTAAATCACCAGTTCTGATACCTGCATCCAAAACCTTTTAACTGCAT CTTCAATGGCCTTACCTTCTTCAGGCAAGTCAATGACAATTTCAACATCATGTCAGCAGACAAGA TAGTGGCGATAGGGTTGACCTTATCTTTGGCAAATCTGGAGCAGAACCGTGGCATGGTTCTGTACA AACCAAATGCGGTGTTCTTGTCTGGCAAAGAGGCCAAGGACGCAGATGGCAACAAACCCAAGGA ACCTGGGATAACGGAGGCTTCATCGGAGATGATATCACCAAACATGTTGCTGGTGATTATAATACCA TTTAGGTGGGTTGGGTTCTTAACCTAGGATCATGGCGGCAGAATCAATCAATGATGTTGAACCTTC AATGTAGGGAATTCGTTCTTGATGGTTTCTCCACAGTTTTCTCCATAATCTTGAAGAGGCCAAA ACATTAGCTTTATCCAAGGACCAAATAGGCAATGGTGGCTCATGTTGTAGGGCCATGAAAGCGGCC ATTCTTGTGATCTTTGCACTTCTGGAACGTTGATGTTCACTATCCCAAGCGACACCATACCA TCGCTTCTTCTTCTTACCAAAGTAAATACCTCCCCTAATCTCTGACAACAACGAAGTCAGTA CCTTTAGCAAATGTGGCTTGATTGGAGTAAGTCTAAAAGAGAGTCGGATGCAAAGTTACATGGT CTTAAGTTGGCGTACAATTTGAAGTTCTTTACGGATTTTTAGTAAACCTTGTTCAGGTTAACACTA CCGGTACCCCATTTAGGACCACCCACAGCACCTAACAAAACGGCATCAGCCTTCTTGGAGGCTTC CAGGCCTCATCTGGAAGTGAACACCTGTAGCATCGATAGCAGCACCACCAATTAATGATTTTC GAAATCGAATTGACATTGGAACGAACATCAGAAATAGCTTTAAGAACCTTAATGGCTTCGGCTG TGATTTCTTGACCAACGTGGTCACCTGGCAAACGACGATCTTCTAGGGGCAGACATAGGGGCA GACATTAGAATGGTATACCTTGAATATATATATATATATGCTGAAATGTAAAAGGTAAGAAAAG TTAGAAAGTAAGACGATTGCTAACCCATTTGGAACCAATAGGTCCTTAAATAATATTGTCA ACTTCAAGTATTGTGATGCAAGCATTTAGTCATGAACGCTTCTCTATTCTATATGAAAAGCCGGTTC CGGCCTCTCACCTTTCCCTTTTCTCCCAATTTTTCAAGTTGAAAAGGTTATATGCGTCAGGCGACC TCTGAAATTAACAAAAAATTTCCAGTCATCGAATTTGATCTGTGCGATAGCGCCCTGTGTGTT TCGTTATGTTGAGGAAAAAATAATGGTTGCTAAGAGATCGAACTCTTGACATCTACGATACCTG AGTATCCACAGTTAACTGCGGTCAAGATATTTCTTGAATCAGGCGCCTTAGACCCTCGGCCAA ACAACCAATTACTTGTGAGAAATAGAGTATAATATCTATAAATAACGTTTTTGAACACACAT GAACAAGGAAGTACAGGACAATGATTTTGAAGAGAATGTGGATTTTGATGTAATGTTGGGATTC CATTTTTAATAAGGCAATAATATTAGGTATATGGATATACTAGAAGTTCTCCTCGACCGGTCGATATG CGGTGTAATACCCGACAGATCGCTAAGGAGAAAAATACCGCATCAGGAATGTAAAGCGTTAAT ATTTTGTAAAATTCGGTTAAATTTTTGTAAAATCAGCTCATTTTTTAAACCAATAGCCGGAATC GGCAAATCCCTTATAAATCAAAAGAATAGACCGAGATAGGGTTGAGTGTGTTCCAGTTTGGAA CAAGAGTCCACTATTAAGAACGTGGACTCCAACGTCAAAGGGCGAAAAACCGTCTATCAGGGCG ATGCCCCACTACGTGAACCATCACCTAATCAAGTTTTTTGGGGTGCAGGTTGCCGTAAGCACTA AATCGGAACCCCTAAAGGGAGCCCCGATTTAGAGCTTGACGGGGAAAGCCGGCGAACGTGGCGA GAAAGGAAGGGAAGAAAGCGAAAGGAGCGGGCGTAGGGCGCTGGCAAGTGTAGCGGTCACGC TGCGGTAACCCACCAACCCCGGCTTAATGCGCCGCTACAGGCGCTTACCTCCGATTCA GGCTGCGCAACTGTTGGGAAGGGGATCGGTGCGGGCCTTTCGCTATTACGCCAGCTGGCGAAA GGGGATGTGCTGCAAGGCGATTAAGTTGGGTAACGCCAGGGTTTTCCAGTCACGACGTTGTAA AACGACGGCCAGTGAGCGCGCTAATACGACTCACTATAGGGCGAATTTGGTACCAGGGCCCCCCC TCGAGGTCGACGGTATCGATAAGCTTGATATCGAATTCCTGCAGCCGGGGGATCCACTAGTTCTA GAGCGCCGCCACCGCGGTGAGGTTCCAGCTTTTGTTCCTTTAGTGAGGGTTAATTTGCGCGCTT GGCGTAATCATGGTCATAGCTGTTTCTGTGTAATTTGTTATCCGCTCACAAATCCACACAACATA CGAGCCGGAAGCATAAAGTGTAAAGCCTGGGTGCCTAATGAGTGAGTAACTCACATTAATTGC GTTGCGCTCACTGCCGCTTCCAGTCGGGAAACCTGTCGTGCCAGCTGCATTAATGAATCGGCC AACGCGCGGGGAGAGGCGGTTTTCGCTATTGGGCGCTTCCGCTTCCGCTCACTGACTGCTGCTG CGCTCGGCTGTTCCGCTGCGGCGAGCGGTATCAGCTCACTCAAAGCGGTAATACGGTTATCCAC AGAATCAGGGGATAACGCAGGAAGAACAATGTGAGCAAAAAGGCCAGCAAAAAGCCAGGAACCC TAAAAAGGCCGCTTGTGGCGTTTTTCCATAGGCTCCGCCCCCTGACGAGCATCACAATAAT CGACGCTCAAAGTCAGAGGTGGCGAAACCCGACAGGACTATAAAGATACCAGGCGTTTCCCCCTG GAAGCTCCCTCGTGCGCTCTCCTGTTCCGACCCCTGCCGCTTACCGGATACCTGTCCGCTTTCTC CCTTCGGGAAGCGTGGCGCTTCTCATAGCTCACGCTGTAGGATCTCAGTTCCGGTGTAGGTCGTT</p>
207bp loading control	<p>ATCTAGTATTAATTAATGAATTCGGATCCACATGCACAGGATGTATATATCTGACACGTGCC TGGAGACTAGGAGTAATCCCTTGGCGGTTAAAACGCGGGGGACAGCGCGTACGTGCGTT TAAGCGGTGCTAGAGCTGTCTACGACCAATGAGCGGCCCTGGCACCGGATTTCTCCAGGGC GGCCGCTATAGGTTCCGAT</p>

References

1. Bellelli, R. and Boulton, S.J. (2021) Spotlight on the Replisome: Aetiology of DNA Replication-Associated Genetic Diseases. *Trends in Genetics*, **37**, 317–336.
2. Escobar, T.M., Loyola, A. and Reinberg, D. (2021) Parental nucleosome segregation and the inheritance of cellular identity. *Nat Rev Genet*, 10.1038/s41576-020-00312-w.
3. Hills, S.A. and Diffley, J.F.X. (2014) DNA Replication and Oncogene-Induced Replicative Stress. *Current Biology*, **24**, R435–R444.
4. Stewart-Morgan, K.R., Petryk, N. and Groth, A. (2020) Chromatin replication and epigenetic cell memory. *Nat Cell Biol*, **22**.
5. Bell, S.P. and Labib, K. (2016) Chromosome duplication in *Saccharomyces cerevisiae*. *Genetics*, **203**, 1027–1067.
6. Pellegrini, L. and Costa, A. (2016) New Insights into the Mechanism of DNA Duplication by the Eukaryotic Replisome. *Trends Biochem Sci*, **41**, 859–871.
7. Li, H. and O'Donnell, M.E. (2018) The Eukaryotic CMG Helicase at the Replication Fork: Emerging Architecture Reveals an Unexpected Mechanism. *BioEssays*, **40**, 1700208.
8. Yeeles, J.T.P., Deegan, T.D., Janska, A., Early, A. and Diffley, J.F.X. (2015) Regulated eukaryotic DNA replication origin firing with purified proteins. *Nature*, **519**, 431–435.
9. Yeeles, J.T.P., Janska, A., Early, A. and Diffley, J.F.X. (2017) How the Eukaryotic Replisome Achieves Rapid and Efficient DNA Replication. *Mol Cell*, **65**, 105–116.
10. Langston, L.D., Zhang, D., Yurieva, O., Georgescu, R.E., Finkelstein, J., Yao, N.Y., Indiani, C. and O'Donnell, M.E. (2014) CMG helicase and DNA polymerase ϵ form a functional 15-subunit holoenzyme for eukaryotic leading-strand DNA replication. *Proc Natl Acad Sci U S A*, **111**, 15390–15395.
11. Zhou, J.C., Janska, A., Goswami, P., Renault, L., Abid Ali, F., Kotecha, A., Diffley, J.F.X. and Costa, A. (2017) CMG-Pol epsilon dynamics suggests a mechanism for the establishment of leading-strand synthesis in the eukaryotic replisome. *Proc Natl Acad Sci U S A*, **114**, 4141–4146.
12. Nick McElhinny, S.A., Gordenin, D.A., Stith, C.M., Burgers, P.M.J. and Kunkel, T.A. (2008) Division of Labor at the Eukaryotic Replication Fork. *Mol Cell*, **30**, 137–144.
13. Burgers, P.M.J. and Kunkel, T.A. (2017) Eukaryotic DNA Replication Fork. *Annu Rev Biochem*, **86**, 417–438.
14. Guillian, T.A. and Yeeles, J.T.P. (2020) An updated perspective on the polymerase division of labor during eukaryotic DNA replication. *Crit Rev Biochem Mol Biol*, **55**, 469–481.
15. Chilkova, O., Stenlund, P., Isoz, I., Stith, C.M., Grabowski, P., Lundstrom, E.-B., Burgers, P.M. and Johansson, E. (2007) The eukaryotic leading and lagging strand DNA polymerases are loaded onto primer-ends via separate mechanisms but have comparable processivity in the presence of PCNA. *Nucleic Acids Res*, **35**, 6588–6597.

- 16.** Georgescu,R.E., Langston,L., Yao,N.Y., Yurieva,O., Zhang,D., Finkelstein,J., Agarwal,T. and O'Donnell,M.E. (2014) Mechanism of asymmetric polymerase assembly at the eukaryotic replication fork. *Nat Struct Mol Biol*, **21**, 664–670.
- 17.** Schauer,G.D. and O'Donnell,M.E. (2017) Quality control mechanisms exclude incorrect polymerases from the eukaryotic replication fork. *Proceedings of the National Academy of Sciences*, **114**, 675–680.
- 18.** Moldovan,G.L., Pfander,B. and Jentsch,S. (2007) PCNA, the Maestro of the Replication Fork. *Cell*, **129**, 665–679.
- 19.** Liu,H.W., Bouchoux,C., Panarotto,M., Kakui,Y., Patel,H. and Uhlmann,F. (2020) Division of Labor between PCNA Loaders in DNA Replication and Sister Chromatid Cohesion Establishment. *Mol Cell*, **78**, 725-738.e4.
- 20.** Yu,C., Gan,H., Han,J., Zhou,Z.X., Jia,S., Chabes,A., Farrugia,G., Ordog,T. and Zhang,Z. (2014) Strand-Specific Analysis Shows Protein Binding at Replication Forks and PCNA Unloading from Lagging Strands when Forks Stall. *Mol Cell*, **56**, 551–563.
- 21.** Sogo,J.M., Stahl,H., Koller,Th. and Knippers,R. (1986) Structure of replicating simian virus 40 minichromosomes. *J Mol Biol*, **189**, 189–204.
- 22.** McKnight,S.L. and Miller,O.L. (1977) Electron microscopic analysis of chromatin replication in the cellular blastoderm drosophila melanogaster embryo. *Cell*, **12**, 795–804.
- 23.** Alabert,C., Barth,T.K., Reverón-Gómez,N., Sidoli,S., Schmidt,A., Jensen,O.N., Imhof,A. and Groth,A. (2015) Two distinct modes for propagation of histone PTMs across the cell cycle. *Genes Dev*, **29**, 585–90.
- 24.** Stewart-Morgan,K.R., Reverón-Gómez,N. and Groth,A. (2019) Transcription Restart Establishes Chromatin Accessibility after DNA Replication. *Mol Cell*, 10.1016/j.molcel.2019.04.033.
- 25.** Escobar,T.M., Oksuz,O., Saldañ A-Meyer,R., Descostes,N., Bonasio,R. and Correspondence,D.R. (2019) Active and Repressed Chromatin Domains Exhibit Distinct Nucleosome Segregation during DNA Replication. *Cell*, **179**, 953–963.
- 26.** Ramachandran,S. and Henikoff,S. (2016) Transcriptional Regulators Compete with Nucleosomes Post-replication. *Cell*, **165**, 580–592.
- 27.** Franklin,R., Murn,J. and Cheloufi,S. (2021) Cell Fate Decisions in the Wake of Histone H3 Deposition. *Front Cell Dev Biol*, **9**.
- 28.** Smith,S. and Stillman,B. (1989) Purification and characterization of CAF-I, a human cell factor required for chromatin assembly during DNA replication in vitro. *Cell*, **58**, 15–25.
- 29.** Houlard,M., Berlivet,S., Probst,A. v., Quivy,J.P., Héry,P., Almouzni,G. and Gérard,M. (2006) CAF-1 is essential for heterochromatin organization in pluripotent embryonic cells. *PLoS Genet*, **2**, 1686–1696.
- 30.** Song,Y., He,F., Xie,G., Guo,X., Xu,Y., Chen,Y., Liang,X., Stagljar,I., Egli,D., Ma,J., *et al.* (2007) CAF-1 is essential for Drosophila development and involved in the maintenance of epigenetic memory. *Dev Biol*, **311**, 213–222.
- 31.** Fischer,S., Prikhozhiy,S., Rau,M.J. and Neumann,C.J. (2007) Mutation of zebrafish *caf-1b* results in S phase arrest, defective differentiation and p53-mediated apoptosis during organogenesis. *Cell Cycle*, **6**, 2962–2969.

- 32.** Cheloufi,S., Elling,U., Hopfgartner,B., Jung,Y.L., Murn,J., Ninova,M., Hubmann,M., Badeaux,A.I., Euong Ang,C., Tenen,D., *et al.* (2015) The histone chaperone CAF-1 safeguards somatic cell identity. *Nature*, **528**, 218–224.
- 33.** Franklin,R., Guo,Y., He,S., Chen,M., Ji,F., Zhou,X., Frankhouser,D., Do,B.T., Chiem,C., Jang,M., *et al.* (2022) Regulation of chromatin accessibility by the histone chaperone CAF-1 sustains lineage fidelity. *Nat Commun*, **13**, 2350.
- 34.** Ye,X., Franco,A.A., Santos,H., Nelson,D.M., Kaufman,P.D. and Adams,P.D. (2003) Defective S phase chromatin assembly causes DNA damage, activation of the S phase checkpoint, and S phase arrest. *Mol Cell*, **11**, 341–351.
- 35.** Hoek,M. and Stillman,B. (2003) Chromatin assembly factor 1 is essential and couples chromatin assembly to DNA replication in vivo. *Proceedings of the National Academy of Sciences*, **100**, 12183–12188.
- 36.** Quivy,J.-P.P., Gérard,A., Cook,A.J.L.L., Roche,D. and Almouzni,G. (2008) The HP1-p150/CAF-1 interaction is required for pericentric heterochromatin replication and S-phase progression in mouse cells. *Nat Struct Mol Biol*, **15**, 972–979.
- 37.** Gaillard,P.H.L., Martini,E.M.D., Kaufman,P.D., Stillman,B., Moustacchi,E. and Almouzni,G. (1996) Chromatin assembly coupled to DNA repair: A new role for chromatin assembly factor I. *Cell*, **86**, 887–896.
- 38.** Cheng,L., Zhang,X., Wang,Y., Gan,H., Xu,X., Lv,X., Hua,X., Que,J., Ordog,T. and Zhang,Z. (2019) Chromatin Assembly Factor 1 (CAF-1) facilitates the establishment of facultative heterochromatin during pluripotency exit. *Nucleic Acids Res*, 10.1093/nar/gkz858.
- 39.** Polo,S.E., Theocharis,S.E., Klijanienko,J., Savignoni,A., Asselain,B., Vielh,P. and Almouzni,G. (2004) Chromatin Assembly Factor-1, a Marker of Clinical Value to Distinguish Quiescent from Proliferating Cells. *Cancer Res*, **64**, 2371–2381.
- 40.** Volk,A., Liang,K., Suraneni,P., Li,X., Zhao,J., Bulic,M., Marshall,S., Pulakanti,K., Malinge,S., Taub,J., *et al.* (2018) A CHAF1B-Dependent Molecular Switch in Hematopoiesis and Leukemia Pathogenesis. *Cancer Cell*, **34**, 707-723.e7.
- 41.** Barbieri,E., de Preter,K., Capasso,M., Chen,Z., Hsu,D.M., Tonini,G.P., Lefever,S., Hicks,J., Versteeg,R., Pession,A., *et al.* (2014) Histone chaperone CHAF1A inhibits differentiation and promotes aggressive neuroblastoma. *Cancer Res*, **74**, 765–774.
- 42.** Zhang,Z., Shibahara,K.I. and Stillman,B. (2000) PCNA connects DNA replication to epigenetic inheritance in yeast. *Nature*, **408**, 221–225.
- 43.** Almouzni,G., Clark,D.J., Méchali,M. and Wolffe,A.P. (1990) Chromatin assembly on replicating DNA in vitro. *Nucleic Acids Res*, **18**, 5767–5774.
- 44.** Smith,S. and Stillman,B. (1991) Immunological characterization of chromatin assembly factor I, a human cell factor required for chromatin assembly during DNA replication in vitro. *J Biol Chem*, **266**, 12041–7.
- 45.** Kaufman,P.D., Kobayashi,R. and Stillman,B. (1997) Ultraviolet radiation sensitivity and reduction of telomeric silencing in *Saccharomyces cerevisiae* cells lacking chromatin assembly factor-I. *Genes Dev*, **11**, 345–357.

- 46.** Kaufman,P.D., Kobayashi,R., Kessler,N. and Stillman,B. (1995) The p150 and p60 subunits of chromatin assembly factor I: A molecular link between newly synthesized histories and DNA replication. *Cell*, **81**, 1105–1114.
- 47.** Verreault,A., Kaufman,P.D., Kobayashi,R. and Stillman,B. (1996) Nucleosome assembly by a complex of CAF-1 and acetylated histones H3/H4. *Cell*, **87**, 95–104.
- 48.** Shibahara,K.I. and Stillman,B. (1999) Replication-dependent marking of DNA by PCNA facilitates CAF-1-coupled inheritance of chromatin. *Cell*, **96**, 575–585.
- 49.** Moggs,J.G., Grandi,P., Quivy,J.-P., Jonsson,Z.O., Hubscher,U., Becker,P.B. and Almouzni,G. (2000) A CAF-1-PCNA-Mediated Chromatin Assembly Pathway Triggered by Sensing DNA Damage. *Mol Cell Biol*, **20**, 1206–1218.
- 50.** Krawitz,D.C., Kama,T. and Kaufman,P.D. (2002) Chromatin assembly factor I mutants defective for PCNA binding require Asf1/Hir proteins for silencing. *Mol Cell Biol*, **22**, 614–25.
- 51.** Tsirkas,I., Dovrat,D., Lei,Y., Kalyva,A., Lotysh,D., Li,Q. and Aharoni,A. (2021) Cac1 WHD and PIP domains have distinct roles in replisome progression and genomic stability. *Curr Genet*, **67**, 129–139.
- 52.** Ben-Shahar,T.R., Castillo,A.G., Osborne,M.J., Borden,K.L.B., Kornblatt,J. and Verreault,A. (2009) Two Fundamentally Distinct PCNA Interaction Peptides Contribute to Chromatin Assembly Factor 1 Function. *Mol Cell Biol*, **29**, 6353–6365.
- 53.** Mattioli,F., Gu,Y., Yadav,T., Balsbaugh,J.L.J.L., Harris,M.R.M.R., Findlay,E.S.E.S., Liu,Y., Radebaugh,C.A.C.A., Stargell,L.A.L.A., Ahn,N.G.N.G., *et al.* (2017) DNA-mediated association of two histone-bound complexes of yeast chromatin assembly factor-1 (CAF-1) drives tetrasome assembly in the wake of DNA replication. *Elife*, **6**, e22799.
- 54.** Mattioli,F., Gu,Y., Balsbaugh,J.L.J.L., Ahn,N.G.N.G. and Luger,K. (2017) The Cac2 subunit is essential for productive histone binding and nucleosome assembly in CAF-1. *Sci Rep*, **7**, 46274.
- 55.** Hibbert,R.G. and Sixma,T.K. (2012) Intrinsic Flexibility of Ubiquitin on Proliferating Cell Nuclear Antigen (PCNA) in Translesion Synthesis. *Journal of Biological Chemistry*, **287**, 39216–39223.
- 56.** Muthurajan,U., Mattioli,F., Bergeron,S., Zhou,K., Gu,Y., Chakravarthy,S., Dyer,P., Irving,T. and Luger,K. (2016) In Vitro Chromatin Assembly: Strategies and Quality Control. In *Methods in Enzymology*. Vol. 573, pp. 3–41.
- 57.** Dyer,P.N., Edayathumangalam,R.S., White,C.L., Bao,Y., Chakravarthy,S., Muthurajan,U.M. and Luger,K. (2004) Reconstitution of Nucleosome Core Particles from Recombinant Histones and DNA. *Methods Enzymol*, **375**, 23–44.
- 58.** Baretic,D., Jenkyn-Bedford,M., Aria,V., Cannone,G., Skehel,M. and Yeeles,J.T.P. (2020) Cryo-EM Structure of the Fork Protection Complex Bound to CMG at a Replication Fork. *Mol Cell*, **78**.
- 59.** Chen,J., Ai,Y., Wang,J., Haracska,L. and Zhuang,Z. (2010) Chemically ubiquitylated PCNA as a probe for eukaryotic translesion DNA synthesis. *Nat Chem Biol*, **6**, 270–272.

- 60.** Gomes, X. v., Gary, S.L. and Burgers, P.M.J. (2000) Overproduction in *Escherichia coli* and characterization of yeast replication factor C lacking the ligase homology domain. *Journal of Biological Chemistry*, **275**, 14541–14549.
- 61.** Yates, L.A., Aramayo, R.J., Pokhrel, N., Caldwell, C.C., Kaplan, J.A., Perera, R.L., Spies, M., Antony, E. and Zhang, X. (2018) A structural and dynamic model for the assembly of Replication Protein A on single-stranded DNA. *Nat Commun*, **9**, 5447.
- 62.** Mattioli, F., Gu, Y. and Luger, K. (2018) Measuring Nucleosome Assembly Activity in vitro with the Nucleosome Assembly and Quantification (NAQ) Assay. *Bio Protoc*, **8**, 1–11.
- 63.** Sato, K., Martin-Pintado, N., Post, H., Altelaar, M. and Knipscheer, P. (2021) Multistep mechanism of G-quadruplex resolution during DNA replication. *Sci Adv*, **7**.
- 64.** Blackledge, N.P., Fursova, N.A., Kelley, J.R., Huseyin, M.K., Feldmann, A. and Klose, R.J. (2020) PRC1 Catalytic Activity Is Central to Polycomb System Function. *Mol Cell*, **77**, 857–874.e9.
- 65.** Quivy, J.P., Roche, D., Kirschner, D., Tagami, H., Nakatani, Y. and Almouzni, G. (2004) A CAF-1 dependent pool of HP1 during heterochromatin duplication. *EMBO Journal*, **23**, 3516–3526.
- 66.** Hammond, C.M., Bao, H., Hendriks, I.A., Carraro, M., García-Nieto, A., Liu, Y., Reverón-Gómez, N., Spanos, C., Chen, L., Rappsilber, J., *et al.* (2021) DNAJC9 integrates heat shock molecular chaperones into the histone chaperone network. *Mol Cell*, 10.1016/j.molcel.2021.03.041.
- 67.** Petryk, N., Dalby, M., Wenger, A., Stromme, C.B., Strandsby, A., Andersson, R. and Groth, A. (2018) MCM2 promotes symmetric inheritance of modified histones during DNA replication. *Science (1979)*, **361**, 1389–1392.
- 68.** Petryk, N., Reverón-Gómez, N., González-Aguilera, C., Dalby, M., Andersson, R. and Groth, A. (2021) Genome-wide and sister chromatid-resolved profiling of protein occupancy in replicated chromatin with ChOR-seq and SCAR-seq. *Nat Protoc*, **16**, 4446–4493.
- 69.** Fursova, N.A., Blackledge, N.P., Nakayama, M., Ito, S., Koseki, Y., Farcas, A.M., King, H.W., Koseki, H. and Klose, R.J. (2019) Synergy between Variant PRC1 Complexes Defines Polycomb-Mediated Gene Repression. *Mol Cell*, **74**, 1020–1036.e8.
- 70.** Yoder, B.L. and Burgers, P.M. (1991) *Saccharomyces cerevisiae* replication factor C. I. Purification and characterization of its ATPase activity. *J Biol Chem*, **266**, 22689–97.
- 71.** Dharadhar, S., Dijk, W.J., Scheffers, S., Fish, A. and Sixma, T.K. (2021) Insert L1 is a central hub for allosteric regulation of USP1 activity. *EMBO Rep*, **22**.
- 72.** Sauer, P. v., Gu, Y., Liu, W.H., Mattioli, F., Panne, D., Luger, K. and Churchill, M.E.A. (2018) Mechanistic insights into histone deposition and nucleosome assembly by the chromatin assembly factor-1. *Nucleic Acids Res*, 10.1093/nar/gky823.
- 73.** Zhang, K., Gao, Y., Li, J., Burgess, R., Han, J., Liang, H., Zhang, Z. and Liu, Y. (2016) A DNA binding winged helix domain in CAF-1 functions with PCNA to stabilize CAF-1 at replication forks. *Nucleic Acids Res*, **44**, 5083–5094.
- 74.** Sauer, P.V., Timm, J., Liu, D., Sitbon, D., Boeri-Erba, E., Velours, C., Mücke, N., Langowski, J., Ochsenein, F., Almouzni, G., *et al.* (2017) Insights into the molecular architecture and histone H3-H4 deposition mechanism of yeast chromatin assembly factor 1. *Elife*, **6**, 835–839.

- 75.** Rosas,R., Aguilar,R.R., Arslanovic,N., Tyler,J.K. and Churchill,M.E.A. (2022) A novel Single Alpha-Helix-DNA-binding domain in CAF-1 promotes gene silencing and DNA damage survival through tetrasome-length DNA selectivity and spacer function. *bioRxiv*, 10.1101/2022.10.11.511754.
- 76.** Liu,W.H., Roemer,S.C., Zhou,Y., Shen,Z.J., Dennehey,B.K., Balsbaugh,J.L., Little,J.C., Nemkov,T., Ahn,N.G., Hansen,K.C., *et al.* (2016) The Cac1 subunit of histone chaperone CAF-1 organizes CAF-1-H3/H4 architecture and tetramerizes histones. *Elife*, **5**, 2852–2861.
- 77.** Young,G., Hundt,N., Cole,D., Fineberg,A., Andrecka,J., Tyler,A., Olerinyova,A., Ansari,A., Marklund,E.G., Collier,M.P., *et al.* (2018) Quantitative mass imaging of single biological macromolecules. *Science* (1979), **360**, 423–427.
- 78.** Mondol,T., Stodola,J.L., Galletto,R. and Burgers,P.M. (2019) PCNA accelerates the nucleotide incorporation rate by DNA polymerase δ . *Nucleic Acids Res*, **47**.
- 79.** Gomes,X. v. and Burgers,P.M.J. (2000) Two modes of FEN1 binding to PCNA regulated by DNA. *EMBO J*, **19**, 3811–3821.
- 80.** Dovrat,D., Stodola,J.L., Burgers,P.M.J. and Aharoni,A. (2014) Sequential switching of binding partners on PCNA during in vitro Okazaki fragment maturation. *Proceedings of the National Academy of Sciences*, **111**, 14118–14123.
- 81.** Bellelli,R., Belan,O., Pye,V.E., Clement,C., Maslen,S.L., Skehel,J.M., Cherepanov,P., Almouzni,G. and Boulton,S.J. (2018) POLE3-POLE4 Is a Histone H3-H4 Chaperone that Maintains Chromatin Integrity during DNA Replication. *Mol Cell*, 10.1016/j.molcel.2018.08.043.
- 82.** Yu,C., Gan,H., Serra-Cardona,A., Zhang,L., Gan,S., Sharma,S., Johansson,E., Chabes,A., Xu,R.M. and Zhang,Z. (2018) A mechanism for preventing asymmetric histone segregation onto replicating DNA strands. *Science* (1979), **361**, 1386–1389.
- 83.** Liu,S., Xu,Z., Leng,H., Zheng,P., Yang,J., Chen,K., Feng,J. and Li,Q. (2017) RPA binds histone H3-H4 and functions in DNA replication-coupled nucleosome assembly. *Science*, **355**, 415–420.
- 84.** Nabet,B., Roberts,J.M., Buckley,D.L., Paulk,J., Dastjerdi,S., Yang,A., Leggett,A.L., Erb,M.A., Lawlor,M.A., Souza,A., *et al.* (2018) The dTAG system for immediate and target-specific protein degradation. *Nat Chem Biol*, **14**, 431–441.
- 85.** Mejlvang,J., Feng,Y., Alabert,C., Neelsen,K.J., Jasencakova,Z., Zhao,X., Lees,M., Sandelin,A., Pasero,P., Lopes,M., *et al.* (2014) New histone supply regulates replication fork speed and PCNA unloading. *Journal of Cell Biology*, **204**, 29–43.
- 86.** Klapholz,B., Dietrich,B.H., Schaffner,C., Hérédia,F., Quivy,J.P., Almouzni,G. and Dostatni,N. (2009) CAF-1 is required for efficient replication of euchromatic DNA in Drosophila larval endocycling cells. *Chromosoma*, **118**, 235–248.
- 87.** Nakamura,K., Saredi,G., Becker,J.R., Foster,B.M., Nguyen,N. v., Beyer,T.E., Cesa,L.C., Faull,P.A., Lukauskas,S., Frimurer,T., *et al.* (2019) H4K20me0 recognition by BRCA1–BARD1 directs homologous recombination to sister chromatids. *Nat Cell Biol*, **21**, 311–318.

- 88.** Saredi,G., Huang,H., Hammond,C.M., Alabert,C., Bekker-Jensen,S., Forne,I., Reverón-Gómez,N., Foster,B.M., Mlejnkova,L., Bartke,T., *et al.* (2016) H4K20me0 marks post-replicative chromatin and recruits the TONSL-MMS22L DNA repair complex. *Nature*, **534**, 714–718.
- 89.** Ray-Gallet,D., Woolfe,A., Vassias,I., Pellentz,C., Lacoste,N., Puri,A., Schultz,D.C., Pchelintsev,N.A., Adams,P.D., Jansen,L.E.T., *et al.* (2011) Dynamics of Histone H3 Deposition In Vivo Reveal a Nucleosome Gap-Filling Mechanism for H3.3 to Maintain Chromatin Integrity. *Mol Cell*, **44**, 928–941.
- 90.** Goswami,P., Abid Ali,F., Douglas,M.E., Locke,J., Purkiss,A., Janska,A., Eickhoff,P., Early,A., Nans,A., Cheung,A.M.C., *et al.* (2018) Structure of DNA-CMG-Pol epsilon elucidates the roles of the non-catalytic polymerase modules in the eukaryotic replisome. *Nat Commun*, **9**.
- 91.** Sun,J., Shi,Y., Georgescu,R.E., Yuan,Z., Chait,B.T., Li,H. and O'Donnell,M.E. (2015) The architecture of a eukaryotic replisome. *Nat Struct Mol Biol*, **22**, 976–982.
- 92.** Lucchini,R., Wellinger,R.E. and Sogo,J.M. (2001) Nucleosome positioning at the replication fork. *EMBO J*, **20**, 7294–7302.
- 93.** Gasser,R., Koller,T. and Sogo,J.M. (1996) The Stability of Nucleosomes at the Replication Fork. *J Mol Biol*, **258**, 224–239.
- 94.** Hogg,M., Osterman,P., Bylund,G.O., Ganai,R.A., Lundström,E.-B., Sauer-Eriksson,A.E. and Johansson,E. (2014) Structural basis for processive DNA synthesis by yeast DNA polymerase ϵ . *Nat Struct Mol Biol*, **21**, 49–55.
- 95.** Baris,Y., Taylor,M.R.G., Aria,V. and Yeeles,J.T.P. (2022) Fast and efficient DNA replication with purified human proteins. *Nature*, **606**, 204–210.
- 96.** Lancey,C., Tehseen,M., Raducanu,V.-S., Rashid,F., Merino,N., Ragan,T.J., Savva,C.G., Zaher,M.S., Shirbini,A., Blanco,F.J., *et al.* (2020) Structure of the processive human Pol δ holoenzyme. *Nat Commun*, **11**.
- 97.** Zheng,F., Georgescu,R.E., Li,H. and O'Donnell,M.E. (2020) Structure of eukaryotic DNA polymerase δ bound to the PCNA clamp while encircling DNA. *Proceedings of the National Academy of Sciences*, **117**.
- 98.** Smith,D.J. and Whitehouse,I. (2012) Intrinsic coupling of lagging-strand synthesis to chromatin assembly. *Nature*, **483**, 434–438.
- 99.** Daigaku,Y., Keszthelyi,A., Müller,C.A., Miyabe,I., Brooks,T., Retkute,R., Hubank,M., Nieduszynski,C.A. and Carr,A.M. (2015) A global profile of replicative polymerase usage. *Nat Struct Mol Biol*, **22**, 192–198.
- 100.** Evrin,C., Maman,J.D., Diamante,A., Pellegrini,L. and Labib,K. (2018) Histone H2A-H2B binding by Pol α in the eukaryotic replisome contributes to the maintenance of repressive chromatin. *EMBO J*, 10.15252/embj.201899021.
- 101.** Li,Z., Hua,X., Serra-Cardona,A., Xu,X., Gan,S., Zhou,H., Yang,W.-S., Chen,C., Xu,R.-M. and Zhang,Z. (2020) DNA polymerase α interacts with H3-H4 and facilitates the transfer of parental histones to lagging strands. *Sci Adv*, **6**.
- 102.** Gan,H., Serra-Cardona,A., Hua,X., Zhou,H., Labib,K., Yu,C. and Zhang,Z. (2018) The Mcm2-Ctf4-Pola axis facilitates parental histone H3-H4 transfer to lagging strands. *Mol Cell*, **72**, 140–151.



3

Enabling PCNA labeling to probe PCNA interactions on DNA using single molecule experiments

Clément Rouillon¹, Kaley McCluskey², Humberto Sanchez González², Theo van Laar²,
Nynke Dekker², Francesca Mattioli¹

¹*Hubrecht Institute-KNAW & University Medical Center Utrecht, Uppsalalaan 8, 3584 CT
Utrecht, The Netherlands*

²*Kavli Institute of Nanoscience Delft, TU Delft, Van der Maasweg 9, 2629 HZ Delft,
The Netherlands*

Abstract

PCNA is an indispensable protein for cell viability, with roles in DNA replication, DNA repair, sister chromatids cohesion, and chromatin assembly. During these processes, PCNA functions as a homotrimeric ring that is loaded onto DNA, where it binds a multitude of proteins. However, the regulation of these interactions on DNA-loaded PCNA remains unclear. This is technically challenging because of the complexity of the DNA loading process and the high mobility of PCNA on DNA, which has hampered the development of quantitative assays. Here, we established a biochemical in bulk readout for PCNA loading and stability on DNA. Moreover, we developed a single-molecule assay using TIRF (Total Internal Reflection Fluorescence)-based CoSMoS (Colocalization Single Molecule Spectroscopy) to visualize individual DNA-loaded PCNA. In the development of these approaches, we found that previous methods used to fluorescently label PCNA render the protein unstable on DNA. Therefore, we set up a sortase-based labeling method that relies on a fluorescent N-terminal extension of PCNA, which instead leads to a stable PCNA homotrimer on DNA, in bulk and in single-molecule CoSMoS. Thus, we have found a new strategy that significantly improves the physiological traits of labeled PCNA, which can now be used to study its interactions at the single-molecule level. This work also underscores the power of comprehensive biochemical reconstitutions that here revealed effects on DNA that were not appreciated with simplified biochemical assays.

Introduction

In the cell, Proliferating Cell Nuclear Antigen (PCNA) plays a pivotal role in various essential processes. This ring-shaped homotrimer is involved in DNA replication, DNA repair, chromatin assembly, and sister chromatid cohesion (reviewed in **1**). During DNA replication, it serves as an essential cofactor for DNA polymerases, tethering them to the DNA template (**1**). On the lagging strand, PCNA recruits multiple proteins that facilitate the maturation of Okazaki fragments (**2**). Subsequently, it recruits CAF-1 and cohesion factors on both sister chromatids, thereby promoting the essential process of chromatin assembly and chromosome cohesion on the daughter strands (**3**). This places PCNA at the heart of chromosome replication.

PCNA is only functional when loaded onto double-stranded DNA (Figure S1A) (**4**). Indeed, PCNA encircles the DNA within the central hole of its homotrimeric structure (**5**). PCNA is loaded onto DNA by ATP-dependent enzymes named clamp loaders that temporarily open the homotrimeric ring and load it onto DNA (**6**). The most studied clamp loader responsible for PCNA loading is the RFC1-5 complex (**6, 7**), but additional homologues have been described to date, including CTF18-RFC (**8**) and ATAD5 (**9**). CTF18-RFC loads PCNA specifically on the leading strand during DNA replication (**10**), while ATAD5 unloads PCNA from chromatin following DNA synthesis (**9**). The distribution of functions between the various loaders is being heavily investigated.

Once loaded onto DNA, the homotrimeric nature of PCNA allows it to bind multiple proteins simultaneously (Figure S1A). These interactions are challenging to dissect using conventional in bulk biochemical methods. Moreover, multiple PCNA molecules can be loaded closely together on DNA (**11**), adding complexity to understanding its roles in cells and *in vitro*. This limits our understanding of how PCNA coordinates all its functions at replication forks. To overcome this challenge, we developed a single-molecule assay, enabling the real-time visualization of individual PCNA molecules loaded onto DNA. To visualize single DNA-loaded PCNA, it is paramount to use fluorescently labeled PCNA at high degree and in controlled positions, and the labeling must not alter the function of the protein. This enables quantitation of stoichiometry and binding kinetics. In parallel, to test functionality of the labeled proteins, we set up in bulk biochemical assays that recapitulate PCNA loading on DNA plasmid. Previous single molecule and biochemical studies using fluorescent PCNA did not use DNA, but rather studied PCNA interactions outside the context of DNA (**12, 13**). Here, we find that these previous labeling approaches (**11–16**) lead to instability of PCNA on DNA. Sortase-based labeling (**17**) instead preserves the structural integrity of PCNA on DNA and also ensures its functionality, making this labeling strategy suitable for moving into single-molecule analysis.

Results

Fluorescent labeling or mutations of the native cysteines of PCNA strongly impairs its stability on DNA

Previous biophysical studies that focused on PCNA outside the context of DNA, employed maleimide chemistry that selectively attaches dyes to sulphur groups found in cysteine residues (13–16). A yeast PCNA monomer contains four cysteines (Figure S1B): C22, C30, C62, and C81. We used a PCNA-C4S-K164C mutant (Figure S1B) where all cysteines are mutated into serines (C22S, C30S, C62S, C81S) and an additional cysteine is added at the surface of the protein, which was previously used in biochemical bulk assays (19). We hypothesized that this mutant may still form a stable trimer due to similarities between cysteine and serine, while allowing for the site-specific labeling on K164C, the sole substrate for maleimide reactions. This PCNA-C4S-K164C mutant (Figure S1B and S1C) behaved similarly to WT-PCNA during protein purification demonstrating that the protein intrinsic stability remained unaffected. We labeled this PCNA with Alexa Fluor 546 (AF546), leading to labeling efficiencies varying between 50-100% across different preparations (Table 1).

To verify that the labeling of PCNA did not affect its loading onto DNA, we used size exclusion chromatography (SEC) and SDS-PAGE to test whether PCNA-C4S-K164C-546 is efficiently loaded on plasmid DNA by the clamp loader RFC1-5 complex, using a previously established assay (18). This assay allows us to also determine the stability of PCNA on DNA over a relatively long time (30-60 minutes). We used unlabeled WT-PCNA as control which is efficiently loaded on DNA, as shown by the co-elution of PCNA with the DNA plasmid that only occurs in the presence of ATP (Figure S1D). Of note, WT-PCNA remained stably loaded throughout the experiment. Interestingly, both labeled and unlabeled PCNA-C4S-K164C (Figure 1A and S1E respectively) showed no co-elution with DNA, suggesting that mutating cysteines into serines, which share chemical properties, is deleterious for the protein stability or loading on DNA. Notably, because these residues do not seem to be crucial for RFC1-5 function (14), we speculate that the native cysteines of PCNA are important for its stability on DNA. On this line, previous work has shown that C81 in PCNA is positioned at the interface between PCNA monomers and that a C81R mutation affects protein stability (20). These data suggest that the PCNA-C4S-K164C construct is not suitable for studying PCNA on DNA.

We therefore engineered a PCNA-K164C mutant (Figure S1B), where all native cysteines were maintained, and K164 was mutated to Cys. We hypothesized that this surface-exposed cysteine might constitute the primary target for dye attachment during labeling procedures, leaving the other cysteines of PCNA non or minimally conjugated. PCNA-K164C protein was purified at a high level of purity (Figure S1C) and behaved as wild-type PCNA (WT-PCNA) during size exclusion chromatography, confirming that it efficiently forms a PCNA homotrimer. Unlabeled PCNA-K164C efficiently loaded onto DNA and was stable throughout the experiment (Figure 1B), suggesting that the added cysteine does not interfere with loading or stability, and confirming that the native cysteines are important for loading or stability on DNA.

We then labeled this mutant with AlexaFluor546 (AF546) at high labeling efficiency (Table 1). Surprisingly, labeled PCNA-K164C displayed poor loading and stability onto DNA (Figure 1C). This result suggests two hypotheses: 1) labeling at the K164C reduces DNA loading or stability, 2) the native cysteines on PCNA can be also (partially) conjugated, leading to destabilization of PCNA.

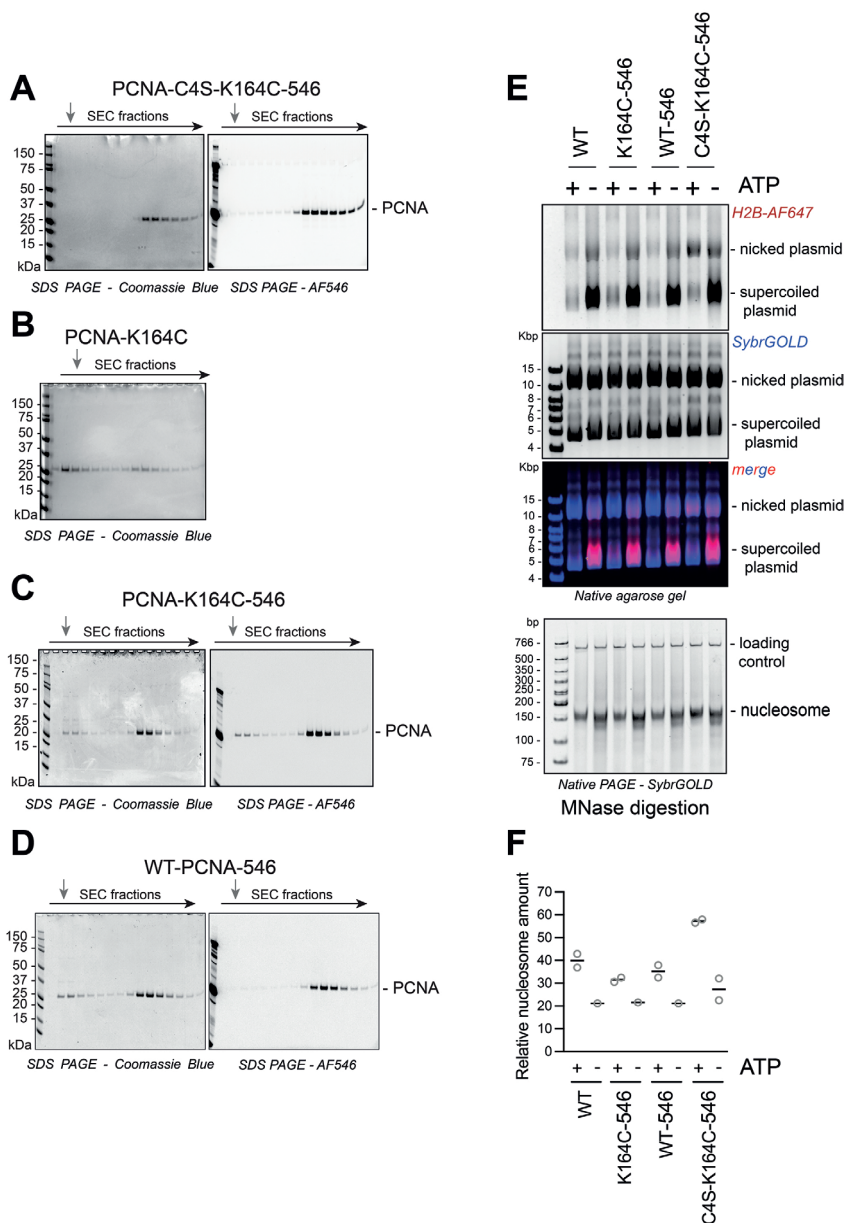


Figure 1: The native cysteines of PCNA play an essential role for its stability on DNA. (A-D) SDS-PAGE analysis following SEC separation of PCNA loading reactions on DNA using (A) labeled PCNA-C4S-K164C-546, (B) PCNA-K164C, (C) labeled PCNA-K164C-546, (D) and labeled WT-PCNA-546. Grey arrows indicate the elution volume of the plasmid DNA used for PCNA loading. (E) Top panel: Native agarose gel analysis of PCNA-NAQ assay reactions with different labeled PCNA. The first gel shows H2B fluorescence, with the signal on nicked plasmid representing PCNA-mediated chromatin assembly. Bottom panel: Native PAGE stained with SybrGOLD following MNase digestion of the samples shown in the top panel. (F) Quantification of H2B fluorescent signal on nicked plasmid, reflecting PCNA-mediated chromatin assembly.

To test these hypotheses, we labeled WT-PCNA with AF546, which cannot be labeled at position 164, where the native lysine is present. We found that the labeling efficiency was low (below 20%) (Table 1), in line with the native cysteines being poorly accessible. Labeled WT-PCNA-546 did not co-elute with the DNA plasmid, and analysis of the SDS PAGE revealed that only an unlabeled fraction was present on DNA (Figure 1D). This shows that attaching dyes or modifying the native cysteines of PCNA disrupt its stability on DNA, which renders this approach invalid to study DNA-loaded PCNA.

PCNA facilitates CAF-1 mediated chromatin assembly with fast kinetics

Our findings indicate that labeling PCNA has an impact on its stability on DNA in the 30-60 minutes time-frame. To understand whether this is caused by a defect in loading by RFC1-5 or by destabilization of PCNA after DNA loading, we used a functional PCNA-dependent nucleosome assembly assay, named PCNA-NAQ assay. The PCNA-NAQ assay measures the PCNA-dependent nucleosome assembly activity of the histone chaperone CAF-1 in bulk conditions (18). This PCNA-dependent activity occurs at short-time frames (within 1 minute), allowing us to differentiate between PCNA loading defects, (which should inactivate CAF-1), or PCNA stability defects, which should not affect its rapid (<1minute) activity at PCNA.

We compared the labeled PCNA variants to WT-PCNA. As previously shown, WT-PCNA facilitates chromatin assembly in a PCNA-dependent manner (i.e., on the nicked plasmid). Inhibition of PCNA loading, by omission of ATP, leads to nucleosome assembly only on the supercoiled plasmid in a PCNA independent manner (Figure 1E and 1F). All labeled PCNA variants successfully facilitated PCNA-dependent CAF-1 activity, as seen by histone deposition on the nicked plasmid, to an extent that is comparable with WT-PCNA (Figure 1E and 1F). Importantly, this activity was dependent on ATP, indicating that PCNA loading by RFC1-5 occurs in these reactions. These data show that fluorescently labeled WT-PCNA PCNA-K164C, PCNA-C4S-K164C are being loaded onto DNA by RFC, confirming that neither PCNA cysteines mutations or labeling significantly affects RFC1-5 activity. We speculate that the fluorescent labels are affecting their stability after loading. Since RFC continuously loads PCNA in the PCNA-NAQ assay, this implies that the instability of PCNA on DNA occurs at a slower rate than the mechanism of chromatin assembly mediated by CAF-1 and PCNA. Interestingly, labeled PCNA-C4S-K164C consistently exhibited enhanced CAF-1 activity on DNA in comparison to WT-PCNA (Figure 1E-F).

An alternative method for the efficient labeling of PCNA

In order to label PCNA and preserve its activity, we tested a protocol based on the sortase enzyme that facilitates the covalent attachment of peptides to protein N-termini (17). This method was previously used for labeling of proteins to be used in CoSMoS (21, 22). We first purified PCNA_{GGG} carrying a sortase-compatible N-terminal sequence (CHHHHHHHHLPETGG). Using sortase (made in house), we fused this PCNA variant to a short peptide harboring a labeled (Cy5) cysteine (Figure 2A). We obtained about 70% of labeling of PCNA (named PCNA_{GGG}-Cy5) (Figure 2A, Table 1), which could be visible also on SDS-PAGE gel, due to the relatively large change in molecular weight because of peptide conjugation (Figure 2A).

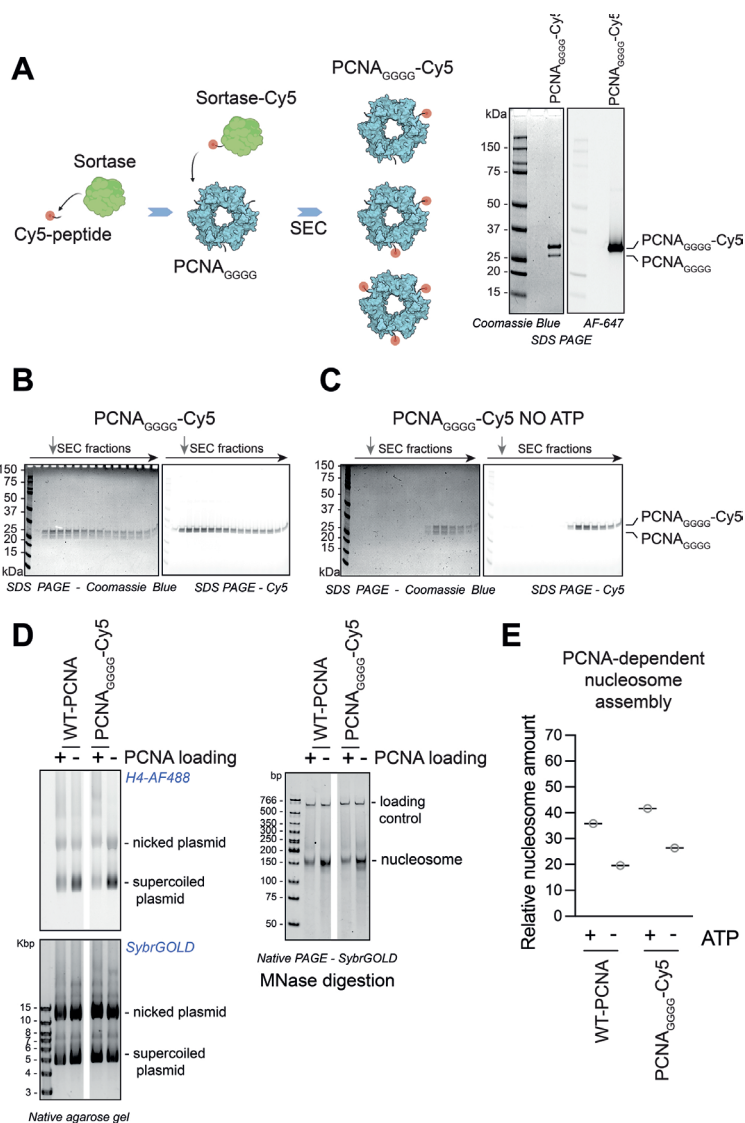


Figure 2: Sortase-mediated labeling of the N-terminal of PCNA produces a robust construct for studying PCNA reactions on DNA. (A) Workflow of the sortase-based labeling of PCNA. A Cy5 labeled peptide is first conjugated to the sortase enzyme and next transferred onto the N-terminus of PCNA. The labeled protein is then purified via SEC and the degree of labeling is determined via SDS PAGE. This image was created with BioRender.com. **(B-C)** SDS-PAGE analysis following SEC separation of PCNA loading reactions on DNA using (B) sortase-labeled PCNA-Cy5 with ATP, (C) or without. In each case, the coomassie staining and fluorescent scan of the SDS PAGE is shown. Grey arrows indicate the elution volume of the plasmid DNA used for PCNA loading. **(D)** Left panel: Native agarose gel analysis of PCNA-NAQ assay reactions with different labeled PCNA. The first gel shows H4 fluorescence, with the signal on nicked plasmid representing PCNA-mediated chromatin assembly. Right panel: Native PAGE stained with SybrGOLD following MNase digestion of the samples shown in the left panel. **(E)** Quantification of H4 fluorescent signal on nicked plasmid, reflecting PCNA-mediated chromatin assembly. Due to limited resources, this experiment was performed only once.

PCNA_{GGGG}-Cy5 efficiently loaded onto DNA in an ATP-dependent manner (Figure 2B and 2C). Notably, both the labeled (top band) and unlabeled PCNA (bottom band) exhibited comparable stability on DNA (Figure 2B), thus reinforcing the assertion that this labeling approach yields a functional construct. This was confirmed when we tested functionality of PCNA_{GGGG}-Cy5 in the PCNA-NAQ assay. PCNA_{GGGG}-Cy5 enabled PCNA-dependent nucleosome assembly by CAF-1 (Figure 2D and 2E). Together, our results show that sortase-based labeling of PCNA is most suitable for retaining PCNA protein stability on DNA and its functionality.

Single molecule TIRF analysis reveals that PCNA labeling can affect its stability on DNA

Our ultimate aim is to develop a single molecule assay to study PCNA interactions at high-temporal resolution. Therefore, we tested if PCNA_{GGGG}-Cy5 would be amenable for such studies.

We opted for a TIRF-based CoSMoS assay, enabling real-time monitoring of PCNA loading events on tethered DNA oligos (Figure 3A). A 79mer DNA oligos was tethered on a passivated surface via biotin-streptavidin. The DNA was conjugated to Digoxigenin (DIG) which was used to block this end with a fragment antigen-binding (Fab). This side of the DNA also harbors an intra-molecular Cy3 fluorophore (Figure 3A). Notably, this setup enables the loading of PCNA by RFC1-5 at the only available 3'-OH end. Subsequently, PCNA slides along the DNA without dissociating due to the blocking complexes on both ends. After incubation with RFC1-5, PCNA and ATP, the surface is washed with buffer to retain the PCNA molecules loaded on DNA, which are then imaged. Sortase-labeled PCNA_{GGGG}-Cy5 showed a substantial level of colocalization between PCNA and DNA (close to 20%, Figure 3B). This was strongly reduced when either ATP or RFC1-5 were omitted from the reaction (Figure 3B), indicating that the signal is dependent on active PCNA loading on DNA by RFC1-5. From this we concluded that the colocalization events indeed represent PCNA loaded onto DNA.

Because residual proteins are washed following PCNA loading, we are able to monitor the stability of PCNA on DNA over time by fitting our data to a linear model. Sortase-labeled PCNA_{GGGG}-Cy5 exhibited remarkable stability throughout the course of the experiment (indicated by the near null slope of the curve), which lasted 20 minutes (Figure 3C). As a control, we used PCNA-K164C-546, which in biochemical experiments showed decreased stability on DNA (Figure 1C). Indeed, this PCNA variant showed a progressive loss of colocalization with DNA over time (20 minutes) in CoSMoS, confirming a decrease in stability on DNA (supported by the negative slope of the curve) (Figure 3D).

In conclusion, the use of sortase-labeled PCNA_{GGGG}-Cy5 enabled monitoring of the stability of individual PCNA molecules on DNA, highlighting the suitability of this labeling approach for precise single-molecule measurements. This method holds great potential for future studies unravelling the biophysical properties of PCNA interactions that occur on DNA, to understand their functional implications.

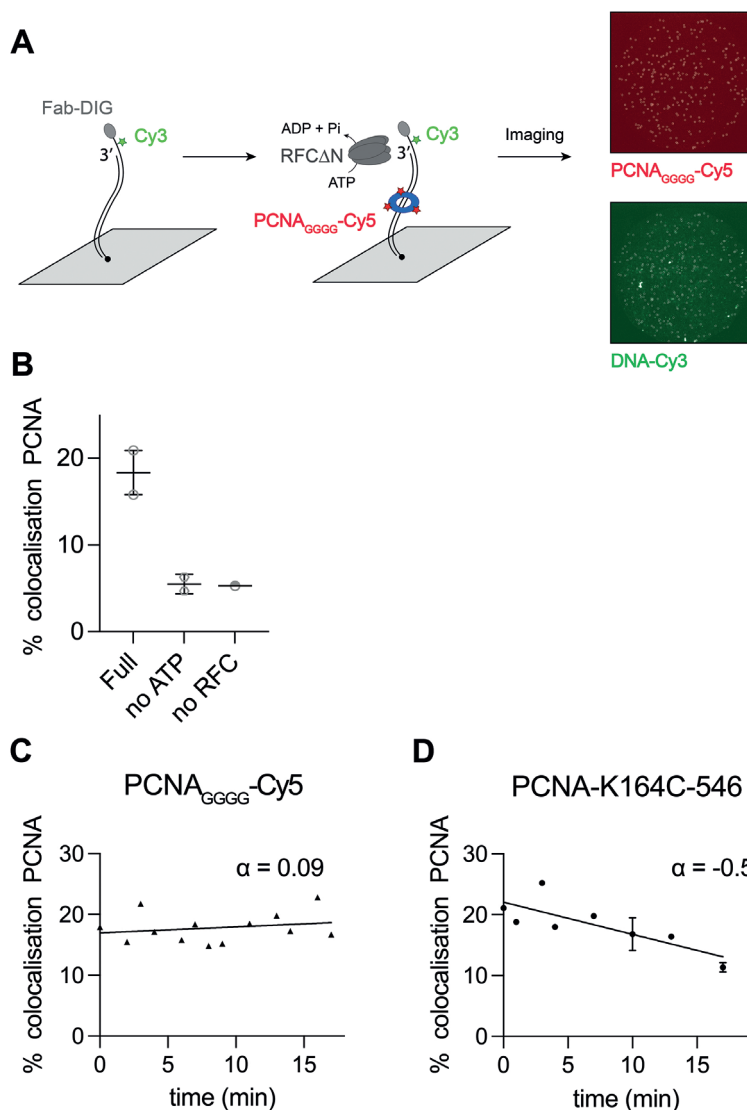


Figure 3: Sortase-mediated labeling of the N-terminal of PCNA produces a robust construct for studying PCNA reactions on DNA. (A) Workflow of the CoSMoS assay for PCNA loading on DNA.

The DNA template was attached to a streptavidin-coated surface using a biotin. It was conjugated to an anti-DIG Fab fragment to block the end of the template, preventing PCNA to slide off during experiments. RFC1-5 and PCNA were injected with imaging buffer and loading reactions were allowed to take place for 5 minutes at 30°C in presence of ATP, before washing away unbound protein with imaging buffer. PCNA and DNA were imaged with excitation at 660 nm and 532 nm respectively. Examples of field of view of a CoSMoS experiment are shown on the right panel (White circles highlight colocalization between PCNA and DNA). (B) Quantification of colocalization between PCNA and the total DNA signal. Each data point is the average colocalization over the course of the experiment (between 15 and 20 minutes) (C-D) Quantification of the colocalization between PCNA and the total DNA signal over time using (C) sortase-labeled PCNA, and (D) PCNA-K164C-546 (Cy5-labeled DNA was used for the PCNA-K164C-546 experiment). A linear regression model was fitted to the data, and the slope of the curve (α) is used to represent the stability of PCNA on DNA over time.

Discussion

Our study reveals the complexity and challenges associated with PCNA reactions occurring on DNA using fluorescently tagged proteins. In particular, we explored various labeling methods and their impacts on PCNA stability. The ultimate goal was to be able to monitor PCNA at high temporal resolution in a single molecule-based assay.

We have recently shown that PCNA-based assays must be performed in the physiological context of loading on DNA, as this severely affects the interactions of PCNA with its binding partners (18). Here, we show that the stability of PCNA on DNA is greatly affected by traditional fluorescent labeling. Indeed, several studies have employed maleimide-based methods for the labeling of yeast PCNA (13–16). These results should be interpreted carefully when examining reactions occurring on DNA as we show that these labeled proteins display low stability once loaded. Our work underscores the essential role of native cysteines in maintaining PCNA stability on DNA. Indeed, previous work showed that a C81R mutation results in a deficiency in the homotrimer intrinsic stability (20). Moreover, structural analysis revealed that a C22Y mutation disrupts the structure of the central DNA binding hole of PCNA (20). Here, we demonstrate that mutating all cysteines into serines is not deleterious for the native assembly of the protein, as the mutants behaved like the wild type protein in gel filtration. However, it affects the stability of PCNA on DNA, despite the shared chemical properties between cysteines and serines. Of note, several studies involving human PCNA have used labeling methods targeting the native cysteines of PCNA (6, 11, 12). Although C22 is not evolutionarily conserved, C81 is highly conserved in this context. Future studies will need to determine whether maleimide approaches are suitable for the fluorescent tagging of human PCNA, and consider sortase-based tagging in that context.

Others have also employed sortase-based methods for the labeling of proteins (21, 23, 24). While this method is powerful and leads to high labeling efficiencies, there are some limitations to this approach. The sortase enzyme facilitates the transfer of a labeled peptide onto PCNA by recognizing the LPXTG/A signal peptide motif (17), where 'X' represents any amino acid (17). This reaction is also reversible as the enzyme recognizes the signal peptide once fused to PCNA. This presents a challenge in achieving nearly complete labeling efficiency, which is a requirement for specific single molecule-based experiments, such as those concerning stoichiometry. Future studies should focus on optimizing this protocol to establish a unidirectional equilibrium, enabling us to bias the reactions toward exclusive PCNA labeling.

Altogether, we established a method to achieve fluorescent labeling of PCNA while preserving the stability of the protein on DNA. This PCNA can be observed at the single molecule level in our CoSMoS-based setup, paving the way for a better understanding of how PCNA regulates its multiple interactions on DNA. Notably, we've recently demonstrated that CAF-1 may not share PCNA with DNA polymerases at DNA replication forks. Our system allows us to monitor these dynamics on individual PCNA homotrimers loaded onto DNA, shedding light on the regulation of interactions on PCNA at replication forks.

Methods

Cloning of PCNA mutants for fluorescent labeling.

For sortase-based labeling, PCNA was mutated in order to harbor 4 glycines at its N-terminus (PCNA_{GGGG}). PCNA_{GGGG} plasmid was generated from a WT-PCNA plasmid using the Q5 Site direct mutagenesis kit (NEB # E0554S). The N-terminal insertion consists of a Histidine affinity tag, followed by a TEV protease recognition site, followed by a GGGG sequence used for peptide attachment by the sortase enzyme (HHHHHHHENLYFQGGGG).

Protein expression and purification

CAF-1, PCNA, PCNA-C4S-K164C, PCNA-K164C, RFC Δ N (hereafter referred to as RFC1-5) and histones were expressed and purified as previously described (18).

Tobacco Etch Virus (TEV) protease:

The plasmid for expression of TEV protease was a generous gift from Titia Sixma. Rosetta2 cells (Novagen) containing the expression plasmid were grown at 37°C in LB medium to OD₆₀₀=0.8. Cultures were incubated at 15°C overnight with 0.2 mM Isopropyl β -D-1-thiogalactopyranoside (IPTG). Cells were harvested by centrifugation at 3200 x g for 15min, and resuspended in Lysis buffer (50 mM Tris pH 8.0, 150 mM NaCl, 1 mM TCEP) in presence of COMPLETE EDTA-free protease inhibitor (Roche) and DNase (Thermo Fischer #88700). Cells were sonicated and the lysate was clarified by centrifugation at 35000xg for 40 min. The lysate was incubated with 2 ml of TALON beads (Takabio #635502) for 1 hour at 4°C. The flow-through was collected and beads were washed with 40 ml of wash buffer (50 mM Tris pH 8.0, 150 mM NaCl, 5 mM Imidazole and 1 mM TCEP). The beads were incubated for one hour at 4°C in 4 ml of elution buffer (50 mM Tris pH 8.0, 150 mM NaCl, 1 mM TCEP, 250 mM imidazole). The eluate was then dialyzed for 2 hours at 4°C (using 12-14 MWCO membrane) against 1L of storage buffer (50 mM Tris pH 8.0, 150 mM NaCl, 5 mM DTT, 1 mM EDTA, 25% glycerol). The buffer was changed and further incubated overnight. The next day the sample was concentrated using AMICON 10 MWCO and stored at -80°C.

PCNA_{GGGG} for sortase labeling:

Rosetta2 cells (Novagen) containing the expression plasmid were grown at 37°C in LB medium to exponential phase (OD₆₀₀=0.4). Cultures were incubated at 16°C overnight with 0.4 mM IPTG. Cells were harvested by centrifugation at 3200 x g for 15min, and resuspended in Lysis buffer (50 mM TRIS pH 7.5, 300 mM NaCl, 10 mM imidazole, 1 mM TCEP) in presence of COMPLETE EDTA-free protease inhibitor (Roche) and DNase (Thermo Fischer #88700). Cells were sonicated and the lysate was clarified by centrifugation at 35000xg for 40 min. The supernatant was recovered and injected on a HisTrap HP 5 ml column (Cytiva) equilibrated in lysis buffer. The column was washed with 50 ml of lysis buffer, and 25 ml of wash buffer (50 mM TRIS pH 7.5, 300 mM NaCl, 20 mM imidazole, 1 mM TCEP). The protein was eluted in a gradient of Buffer B (50 mM TRIS pH 7.5, 300 mM NaCl, 300 mM imidazole, 1 mM TCEP) along 100 ml. Next, the histidine affinity tag was removed using a 1:100 ratio of homemade TEV protease per PCNA for 2 hours at 4°C while dialyzing (using 12-14 MWCO membrane) against 2L of dialysis buffer (20 mM TRIS pH 7.5, 125 mM NaCl, 10 mM Imidazole, 1 mM TCEP). This step was performed to

remove excess imidazole that inhibits the TEV protease. The dialysis buffer was changed for 2L of fresh buffer and further incubated overnight at 4°C. The next day, the sample was purified via a second nickel pull down in order to remove undigested PCNA and TEV protease. The sample was mixed with 10 ml of nickel-shepharose beads equilibrated in lysis buffer (without imidazole), and the flow through containing PCNA_{GGGG} was recovered and the beads were further washed with 15 ml of lysis buffer (no imidazole). Flow through and wash samples were pooled and diluted with lysis buffer (no imidazole and NaCl) to reach a NaCl concentration of 160 mM. The sample was injected on HiTrap Q HP 5 ml (Cytiva) equilibrated in QA buffer (20 mM Tris pH 7.5, 125 mM NaCl, 1 mM TCEP). The column was washed with 50 ml of QA buffer and PCNA_{GGGG} was eluted in a gradient of QB buffer (20 mM Tris pH 7.5, 1000 mM NaCl, 1 mM TCEP) along 100 ml. Fractions containing PCNA_{GGGG} were pooled together, concentrated using AMICON 10 MWCO and injected on Superdex 200 10-300 increase GL (Cytiva), prior to elution in 20 mM HEPES pH 7.5, 125 mM NaCl, and 1 mM TCEP. PCNA_{GGGG} was concentrated using AMICON 0.5ml MWCO and stored at -80°C.

Sortase A

Sortase A was expressed in BL21(DE3) from plasmid pET30b-7m SrtA (Addgene #51141). Cells were harvested by centrifugation at 3200 x g for 15min and resuspended in lysis buffer (50 mM TRIS-HCl pH 7.2, 150 mM NaCl, 10% glycerol and 10 mM imidazole) and lysed by sonication. The lysate was cleared in an Avanti JXN-26 centrifuge for 25 minutes at 16000 x g.

Sortase A was pulled-down with Ni-NTA agarose beads, eluted from the beads with elution buffer (50 mM TRIS-HCl pH 7.2, 150 mM NaCl, 10% glycerol and 500 mM imidazole) and subsequently dialyzed (using 7-8 MWCO membrane) against dialysis buffer (50 mM TRIS-HCl pH 7.2, 150 mM NaCl and 10% glycerol). Protein concentration was determined using Bradford.

Maleimide-based labeling of PCNA variants

PCNA-C4S-K164C and PCNA-K164C were labeled with AlexaFluor546 (AF546) as previously described (18).

For each reaction, the degree of labeling was assessed as follows. PCNA concentration was determined by SDS-PAGE using a gradient of BSA as standard. The molarity of AF546 in the sample was measured with a nanodrop. The degree of labeling was defined as the molar ratio of dye per PCNA monomer.

Sortase labeling of PCNA_{GGGG} (PCNA_{GGGG}-Cy5)

10 μM of PCNA_{GGGG} was subjected to a labeling procedure using 600 μM of labeled peptide bearing a Cy5 fluorophore and a N-terminal His-tag (Cy5-CHHHHHHHHLPETGG - Lifetein). The labeling reaction was catalyzed by sortase enzyme (10 μM) in the presence of 5 mM CaCl₂. The reaction was incubated for 20 minutes at room temperature and subsequently quenched with 20 mM EDTA. To purify the labeled protein, size exclusion chromatography was employed using a Superose 6 Increase 10/300 GL column. The chromatographic separation was performed in a buffer composed of 50 mM HEPES at pH 7.5, 150 mM NaCl, 10% glycerol, and 1 mM TCEP. This step ensured the isolation of the labeled PCNA_{GGGG} from unreacted components and reaction by-products.

Degree of labeling: Because the labeled protein runs slower than unlabeled PCNA on SDS-PAGE (Figure 2A), we determine the degree of labeling as the ratio of the labeled PCNA over the total signal within a lane on SDS-PAGE.

PCNA loading on SEC

These experiments were performed as previously described (18). We used a nicked pUC19 plasmid as template for PCNA loading. The plasmid was incubated with Nt.BspQI for 8 h at 50°C, and subsequently purified via phenol chloroform extraction. PCNA (30 μM monomer) was incubated with RFC1-5 (0.5 μM) and nicked pUC19 (0.3 μM) in presence of 10 mM MgCl₂ and 3 mM ATP in PCNA loading buffer (50 mM HEPES pH 7.5, 200 mM NaCl, 0.01% IGEPAL CA-360, 1 mM TCEP). This reaction was incubated for 5 minutes at 30°C before injection on Superose 6 increase 3.2–300 columns connected to an AKTA pure system fitted with PEEK I.D. 0.25 mm tubing. The reaction was eluted in PCNA loading buffer supplemented with 10 mM MgCl₂, and samples were analyzed on 4–12% gradient SDS-PAGE run in MES buffer.

PCNA-NAQ assay

These experiments were performed as previously described (18). We used pRC1765 (Addgene #141346) for PCNA loading and chromatin assembly. pRC1765 was nicked using Nt.BbvCI for 6 h at 37°C, and was then purified via phenol chloroform extraction.

Briefly, the following components were incubated together in 11 μl using PCNA loading buffer: 50 nM of supercoiled pRC1765, 50 nM of nicked pRC1765, 1.1 μM of RFC1-5, 10.9 μM of PCNA monomer, 10.9 mM ATP and 8 mM MgCl₂. This reaction was incubated for 5 minutes at 30°C. Subsequently, 25 μl NA buffer were added (25 mM Tris pH 7.5, 150 mM NaCl, 1 mM EDTA, 0.02% Tween-20, 1 mM TCEP). CAF-1 prebound to H3-H4 dimers (100 nM each) were added to the reaction and incubated 15 minutes at room temperature. Fluorescently labeled H2A-H2B dimers (100 nM) were then added to allow full nucleosome assembly, and incubated for 15 minutes at room temperature. Samples were spun down for 5 minutes at 170000xg to remove potential precipitates. 1 μl of reactions was mixed with 5 μl of loading buffer (NA buffer + 5% sucrose). Samples were separated on 0.8% native agarose gel, run in 1X TAE (Tris-Acetate EDTA) for 90 minutes.

MNase reactions were then performed with the rest of the PCNA-NAQ reactions. Briefly, 25 μl of sample was incubated with 80 units of MNase (NEB #M0247S) in 100 μl final volume of 50 mM Tris pH 7.9, 5 mM CaCl₂. Samples were incubated 10 minutes at 37°C prior to inactivation using 20 mM EDTA. Proteins were then digested with ProteinaseK (NEB #P8107S) for 20 minutes at 50°C. A 621 bp DNA fragments was added as loading control, and the digested DNA was purified using the MinElute PCR purification kit (Qiagen #28006) according to the manufacturer's instructions. MNase-digested samples were run on 6% native PAGE, and stained with SybrGOLD.

Single molecule measurements

Experiments were performed in the imaging buffer (10 mM Tris pH 7.4, 150 mM NaCl, 10 mM MgCl₂, 0.01% NP-40, 1 mM DTT, 10% glycerol, 1 mM ATP). Trolox and glucose oxidase/catalase with 7% glucose were added as dye protection solutions.

The DNA template was annealed at 98°C for 5 minutes and allowed to cool down until it reached room temperature. 50 nM PCNA was incubated alone or with 50 nM RFC1-5, with or

without ATP as appropriate, for 5 minutes at room temperature. Samples were then introduced to a flow cell containing Cy3-labeled 79mer DNA with a 14 nt single-strand overhang (Table 2), terminally blocked with anti-DIG Fab fragment (Figure 3A). After 5 minutes of incubation, excess protein was flushed out using imaging buffer.

Experiments were conducted on a micromirror TIRF microscope with red excitation at 660 nm, 6 mW, and green excitation at 532 nm, 6 mW, and integration time 100 ms/frame.

The red and green channels were registered using polynomial decomposition (Global correction of optical distortions in multicolor single-molecule microscopy using Zernike polynomial gradients) and fluorophores were detected using custom Python scripts.

The results were analyzed using GraphPad prism and a linear regression model was fitted to the data. We use the slope of the curve to assess the stability of PCNA on DNA.

Table 1

Constructs	labeling Efficiencies	Stability on DNA
PCNA-C4S-K164C-546	50-100%	Poor
PCNAK164C-546	100%	Poor
WT-PCNA-546	<20%	Poor
PCNA _{GGGG} -Cy5	70%	Good

Table 2

short	3'-CAATCCGGCTAGGTTGAATACGAGTTTGCTTAGCCTACAAACAGAGCGCATA GTAGCCCGATTTCCGGTTACGGTGACAT-5'
long	5DigN/TTTTTTT/ICy3N/TTTTTTTGTAGGCCGATCCAACCTATGCTCAAACGAATCGGATGT TTGTCTCGCGTATCATCGGGCTA AAGCCAATGCCACGTGATTTTTTT/3Bio/

Acknowledgments

We thank Zhihao Zhuang for sharing the plasmid for PCNA-C4S-K16C expression, and Anuj Kumar and Serge Vincent for preliminary work on the CoSMoS experiment and PCNA labeling.

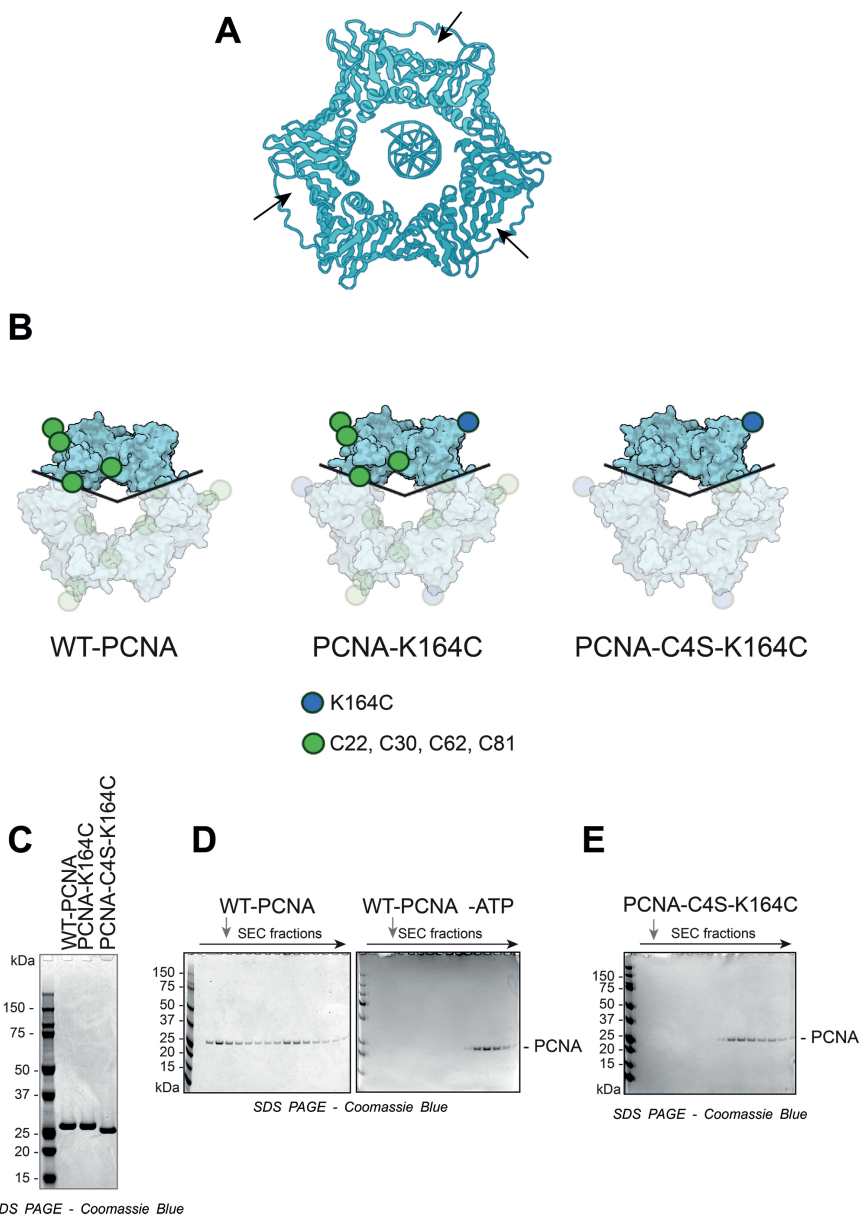
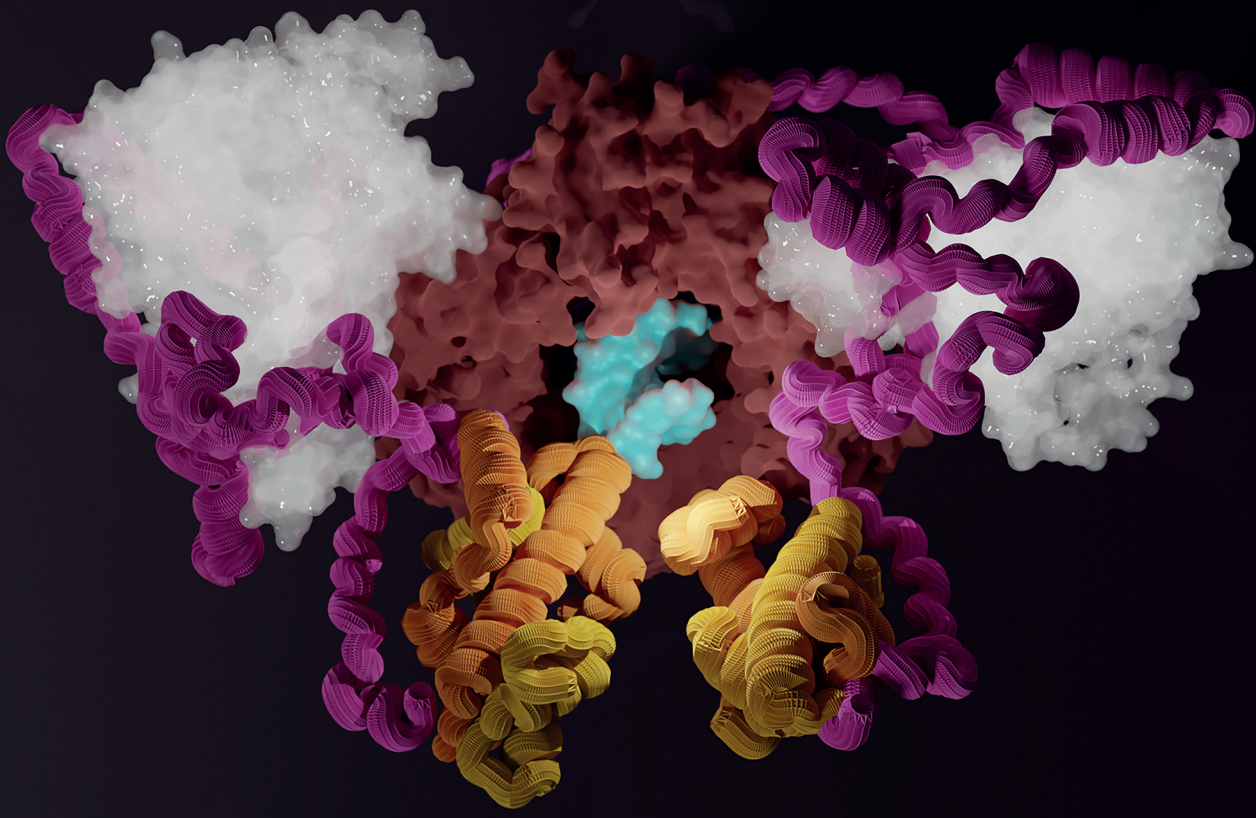


Figure S1: (A) Structure of the PCNA homotrimer loaded on dsDNA (PDB: 6GIS). Black arrows indicate the PIP binding region on each monomer. This image was created with BioRender.com. (B) Structure of PCNA homotrimer where the native cysteines of the protein are highlighted in green and additional ones in blue. Only one monomer is detailed for clarity. This image was created with BioRender.com. (C) SDS-PAGE of purified WT-PCNA, PCNA-K164C and PCNA-C4S-K164C. WT-PCNA and PCNA-K164C harbor a N-terminal Histidine affinity tag, resulting in a slower migration on SDS-PAGE. (D) SDS-PAGE analysis following SEC separation of WT-PCNA loading reactions on DNA with (left panel) and without ATP (right panel). Grey arrows indicate the elution volume of the plasmid DNA used for PCNA loading. (E) SDS-PAGE analysis following SEC separation of unlabeled PCNA-C4S-K164C loading reactions on DNA. Grey arrows indicate the elution volume of the plasmid DNA used for PCNA loading.

References

1. K. N. Choe, G.-L. Moldovan, Forging Ahead through Darkness: PCNA, Still the Principal Conductor at the Replication Fork. *Mol. Cell* **65**, 380–392 (2017).
2. H. Sun, L. Ma, Y.-F. Tsai, T. Abeywardana, B. Shen, L. Zheng, Okazaki fragment maturation: DNA flap dynamics for cell proliferation and survival. *Trends Cell Biol.* **33**, 221–234 (2023).
3. Z. Zhang, K. Shibahara, B. Stillman, PCNA connects DNA replication to epigenetic inheritance in yeast. *408*, 5 (2000).
4. A. González-Magaña, F. J. Blanco, Human PCNA Structure, Function, and Interactions. *Biomolecules* **10**, 570 (2020).
5. M. De March, N. Merino, S. Barrera-Vilarmau, R. Crehuet, S. Onesti, F. J. Blanco, A. De Biasio, Structural basis of human PCNA sliding on DNA. *Nat. Commun.* **8**, 13935 (2017).
6. M.-S. Kang, E. Ryu, S.-W. Lee, J. Park, N. Y. Ha, J. S. Ra, Y. J. Kim, J. Kim, M. Abdel-Rahman, S. H. Park, K. Lee, H. Kim, S. Kang, K. Myung, Regulation of PCNA cycling on replicating DNA by RFC and RFC-like complexes. *Nat. Commun.* **10**, 2420 (2019).
7. Multistep loading of a DNA sliding clamp onto DNA by replication factor C | eLife. <https://elifesciences.org/articles/78253>.
8. V. P. Bermudez, Y. Maniwa, I. Tappin, K. Ozato, K. Yokomori, J. Hurwitz, The alternative Ctf18-Dcc1-Ctf8-replication factor C complex required for sister chromatid cohesion loads proliferating cell nuclear antigen onto DNA. *Proc. Natl. Acad. Sci. U. S. A.* **100**, 10237–10242 (2003).
9. T. Kubota, K. Nishimura, M. T. Kanemaki, A. D. Donaldson, The Elg1 Replication Factor C-like Complex Functions in PCNA Unloading during DNA Replication. *Mol. Cell* **50**, 273–280 (2013).
10. H. W. Liu, C. Bouchoux, M. Panarotto, Y. Kakui, H. Patel, F. Uhlmann, Division of Labor between PCNA Loaders in DNA Replication and Sister Chromatid Cohesion Establishment. *Mol. Cell* **78**, 725-738.e4 (2020).
11. A. B. Kochaniak, S. Habuchi, J. J. Loparo, D. J. Chang, K. A. Cimprich, J. C. Walter, A. M. van Oijen, Proliferating Cell Nuclear Antigen Uses Two Distinct Modes to Move along DNA. *J. Biol. Chem.* **284**, 17700–17710 (2009).
12. J. K. Binder, L. G. Douma, S. Ranjit, D. M. Kanno, M. Chakraborty, L. B. Bloom, M. Levitus, Intrinsic stability and oligomerization dynamics of DNA processivity clamps. *Nucleic Acids Res.* **42**, 6476–6486 (2014).
13. J. A. Thompson, M. R. Marzahn, M. O'Donnell, L. B. Bloom, Replication factor C is a more effective proliferating cell nuclear antigen (PCNA) opener than the checkpoint clamp loader, Rad24-RFC. *J. Biol. Chem.* **287**, 2203–2209 (2012).
14. M. R. Marzahn, J. N. Hayner, J. A. Meyer, L. B. Bloom, Kinetic analysis of PCNA clamp binding and release in the clamp loading reaction catalyzed by *Saccharomyces cerevisiae* replication factor C. *Biochim. Biophys. Acta* **1854**, 31–38 (2015).
15. R. Kumar, V. C. Nashine, P. P. Mishra, S. J. Benkovic, T.-H. Lee, Stepwise loading of yeast clamp revealed by ensemble and single-molecule studies. *Proc. Natl. Acad. Sci. U. S. A.* **107**, 19736–19741 (2010).

- 16.** Z. Zhuang, B. L. Yoder, P. M. J. Burgers, S. J. Benkovic, The structure of a ring-opened proliferating cell nuclear antigen–replication factor C complex revealed by fluorescence energy transfer. *Proc. Natl. Acad. Sci.* **103**, 2546–2551 (2006).
- 17.** C. S. Theile, M. D. Witte, A. E. M. Blom, L. Kundrat, H. L. Ploegh, C. P. Guimaraes, Site-specific N-terminal labeling of proteins using sortase-mediated reactions. *Nat. Protoc.* **8**, 1800–1807 (2013).
- 18.** C. Rouillon, B. V. Eckhardt, L. Kollenstart, F. Gruss, A. E. E. Verkennis, I. Rondeel, P. H. L. Krijger, G. Ricci, A. Biran, T. van Laar, C. M. Delvaux de Fenffe, G. Luppens, P. Albanese, K. Sato, R. A. Scheltema, W. de Laat, P. Knipscheer, N. H. Dekker, A. Groth, F. Mattioli, CAF-1 deposits newly synthesized histones during DNA replication using distinct mechanisms on the leading and lagging strands. *Nucleic Acids Res.*, gkad171 (2023).
- 19.** J. Chen, Y. Ai, J. Wang, L. Haracska, Z. Zhuang, Chemically ubiquitylated PCNA as a probe for eukaryotic translesion DNA synthesis. *Nat. Chem. Biol.* **6**, 270–272 (2010).
- 20.** L. M. Dieckman, E. M. Boehm, M. M. Hingorani, M. T. Washington, Distinct Structural Alterations in Proliferating Cell Nuclear Antigen Block DNA Mismatch Repair. *Biochemistry* **52**, 5611–5619 (2013).
- 21.** S. Ticau, L. J. Friedman, N. A. Ivica, J. Gelles, S. P. Bell, Single-Molecule Studies of Origin Licensing Reveal Mechanisms Ensuring Bidirectional Helicase Loading. *Cell* **161**, 513–525 (2015).
- 22.** A. Zhang, L. J. Friedman, J. Gelles, S. P. Bell, Changing protein–DNA interactions promote ORC binding-site exchange during replication origin licensing. *Proc. Natl. Acad. Sci.* **120**, e2305556120 (2023).
- 23.** H.-J. Jeong, G. C. Abhiraman, C. M. Story, J. R. Ingram, S. K. Dougan, Generation of Ca²⁺-independent sortase A mutants with enhanced activity for protein and cell surface labeling. *PLOS ONE* **12**, e0189068 (2017).
- 24.** K. E. Dillard, J. M. Schaub, M. W. Brown, F. A. Saifuddin, Y. Xiao, E. Hernandez, S. D. Dahlhauser, E. V. Anslyn, A. Ke, I. J. Finkelstein, Sortase-mediated fluorescent labeling of CRISPR complexes. *Methods Enzymol.* **616**, 43–59 (2019).



4

CAF-1 uses an extended binding interface on PCNA for its recruitment on newly synthesized DNA

Clément Rouillon¹, Charlotte M Delvaux de Fenffe¹, Maaike Steenkamp¹, Francesca Mattioli¹

¹*Hubrecht Institute-KNAW & University Medical Center Utrecht, Uppsalalaan 8, 3584 CT Utrecht, The Netherlands*

Abstract

Before cells divide, they must duplicate their genetic content to provide a copy of the genome to the future daughter cells. In addition, the epigenetic cell memory must be preserved as it controls vital cellular processes and controls cell fate. The histone chaperone CAF-1 is essential in this process as it propagates chromatin information on sister chromatids during DNA replication. Its action is regulated by PCNA, a core component of the DNA replication machinery. How the CAF-1-PCNA complex assembles and how this interaction is regulated at replication forks remain unclear. Structural information of these complexes would greatly advance our understanding of chromatin replication. Here we use AlphaFold-Multimer modelling, and biochemical assays to investigate the structural properties of the CAF-1-H3-H4 complex and its interaction with PCNA. This interaction involves an interplay between the two canonical PCNA Interacting Peptides (PIPs) in CAF-1 and a new interface between PCNA and the small subunit of CAF-1. The latter occurs through a unique PCNA surface, whose mutation was previously described to partially phenocopy CAF-1 deletion in yeast cells. This work highlights the complex nature of the CAF-1-PCNA interaction, where multiple domains are involved. This paves the way for structural studies that will visualize this complex at high spatial resolution.

Introduction

Chromatin dynamics control fundamental processes in our cells, including transcription, DNA replication and DNA repair. Moreover, mutations in factors that govern chromatin homeostasis often lead to cancer (1, 2). Therefore, structural studies are required to better characterize the impact of these mutations, and for the development of inhibitors targeting these proteins during tumorigenesis (3). To ensure that chromatin information is preserved when cells divide, epigenetic information carried by histone proteins must be faithfully transmitted (4, 5). In S phase, the chromatin structure is disrupted by DNA replication, and parental histones are removed from DNA and redeposited on each sister chromatid (4, 5). In addition, newly synthesized histones are *de novo* incorporated on replicated DNA to maintain chromatin density. This is a stepwise process known as nucleosome assembly, where two H3-H4 histone dimers are brought together as a (H3-H4)₂ tetramer (6). It is next deposited onto DNA where two H2A-H2B dimers get incorporated, resulting in an octamer of histones wrapped by about 150bp of DNA (6).

These histone dynamics depend on a complex network of proteins known as histone chaperones, that bind histones using acidic domains, and control their deposition throughout the cell cycle (7). CAF-1 is the key histone chaperone that assembles newly synthesized histones on replicated DNA (8). It is a heterotrimer made of the large subunit Cac1, the middle subunit Cac2 and the small subunit Cac3 in *S.cerevisiae*, and this composition is highly conserved through evolution (9–11). Modelling of the Cac2 and Cac3 subunits results in globular proteins harboring a typical WD40 fold (12, 13), while Cac1 has an elongated shape suggesting a high degree of disorder (12, 14, 15). It was shown that CAF-1 binds H3-H4 via a composite interface that involves the Cac2 subunit and the acidic domain in Cac1 (12, 14, 15). Recent work determined the structure of a human CAF-1 subcomplex bound to H3-H4 (16), whose features are in line with previous biochemical data using the yeast complex (reviewed in (9)).

In the course of DNA synthesis, CAF-1 assembles chromatin on both leading and lagging strands (17) through its recruitment by PCNA. During chromatin assembly, two CAF-1-H3-H4 complexes assemble on PCNA (17). They coordinate their action on PCNA via DNA binding by the WHD domain to promote the assembly of a (H3-H4)₂ tetramer, and its deposition onto DNA (14, 15, 17).

PCNA is a ring-shaped homotrimer (18) (Figure S1A) that encircles DNA during DNA synthesis (19), where it acts as the processivity factor for DNA polymerases ϵ and δ (20). Due to its asymmetry, we distinguish the front side of PCNA where the polymerases bind (21), and the back side of the protein (Figure S1A). PCNA interactors carry conserved PCNA Interacting Peptides (PIPs) that bind in a conserved pocket located on the front side of PCNA (hereafter referred to as the PIP binding region) (Figure S1A).

CAF-1 is recruited to PCNA via a direct interaction mediated by its two PIPs, PIP1 and PIP2, and via DNA binding by the KER domain (17, 22–24). An early study in yeast found a PCNA mutation that phenocopies CAF-1 mutations (PCNA-RD; R61A, D63A) (22), without affecting the PCNA trimer structure (25). Interestingly, the mutated amino acids are protruding on the back side of PCNA (far from the PIP binding region) where nucleosomes are thought to be made (17) (Figure S1A). Recent work established that PCNA-RD leads to transient loss of silencing in heterochromatin (26), further linking this mutation to CAF-1-related mechanisms. Due to these studies, CAF-1 is thought to bind the back side of PCNA, but this remains to be directly tested.

Here, we combine AlphaFold-Multimer (AF-Multimer) structure prediction on the CAF-1-PCNA-H3-H4 complex with biochemical reconstitutions to study how CAF-1 and PCNA interact. We found that CAF-1 binds PCNA in a unique mode involving PIP domains and a novel interface between the Cac3 subunit and the RD region in PCNA, which is indeed mutated in the PCNA_RD mutant. CAF-1 seems to embrace PCNA in a unique way from the known PCNA interactors. This organization favors the positioning of the histone binding core of CAF-1 towards the back of the PCNA ring, where we hypothesize that histones must be deposited during DNA replication. Using biochemical reconstitution, we tested these structural hypotheses. First, we confirmed individual roles for both PIP domains in CAF-1 recruitment to PCNA and chromatin assembly activity. Interestingly, mutations of PCNA at the RD region lead to no significant defects in PCNA binding and PCNA-dependent chromatin assembly *in vitro*. This work shows that CAF-1 uses a complex set of interactions on PCNA.

Results

The PIPs of CAF-1 have distinct functions in PCNA recruitment and activity

Previous work in cells determined that the CAF-1-PCNA interaction is primarily occurring through the PIP2 domain in Cac1 (17, 24). Yet, Cac1 harbors a second canonical PIP domain in its N-terminus named PIP1 (Figure S1B), and we sought to determine the individual role of both PIPs in PCNA recruitment using recombinant yeast proteins.

As previously shown, CAF-1 forms a stable interaction with DNA-loaded PCNA (Figure 1A) and we have shown that this interaction is dependent on the integrity of both PIP domains (Figure 1B) (17). We next introduced mutations in either PIP1 or PIP2 to study their contribution separately (Figure S1B and S1C). PIP1 mutations did not affect CAF-1 recruitment to DNA-loaded PCNA (Figure 1C). Mutating the PIP2 domain did not abrogate the CAF-1-PCNA interaction either (Figure 1D). This was unexpected as previous work in yeast cells showed that this mutation impacts CAF-1 activity on chromatin (24). This indicates that either PIPs on CAF-1 can promote CAF-1 recruitment to PCNA.

We find that either PIP1 or PIP2 can promote CAF-1 recruitment to PCNA, and we hypothesized that their role may differ during chromatin assembly, based on their different phenotypes in cells (23). Therefore, we used the recently developed PCNA-NAQ assay that specifically measures the PCNA-dependent activity of CAF-1 (17). In this assay, PCNA is loaded on plasmid DNA and recruits CAF-1 where chromatin assembly reactions take place (Figure 1E and 1F). As previously shown, WT-CAF-1 efficiently assembles chromatin on DNA where PCNA is loaded, while CAF-1_PIP** shows a drastic loss of activity (Figure 1E and 1F). Consistent with binding experiments (Figure 1C), the chromatin assembly efficiency of CAF-1_PIP1* was comparable to WT-CAF-1 (Figure 1E and 1F). Surprisingly, CAF-1_PIP2* failed to assemble chromatin on PCNA (Figure 1E and 1F), while retaining its chromatin assembly activity independently of PCNA (Figure 1E, right panel), indicating that PIP2 is required for the activity of CAF-1 on PCNA.

Overall, these results show that the two CAF-1 PIPs have distinct activities. Either PIP is dispensable for CAF-1 recruitment to PCNA, suggesting that they each are able to mediate this interaction. Yet, only PIP2 is essential to mediate CAF-1 activity on PCNA. This suggests that PIP2 may control other aspects of the CAF-1-PCNA interaction such as the stoichiometry of the complex, its organization or its binding properties.

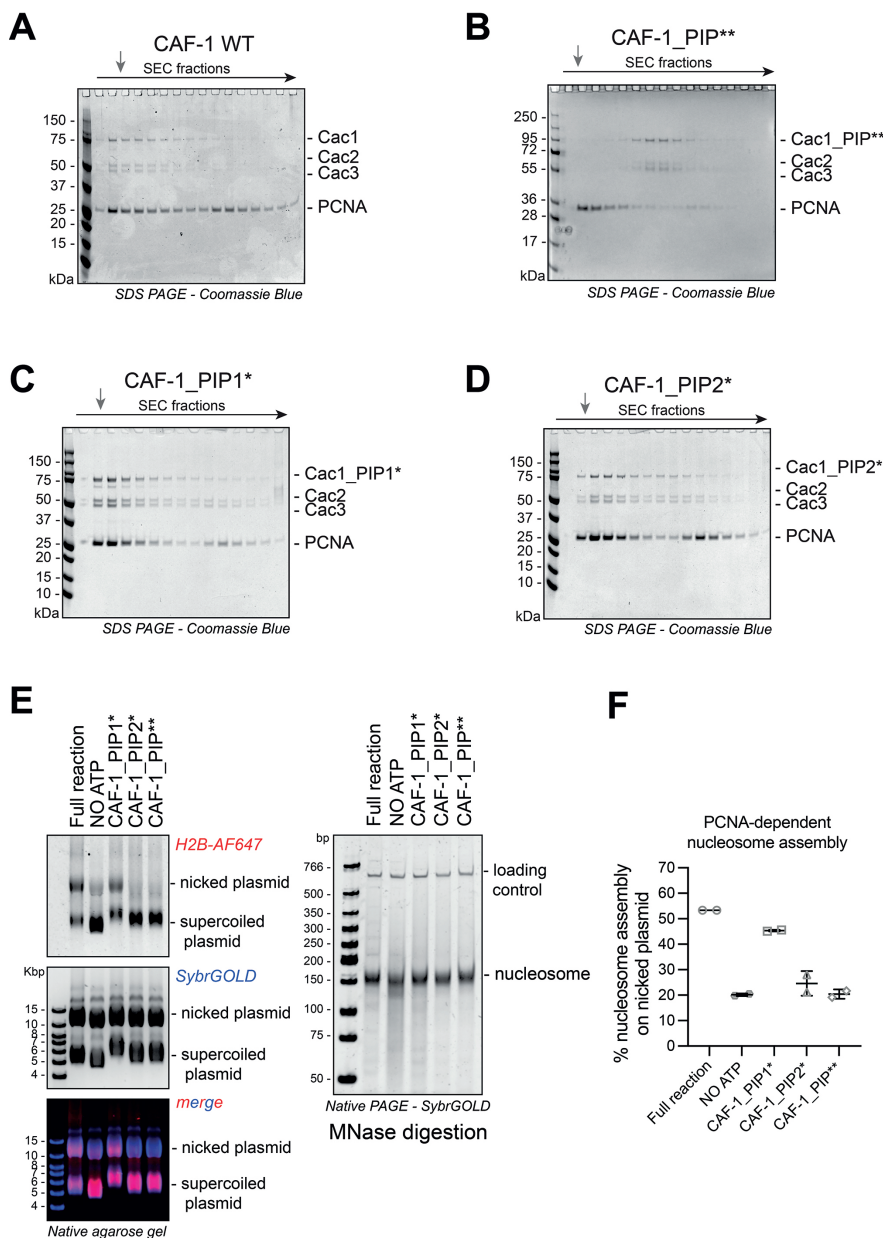


Figure 1: CAF-1 uses several PIP domains to bind DNA-loaded PCNA. (A-D) SDS-PAGE following SEC analysis of PCNA loading experiments in presence of ATP and RFC with (A) CAF-1 WT, (B) CAF-1_PIP**, (C) CAF-1_PIP1* and (D) CAF-1_PIP2*. Grey arrows indicate the elution volume of the plasmid DNA used for PCNA loading. **(E)** Left panel: Native agarose gel analysis of PCNA-NAQ assay reactions with CAF-1_PIP1*, CAF-1_PIP2* or CAF-1_PIP**. The first gel shows H2B fluorescence, with the signal on nicked plasmid representing PCNA-mediated chromatin assembly. Right panel: Native PAGE stained with SybrGOLD following Micrococcal Nuclease (MNase) digestion of the samples shown in the left panel. **(F)** Quantification of H2B fluorescent signal on nicked plasmid in (E), reflecting PCNA-mediated chromatin assembly.

Additional low affinity interfaces exist between CAF-1 and PCNA

We further studied this interaction outside of the context of DNA, using crosslinking experiments and fluorescence polarization. We and others previously showed that in absence of DNA, histone binding to CAF-1 further promotes interaction with PCNA (10, 17) (Figure S1D). We wondered if this DNA-independent and histone-dependent interaction is also promoted by the PIPs on CAF-1.

Interestingly, crosslinking experiments revealed that this interaction is not dependent on the PIPs of CAF-1 (Figure S1D). Using fluorescence polarization experiments, we found that the affinity of this PIP-independent interaction is low ($K_D > 8\mu\text{M}$, K_D was estimated using the equation provided due to lack of a clear maximal response) (Figure S1E), compared to the binding affinity that we previously estimated between CAF-1 and PCNA in the presence of DNA (~100 nM) (17), suggesting that it plays a minor role in driving the assembly of a CAF-1-PCNA complex. These data suggest that histone binding to CAF-1 may unmask low-affinity additional interfaces that are distinct from the PIPs to bind PCNA. These interfaces may finetune the interaction and organization of the CAF-1-PCNA complex.

AlphaFold predicts an extended interaction between CAF-1 and PCNA

In order to obtain a comprehensive model of how CAF-1 and PCNA interact, we performed structure predictions using AF-Multimer. The resulting model of an isolated CAF-1 complex (Figure S2A-G) confirms previous biochemical findings showing that it is a highly flexible heterotrimeric complex, where the large subunit (Cac1) is highly disordered, while the small and middle subunits (Cac3 and Cac2 respectively) are globular and spatially separated (Figure S2A-G) (14, 15). Moreover, the global organization of the Cac1 subunit is in line with previous work from several groups (12, 14, 15, 17, 24, 29, 30), increasing the likelihood of this predicted organization. This organization was also confirmed by a recent structure of a human CAF-1 sub-complex (16).

We previously reported that two CAF-1 assemble on DNA-loaded PCNA using biochemical analysis with mass photometry of the isolated complex (17). We also found that the interaction of CAF-1 with PCNA is regulated by the binding of H3-H4 to the acidic domain in the large subunit of CAF-1 (17). Therefore, we used AF-Multimer to predict the organization of two CAF-1-H3-H4 complexes on a PCNA homotrimer. The predicted assembly of these complexes largely aligns with previously published work (12, 14, 15, 17, 24, 29, 30). The two H3-H4 dimers associate in a (H3-H4)₂ tetramer (6) that is wrapped on each side by the disordered acidic domains of the two Cac1 subunits. As previously reported, the Cac2 subunit is also predicted to bind to H3-H4 (12).

AF-Multimer successfully predicted an interaction between PCNA and the two CAF-1 (Figure 2A-B, and Figure S3A-E). CAF-1 sits on the edge of PCNA, and extends on the front and the back side of the ring, suggesting an extended interaction that, to our knowledge, has not yet been seen in other PCNA-binding proteins (Figure 2A-B and S3A-E). CAF-1 wraps PCNA and DNA on the front side of PCNA, while the back side consists of the histone binding and chromatin assembly module. Notably, PCNA and histones mediate the association of the two CAF-1 complexes and no interactions are predicted between the two CAF-1, in line with previous data showing that CAF-1 complexes do not dimerize (14, 15). Each CAF-1 binds PCNA via the PIP2 domains in Cac1, in line with our experimental data (Figure 1A-D). Interestingly, PIP1 was not predicted to interact with PCNA in those conditions.

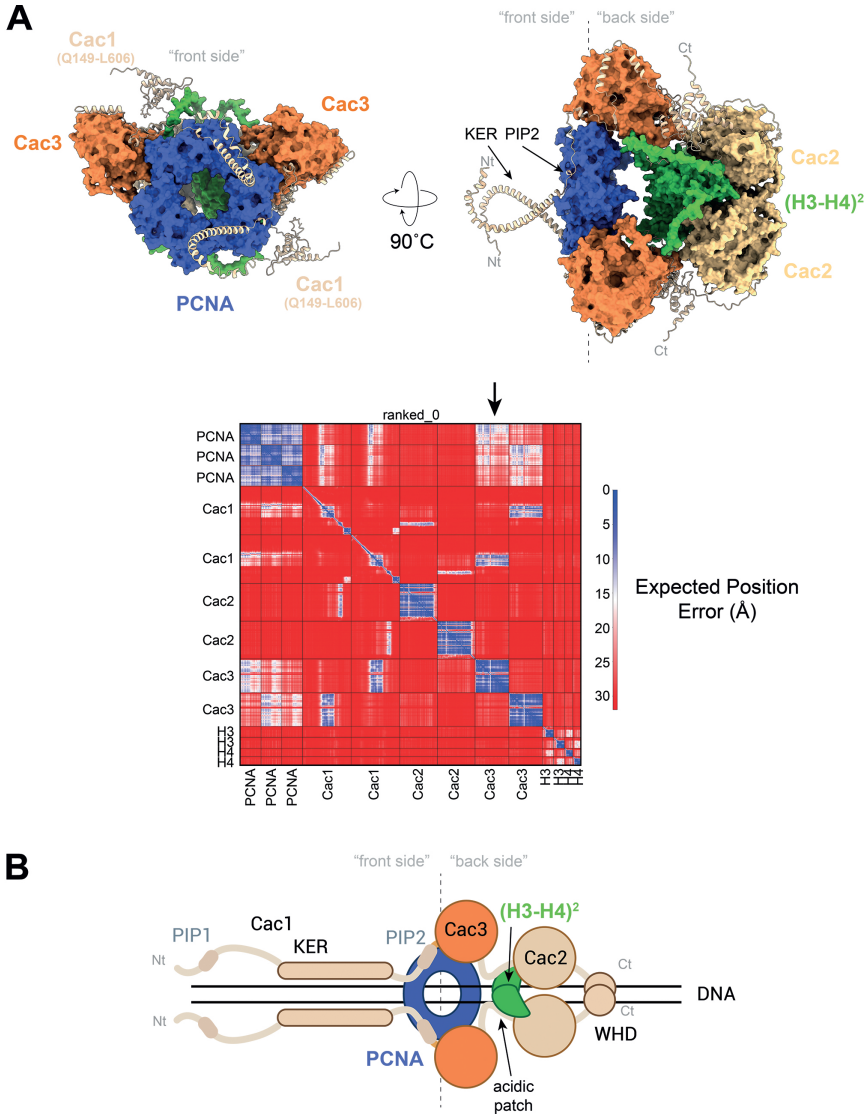


Figure 2: CAF-1 uses an extended interface to bind PCNA. (A) Top panels: AlphaFold-Multimer prediction of a PCNA homotrimer and two CAF-1-H3-H4 complexes (*S.cerevisiae*). The residues Q149 to L606 are shown for each Cac1 subunit (including KER, PIP2, Cac3 and Cac2 binding site, the acidic domain and the WHD) and the N-termini and C-termini are indicated for each Cac1. Due to their high degree of disorder, the Cac1 subunits are shown using a cartoon style, while all other subunits are depicted using a surface style. The front side refers to the PCNA interface where the PIP binding pocket is, while the back side refers to the opposite side. Bottom panel: The Predicted Alignment Error (PAE) matrix is shown for the highest-ranked prediction (ranked_0). An example of the low expected position error between PCNA and Cac3 is indicated by an arrow. **(B)** Cartoon representation depicting two CAF-1-H3-H4 complexes assembling on DNA-loaded PCNA. PIP1 is predicted unstructured, while each PIP2 are bound to distinct PCNA monomers. The KER and the WHD bind DNA as previously described (14, 15, 17, 30). Both Cac3 bind PCNA in the RD region, placing the acidic domains face to face. The acidic domains cooperate with Cac2 for the binding of (H3-H4)₂ as previously described (12, 14, 15).

We find that the relative orientation of the two CAF-1 to each other ideally positions the acidic domains “face to face” allowing for H3-H4 tetramerization, the first step of chromatin assembly (Figure 2A-B and S3A-E). This optimal orientation is largely due to a novel predicted interaction between Cac3 and PCNA (Figure 2A-B and S3A-E). The novel PCNA-Cac3 interaction occurs near the RD residues on PCNA, which are mutated in PCNA-RD (22). This interaction was found in all 5 predictions, increasing its likelihood (Figure 2A-B and S3A-E). Further analysis of the interfaces involved (using PDBePISA) indicates that PCNA uses an extended set of residues for this interaction. It includes its N-terminus (residues 1-5), the RD region (residues 59-64) and residues 89 to 94. On the other hand, Cac3 uses a unique sequence that encompasses residues 159 to 172. Taken together, these residues form 14 ionic bonds over 500 Å². Sequence alignment of Cac3 and PCNA across several species revealed a high degree of conservation of the interfaces involved in this interaction (Figure S4A-B). This strongly suggests that the RD residues may regulate CAF-1 recruitment to PCNA, explaining the cellular phenotypes observed previously (22, 26). Based on this AF prediction, CAF-1 thus binds PCNA using an extended interface: beyond the canonical PIP interaction, CAF-1 may bind via the Cac3 subunit the RD region on PCNA.

PCNA_RD does not influence CAF-1 function *in vitro*

We directly tested the effect of the PCNA_RD mutation on CAF-1 function. We expressed and purified PCNA-RD (Figure S4C), and tested its ability to recruit CAF-1 on DNA using size exclusion chromatography. PCNA-RD was efficiently loaded on DNA by RFC (Figure 3A), suggesting that defects previously observed with this mutant are not due to deficiencies in DNA loading or PCNA instability on DNA. Moreover, PCNA-RD recruited CAF-1 on DNA (Figure 3B) with a similar efficiency to wild type PCNA (Figure 1A), suggesting that this interface is dispensable for the interaction of CAF-1 and PCNA on DNA, again supporting the primary role of the PIPs in CAF-1 recruitment

It was previously shown that the CAF-1-PCNA interaction competes with DNA polymerase epsilon (Pole) binding to PCNA, and therefore slows down DNA synthesis (17). Therefore, we wondered if PCNA-RD also promotes the CAF-1-mediated inhibition of the polymerase, as an independent way to further test that PCNA-RD can efficiently bind CAF-1. Both WT and PCNA-RD stimulated DNA synthesis by Pole, indicating that this mutation does not affect the PCNA function towards DNA polymerases (Figure 3C). Moreover, CAF-1 inhibited Pole activity also in the presence of the PCNA-RD mutant (Figure 3C). This confirms that the RD mutation does not significantly affect CAF-1 recruitment to PCNA, consistent with the results of the binding assay (Figure 3B). Therefore, we show that the Cac3-PCNA interaction is not a strong driver of the CAF-1-PCNA complex assembly.

Next, we tested the ability of PCNA-RD to stimulate CAF-1 nucleosome assembly activity using the PCNA-NAQ assay. PCNA-RD leads to no significant differences (Figure 3D and 3E). This indicates that the PCNA-RD mutation does not affect the PCNA-mediated activity of CAF-1, which is mostly driven by PIP interactions.

Overall, from our data it remains unclear what is the role of the Cac3-PCNA interface for CAF-1 function. Experimental determination of the CAF-1-PCNA structure is required to confirm this interface and understand its function.

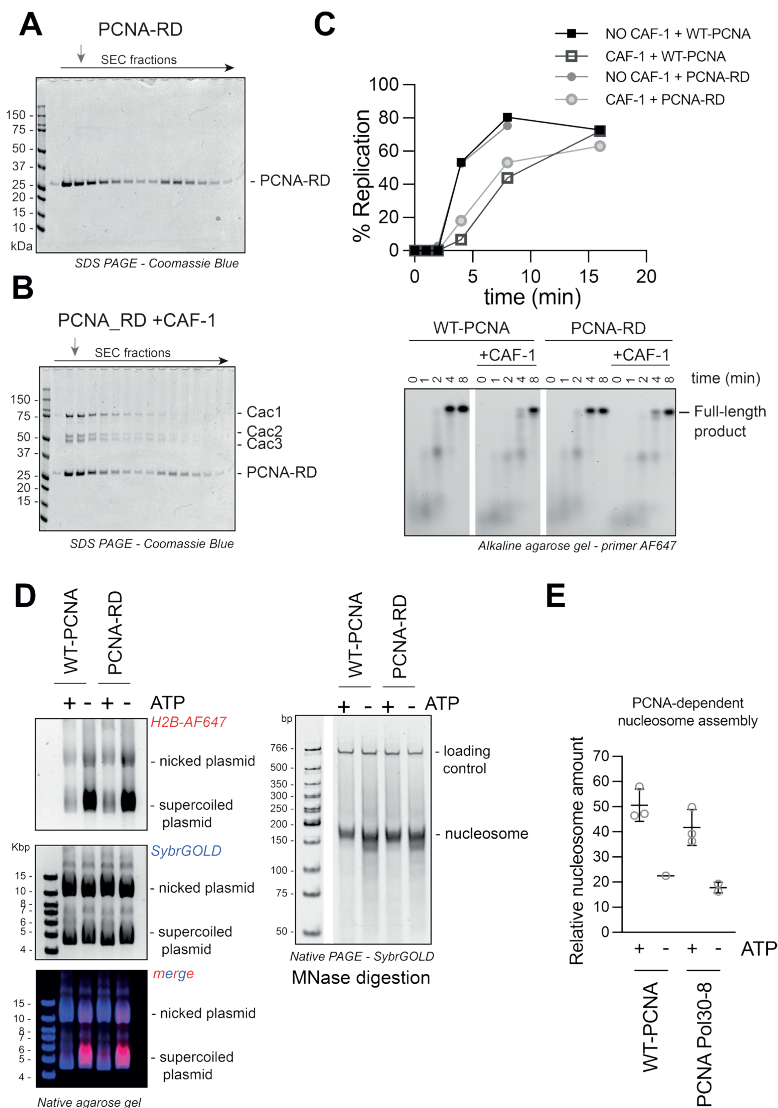


Figure 3: PCNA-RD promotes CAF-1 recruitment on DNA and stimulates its chromatin assembly activity. (A-B) SDS-PAGE following SEC analysis of PCNA loading experiments in presence of ATP and RFC with (A) PCNA-RD alone, and (B) PCNA-RD with CAF-1. Grey arrows indicate (C) Top panel: Quantification of the % of replication following a primer extension experiment with Pole. %Replication represents the intensity of the full-length product band relative to the total fluorescence in each lane (expressed in percentages) from the bottom panels. Bottom panel, Fluorescence scan of a denaturing alkaline agarose gel of primer extension reactions with Pole, comparing WT-PCNA to PCNA-RD in presence or absence of CAF-1. The experiment was only performed once and should be repeated for statistical significance. (D) Left panel: Native agarose gel analysis of PCNA-NAQ assay reactions with WT-PCNA or PCNA-RD. The first gel shows H2B fluorescence, with the signal on nicked plasmid representing PCNA-mediated chromatin assembly. Right panel: Native PAGE stained with SybrGOLD following Micrococcal Nuclease (MNase) digestion of the samples shown in the left panel. (E) Quantification of H2B fluorescent signal on nicked plasmid in (D), reflecting PCNA-mediated chromatin assembly.

Discussion

In this work, we investigate the molecular assembly of the CAF-1-PCNA complex using structure prediction tools and biochemical reconstitutions. We show that similarly to other PCNA interactors (31), CAF-1 carries multiple PIP domains that each regulate its function on PCNA. Moreover, we provide evidence for a novel extended interface between CAF-1 and PCNA, involving the small CAF-1 subunit Cac3 and the RD region on PCNA. Our work highlights the complexity of this critical interaction for epigenome stability, identifying a novel interface in this process, and enabling a structural understanding of this mechanism.

CAF-1 uses several PIP domains with distinct functions during chromatin assembly

We report here that additionally to PIP2, the PIP1 domain (unknown in yeast so far) is involved in recruiting CAF-1 to PCNA. Previous works has shown that it is common for PCNA binding protein to use several PIP domains to act on PCNA (32): One (at least) is localized in long disordered region similarly to PIP1, and a second one like PIP2, is in the core of the protein. So why does CAF-1 have two PIPs and how do these regulate its function? Several hypotheses can be envisioned. PIP1 may be used for the initial recruitment of CAF-1 to PCNA and is then replaced by PIP2. Yet, three PIP binding sites are available on PCNA, so replacing might not be necessary *per se*. As two CAF-1 complexes are required for nucleosome assembly, it is possible that these interactions coordinate CAF-1 stoichiometry on PCNA. Another attractive model suggests that CAF-1 may bind distinct PCNA trimers at the same time using both PIP1 and PIP2. Further studies are needed to disentangle these hypotheses, using high resolution methods such as CryoEM and single molecule-based assays.

Previous work in yeast and human cells found that a single mutation of PIP1 or PIP2 is not sufficient to fully abrogate CAF-1 recruitment to PCNA (23, 24). Here, our biochemical reconstitutions show a redundancy of PIP1 and PIP2 in CAF-1 recruitment to PCNA. Interestingly we find that only PIP2 is essential during PCNA-dependent chromatin assembly, while it is dispensable for CAF-1 recruitment to PCNA. Previous work showed similar phenotypes when mutating the WHD in Cac1 (17). Using mass photometry, it was shown that this domain may control the stoichiometry of CAF-1 on DNA-loaded PCNA. Therefore, we speculate that the PIP2 domain may affect the association of a second CAF-1 with PCNA on DNA. This hypothesis would suggest that one CAF-1 complex must be bound to DNA-loaded PCNA in order to recruit a second one.

An interaction between Cac3 and PCNA may promote the positioning of CAF-1 that drives H3-H4 tetramerization

Using AF-Multimer and biochemical evidences (22, 26, 33), we identified a new binding interface between PCNA and the Cac3 subunit of CAF-1. This novel interaction optimally positions both CAF-1-H3-H4 on PCNA, therefore promoting H3-H4 tetramerization, and subsequent nucleosome assembly. This work allows us to get a first glance at how CAF-1 deposits histones on DNA.

It has been shown in cells that PCNA-RD strongly impedes CAF-1 function (22, 26, 33). Here, we show that this mutant does not affect CAF-1 recruitment, nor its PCNA-dependent activity.

Therefore, the phenotypes observed in cells emerge from problems that our reconstitutions do not yet recapitulate. Here, we show that the Cac3-PCNA interaction at the RD interface optimally positions the chromatin assembly modules of CAF-1 on the back side of PCNA. It is conceivable that mutating the RD region could result in a reverse binding of CAF-1 to PCNA, leading to chromatin assembly on the front side of PCNA. Future studies need to develop suitable experiments to investigate this possibility and how this may affect other chromatin processes, such as recycling of parental histones for instance.

The predicted assembly of a CAF-1-PCNA complex leads us to reconsider the model of how new histones are deposited at forks.

Current models of chromatin assembly during DNA replication suggest that CAF-1 function is physically coupled to DNA synthesis (4, 5). This means that PCNA binds CAF-1 and the DNA polymerases ϵ/δ at the same time (31). This allows replicated DNA to be readily assembled into chromatin. Recently, we have demonstrated that PCNA is unable to share simultaneously CAF-1 and Pole, the DNA polymerase of the leading strand (17), indicating that more complex dynamics are at play on PCNA molecules at replication forks. In light of the data presented here, where CAF-1 has extensive contacts with the back and front side of PCNA, we hypothesize that PCNA sharing may not be possible with Pol δ on the lagging strand, and likely with many more PCNA-binding proteins that are present at forks. Therefore, additional mechanisms need to be investigated to understand the integration of DNA and chromatin replication. The availability of PCNA molecules at fork may well regulate such integration, placing PCNA loading and unloading at the heart of these processes.

Methods

Protein expression and Purification

All proteins used in this study were expressed, purified as previously described (17). All fluorescent labeling reactions were conducted as reported in (17). PCNA-RD (R61A, D63A), CAF-1_PIP1* (F22A, F23A) and CAF-1_PIP2* (F233A, F234A) were generated using standard mutagenesis protocols, and they were expressed and purified with the same protocol that the wild type proteins used in (17).

PCNA-CAF-1 binding experiments on SEC

We used nicked pUC19 as template for PCNA loading. The plasmid was digested with the nicking enzyme Nt.BspQI for 8 h at 50°C, before being purified via phenol chloroform extraction. Nicked pUC19 (0,3 μ M) was then incubated with PCNA (30 μ M monomer), RFC (0.5 μ M), ATP (3 mM), and MgCl₂ (10 mM), in PCNA loading buffer (50 mM HEPES pH 7.5, 200 mM NaCl, 0.01% IGEPAL CA-360, 1mM TCEP). After 5 minutes at 30°C, CAF-1 was added to the reactions (5 μ M) and further incubated at room temperature for 15 minutes. Samples were then injected on Superose 6 increase 3.2–300 columns connected to an AKTA pure system fitted with PEEK I.D. 0.25 mm tubing. The reaction was eluted in PCNA loading buffer supplemented with 10 mM MgCl₂, and samples were analyzed on 4-12% gradient SDS-PAGE run in MES buffer.

PCNA-NAQ assay

We used nicked pRC1765 (Addgene #141346) for PCNA loading and chromatin assembly. The plasmid was digested with the nicking enzyme Nt.BbvCI for 6 h at 37°C, and was then purified via phenol chloroform extraction. The nicked plasmid (50 nM) was mixed with supercoiled pRC1765 (50 nM), 1,1 μM of RFC, 10,9 μM of PCNA monomer, 10,9 mM ATP and 8 mM MgCl₂ in PCNA loading buffer. Typically, this reaction was performed in 11 μl final volume. The reactions were incubated for 5 minutes at 30°C. Samples were then diluted 3-fold with NA buffer to lower the MgCl₂ concentration that otherwise inhibits chromatin assembly. CAF-1 prebound to H3-H4 dimers (100 nM each) were added to the reaction and incubated 15 minutes at room temperature. Fluorescently labeled H2A-H2B dimers (100 nM) were then added to allow full nucleosome assembly, and incubated for 15 minutes at room temperature. Samples were spun down for 5 minutes at 170000 x g to remove potential precipitates. 1 μl of reactions was mixed with 5 μl of loading buffer (NA buffer + 5% sucrose). Samples were separated on 0.8% native agarose gel, run in 1X TAE (Tris-Acetate EDTA) for 90 minutes.

MNase reactions were then performed with the rest of the PCNA-NAQ reactions. Briefly, 25 μl of sample was incubated with 80 units of MNase (NEB #M0247S) in 100 μl final volume of 50 mM Tris pH 7.9, 5 mM CaCl₂. Samples were incubated 10 minutes at 37°C prior to inactivation using 20 mM EDTA. Proteins were then digested with ProteinaseK (NEB #P8107S) for 20 minutes at 50°C. A 621bp DNA fragments was added as loading control, and the digested DNA was purified using the MinElute PCR purification kit (Qiagen #28006) according to the manufacturer's instructions. MNase-digested samples were run on 6% native PAGE, and stained with SybrGOLD

AlphaFold, Structure analysis and Sequence alignment

AlphaFold-Multimer (v2.3.2) predictions (27) were run on a Linux cluster using a GPU NVIDIA A100 80GB PCIE, at the High Performance and Cloud computing centre of Utrecht University, through a wrapper script from https://github.com/kalininalab/alphafold_non_docker. Databases and software were downloaded on October 31st, 2024. Predicted structures were relaxed, and the maximum template release data used was 09-11-2023. For each AlphaFold-Multimer run, 5 predictions are shown from ranked_0 to ranked_4, where ranked_0 is the best. The novel Cac3-PCNA interaction was analyzed using PDBePISA from the EMBL-EBI. Protein sequence alignments were performed using Cluster Omega from the EMBL-EBI using the standard procedure, and results of these alignments were further assessed in ChimeraX.

Primer extension

Primer extensions experiments with Pole were performed as previously described (17). Reactions were performed in 25 mM HEPES-KOH pH 7.5, 150 mM potassium acetate, 8 mM magnesium acetate, 1mM TCEP, 1 mM ATP and 0.2 mg/ml BSA. The DNA template was coated with RPA, and incubated for 5 minutes at 30°C. Next, PCNA and RFCΔN were added and loaded onto RPA-coated DNA and incubated 5 minutes at 30°C. Pole was added with dCTP, dATP and dGTP and incubated for 5 minutes at 30°C. Finally, CAF-1 and dTTP were added to fully start DNA synthesis. Samples were quenched in 10 mM EDTA final concentration at the reported time points, and separated on 1.2% denaturing (alkaline) agarose gel.

In-solution crosslinking experiments

Crosslinking experiments were performed in 50 mM HEPES pH 7.5, 200 mM NaCl, 0.01% IGEPAL CA-360, 1mM TCEP. PCNA (6 μ M monomers) was incubated with CAF-1 (2 μ M) for 10 minutes at room temperature. Complexes were crosslinked with 1mM disuccinimidyl suberate (DSS) for 10 minutes at room temperature, prior to quenching with 150 mM TRIS pH 8.0. Samples were separated on 12% SDS-PAGE (BioRad - Criterion), and stained with Coomassie Blue.

Fluorescence Polarization

Fluorescence polarization experiments were performed as previously described (17) in 25mM TRIS pH 7.5, 300 mM NaCl, 5% glycerol, 1 mM EDTA, 0.01% IGEPAL ca-630 (added fresh), 0.01% CHAPS (added fresh), 1 mM DTT (added fresh). 40 nM of PCNA-C4S-K164C labeled with Alexa Fluor 488 (17) were incubated with increasing concentrations of CAF-1 in CORNING low flange 384 well black microplates. Fluorescence polarization was measured with a CLARIOstar (BMG LabTech) plate reader. The binding affinity was determined using a One Site binding curve (not accounting for fluorescent label depletion) in GraphPad PRISM ($y=B_{max} * x / K_d + x + Background$, where B_{max} is the maximum specific binding, K_d is the equilibrium dissociation constant and Background is the measured binding with no added ligand). When no maximal response could be achieved due to low binding affinity, we estimated a minimal K_d based on the One Site binding curve equation. Fluorescence Polarization was measured three times over the course of 15 minutes for each sample, to ensure equilibration of the binding. Each experiment was performed in triplicate.

Acknowledgments

We thank Ren Xie for his help and advice on generating figures related to AF-Multimer analysis.

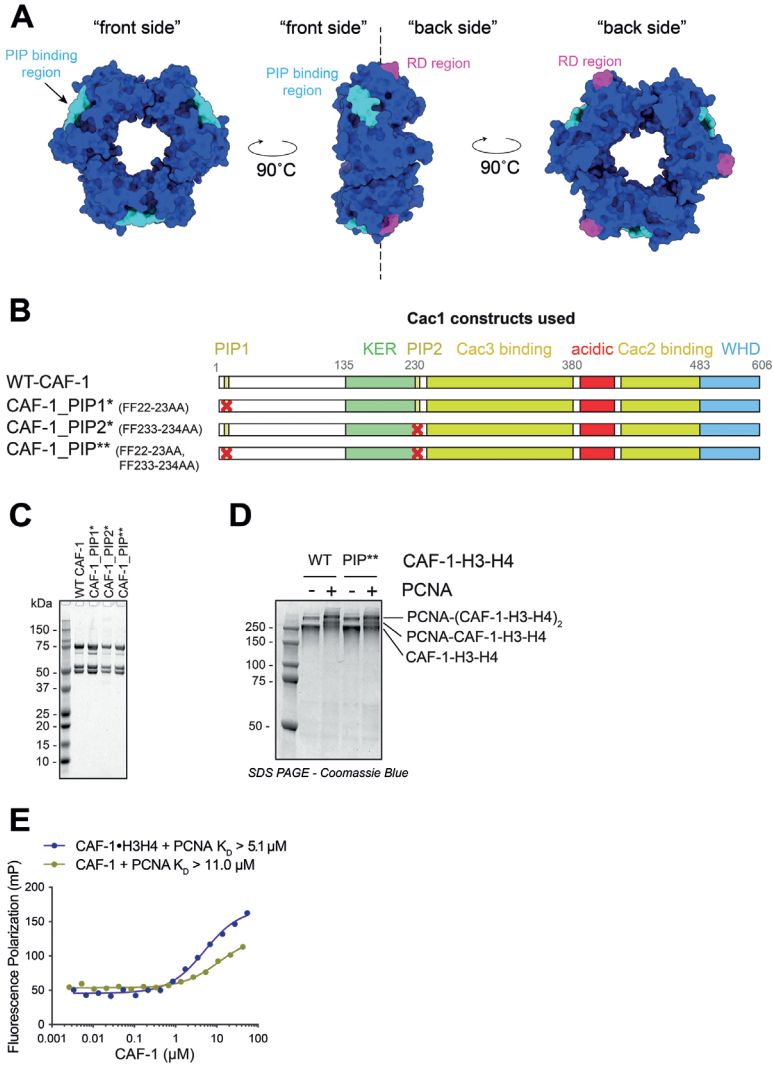


Figure S1: (A) Structure of yeast PCNA homotrimer (PDB: 1PLQ). The front side harbors the PIP binding pocket (cyan) while the RD region (magenta) protrudes towards the back side of PCNA. (B) Cartoons of the Cac1 (large CAF-1 subunit) domains and the mutants used in this study. All complexes contain Cac2 and Cac3, in addition to the indicated Cac1 construct. (C) SDS-PAGE of the purified WT CAF-1 mutants shown in (B). (D) SDS-PAGE of crosslinking reactions containing PCNA, and CAF-1 prebound to H3-H4 dimers as previously described (17). WT CAF-1 and CAF-1_PIP** are compared here. (E) Fluorescence Polarization experiments using fluorescently labeled PCNA and increasing concentrations of CAF-1 or CAF-1 prebound to H3-H4 dimers. The data points were fitted to a one site binding curve and the K_D were calculated in GraphPad. K_D were estimated due to the lack of a clear maximal response.

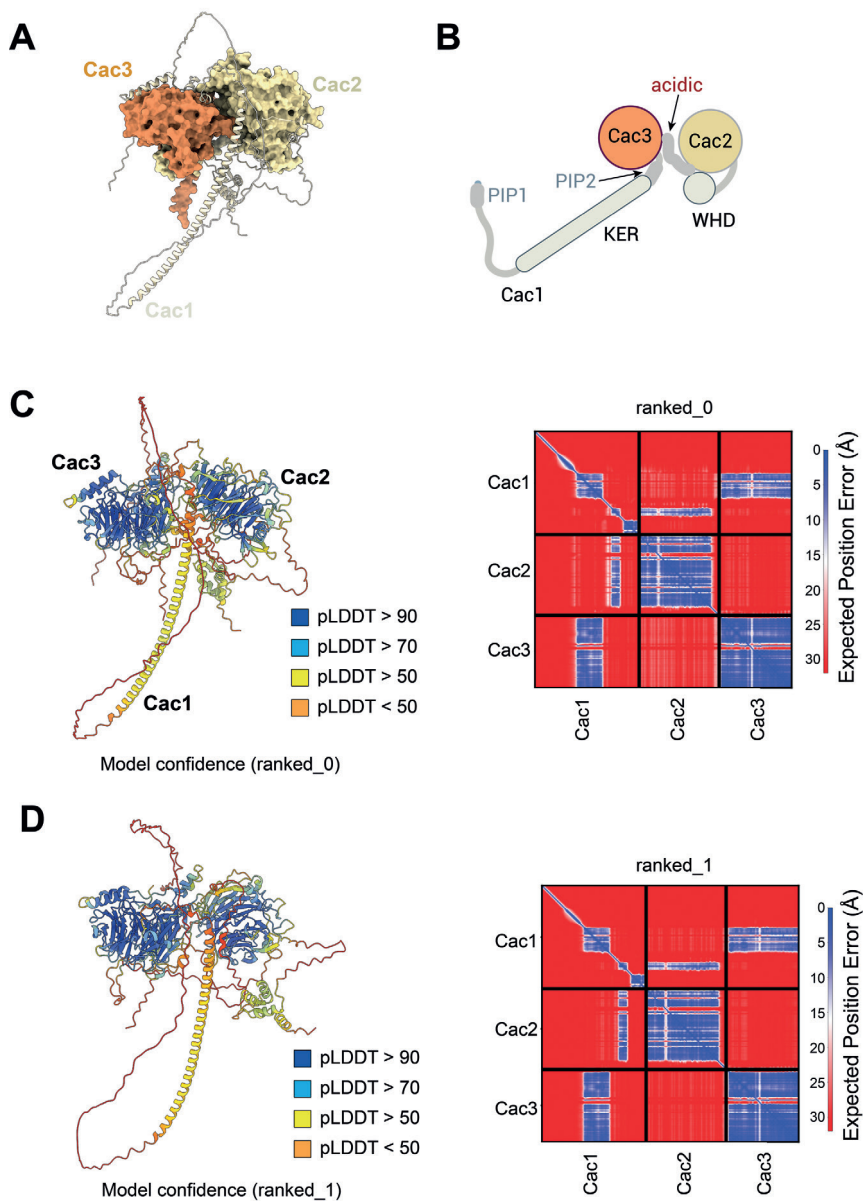


Figure S2: (legend on next page)

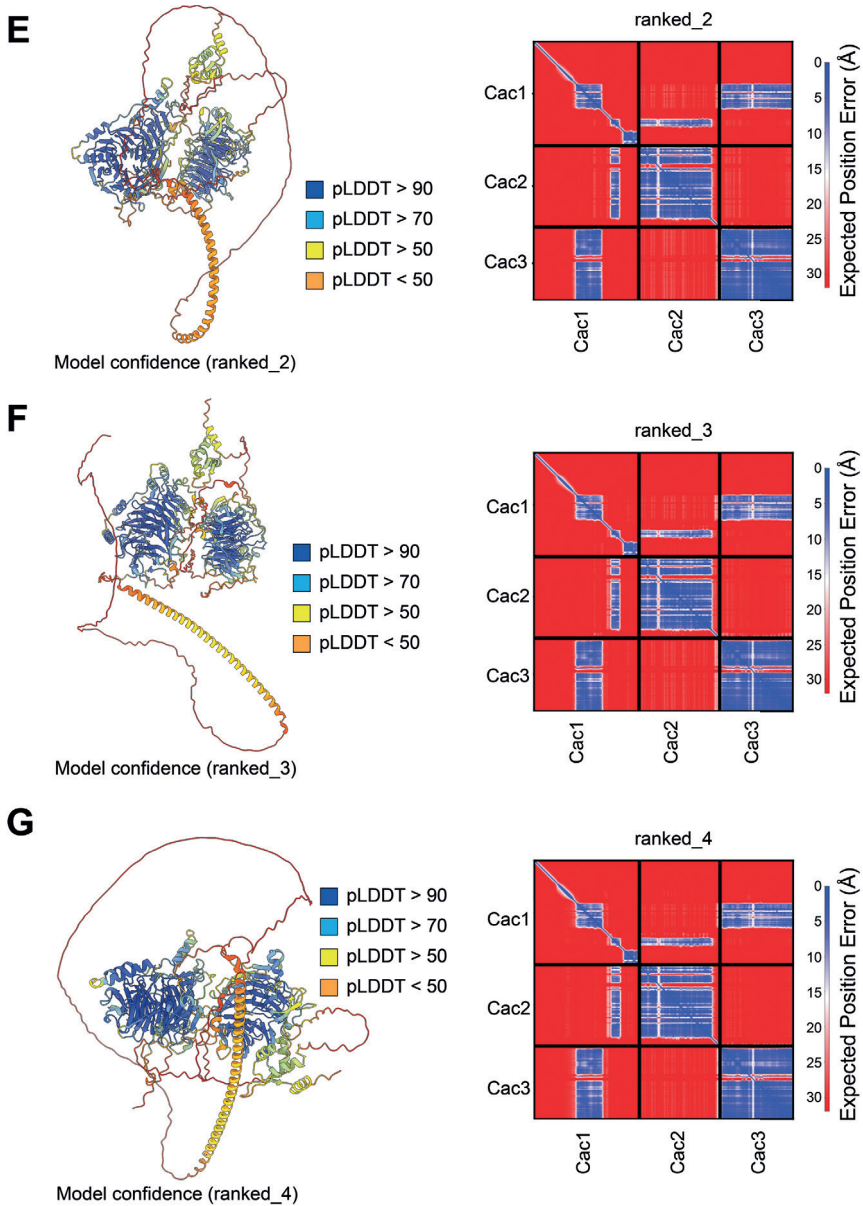
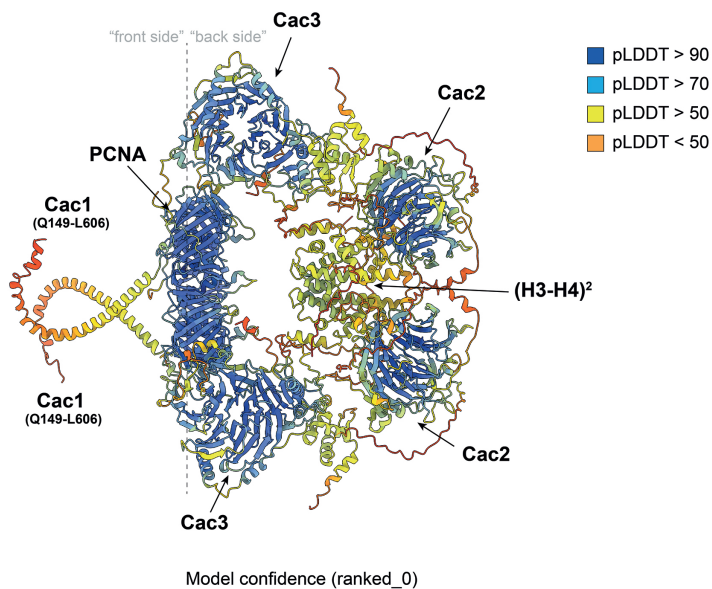


Figure S2: (A) AlphaFold-Multimer prediction of the CAF-1 complex (*S.cerevisiae*). The Cac1 subunit is largely disordered while Cac2 and Cac3 are globular. Due to its high degree of disorder, the Cac1 subunit is shown using a cartoon style, while Cac2 and Cac3 are depicted using a surface style. (B) Cartoon representation of the AF-Multimer prediction shown in (A). In its N-terminus, Cac1 harbors two PCNA Interacting Peptides (PIPs) that flank the KER DNA binding domain, while the C-terminus folds as a WHD DNA binding domain. (C-G) Assessment of the AF-Multimer predictions from ranked_0 to ranked_4 (respectively). Left panels: Cartoon style of the AF-Multimer predictions colored by pLDDT (Local Distance Difference Test). Right panels: PAE matrices indicating the expected position error between Cac1, Cac2 and Cac3.

A



B

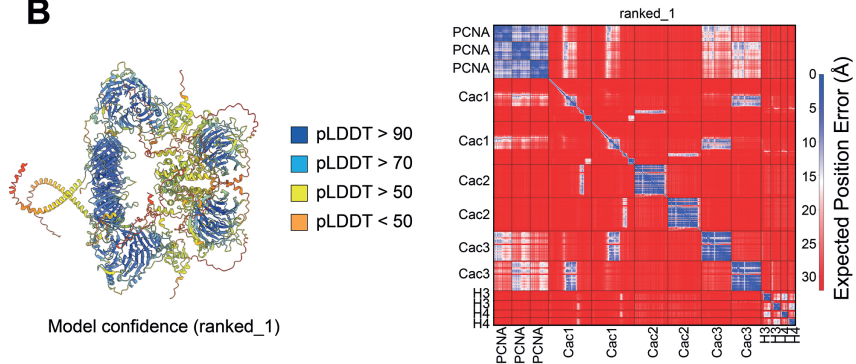


Figure S3: (legend on next page)

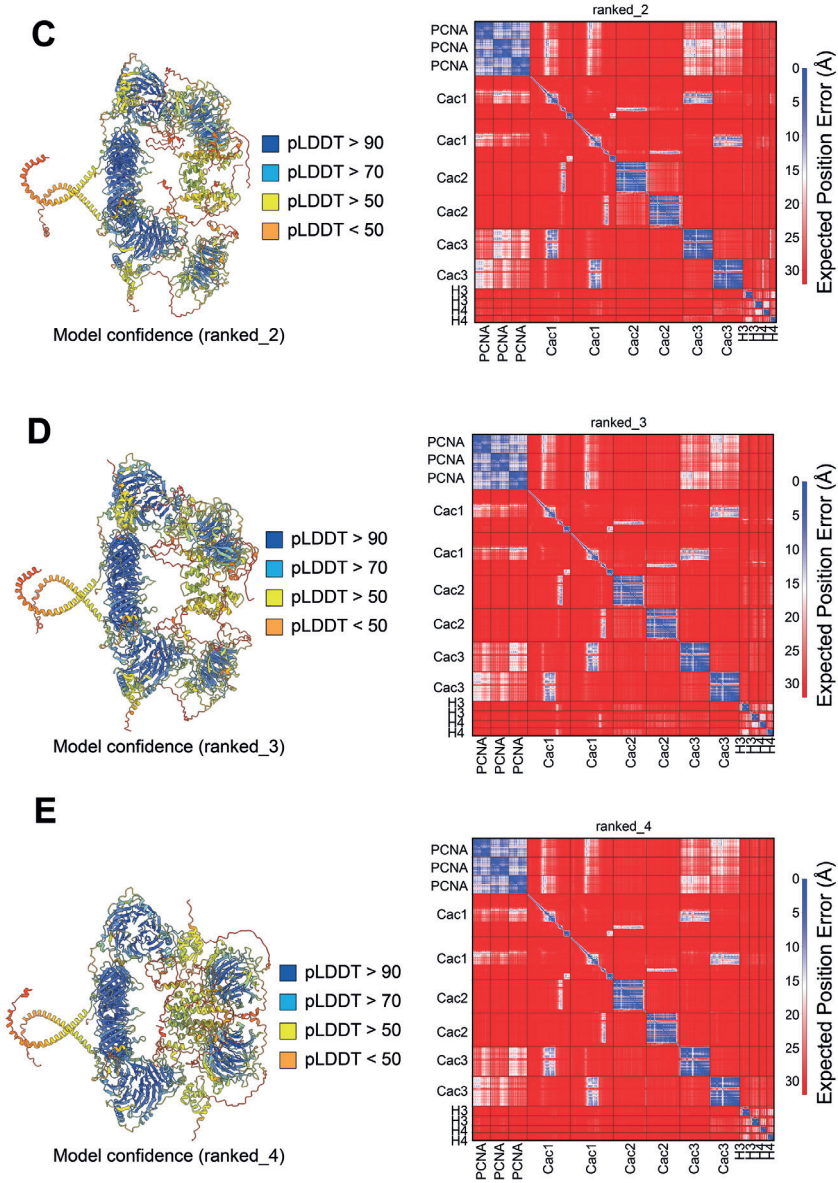


Figure S3: (A) Cartoon style of the AF-Multimer prediction from Figure 2. Prediction ranked_0 colored by pLDDT is shown. (B-E) Assessment of the AF-Multimer predictions from ranked_1 to ranked_4 (respectively). Left panels: Cartoon style of the AF-Multimer predictions colored by pLDDT. Right panels: PAE matrices indicating the expected position error between the individual subunits of one PCNA homotrimer, two CAF-1 heterotrimers, and two H3-H4 dimers.

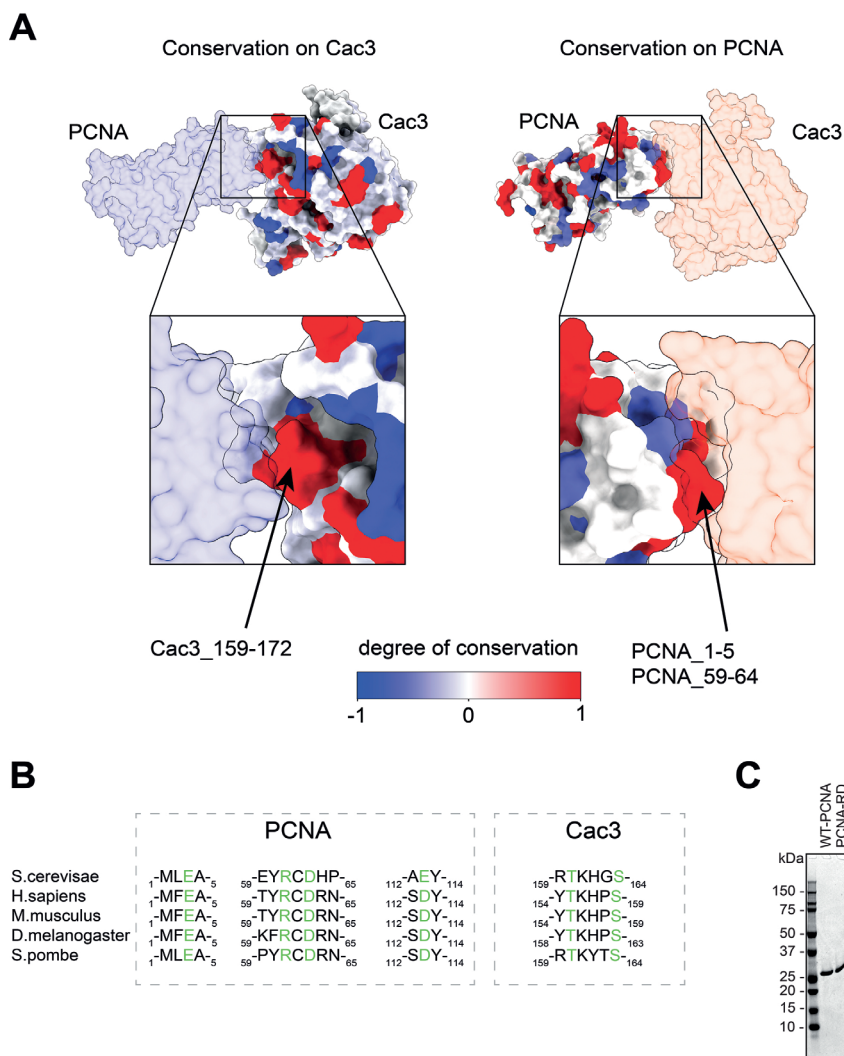


Figure S4: (A) Surface representation of the AF-Multimer prediction ranked_0, colored by level of conservation for Cac3 (left panel) and PCNA (right panel). Cac3 and PCNA were analyzed for conservation between *S.cerevisiae*, *H.Sapiens*, *M.Musculus*, *D.Melanogaster* and *S.Pombe*, and results were imported in ChimeraX. For each protein, the residues involved in the Cac3-PCNA interaction are indicated. (B) Protein sequence alignment of the domain involved in the newly predicted interaction between Cac3 and the RD region of PCNA. Residues highlighted in green are predicted to directly mediate this interaction. (C) SDS-PAGE of purified WT-PCNA and PCNA_RD (yeast).

References

1. M. A. Morgan, A. Shilatifard, Chromatin signatures of cancer. *Genes Dev.* **29**, 238–249 (2015).
2. M. Wang, B. D. Sunkel, W. C. Ray, B. Z. Stanton, Chromatin structure in cancer. *BMC Mol. Cell Biol.* **23**, 35 (2022).
3. M. Bakail, A. Gaubert, J. Andreani, G. Moal, G. Pinna, E. Boyarchuk, M.-C. Gaillard, R. Courbeyrette, C. Mann, J.-Y. Thuret, B. Guichard, B. Murciano, N. Richet, A. Poitou, C. Frederic, M.-H. Le Du, M. Agez, C. Roelants, Z. A. Gurard-Levin, G. Almouzni, N. Cherradi, R. Guerois, F. Ochsenbein, Design on a Rational Basis of High-Affinity Peptides Inhibiting the Histone Chaperone ASF1. *Cell Chem. Biol.* **26**, 1573-1585.e10 (2019).
4. K. R. Stewart-Morgan, N. Petryk, A. Groth, Chromatin replication and epigenetic cell memory. *Nat. Cell Biol.* **22**, 361–371 (2020).
5. T. M. Escobar, A. Loyola, D. Reinberg, Parental nucleosome segregation and the inheritance of cellular identity. *Nat. Rev. Genet.* **22**, 379–392 (2021).
6. K. Luger, A. W. Mäder, R. K. Richmond, D. F. Sargent, T. J. Richmond, Crystal structure of the nucleosome core particle at 2.8 Å resolution. *Nature* **389**, 251–260 (1997).
7. C. M. Hammond, C. B. Strømme, H. Huang, D. J. Patel, A. Groth, Histone chaperone networks shaping chromatin function. *Nat. Rev. Mol. Cell Biol.* **18**, 141–158 (2017).
8. S. Smith, B. Stillman, Purification and characterization of CAF-1, a human cell factor required for chromatin assembly during DNA replication in vitro. *Cell* **58**, 15–25 (1989).
9. P. V. Sauer, Y. Gu, W. H. Liu, F. Mattioli, D. Panne, K. Luger, M. E. Churchill, Mechanistic insights into histone deposition and nucleosome assembly by the chromatin assembly factor-1. *Nucleic Acids Res.* **46**, 9907–9917 (2018).
10. F. Ouasti, M. Audin, K. Freon, J.-P. Quivy, M. Tachekort, E. Cesard, A. Thureau, V. Ropars, P. F. Varela, G. Moal, I. S. Amadou, A. Uryga, P. Legrand, J. Andreani, R. Guerois, G. Almouzni, S. Lambert, F. Ochsenbein, Disordered regions and folded modules in CAF-1 promote histone deposition in *S. pombe*. bioRxiv [Preprint] (2023). <https://doi.org/10.1101/2023.06.02.543505>.
11. H. Kaya, K. Shibahara, K. Taoka, M. Iwabuchi, B. Stillman, T. Araki, FASCIATA Genes for Chromatin Assembly Factor-1 in Arabidopsis Maintain the Cellular Organization of Apical Meristems. *Cell* **104**, 131–142 (2001).
12. F. Mattioli, Y. Gu, J. L. Balsbaugh, N. G. Ahn, K. Luger, The Cac2 subunit is essential for productive histone binding and nucleosome assembly in CAF-1. *Sci. Rep.* **7**, 46274 (2017).
13. D. Kim, D. Setiাপutra, T. Jung, J. Chung, A. Leitner, J. Yoon, R. Aebersold, H. Hebert, C. K. Yip, J.-J. Song, Molecular Architecture of Yeast Chromatin Assembly Factor 1. *Sci. Rep.* **6** (2016).
14. F. Mattioli, Y. Gu, T. Yadav, J. L. Balsbaugh, M. R. Harris, E. S. Findlay, Y. Liu, C. A. Radebaugh, L. A. Stargell, N. G. Ahn, I. Whitehouse, K. Luger, DNA-mediated association of two histone-bound complexes of yeast Chromatin Assembly Factor-1 (CAF-1) drives tetrasome assembly in the wake of DNA replication. *eLife* **6** (2017).

- 15.** P. V. Sauer, J. Timm, D. Liu, D. Sitbon, E. Boeri-Erba, C. Velours, N. Mücke, J. Langowski, F. Ochsenbein, G. Almouzni, D. Panne, Insights into the molecular architecture and histone H3-H4 deposition mechanism of yeast Chromatin assembly factor 1. *eLife* **6**, e23474 (2017).
- 16.** C.-P. Liu, Z. Yu, J. Xiong, J. Hu, A. Song, D. Ding, C. Yu, N. Yang, M. Wang, J. Yu, P. Hou, K. Zeng, Z. Li, Z. Zhang, X. Zhang, W. Li, Z. Zhang, B. Zhu, G. Li, R.-M. Xu, Structural insights into histone binding and nucleosome assembly by chromatin assembly factor-1. *Science* **381**, eadd8673 (2023).
- 17.** C. Rouillon, B. V. Eckhardt, L. Kollenstart, F. Gruss, A. E. E. Verkennis, I. Rondeel, P. H. L. Krijger, G. Ricci, A. Biran, T. van Laar, C. M. Delvaux de Fenffe, G. Luppens, P. Albanese, K. Sato, R. A. Scheltema, W. de Laat, P. Knipscheer, N. H. Dekker, A. Groth, F. Mattioli, CAF-1 deposits newly synthesized histones during DNA replication using distinct mechanisms on the leading and lagging strands. *Nucleic Acids Res.*, gkad171 (2023).
- 18.** T. S. R. Krishna, X.-P. Kong, S. Gary, P. M. Burgers, J. Kuriyan, Crystal structure of the eukaryotic DNA polymerase processivity factor PCNA. *Cell* **79**, 1233–1243 (1994).
- 19.** R. McNally, G. D. Bowman, E. R. Goedken, M. O'Donnell, J. Kuriyan, Analysis of the role of PCNA-DNA contacts during clamp loading. *BMC Struct. Biol.* **10**, 3 (2010).
- 20.** T. A. Guilliam, J. T. P. Yeeles, An updated perspective on the polymerase division of labor during eukaryotic DNA replication. *Crit. Rev. Biochem. Mol. Biol.* **55**, 469–481 (2020).
- 21.** C. Lancey, M. Tehseen, V.-S. Raducanu, F. Rashid, N. Merino, T. J. Ragan, C. G. Savva, M. S. Zaher, A. Shirbini, F. J. Blanco, S. M. Hamdan, A. De Biasio, Structure of the processive human Pol δ holoenzyme. *Nat. Commun.* **11**, 1109 (2020).
- 22.** Z. Zhang, K. Shibahara, B. Stillman, PCNA connects DNA replication to epigenetic inheritance in yeast. **408**, 5 (2000).
- 23.** T. R. Ben-Shahar, A. G. Castillo, M. J. Osborne, K. L. B. Borden, J. Kornblatt, A. Verreault, Two Fundamentally Distinct PCNA Interaction Peptides Contribute to Chromatin Assembly Factor 1 Function. *Mol. Cell. Biol.* **29**, 6353–6365 (2009).
- 24.** K. Zhang, Y. Gao, J. Li, R. Burgess, J. Han, H. Liang, Z. Zhang, Y. Liu, A DNA binding winged helix domain in CAF-1 functions with PCNA to stabilize CAF-1 at replication forks. *Nucleic Acids Res.* **44**, 5083–5094 (2016).
- 25.** C. M. Kondratick, J. M. Litman, K. V. Shaffer, M. T. Washington, L. M. Dieckman, Crystal structures of PCNA mutant proteins defective in gene silencing suggest a novel interaction site on the front face of the PCNA ring. *PLOS ONE* **13**, e0193333 (2018).
- 26.** M. Brothers, J. Rine, Mutations in the PCNA DNA Polymerase Clamp of *Saccharomyces cerevisiae* Reveal Complexities of the Cell Cycle and Ploidy on Heterochromatin Assembly. *Genetics* **213**, 449–463 (2019).

- 27.** R. Evans, M. O'Neill, A. Pritzel, N. Antropova, A. Senior, T. Green, A. Žídek, R. Bates, S. Blackwell, J. Yim, O. Ronneberger, S. Bodenstein, M. Zielinski, A. Bridgland, A. Potapenko, A. Cowie, K. Tunyasuvunakool, R. Jain, E. Clancy, P. Kohli, J. Jumper, D. Hassabis, Protein complex prediction with AlphaFold-Multimer. *bioRxiv [Preprint]* (2022). <https://doi.org/10.1101/2021.10.04.463034>.
- 28.** M. A. Cianfrocco, M. Wong-Barnum, C. Youn, R. Wagner, A. Leschziner, "COSMIC2: A Science Gateway for Cryo-Electron Microscopy Structure Determination" in *Proceedings of the Practice and Experience in Advanced Research Computing 2017 on Sustainability, Success and Impact* (Association for Computing Machinery, New York, NY, USA, 2017; <https://dl.acm.org/doi/10.1145/3093338.3093390>) *PEARC17*, pp. 1–5.
- 29.** W. H. Liu, S. C. Roemer, Y. Zhou, Z.-J. Shen, B. K. Dennehey, J. L. Balsbaugh, J. C. Liddle, T. Nemkov, N. G. Ahn, K. C. Hansen, J. K. Tyler, M. E. Churchill, The Cac1 subunit of histone chaperone CAF-1 organizes CAF-1-H3/H4 architecture and tetramerizes histones. *eLife* **5** (2016).
- 30.** R. Rosas, R. R. Aguilar, N. Arslanovic, A. Seck, D. J. Smith, J. K. Tyler, M. E. Churchill, A novel single alpha-helix DNA-binding domain in CAF-1 promotes gene silencing and DNA damage survival through tetrasome-length DNA selectivity and spacer function. *eLife* **12**, e83538 (2023).
- 31.** K. N. Choe, G.-L. Moldovan, Forging Ahead through Darkness: PCNA, Still the Principal Conductor at the Replication Fork. *Mol. Cell* **65**, 380–392 (2017).
- 32.** S. M. Hamdan, A. De Biasio, Functional hierarchy of PCNA-interacting motifs in DNA processing enzymes. *BioEssays* **45**, 2300020 (2023).
- 33.** X. Bi, Y. Ren, M. Kath, Proliferating cell nuclear antigen (PCNA) contributes to the high-order structure and stability of heterochromatin in *Saccharomyces cerevisiae*. *Chromosome Res.* **25**, 89–100 (2017).



5

Reconstitution of nucleosome assembly by human CAF-1 reveals plasticity in histone and PCNA binding

Clément Rouillon¹, Rosanne van Hooijdonk¹, Giulia Ricci¹, Charlotte M Delvaux de Fenffe¹, Felicia Piek¹, Yajie Gu², Jan Dreyer¹, Francesca Mattioli¹

¹*Hubrecht Institute-KNAW & University Medical Center Utrecht, Uppsalalaan 8, 3584 CT Utrecht, The Netherlands*

²Department of Cellular and Molecular Medicine, University of California, San Diego, La Jolla, CA 92093, USA.

Abstract

In human cells, the histone chaperone CAF-1 acts on H3-H4 dimers carrying specific modifications (H4K20me0) and containing variants (H3.1) during DNA replication and repair. How this selectivity is achieved remains unclear. To tackle this question, we use biochemical reconstitutions with human proteins. First, we were able to purify the human CAF-1 complex at high purity and yield. Human CAF-1 binds histones at high affinity and deposits them onto DNA to form nucleosomes, using a similar mechanism as the yeast complex. Histone variants (H3.1 or H3.3) as well as post-translational modifications (methylation of H3K9 or H4K20) do not affect the binding affinity of CAF-1. These data argue that CAF-1 does not intrinsically select for specific H3-H4 dimers, but that the observed binding specificity in cells is likely the result of additional regulatory factors (e.g. interactors or localization). CAF-1 is recruited by PCNA during DNA replication and repair, and a subset of PCNAs are post-translationally modified in these processes. These molecules may localize CAF-1 to specific sites, functioning as such regulatory factors. We thus used purified and homogeneously monoubiquitinated PCNA to test if this would affect the interaction with CAF-1. We find that PCNA ubiquitination does not affect CAF-1 binding on DNA. This suggests that CAF-1 can function on PCNA molecules that are modified by ubiquitin at lysine 164, and that this modification cannot act as a discriminatory signal for CAF-1 localization. Future studies in more comprehensive reconstitutions will address how other modifications on PCNA or histones may directly affect CAF-1 function, to explain how the cellular specificity of CAF-1 is achieved.

Introduction

Eukaryotic cells replicate their DNA and the associated chromatin before each cell division. Faithful inheritance of chromatin domains ensures homeostasis and maintenance of transcriptional programs that in turn safeguard cell fate. Consequently, failure to properly transmit chromatin information during mitosis results in developmental defects (1, 2) and diseases such as cancer (3–5).

The histones within chromatin carry post translational modifications (PTMs) that control the structure and the function of the genome. In order to properly copy the epigenetic landscape, these PTMs must be accurately re-established at the right genomic location in both daughter cells. This process begins in the mother cell during DNA replication, where a complex machinery called the replisome copies the DNA. The passage of the replisome disrupts the chromatin ahead of the fork via the controlled actions of histone chaperones (6). The parental histones are then recycled with their modifications on the two sister chromatids. These histones are notably marked by local PTMs, such as H3K9me3 and H4K20me2 (6). H3K9me3 marks the compact constitutive heterochromatin and provides specificity for heterochromatin protein 1 (HP1) binding in human cells. Inheritance of H3K9me3 constitutes a critical step for cell fate control (7). On the other hand, H4K20me2 marks the age of histone proteins as it accumulates over time following protein synthesis and histone deposition (8). This mark also regulates recruitment of DNA repair factors on chromatin (9).

Distinct histone chaperones control parental histone recycling on leading and lagging strands. The MCM2 subunit of the MCM helicase, the primase Pol α and the ssDNA binding protein RPA mediate parental histones recycling towards the lagging strand (8, 10, 11). DNA polymerase δ controls parental histones recycling to the leading strand (12), where additional factors may well be involved (13). Concurrently to parental histone recycling, the histone chaperone CAF-1 deposits newly synthesized H3-H4 histones on both leading and lagging strands (13, 14), in order to maintain chromatin density on both strands. These new histones contain the H3.1 variant (15) and are characterized by lack of methylation marks, particularly on H4K20 (6, 16). As a result, the newly synthesized chromatin harbors a mixture of old and new histones. Here, enzymes responsible for chromatin modification identify marks on the recently recycled parental histones and copy these marks to the new histones, leading to chromatin maturation and the re-establishment of the epigenome. This mechanism ensures the preservation of local chromatin marks at their correct genomic location. Of note, various studies have linked CAF-1 function to the stability of H3K9me3 domains after DNA replication (17–19).

Interestingly, the recent structure of the human CAF-1-H3-H4 complex shows that the few amino acids that differ H3.1 from H3.3 do not interact with CAF-1 (20). This raises questions as to how CAF-1 controls its interaction with the H3.1 variant during S phase. Because CAF-1 acts at replication forks after recruitment by the DNA polymerase processivity factor called PCNA (13, 21), this suggests that this factor may contribute to regulating CAF-1 specificity for unmethylated H3.1-H4. PCNA is involved in several essential functions at replication forks (22), which are further regulated by PTMs on PCNA itself. A key PTM is the mono-ubiquitination at lysine 164 by the RAD6-RAD18 complex which facilitates TransLesion Synthesis (TLS) on damaged DNA (23). Recent studies in human and *S.pombe* have revealed that PCNA is also ubiquitinated at K164 during unperturbed DNA replication, and that this modification is functionally linked to Okazaki fragments maturation and CAF-1-mediated chromatin assembly (24, 25). These observations

suggest that PCNA ubiquitination may act as a regulatory factor for CAF-1 function at replication fork.

In this work we test whether PCNA and histones PTMs or variants provide direct specificity for CAF-1 histone chaperone function. To this end, we developed *in vitro* reconstitutions with human proteins. We show that CAF-1 has a low intrinsic specificity for histone H3 variants, and its modifications. Similarly, PCNA ubiquitination does not affect CAF-1 function. Together this indicates that CAF-1 is a malleable complex that can directly bind several histones H3-H4 cargoes and PCNA in different modified states. Therefore, we conclude that other regulatory factors control the specificity of CAF-1 observed in cells.

Results

A conserved nucleosome assembly mechanism by CAF-1 *in vitro*

To investigate the mechanism of nucleosome assembly by CAF-1 in humans, we first purified the human CAF-1 complex. The heterotrimeric complex (p150, p60 and p48) elutes as a single peak from gel filtration, and SDS-PAGE analysis reveals stoichiometric amounts of each subunit (Figure S1A and S1B). First, we tested the ability of CAF-1 to bind H3-H4 using fluorescence polarization. We found that CAF-1 bound H3-H4 in the low nM range (5 nM), consistent with the binding affinity of histone chaperones for their cognate histones (13, 28) (Figure 1A). Previous studies on the yeast CAF-1 complex identified a sub-complex lacking the N-terminal domain of the large subunit (tCAF-1) capable of histone binding and nucleosome assembly *in vitro*. (28–30). To confirm that this organization is conserved from yeast to human (Figure S1A), we successfully purified tCAF-1 from human (Figure S1A and S1B). This sub-complex contained all three subunits (Figure S1B) and bound H3-H4 dimers with similar affinities compared to the full-length complex (Figure 1A). Moreover, cooperativity in histone binding was observed with both constructs ($h=1.7$ for tCAF-1, $h=2.4$ for FL-CAF-1). These data show that the overall organization of the CAF-1 complex and its binding to H3-H4 is conserved between yeast and human. These results aligned with a recent study that determined the structure of human tCAF-1 bound to a H3-H4 dimer (20).

In order to test if human CAF-1 assembles chromatin, we used a previously developed assay, named nucleosome assembly and quantification (or NAQ) assay to assess nucleosome assembly capacity (28, 31). Human CAF-1 is functional and efficiently assembles nucleosomes on linear DNA (Figure 1B). Nucleosome assembly was most efficient when using a 2-fold ratio of human CAF-1 per H3-H4 tetramer, which is consistent with the binding stoichiometry of one H3-H4 dimer per CAF-1 complex (28). The tCAF-1 complex was also active and assembled nucleosomes, albeit with less efficiency than the full-length complex (Figure 1B). This indicates that although the core histone deposition function is retained in this part of the complex, the N-terminus of p150 (residues 1-447) may further promote nucleosome assembly, perhaps by facilitating the interaction between the KER domain and DNA. Importantly the integrity of the WHD domain was essential for nucleosome assembly by tCAF-1 (Figure 1B, S1A and S1B) (tCAF-1 Δ WHD), confirming its critical role in nucleosome assembly (28, 30, 32).

Together these data show that recombinant human CAF-1 is active, and its mechanism of nucleosome assembly is generally conserved, with a high dependency on the WHD domain. We identify a potential activating role for the p150 N-terminus in nucleosome assembly.

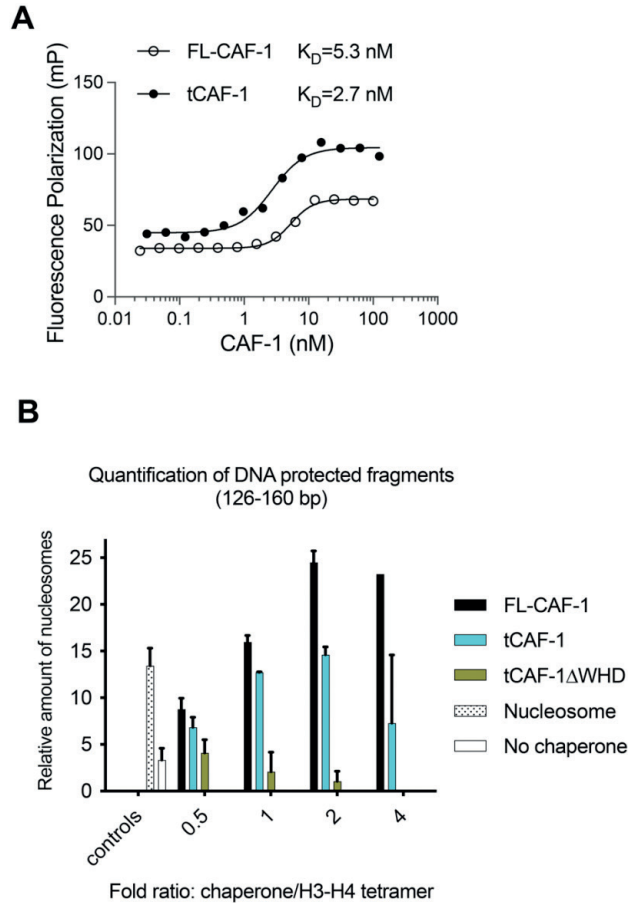


Figure 1: The mechanism of CAF-1-mediated chromatin assembly is globally conserved from yeast to human. (A) Fluorescence polarization experiments performed between CAF-1 or tCAF-1 with H3.1-H4 dimers (where H4 is labelled at E63C with Alex Fluor 488). **(B)** Quantification of DNA-protected fragments issued from NAQ experiments. The MNase-digested samples (126-160 bp) were quantified using DNA chips on bioanalyzer, and normalized to the loading control within each lane. Different ratios of CAF-1 per H3-H4 tetramer were used to determine the optimal stoichiometry to achieve maximal chromatin assembly efficiency.

Histone post-translational modifications and variants do not alter CAF-1 dependent binding and activity *in vitro*

During S phase in human cells, CAF-1 deposits newly synthesized histones H3.1-H4 following DNA replication (15). Notably, these histones are characterized by the absence of lysine methylation and the presence of histone acetylation marks, a feature that distinguishes them from parental histones (6, 33). We wondered whether histone PTMs may determine the binding specificity of CAF-1. Because CAF-1 was shown to deposit H4K20me0 on DNA (16), and to promote the establishment of H3K9me3 (17), we focused on these two lysines, that are unmethylated in new histones, as opposed to parental histones which are tri- and di-methylated respectively at these sites (34–36). We introduced chemical modifications at these single sites and used the

methyl-lysine analogs (MLA) approach (27) to mimic these modifications in human H3 and H4 (Figure S2A). We confirmed the installation of these PTM mimics via western blotting (Figure S2B). The histone preparation behaved as expected and ran in stoichiometric amounts on SDS-PAGE following their refolding (Figure S2A and S2B), indicating that the MLA-histones are functional.

We tested whether these modifications, namely H3K9 and H4K20 methylation, influence CAF-1 binding in fluorescence polarization experiments. Interestingly, H3-H4 dimers containing H4K20me2 or H3K9me3 exhibited binding affinities towards CAF-1 that were comparable to those observed with unmodified histones (Figure 2A). Furthermore, our analysis of the binding between CAF-1 and H3K9me3 revealed a Hill coefficient of 1.8, indicating that CAF-1 employs a cooperative binding mode in this context, similarly to the unmodified histones (Figure 1A). We next asked whether H3K9 and H4K20 modifications affect the chromatin assembly activity of CAF-1. We therefore used NAQ experiments (31) to evaluate the impact of those PTMs for CAF-1 mediated histone deposition. None of the modified histones affects the nucleosome assembly efficiency compared to their unmodified counterparts (Figure 2B). This indicates that CAF-1 is able to bind and deposit H3-H4 dimers containing H3K9me3 or H4K20me2, suggesting that the observed specificity of CAF-1 for unmethylated H3-H4 in cells (15, 16) is not due to intrinsic binding preferences, but rather to other regulatory factors.

Similarly, CAF-1 binds primarily H3.1-H4 and not the replication-independent variant H3.3-H4 (15). We prepared both H3-H4 dimers and tested how CAF-1 binds and deposits these two variants (Figure S2A). CAF-1 exhibited a similar binding affinity for H3.1 and H3.3 (Figure 2C) with cooperative binding characterized by a Hill coefficient of 2.0 in both cases. Additionally, in NAQ assays, CAF-1 was equally active with H3.1 or H3.3-containing H3-H4 (Figure 2D). These data confirm that CAF-1 is also not intrinsically specific for the H3.1 variant, supporting a general plasticity in its mechanism of action.

Human CAF-1 and PCNA form unanticipated interactions outside of DNA

In cells, CAF-1 requires PCNA for its activity at forks, via the p150 N-terminus (Figure S1A) (21, 37). Abrogating their interaction leads to mistargeting of CAF-1 on chromatin (37), defects in DNA repair (38) and failure in heterochromatin silencing (21). We reasoned that PCNA may further regulate CAF-1 specificity. To study this, we set out to reconstitute CAF-1-mediated chromatin assembly via PCNA recruitment using human proteins.

We used size exclusion chromatography (SEC) to study the interaction between CAF-1 and PCNA loaded on plasmid DNA (13). As anticipated, our SEC analysis demonstrated the co-elution of CAF-1, PCNA and the plasmid DNA (Figure 3A, +ATP +CAF-1) suggesting that the complex efficiently formed on circular DNA. Previous work has shown that the N-terminus of p150 contains PCNA interacting peptides (PIP) and a DNA binding domain important for CAF-1 recruitment (13, 37). Similarly, human tCAF-1 failed to interact with DNA-loaded PCNA (Figure 3B) arguing that the N-terminal domain of p150 constitutes the primary interface between CAF-1 and PCNA. To validate the specificity of this interaction with DNA-loaded PCNA, we performed a control experiment in which all proteins are present, but where PCNA cannot be loaded onto DNA due to the omission of ATP (Figure 3A, -ATP +CAF-1). Here, CAF-1 no longer co-eluted with DNA, indicating that PCNA is required for binding to the plasmid in this experiment. Surprisingly, this experiment revealed that a population of free PCNA coeluted with CAF-1, as shown by a shift of the PCNA molecules to higher molecular weight fractions (Figure 3A, shift from fractions 10-11 to 7-8 when comparing

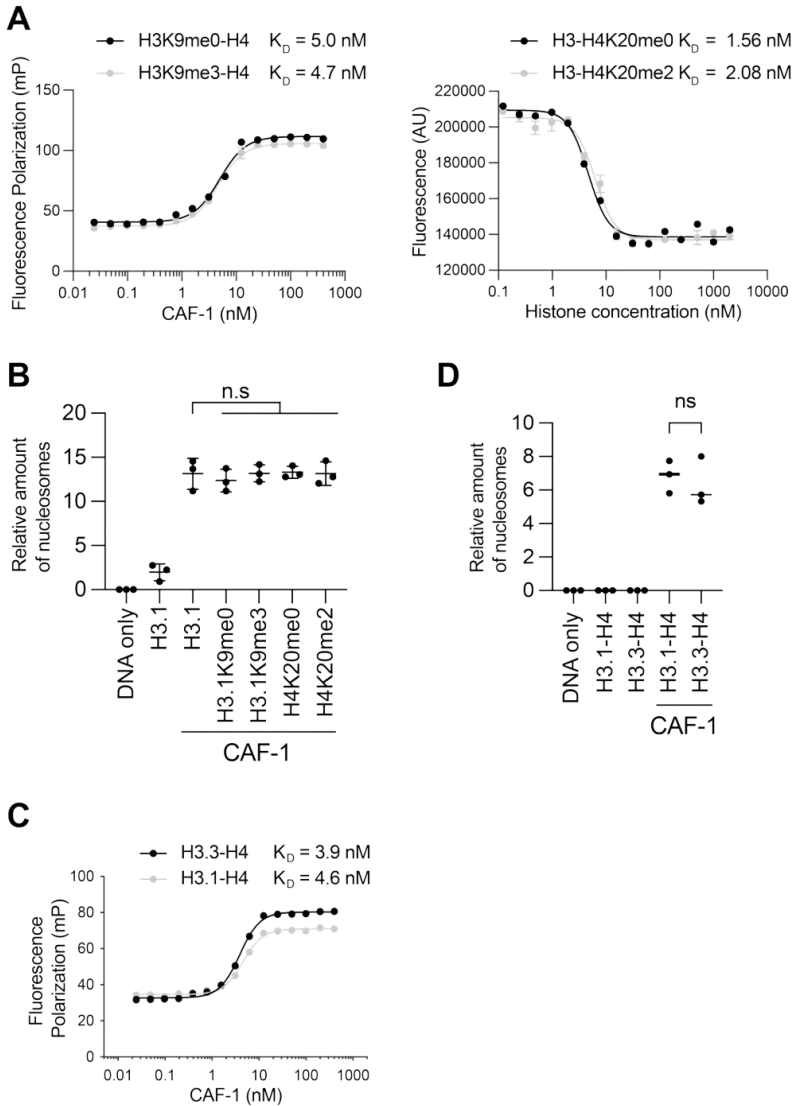


Figure 2: CAF-1 exhibits low specificity for modified H3K9 and H4K20 as well as for H3 variants.

(A) Left panel: Fluorescence polarization experiments testing the effect of H3.1K9 trimethylation on CAF-1 binding affinity. H4-T71C was labelled with AlexaFluor 488. Right panel: Competition fluorescence polarization experiment testing the effect of H4K20 dimethylation on CAF-1 binding affinity. **(B)** Bioanalyzer-based quantification of nucleosome assembly reactions (126-165 bp) normalized to the 621 bp loading control within each lane. The impact of H3K9 trimethylation and H4K20 dimethylation on CAF-1-mediated chromatin assembly was assessed using NAQ assays. Mean \pm SD is shown, (one-way ANOVA comparing WT CAF-1 to control conditions). **(C)** Fluorescence polarization experiments comparing the binding affinity of CAF-1 with the variants H3.1 and H3.3 (where H4 is labelled at E63C with Alex Fluor 488). **(D)** Bioanalyzer-based quantification of nucleosome assembly reactions (126-165 bp) normalized to the 621 bp loading control within each lane. Mean \pm SD is shown, (unpaired t-test was used). The impact of H3 variants on CAF-1-mediated chromatin assembly was assessed using NAQ assays.

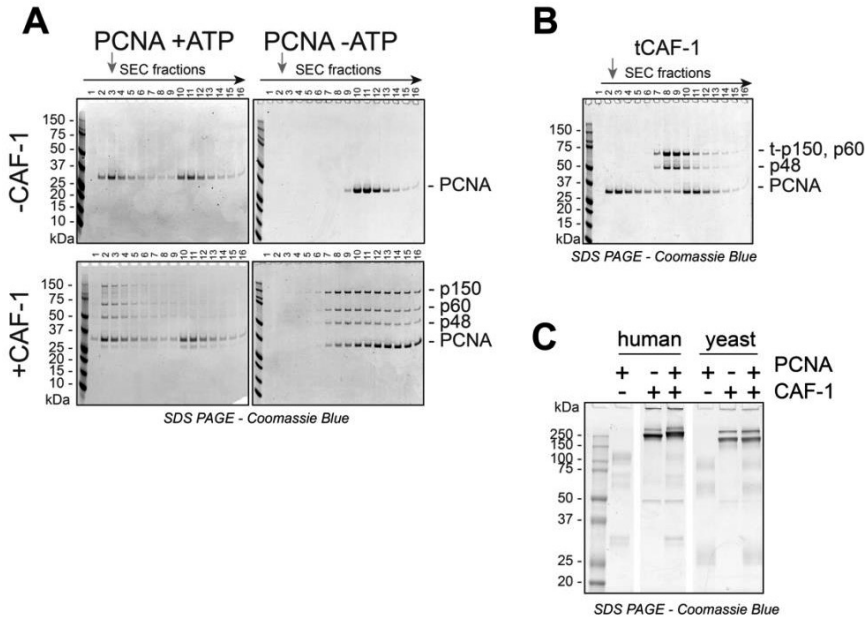


Figure 3: The interaction between human CAF-1 and PCNA shows a low dependency on DNA. (A-B)

SDS-PAGE following SEC analysis of PCNA loading experiments, in absence of CAF-1 (top panels) or in presence of CAF-1 (bottom panels). Experiments were conducted with ATP (left panels) or without ATP (right panels), and (B) where a tCAF-1 mutant lacking the N-terminal domain of p150 is used in presence of ATP. Grey arrows indicate the elution volume of the plasmid DNA used for PCNA loading. Fractions are indicated above each respective lane of the SDS-PAGE. (C) SDS-PAGE analysis following crosslinking between CAF-1 and PCNA in absence of DNA. The binding of the human and yeast proteins was directly compared in this experiment.

-ATP -CAF-1 to -ATP +CAF-1 control). This suggests that CAF-1 and PCNA may interact in the absence of DNA. This was unexpected, as a previous study with yeast proteins showed that CAF-1 only binds PCNA that is loaded onto DNA (13).

To further test this hypothesis, we used crosslinking experiments to test the presence of a DNA-independent interaction between human CAF-1 and PCNA in solution. Consistent with SEC analysis, CAF-1 efficiently crosslinked with PCNA in the absence of DNA, while the yeast proteins were unable to interact (Figure 3C). These data reveal that the interaction between human PCNA and CAF-1 does not require DNA, opposite to what is observed with the yeast proteins. This raises new questions on the implications of this difference within a highly conserved pathway.

Mono-ubiquitination of PCNA on K164 enables CAF-1 binding and activity

During physiological DNA replication and replication stress, PCNA undergoes a series of PTM (23, 25, 39). A key modification is the mono-ubiquitination of lysine 164 (Ub-PCNA), a hallmark of replication stress that promotes TLS (23). More recently, several studies found that a subset of PCNAs are also ubiquitinated during unperturbed DNA replication, and this modification is functionally linked to Okazaki fragment maturation, PCNA unloading from DNA, and CAF-1-mediated chromatin assembly (24, 25). Remarkably, a recent study suggests that

CAF-1 itself stimulates the ubiquitination of PCNA during TLS by recruiting the E3 ligase Rad18 to PCNA (40). These intriguing findings establish a functional link between nucleosome assembly and the ubiquitination of PCNA. Therefore, we wondered how Ub-PCNA affects CAF-1 recruitment and activity.

First, we isolated pure Ub-PCNA, following a previously established protocol (41) (Figure S2C), and confirmed its functionality in RFC-mediated loading on DNA using SEC experiments (26) (Figure 4A, +ATP -CAF-1). We therefore used Ub-PCNA in our biochemical assays to establish its effect on CAF-1-mediated mechanisms. In a similar fashion to reactions involving unmodified PCNA (Figure 3A), CAF-1 and Ub-PCNA coeluted with DNA in the presence of ATP (Figure 4A, +ATP +CAF-1), providing evidence that the complex can form on DNA. Importantly, the amount of Ub-PCNA co-eluting with CAF-1 and DNA was equal to that observed when unmodified PCNA was used (Figure 3A). This suggests that ubiquitination does not affect the stability of Ub-PCNA on DNA, nor its binding to CAF-1. Furthermore, when ATP was omitted (Figure 4A, -ATP +CAF-1), Ub-PCNA still shifted to higher molecular weight fractions, overlapping with CAF-1 (Figure 4A, shift from fractions 10-11 to 7-8 when comparing -ATP -CAF-1 to -ATP +CAF-1 control), indicating that the DNA-independent interaction of PCNA with CAF-1 was not affected. This interaction was confirmed through crosslinking experiments, where Ub-PCNA exhibited DNA-independent interactions with CAF-1 comparable to that of unmodified PCNA (Figure 4B).

Collectively, these findings indicate that ubiquitin neither hinders nor stimulates CAF-1 binding, suggesting that CAF-1 may well be recruited to Ub-PCNA.

While Ub-PCNA does not affect CAF-1 binding, we were interested in understanding if it could affect its activity. Therefore, we used the recently established PCNA-NAQ assay, designed to specifically assess the PCNA-dependent activity of CAF-1 (13). This assay uses a mixture of nicked plasmid where PCNA can be loaded, and a supercoiled plasmid where the PCNA-independent activity of CAF-1 takes place. Human CAF-1 efficiently assembled chromatin on nicked DNA when PCNA was loaded, while this activity was strongly reduced in the absence of ATP (Figure 4C and 4D), demonstrating that this assay reconstitutes its PCNA-dependent nucleosome assembly activity. Moreover, truncated tCAF-1 displayed only background assembly on nicked plasmid (Figure 4C and 4D), confirming that the activity of human CAF-1 depends on its interaction with PCNA via the N-terminus of p150 (containing the PIPs and the KER). When we used Ub-PCNA in these reactions, we could not observe any effect of the ubiquitin fusion on CAF-1 activity (Figure 4C and 4D).

In conclusion, we show that Ub-PCNA enables CAF-1 recruitment and its chromatin assembly activity, with no detectable differences compared to unmodified PCNA. These results suggest that ubiquitination of PCNA on K164 has no direct effect on CAF-1 binding and function, hinting at an indirect interplay between these two factors (24, 25) that needs to be further elucidated.

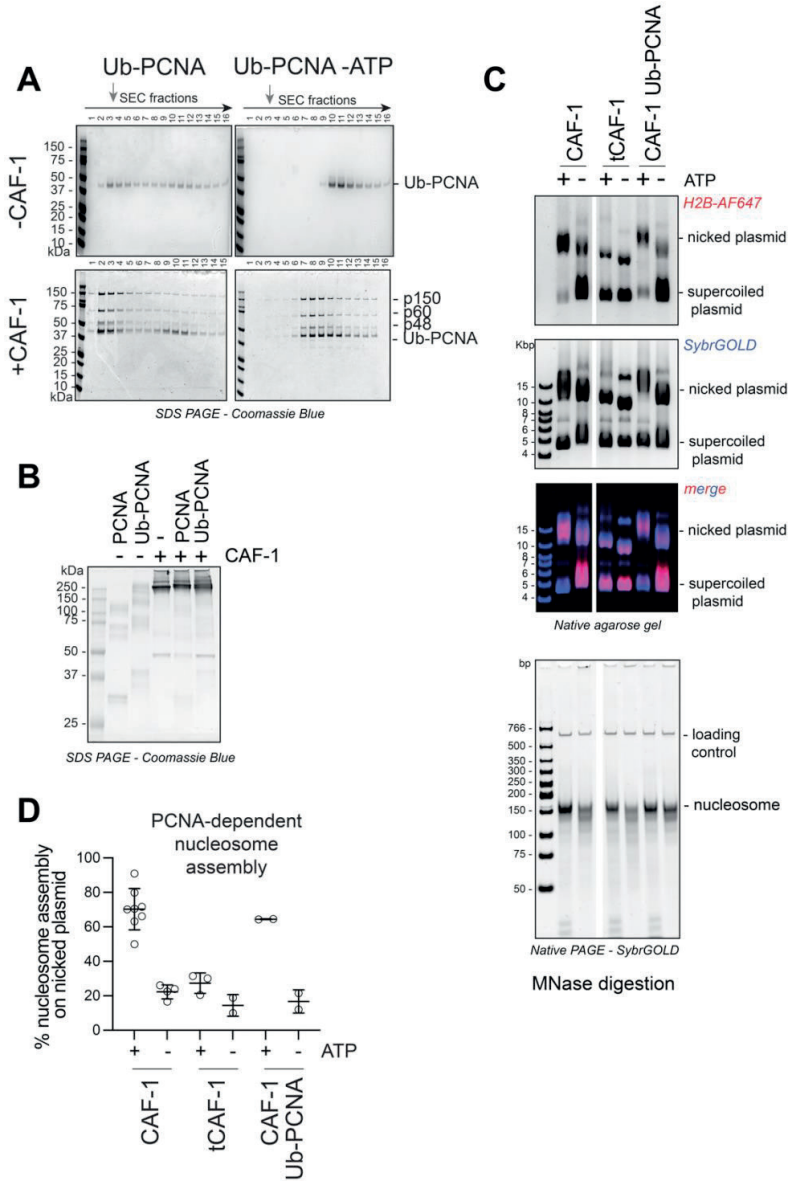


Figure 4: Ub-PCNA functions similarly to unmodified PCNA during CAF-1 mediated chromatin assembly. (A) SDS-PAGE following SEC analysis of Ub-PCNA loading experiments in presence of ATP (top left panel) or when ATP is omitted (top right panel), in absence of CAF-1 in these reactions (top panels) or in presence of CAF-1 (bottom panels). Grey arrows indicate the elution volume of the plasmid DNA used for PCNA loading. Fractions numbers are indicated above each respective lane of the SDS-PAGE. (B) SDS-PAGE analysis following crosslinking between CAF-1 and PCNA or Ub-PCNA in absence of DNA. (C) Top panel: Native agarose gel analysis of PCNA-NAQ assay reactions. The first gel shows H2B fluorescence, with the signal on nicked plasmid representing PCNA-mediated chromatin assembly. Bottom panel: Native PAGE stained with SybrGOLD following MNase digestion of the samples shown in the top panel. (D) Quantification of H2B fluorescent signal on nicked plasmid, reflecting the PCNA-dependent chromatin assembly.

Discussion

Our study presents the reconstitution of nucleosome assembly by the human CAF-1 complex and its dependency on PCNA. We show that CAF-1 function is largely conserved from yeast to human, and its activity is unaffected by histone variants and modifications on H3K9 and H4K20. We reconstituted the dependency of CAF-1 for PCNA using human proteins, and found that PCNA ubiquitination on K164 does not hinder the recruitment of CAF-1 and subsequent chromatin assembly.

Overall, our work reveals that CAF-1 exhibits low specificity for histone H3-H4 modifications or variants, and it does not discriminate between unmodified and Ub-PCNA. This suggests that the observed specificity of CAF-1 for unmodified H3.1-H4 histones in cells stems from additional regulatory steps, and not from an intrinsic binding specificity.

Where does the histone specificity of CAF-1 originate?

First, since this work was carried out, a structure of human CAF-1 was published. This revealed that the N-terminal tail of the histone H3 directly interacts with the small subunit of CAF-1 (p48) (20). Interestingly, H3K9 and H4K20 do not stably bind CAF-1, in line with our results suggesting that they can be modified. On the other hand, H3K4 closely interacts with p48. It remains to be studied if modifications at this site affect the affinity of CAF-1 for histones. Along the same lines, new histones are acetylated primarily on the H4 N-terminal tail. Interestingly, this tail is not visible in the recent structure (20), it would nonetheless be interesting to test whether H4 N-terminal acetylation stimulates CAF-1 binding.

Next, there are few factors that may confer specificity of CAF-1 for new histones in the cellular context: 1. other histone chaperones, 2. its localization, and 3. Its expression timing.

1. ASF1 hands over histones H3.1-H4 to CAF-1 before chromatin assembly (42). Thus, this histone chaperone might determine specificity for CAF-1. However, ASF1 also binds both H3.1 and H3.3 histone variants (43), and does not interact with histone tails that contain PTMs (44), therefore it seems unlikely that ASF1 plays a role in histone specificity.

While CAF-1 itself does not show specificity for H3.1, it is possible that the H3.3 chaperones HIRA and DAXX (15, 45) are highly selective and do not bind H3.1, indirectly stimulating CAF-1 binding to H3.1 in the crowded nuclear environment. Furthermore, H3.1 is highly abundant during S phase in comparison to H3.3 (46), which may provide further selectivity for CAF-1.

2. CAF-1 is localized behind replication forks via its recruitment by PCNA (13, 21). Notably, we have shown that CAF-1 binds to PCNAs that are not physically connected to DNA polymerase epsilon, hence the replisome (13). This suggests that sites of new histones deposition are spatially displaced from the replisome where the parental histones are recycled (6, 33). This spatial selectivity may provide specificity in CAF-1 function, preventing an interaction with e.g. parental methylated histones H3-H4 (containing any H3 variants).

3. Finally, another level of regulation may arise from the expression timing of CAF-1 and H3.1. Both proteins are specifically expressed at the G1/S transition (14, 47–49), where they raise rapidly and dramatically (50). This temporal synchrony may facilitate their interaction, resulting in apparent binding specificity.

What is the link between CAF-1 and bulky PCNA modifications?

Previous studies have established a functional link between CAF-1 activity and the ubiquitination of PCNA during unperturbed DNA synthesis (24, 25). Our data shows that ubiquitin conjugated on PCNA K164 does not affect CAF-1 binding nor its nucleosome assembly activity. This makes sense based on the location of the ubiquitin moiety and the predicted binding site for CAF-1 at the PIP binding region on PCNA (13, 37). Whereas ubiquitination of K164 does not impact CAF-1 function, we cannot exclude the opposite scenario whereby CAF-1 itself regulates PCNA ubiquitination. Indeed, experiments in cells indicate that CAF-1 facilitates PCNA ubiquitination by directly interacting with the Rad18 ubiquitin ligase complex (40). This implies that CAF-1 may act as a regulator of PCNA ubiquitination during unperturbed DNA replication, potentially influencing other PCNA-associated processes like Okazaki fragment maturation or PCNA unloading by the ATAD5-RFC complex, as previously proposed (24, 51). Furthermore, Because the ubiquitination of PCNA governs the recruitment of other factors on chromatin (22), it is plausible that during DNA replication, Ub-PCNA binds other proteins that may subsequently regulate CAF-1 function. This could explain why we do not see any effects in our reconstitutions that use CAF-1 alone. To unravel these differences, further work should determine the interactome of CAF-1 with PCNA and Ub-PCNA in cellular context during physiological DNA synthesis.

A functional link between CAF-1 and SUMOylated PCNA has also been drawn (52). SUMO is an ubiquitin-like molecule that is conjugated to PCNAK164 during unperturbed DNA replication (22), thus adding a possible new regulator of chromatin assembly by CAF-1. The mechanistic basis of these interplays remains unclear.

In order to disentangle the complex relationship between CAF-1 and PCNA, along with its regulation by PCNA modifications, further studies must explore the precise mechanistic links and regulatory factors governing their interaction. These experiments will bring a substantial understanding of how PCNA modifications regulates replication forks and its implication for DNA replication, chromatin assembly and cycling of PCNA on chromatin.

Methods

Protein expression and purification

All proteins were expressed and purified as previously described. This includes PCNA (26), ubiquitin (26), E1 (Uba1) (26), E2 (UbcH5c S22R) (26), RFC Δ N (hereafter referred to as RFC) (13), CAF-1 (13), and histones (13, 27). Histones used for the PCNA-NAQ assay were fluorescently labelled with Alexa Fluor 647 as previously described (13). Histones used for fluorescence polarization were labelled with Alexa Fluor 488 as previously described (13). H3.1-H4 and H3.3-H4 were labelled on H4-E63C. Mono-ubiquitinated PCNA was prepared as previously described (26).

Preparation of modified H3K9me3 and H4K20me2

H3K9me3 and H4K20me2 (and their me0 counterpart) were prepared using the methyl-lysine analogue procedure (27). H3K9me3 was fluorescently labelled with Alexa Fluor 488 on H4-T71C.

H3K9me3

9 mg of lyophilized H3K9C-C110A (The histone source) were dissolved in alkylation buffer (4 M guanidine hydrochloride, 1 M HEPES pH 7.8, 10 mM DL-methionine and 20mM fresh DTT) and incubated for 1 hour at 37°C.

50 mM (2-bromoethyl)-ammonium bromide or (2-bromoethyl)-trimethylammonium bromide solution prepared fresh were added to prepare H3K9me0 and H3K9me3 respectively. Samples were incubated at room temperature for 2.5 hours with occasional mixing, covered in aluminum foil before 10 mM of fresh DTT was added. After an additional 2.5 hours, the reaction was quenched with 2-Mercaptoethanol and incubated at room temperature for 30 min. Methylated H3 was then purified using a PD-10 column equilibrated in 2 mM 2-Mercaptoethanol/H₂O. The protein was lyophilized and H3-H4 tetramers were refolded as previously described (13).

H4K20me2

10.5 mg of lyophilized H4K20C (The histone source, Colorado) were dissolved in alkylation buffer (4 M guanidine hydrochloride, 1 M HEPES pH 7.8, 10 mM DL-methionine and 20mM fresh DTT) and incubated for 1 hour at 37°C.

50 mM (2-bromoethyl)-ammonium bromide or (2-bromoethyl)-dimethylammonium bromide solution prepared fresh were added to prepare H4K20me0 and H4K20me2 respectively. Samples were incubated at room temperature for 2.5 hours with occasional mixing, covered in aluminum foil before 10 mM of fresh DTT was added. After an additional 2.5 hours, the reaction was quenched with 2-Mercaptoethanol and incubated at room temperature for 30 min. Methylated H3 was then purified using a PD-10 column equilibrated in 2-Mercaptoethanol/H₂O. The protein was lyophilized and H3-H4 tetramers were refolded as previously described (13).

Fluorescence polarization

Fluorescence polarization experiments were conducted as previously reported (13). Increasing concentrations of CAF-1 were incubated with 15 nM H3-H4 (E63C-AF488) dimers in 25 mM TRIS pH 7.5, 300 mM NaCl, 5% Glycerol, 1 mM EDTA, 0.01% IGEPAL ca-630, 0.01% CHAPS and 1 mM TCEP. 30 μ l reactions were performed in CORNING low flange 384 well black microplates (CLS3575), and fluorescence polarization was measured with CLARIOstar (BMG LabTech) plate reader. The data were analyzed using GraphPad Prism, and fitted to a One Site binding curve (not accounting for fluorescent label depletion) with hill coefficient to determine the K_D ($y = B_{max} * x^h / K_D^h + x^h$, where B_{max} is the maximum specific binding, K_D is the equilibrium dissociation constant and h is the hill coefficient). Each experiment was repeated at least 3 times.

Competition experiments were performed by incubating 30 nM tCAF-1-H3-H4 (H4-T71C-AF488) complex with increasing amount of unlabeled H3-H4K20me2 or H3-H4K20me0. The data were analyzed using GraphPad Prism, and fitted to a One Site competition curve with hill coefficient (not accounting for fluorescent label depletion) to determine the EC50 (the concentration of H4K20me2 where half of the CAF-1-H4K20me0 is dissociated) ($y = B_{min} + (B_{max} - B_{min}) / (1 + x^h / EC50^h)$), where B_{max} is the value measured when no competitor was added, B_{min} is the value measured when the competitor completely outcompetes H3-H4-T71C-AF488, h is the hill coefficient and EC50 is the concentration of competitor that results in 50% binding of H3-H4K20me2 (or H3-H4K20me0). The K_D was derived using the formula provided in Graphpad: $K_D = EC50 / (1 + B / K_D AB)$ where EC50 is the concentration of competitor that results in 50% binding

of H3-H4K20me2 (or H3-H4K20me0), B is the concentration of tCAF-1 and K_D AB is the known K_D between tCAF-1 and H3-H4-T71C-AF488. Each experiment was repeated at least 3 times.

NAQ assay

The nucleosome assembly reactions were performed as follows. CAF-1 (400 nM) and H3-H4 dimers (400nM) were mixed in NA buffer (25 mM TRIS pH 7.5, 150 mM NaCl, 1 mM EDTA, 0.02% Tween-20 and 1 mM TCEP), for 10 minutes at room temperature. Next, 207 bp DNA (200 nM) or pUC19 (13 nM) was added to the CAF-1-H3-H4 mix and further incubated for 10 minutes. Finally, H2A-H2B dimers (400 nM) were added to the reactions and incubated for 10 minutes at room temperature. After incubation, reactions were digested for 10 minutes at 37°C with 30 units of MNase (NEB #M0247S) in buffers containing 50 mM TRIS pH 8.0 and 5 mM CaCl_2 . The digestion was quenched with 50 mM EDTA. 50 ng of DNA loading control (621 bp). The nucleosomal DNA was retrieved and purified using MinElute PCR purification kit (QIAGEN #28004) according to the manufacturer instructions. 3 μ l of samples were loaded on 6% PAGE and stained with SybrGOLD. 1 μ l of each reaction was analyzed with DNA chips (Agilent DNA 1000 kit) on Bioanalyzer (Agilent) for quantification. The amount of nucleosomal bands (125-165bp) were normalized to the loading control for each sample as in (13). Data were plotted with Graphad Prism.

PCNA loading on SEC

We used nicked pUC19 as template for PCNA loading. The plasmid was digested with the nicking enzyme Nt.BspQI for 8 h at 50°C, before being purified via phenol chloroform extraction. Nicked pUC19 (0,3 μ M) was then incubated with PCNA (30 μ M monomer), RFC (0.5 μ M), ATP (3 mM), and MgCl_2 (10 mM), in PCNA loading buffer (50 mM HEPES pH 7.5, 200 mM NaCl, 0.01% IGEPAL CA-360, 1mM TCEP). After 5 minutes at 30°C, CAF-1 was added to the reactions (5 μ M) and further incubated at room temperature for 15 minutes. Samples were then injected on Superose 6 increase 3.2–300 columns connected to an AKTA pure system fitted with PEEK I.D. 0.25 mm tubing. The reaction was eluted in PCNA loading buffer supplemented with 10 mM MgCl_2 , and samples were analyzed on 4-12% gradient SDS-PAGE run in MES buffer.

Crosslinking between PCNA and CAF-1

PCNA or Ub-PCNA (6 μ M monomer) were mixed with CAF-1 (2 μ M) for 10 min at room temperature in PCNA loading buffer. Samples were then crosslinked using 1 mM DSS (disuccinimidyl suberate) and further incubated for 10 minutes at room temperature. The crosslinker was then quenched with TRIS pH 7.5 and incubated for 10 more minutes at room temperature. The samples were run on 12% SDS-PAGE (BioRad) in XT MOPS buffer (#1610793 BioRad) for 30 minutes at 20 mA and an additional 2h30 at 40 mA. Gels were stained with Coomassie brilliant blue for detection of crosslinked complexes.

PCNA-NAQ assay

We used nicked pRC1765 (Addgene #141346) for PCNA loading and chromatin assembly. The plasmid was digested with the nicking enzyme Nt.BbvCI for 6 h at 37°C, and was then purified via phenol chloroform extraction. The nicked plasmid (50 nM) was mixed with supercoiled pRC1765 (50 nM), 1,1 μ M of RFC, 10,9 μ M of PCNA monomer, 10,9 mM ATP and 8 mM MgCl_2 in PCNA loading buffer. Typically, this reaction was performed in 11 μ l final volume. The reactions

were incubated for 5 minutes at 30°C. Samples were then diluted 3-fold with NA buffer to lower the MgCl₂ concentration that otherwise inhibits chromatin assembly. CAF-1 prebound to H3-H4 dimers (100 nM each) were added to the reaction and incubated 15 minutes at room temperature. Fluorescently labelled H2A-H2B dimers (100 nM) were then added to allow full nucleosome assembly, and incubated for 15 minutes at room temperature. Samples were spun down for 5 minutes at 170000 x g to remove potential precipitates. 1µl of sample was mixed with 5µl of loading buffer (NA buffer + 5% sucrose). Samples were separated on 0.8% native agarose gel, run in 1X TAE (Tris-Acetate EDTA) for 90 minutes at 90 volts.

MNase reactions were then performed with the rest of the PCNA-NAQ reactions. Briefly, 25µl of sample was incubated with 80 units of MNase (NEB #M0247S) in 100 µl final volume of 50 mM Tris pH 7.9, 5 mM CaCl₂. Samples were incubated 10 minutes at 37°C prior to inactivation using 20 mM EDTA. Proteins were then digested with ProteinaseK (NEB #P8107S) for 20 minutes at 50°C. A 621 bp DNA fragments was added as loading control, and the digested DNA was purified using the MinElute PCR purification kit (Qiagen #28006) according to the manufacturer's instructions. MNase-digested samples were run on 6% native PAGE, and stained with SybrGOLD.

Acknowledgments

We thank Titia Sixma for sharing plasmids for the E1, E2 and ubiquitin, Paul Kaufmann for sharing the cDNAs of the human CAF-1 subunits. We thank Fabian Gruss for providing purified human CAF-1 protein.

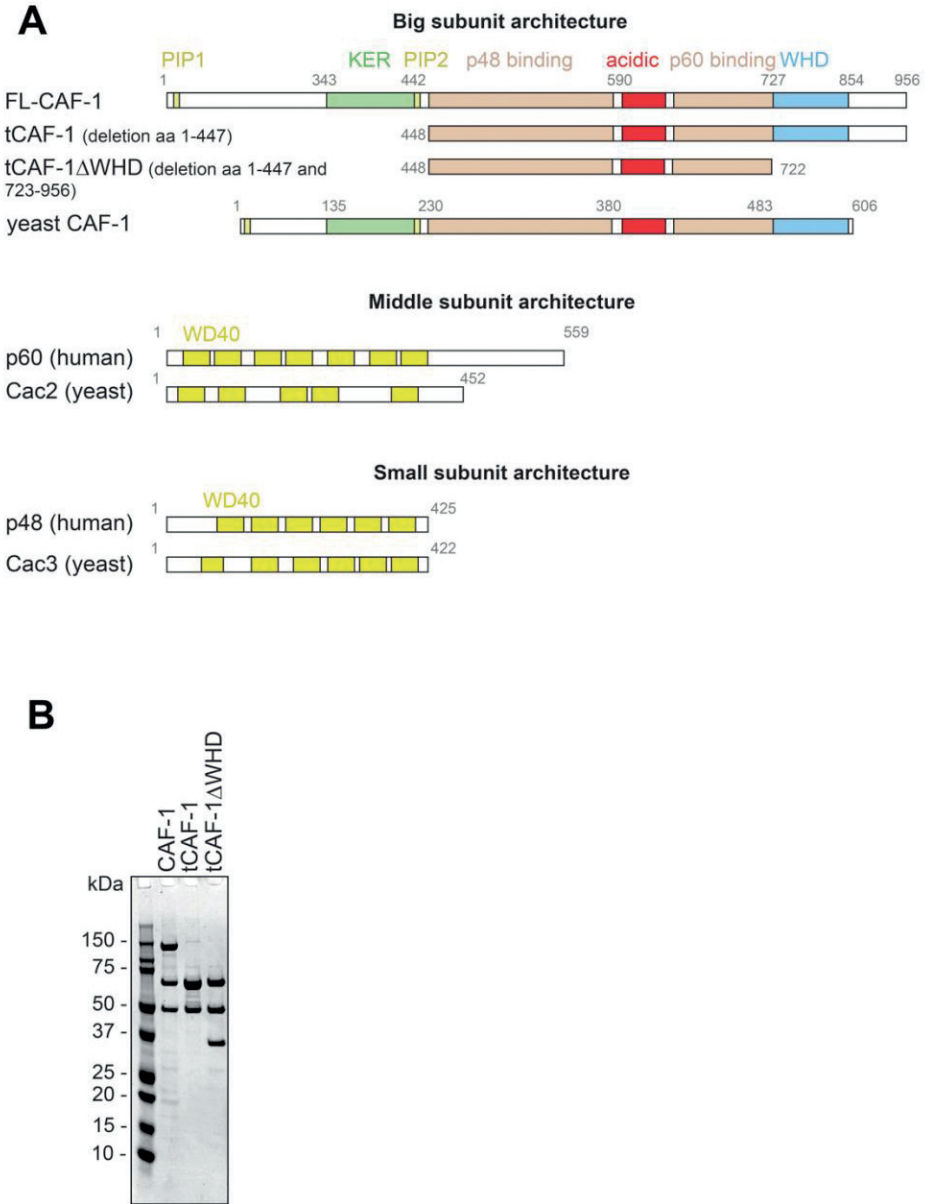


Figure S1: (A) Cartoons of the p150 (large CAF-1 subunit) domains and the mutants used in this study. Each subunit architecture is compared to its yeast counterpart. (B) SDS-PAGE of the purified CAF-1 used in this study. tCac1 runs at the same height as Cac2.

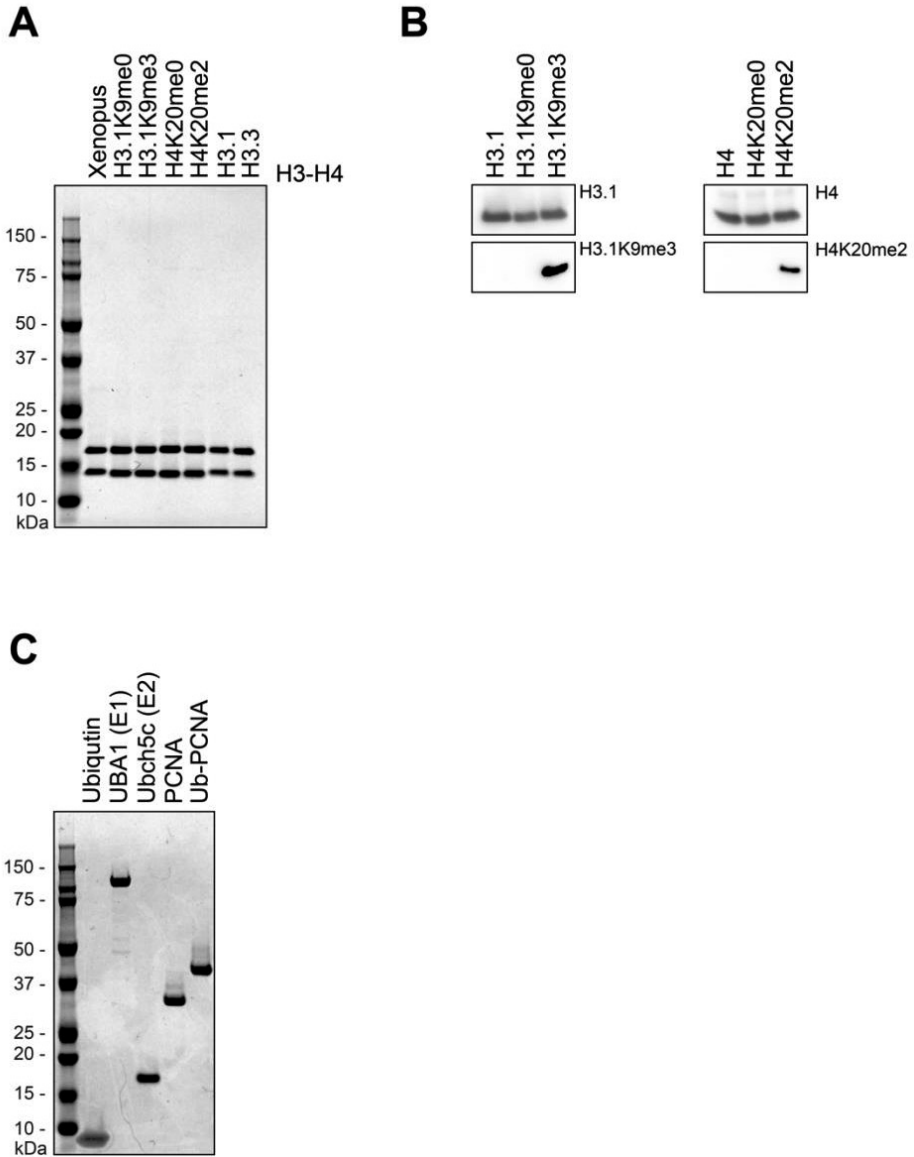


Figure S2: (A) SDS-PAGE of the refolded human H3-H4 tetramers used in this study. (B) Western Blot analysis of the methylation state of the refolded H3K9me0 vs H3K9me3 and H4K20me0 vs H4K20me2. (C) SDS-PAGE of the purified E1, E2, PCNA and Ub-PCNA used in this study.

References

1. Q. Wen, J. Zhou, C. Tian, X. Li, G. Song, Y. Gao, Y. Sun, C. Ma, S. Yao, X. Liang, X. Kang, N. Wang, Y. Yao, H. Wang, X. Liang, J. Tang, S. M. Offer, X. Lei, C. Yu, X. Liu, Z. Liu, Z. Wang, H. Gan, Symmetric inheritance of parental histones contributes to safeguarding the fate of mouse embryonic stem cells during differentiation. *Nat. Genet.* **55**, 1555–1566 (2023).
2. A. Wenger, A. Biran, N. Alcaraz, A. Redó-Riveiro, A. C. Sell, R. Krautz, V. Flury, N. Reverón-Gómez, V. Solís-Mezarino, M. Völker-Albert, A. Imhof, R. Andersson, J. M. Brickman, A. Groth, Symmetric inheritance of parental histones governs epigenome maintenance and embryonic stem cell identity. *Nat. Genet.* **55**, 1567–1578 (2023).
3. M. R. Rountree, K. E. Bachman, J. G. Herman, S. B. Baylin, DNA methylation, chromatin inheritance, and cancer. *Oncogene* **20**, 3156–3165 (2001).
4. R. Bellelli, S. J. Boulton, Spotlight on the Replisome: Aetiology of DNA Replication-Associated Genetic Diseases. *Trends Genet.* **37**, 317–336 (2021).
5. S. Cheloufi, U. Elling, B. Hopfgartner, Y. L. Jung, J. Murn, M. Ninova, M. Hubmann, A. I. Badeaux, C. Euong Ang, D. Tenen, D. J. Wesche, N. Abazova, M. Hogue, N. Tasdemir, J. Brumbaugh, P. Rathert, J. Jude, F. Ferrari, A. Blanco, M. Fellner, D. Wenzel, M. Zinner, S. E. Vidal, O. Bell, M. Stadtfeld, H. Y. Chang, G. Almouzni, S. W. Lowe, J. Rinn, M. Wernig, A. Aravin, Y. Shi, P. J. Park, J. M. Penninger, J. Zuber, K. Hochedlinger, The histone chaperone CAF-1 safeguards somatic cell identity. *Nature* **528**, 218–224 (2015).
6. K. R. Stewart-Morgan, N. Petryk, A. Groth, Chromatin replication and epigenetic cell memory. *Nat. Cell Biol.* **22**, 361–371 (2020).
7. Z. Li, S. Duan, X. Hua, X. Xu, Y. Li, D. Menolfi, H. Zhou, C. Lu, S. Zha, S. P. Goff, Z. Zhang, Asymmetric distribution of parental H3K9me3 in S phase silences L1 elements. *Nature* **623**, 643–651 (2023).
8. N. Petryk, M. Dalby, A. Wenger, C. B. Stromme, A. Strandsby, R. Andersson, A. Groth, MCM2 promotes symmetric inheritance of modified histones during DNA replication. *Science* **361**, 1389–1392 (2018).
9. K. L. Paquin, N. G. Howlett, Understanding the Histone DNA Repair Code: H4K20me2 Makes Its Mark. *Mol. Cancer Res.* **16**, 1335–1345 (2018).
10. S. Liu, Z. Xu, H. Leng, P. Zheng, J. Yang, K. Chen, J. Feng, Q. Li, RPA binds histone H3-H4 and functions in DNA replication-coupled nucleosome assembly. *Science* **355**, 415–420 (2017).
11. H. Gan, A. Serra-Cardona, X. Hua, H. Zhou, K. Labib, C. Yu, Z. Zhang, The Mcm2-Ctf4-Pola Axis Facilitates Parental Histone H3-H4 Transfer to Lagging Strands. *Mol. Cell* **72**, 140–151.e3 (2018).
12. A mechanism for preventing asymmetric histone segregation onto replicating DNA strands | Science. <https://www-science-org.proxy.library.uu.nl/doi/10.1126/science.aat8849>.

- 13.** C. Rouillon, B. V. Eckhardt, L. Kollenstart, F. Gruss, A. E. E. Verkennis, I. Rondeel, P. H. L. Krijger, G. Ricci, A. Biran, T. van Laar, C. M. Delvaux de Fenffe, G. Luppens, P. Albanese, K. Sato, R. A. Scheltema, W. de Laat, P. Knipscheer, N. H. Dekker, A. Groth, F. Mattioli, CAF-1 deposits newly synthesized histones during DNA replication using distinct mechanisms on the leading and lagging strands. *Nucleic Acids Res.*, gkad171 (2023).
- 14.** S. Smith, B. Stillman, Purification and characterization of CAF-I, a human cell factor required for chromatin assembly during DNA replication in vitro. *Cell* **58**, 15–25 (1989).
- 15.** H. Tagami, D. Ray-Gallet, G. Almouzni, Y. Nakatani, Histone H3.1 and H3.3 Complexes Mediate Nucleosome Assembly Pathways Dependent or Independent of DNA Synthesis. *Cell* **116**, 51–61 (2004).
- 16.** T.-H. Huang, F. Fowler, C.-C. Chen, Z.-J. Shen, B. Sleckman, J. K. Tyler, The Histone Chaperones ASF1 and CAF-1 Promote MMS22L-TONSL-Mediated Rad51 Loading onto ssDNA during Homologous Recombination in Human Cells. *Mol. Cell* **69**, 879–892.e5 (2018).
- 17.** Y. Hatanaka, K. Inoue, M. Oikawa, S. Kamimura, N. Ogonuki, E. N. Kodama, Y. Ohkawa, Y. Tsukada, A. Ogura, Histone chaperone CAF-1 mediates repressive histone modifications to protect preimplantation mouse embryos from endogenous retrotransposons. *Proc. Natl. Acad. Sci.* **112**, 14641–14646 (2015).
- 18.** M. Houlard, S. Berlivet, A. V. Probst, J.-P. Quivy, P. Héry, G. Almouzni, M. Gérard, CAF-1 Is Essential for Heterochromatin Organization in Pluripotent Embryonic Cells. *PLoS Genet.* **2**, e181 (2006).
- 19.** A. Loyola, H. Tagami, T. Bonaldi, D. Roche, J. P. Quivy, A. Imhof, Y. Nakatani, S. Y. R. Dent, G. Almouzni, The HP1 α -CAF1-SetDB1-containing complex provides H3K9me1 for Suv39-mediated K9me3 in pericentric heterochromatin. *EMBO Rep.* **10**, 769–775 (2009).
- 20.** C.-P. Liu, Z. Yu, J. Xiong, J. Hu, A. Song, D. Ding, C. Yu, N. Yang, M. Wang, J. Yu, P. Hou, K. Zeng, Z. Li, Z. Zhang, X. Zhang, W. Li, Z. Zhang, B. Zhu, G. Li, R.-M. Xu, Structural insights into histone binding and nucleosome assembly by chromatin assembly factor-1. *Science* **381**, eadd8673 (2023).
- 21.** Z. Zhang, K. Shibahara, B. Stillman, PCNA connects DNA replication to epigenetic inheritance in yeast. **408**, 5 (2000).
- 22.** K. N. Choe, G.-L. Moldovan, Forging Ahead through Darkness: PCNA, Still the Principal Conductor at the Replication Fork. *Mol. Cell* **65**, 380–392 (2017).
- 23.** C. Hoegel, B. Pfander, G.-L. Moldovan, G. Pyrowolakis, S. Jentsch, RAD6-dependent DNA repair is linked to modification of PCNA by ubiquitin and SUMO. *Nature* **419**, 135–141 (2002).
- 24.** T. Thakar, W. Leung, C. M. Nicolae, K. E. Clements, B. Shen, A.-K. Bielinsky, G.-L. Moldovan, Ubiquitinated-PCNA protects replication forks from DNA2-mediated degradation by regulating Okazaki fragment maturation and chromatin assembly. *Nat. Commun.* **11**, 2147 (2020).
- 25.** Y. Daigaku, T. J. Etheridge, Y. Nakazawa, M. Nakayama, A. T. Watson, I. Miyabe, T. Ogi, M. A. Osborne, A. M. Carr, PCNA ubiquitylation ensures timely completion of unperturbed DNA replication in fission yeast. *PLoS Genet.* **13**, e1006789 (2017).

- 26.** S. Dharadhar, W. J. Dijk, S. Scheffers, A. Fish, T. K. Sixma, Insert L1 is a central hub for allosteric regulation of USP1 activity. *EMBO Rep.* **22** (2021).
- 27.** M. D. Simon, F. Chu, L. R. Racki, C. C. de la Cruz, A. L. Burlingame, B. Panning, G. J. Narlikar, K. M. Shokat, The site-specific installation of methyl-lysine analogs into recombinant histones. *Cell* **128**, 1003–1012 (2007).
- 28.** F. Mattioli, Y. Gu, T. Yadav, J. L. Balsbaugh, M. R. Harris, E. S. Findlay, Y. Liu, C. A. Radebaugh, L. A. Stargell, N. G. Ahn, I. Whitehouse, K. Luger, DNA-mediated association of two histone-bound complexes of yeast Chromatin Assembly Factor-1 (CAF-1) drives tetrasome assembly in the wake of DNA replication. *eLife* **6** (2017).
- 29.** F. Mattioli, Y. Gu, J. L. Balsbaugh, N. G. Ahn, K. Luger, The Cac2 subunit is essential for productive histone binding and nucleosome assembly in CAF-1. *Sci. Rep.* **7**, 46274 (2017).
- 30.** P. V. Sauer, J. Timm, D. Liu, D. Sitbon, E. Boeri-Erba, C. Velours, N. Mücke, J. Langowski, F. Ochsenbein, G. Almouzni, D. Panne, Insights into the molecular architecture and histone H3-H4 deposition mechanism of yeast Chromatin assembly factor 1. *eLife* **6**, e23474 (2017).
- 31.** F. Mattioli, Y. Gu, K. Luger, Measuring Nucleosome Assembly Activity in vitro with the Nucleosome Assembly and Quantification (NAQ) Assay. *BIO-Protoc.* **8** (2018).
- 32.** K. Zhang, Y. Gao, J. Li, R. Burgess, J. Han, H. Liang, Z. Zhang, Y. Liu, A DNA binding winged helix domain in CAF-1 functions with PCNA to stabilize CAF-1 at replication forks. *Nucleic Acids Res.* **44**, 5083–5094 (2016).
- 33.** T. M. Escobar, A. Loyola, D. Reinberg, Parental nucleosome segregation and the inheritance of cellular identity. *Nat. Rev. Genet.* **22**, 379–392 (2021).
- 34.** G. Saredi, H. Huang, C. M. Hammond, C. Alabert, S. Bekker-Jensen, I. Forne, N. Reverón-Gómez, B. M. Foster, L. Mlejnkova, T. Bartke, P. Cejka, N. Mailland, A. Imhof, D. J. Patel, A. Groth, H4K20me0 marks post-replicative chromatin and recruits the TONSL–MMS22L DNA repair complex. *Nature* **534**, 714–718 (2016).
- 35.** A. N. D. Scharf, K. Meier, V. Seitz, E. Kremmer, A. Brehm, A. Imhof, Monomethylation of Lysine 20 on Histone H4 Facilitates Chromatin Maturation. *Mol. Cell. Biol.* **29**, 57–67 (2009).
- 36.** A. Loyola, T. Bonaldi, D. Roche, A. Imhof, G. Almouzni, PTMs on H3 Variants before Chromatin Assembly Potentiate Their Final Epigenetic State. *Mol. Cell* **24**, 309–316 (2006).
- 37.** T. R. Ben-Shahar, A. G. Castillo, M. J. Osborne, K. L. B. Borden, J. Kornblatt, A. Verreault, Two Fundamentally Distinct PCNA Interaction Peptides Contribute to Chromatin Assembly Factor 1 Function. *Mol. Cell. Biol.* **29**, 6353–6365 (2009).
- 38.** J. G. Moggs, P. Grandi, J.-P. Quivy, Z. O. Jónsson, U. Hübscher, P. B. Becker, G. Almouzni, A CAF-1–PCNA-Mediated Chromatin Assembly Pathway Triggered by Sensing DNA Damage. *Mol. Cell. Biol.* **20**, 1206–1218 (2000).
- 39.** G. Bellí, N. Colomina, L. Castells-Roca, N. P. Lorite, Post-Translational Modifications of PCNA: Guiding for the Best DNA Damage Tolerance Choice. *J. Fungi* **8**, 621 (2022).

- 40.** B. Wen, H.-X. Zheng, D.-X. Deng, Z.-D. Zhang, J.-H. Heng, L.-D. Liao, L.-Y. Xu, E.-M. Li, CHAF1A promotes the translesion DNA synthesis pathway in response to DNA replication stress. *bioRxiv [Preprint]* (2023). <https://doi.org/10.1101/2023.04.21.537900>.
- 41.** R. G. Hibbert, T. K. Sixma, Intrinsic Flexibility of Ubiquitin on Proliferating Cell Nuclear Antigen (PCNA) in Translesion Synthesis. *J. Biol. Chem.* **287**, 39216–39223 (2012).
- 42.** J. K. Tyler, K. A. Collins, J. Prasad-Sinha, E. Amiot, M. Bulger, P. J. Harte, R. Kobayashi, J. T. Kadonaga, Interaction between the Drosophila CAF-1 and ASF1 chromatin assembly factors. *Mol. Cell. Biol.* **21**, 6574–6584 (2001).
- 43.** Y. Tang, M. V. Poustovoitov, K. Zhao, M. Garfinkel, A. Canutescu, R. Dunbrack, P. D. Adams, R. Marmorstein, Structure of a human ASF1a–HIRA complex and insights into specificity of histone chaperone complex assembly. *Nat. Struct. Mol. Biol.* **13**, 921–929 (2006).
- 44.** C. M. English, M. W. Adkins, J. J. Carson, M. E. A. Churchill, J. K. Tyler, Structural basis for the histone chaperone activity of Asf1. *Cell* **127**, 495–508 (2006).
- 45.** L. Huang, T. Agrawal, G. Zhu, S. Yu, L. Tao, J. Lin, R. Marmorstein, J. Shorter, X. Yang, DAXX represents a new type of protein-folding enabler. *Nature* **597**, 132–137 (2021).
- 46.** K. Delaney, N. Weiss, G. Almouzni, The cell-cycle choreography of H3 variants shapes the genome. *Mol. Cell* **0** (2023).
- 47.** R. Siddaway, S. Milos, É. Coyaud, H. Y. Yun, S. M. Morcos, S. Pajovic, E. I. Campos, B. Raught, C. Hawkins, The in vivo Interaction Landscape of Histones H3.1 and H3.3. *Mol. Cell. Proteomics* **21** (2022).
- 48.** A. Santos, R. Wernersson, L. J. Jensen, Cyclebase 3.0: a multi-organism database on cell-cycle regulation and phenotypes. *Nucleic Acids Res.* **43**, D1140–D1144 (2015).
- 49.** N. Battich, J. Beumer, B. de Barbanson, L. Krenning, C. S. Baron, M. E. Tanenbaum, H. Clevers, A. van Oudenaarden, Sequencing metabolically labeled transcripts in single cells reveals mRNA turnover strategies. *Science* **367**, 1151–1156 (2020).
- 50.** R. S. Wu, S. Tsai, W. M. Bonner, Patterns of histone variant synthesis can distinguish G0 from G1 cells. *Cell* **31**, 367–374 (1982).
- 51.** M.-S. Kang, E. Ryu, S.-W. Lee, J. Park, N. Y. Ha, J. S. Ra, Y. J. Kim, J. Kim, M. Abdel-Rahman, S. H. Park, K. Lee, H. Kim, S. Kang, K. Myung, Regulation of PCNA cycling on replicating DNA by RFC and RFC-like complexes. *Nat. Commun.* **10**, 2420 (2019).
- 52.** M. Li, X. Xu, C.-W. Chang, L. Zheng, B. Shen, Y. Liu, SUMO2 conjugation of PCNA facilitates chromatin remodeling to resolve transcription-replication conflicts. *Nat. Commun.* **9**, 2706 (2018).



6

General Discussion

The mechanism of CAF-1 chromatin assembly at replication forks unraveled

This thesis presents the study of how the histone chaperone CAF-1 functions at DNA replication forks. More specifically, our investigation centers on how CAF-1 is regulated by the DNA polymerase processivity factor PCNA, and how together, they orchestrate the assembly of chromatin on newly replicated DNA. Our findings in **Chapters 2, 4 and 5** highlight the complexity of the interaction between these two proteins through the use of multidisciplinary approaches such as biochemical reconstitutions, genomic-based assays, and structure predictions using AlphaFold (AF) Multimer. Subsequent studies to our work have validated our findings, emphasizing the role of histones and DNA in regulating the recruitment of CAF-1 to PCNA (1, 2). Intriguingly, their findings suggest that the WHD, a DNA binding domain within the big subunit of CAF-1, is less critical for CAF-1 function in *S.pombe* (2) than previously reported for *S.cerevisiae* (3, 4), indicating potential evolutionary divergence in CAF-1 function. This underscores the necessity to further investigate these reconstitutions with human proteins, as we set up in **Chapter 5**.

Our AF predictions are supported by a crystal structure of the KER domain of CAF-1, that reveals a distinctive long single α -helix configuration exposing positively charged residues on one side (7). As shown in **Chapter 2**, this structure confirms that the length of this α -helix drives the selectivity of CAF-1 for DNA that can sustain tetrasome assembly.

Building on that, a structure of a human CAF-1 subcomplex was recently solved, highlighting the structural impact of binding partners, particularly histones, on CAF-1 (5). In light of our findings on the effect of histones, PCNA and DNA on CAF-1, this underscores the importance of including those components in future structural investigations of the full-length complex to obtain physiologically relevant structures.

In **Chapter 2**, we combined complex reconstitution of eukaryotic DNA replication with a genomic-based assay in cells, revealing that CAF-1 is active on both the leading and lagging strands. However, we found that CAF-1 cannot share PCNA with the DNA polymerases, resulting in the inhibition of DNA synthesis, particularly on the leading strand. We propose a model where CAF-1 and replicative DNA polymerases use distinct PCNA homotrimers at DNA replication forks. This physical uncoupling of chromatin assembly from sites of DNA synthesis prompts new inquiries about PCNA and chromatin dynamics during DNA replication, that we discuss below.

While it is widely accepted that several PCNA exist on the lagging strand, the loading of distinct PCNA entities on the leading strand is a novel concept requiring further exploration. Recent genomic studies in yeast indicate comparable abundance of PCNA on both strands (6), implying a model where multiple PCNA are loaded on the leading strand. The CTF18-RFC clamp loader, known to interact with Pole during unperturbed DNA replication (7), emerges as a potential player in this process, having demonstrated a role in promoting rapid DNA synthesis on the leading strand in vitro (8). Future studies should describe the involvement of CTF18-RFC on the leading strand in the context of chromatin assembly at DNA replication forks.

On the lagging strand, PCNA is loaded at each Okazaki fragment to synthesize DNA with Pol δ , where it also orchestrates Okazaki fragment maturation by recruiting FEN1 and Cdc9 (9). Structural insights have shown that PCNA can bind simultaneously FEN1 and Pol δ (10), suggesting that DNA synthesis and maturation of Okazaki fragment may occur concomitantly. Our AF predictions in **Chapter 4** suggest a different scenario during chromatin assembly, where the interaction between CAF-1 and PCNA prevents the simultaneous binding of any other protein

to PCNA. As a result, it appears that chromatin assembly by CAF-1 on the lagging strand is uncoupled from DNA synthesis, akin to the situation observed on the leading strand. Despite these observations, the regulatory mechanisms governing these interactions on PCNA remain unclear. Specifically, unraveling the temporal sequence of events between Okazaki fragment maturation and CAF-1-mediated chromatin assembly poses an intriguing question. To address this, further exploration of these dynamics is crucial, and the single-molecule-based assays developed in **Chapter 3** emerges as a valuable tool for probing and understanding these intricate processes.

While our research centered on CAF-1, a novel histone chaperone, the DNA repair factor TONSL, has recently emerged as a potential regulator of new histone deposition at DNA replication forks (11, 12). Initially identified for its role in homologous recombination, TONSL, similarly to CAF-1, exhibits specific binding to H3.1 and is notably enriched on newly replicated DNA (13). Recent studies have demonstrated that TONSL acts as a chaperone for H3.1-H4 dimers in both human and plant systems. However, its precise function and whether it can directly assemble nucleosomes remain unknown. To improve our understanding of TONSL chaperoning activity, it is crucial to further characterize its functions using biochemical reconstitutions similar to those employed in **Chapter 2** of this thesis. This approach will contribute valuable insights into the mechanisms underlying TONSL-mediated histone chaperoning at DNA replication forks.

Unveiling the diverse functions of CAF-1: Investigating its role beyond chromatin assembly

Our work focused on the critical role of CAF-1 as the key chromatin assembly factor at DNA replication forks. However, it is noteworthy that CAF-1 has been implicated in various crucial cellular functions, including DNA repair, heterochromatin maintenance, and the regulation of PCNA abundance on chromatin. Despite these important roles, our understanding of these functions remains limited, largely due to the absence of detailed biochemical reconstitutions.

Previous studies established CAF-1 as an important DNA repair factor, particularly during homologous recombination (14, 15). Yet our understanding of its function in this context remains limited. Recent advancements, particularly using AF, have enabled high-throughput predictions of interactions between distinct proteins. The Walter lab, focusing on proteins involved in genome maintenance, has generated a database providing scores that reflect the likelihood of these predictions (predictomes.org) (16, 17). Interestingly, CAF-1 exhibits high predictions of interaction with proteins involved in Non-Homologous End Joining (NHEJ), such as the scaffolding protein PAXX (18) (predictomes.org). A previous study has shown that CAF-1 may contribute to NHEJ through interactions with the KU complex and 14-3-3 proteins (19). This opens exciting questions regarding the role that CAF-1 might play in this error-prone DNA repair pathway and how it may influence it. In order to understand CAF-1 function in DNA repair, particularly in the context of error prone pathways involved in various diseases (20) it is crucial to combine cellular investigations with detailed biochemical reconstitutions.

CAF-1 is directly associated with the maintenance of heterochromatin in cells, primarily through its interaction with heterochromatin protein 1 (HP1) (21–23). HP1 binds to nucleosomes in heterochromatic regions, promoting their close associations and resulting in compact and transcriptionally silent chromatin (24). Despite this established connection, the precise role of CAF-1 in heterochromatin maintenance remains unclear. Its significance lies in promoting the inheritance of gene silencing, a crucial factor in safeguarding cell fate (23, 25). The specific

contribution of CAF-1, whether it involves depositing HP1 in heterochromatic regions or facilitating downstream events that support heterochromatin maintenance, remains to be determined. Notably, CAF-1 is also thought to contribute to the propagation of DNA and histones methyl marks in heterochromatin (26–28). Despite the importance of this function in maintaining cell fate and safeguarding the genome, detailed insights into the role of CAF-1 in this context are still missing. Future studies are essential to determine how CAF-1 contributes to preserving heterochromatin domains and to understand the potential consequences of disruptions in its function, particularly in the context of diseases.

In **Chapter 5**, our investigation focused on understanding how bulky modifications on PCNA, such as ubiquitin, might impact CAF-1 activity. We observed no discernible difference when compared to unmodified PCNA, indicating that these interactions may well occur *in vivo*. Recently, two independent studies established a functional link between CAF-1 and PCNA ubiquitination during unperturbed DNA synthesis (29, 30). CAF-1 was found to facilitate PCNA modifications on K164 by directly interacting with the ubiquitin ligase Rad6/Rad18, responsible for ubiquitinating PCNA at this position (29). Interestingly, this modification is thought to positively regulate PCNA unloading from chromatin during unperturbed DNA synthesis (30, 31). Considering previous evidence demonstrating that CAF-1 deletion in human cells leads to PCNA accumulation on chromatin (32), it raises the possibility that CAF-1 may play a role in promoting PCNA modifications signaling its unloading from chromatin by the ATAD5 PCNA unloader. Further investigations are needed to explore whether the interaction between CAF-1 and PCNA forms the basis for the regulation of PCNA unloading from chromatin, carrying significant implications for the control of PCNA activity at DNA replication forks.

The prospects of targeting CAF-1 in cancer therapy/diagnosis

Uncontrolled cell proliferation, a hallmark of cancer development, is characterized by elevated expression of proteins involved in cell division. Given its pivotal role in S phase and consequently in proliferative cells, CAF-1 is particularly important in cancer tumorigenesis (reviewed in (33)). CAF-1 is markedly overexpressed in various cancers, including head and neck squamous cell carcinoma, acute myeloid leukemia, skin melanomas, breast, prostate, oral, tongue, and salivary gland cancers (34–40).

While cancer research continues to advance, there remains a substantial need for identifying new therapeutic targets and markers for establishing diagnoses and prognostics. In recent years, CAF-1 has emerged as a relevant biomarker for cancer development and tumor proliferation (33, 40). Notably, the expression of the large and middle subunits of CAF-1 (p150 and p60 in humans) strongly correlates with the expression of Ki67 in cancer cells, a routine marker in immunohistochemistry diagnosis in pathology laboratories (33). Consequently, CAF-1 may serve as a clinical marker for cancer development and tumorigenesis. Future studies should explore whether it could be utilized for grading certain types of cancers, particularly in cases where other markers like Ki67 may be less reliable (33).

As of now, there are no cancer therapies specifically targeting CAF-1. However, recent studies explored whether CAF-1 could be targeted in neuroblastoma (41), in AML (42) and in liver cancer using cell and mouse models (43). All studies found that CAF-1 knockdowns strongly limit the development of cancer cells *in vitro*. Additionally, a study revealed that targeting CAF-1 led to the release of genomic DNA into the cytosol of cancer cells, triggering an intrinsic immune

response that could potentially enhance certain chemotherapies (43). Given the potential of CAF-1 as a therapeutic target in cancer, our novel finding demonstrating CAF-1 binding to PCNA in a previously uncharacterized binding interface (Chapter 4), could also be targeted through inhibitors. Our work may pave the way for the development of tools that could enable the use of CAF-1 as a routine biomarker in cancer diagnosis and potentially as a therapeutic target.

References

1. R. Rosas, R. R. Aguilar, N. Arslanovic, A. Seck, D. J. Smith, J. K. Tyler, M. E. Churchill, A novel single alpha-helix DNA-binding domain in CAF-1 promotes gene silencing and DNA damage survival through tetrasome-length DNA selectivity and spacer function. *eLife* **12**, e83538 (2023).
2. F. Ouasti, M. Audin, K. Freon, J.-P. Quivy, M. Tachekort, E. Cesard, A. Thureau, V. Ropars, P. F. Varela, G. Moal, I. S. Amadou, A. Uryga, P. Legrand, J. Andreani, R. Guerois, G. Almouzni, S. Lambert, F. Ochsenein, Disordered regions and folded modules in CAF-1 promote histone deposition in *S. pombe*. bioRxiv [Preprint] (2023). <https://doi.org/10.1101/2023.06.02.543505>.
3. F. Mattioli, Y. Gu, T. Yadav, J. L. Balsbaugh, M. R. Harris, E. S. Findlay, Y. Liu, C. A. Radebaugh, L. A. Stargell, N. G. Ahn, I. Whitehouse, K. Luger, DNA-mediated association of two histone-bound complexes of yeast Chromatin Assembly Factor-1 (CAF-1) drives tetrasome assembly in the wake of DNA replication. *eLife* **6** (2017).
4. P. V. Sauer, J. Timm, D. Liu, D. Sitbon, E. Boeri-Erba, C. Velours, N. Mücke, J. Langowski, F. Ochsenein, G. Almouzni, D. Panne, Insights into the molecular architecture and histone H3-H4 deposition mechanism of yeast Chromatin assembly factor 1. *eLife* **6**, e23474 (2017).
5. C.-P. Liu, Z. Yu, J. Xiong, J. Hu, A. Song, D. Ding, C. Yu, N. Yang, M. Wang, J. Yu, P. Hou, K. Zeng, Z. Li, Z. Zhang, X. Zhang, W. Li, Z. Zhang, B. Zhu, G. Li, R.-M. Xu, Structural insights into histone binding and nucleosome assembly by chromatin assembly factor-1. *Science* **381**, eadd8673 (2023).
6. H. W. Liu, C. Bouchoux, M. Panarotto, Y. Kakui, H. Patel, F. Uhlmann, Division of Labor between PCNA Loaders in DNA Replication and Sister Chromatid Cohesion Establishment. *Mol. Cell* **78**, 725-738.e4 (2020).
7. K. Stokes, A. Winczura, B. Song, G. De Piccoli, D. B. Grabarczyk, Ctf18-RFC and DNA Pol ϵ form a stable leading strand polymerase/clamp loader complex required for normal and perturbed DNA replication. *Nucleic Acids Res.* **48**, 8128–8145 (2020).
8. Y. Baris, M. R. G. Taylor, V. Aria, J. T. P. Yeeles, Fast and efficient DNA replication with purified human proteins. *Nature* **606**, 204–210 (2022).
9. H. Sun, L. Ma, Y.-F. Tsai, T. Abeywardana, B. Shen, L. Zheng, Okazaki fragment maturation: DNA flap dynamics for cell proliferation and survival. *Trends Cell Biol.* **33**, 221–234 (2023).
10. C. Lancey, M. Tehseen, V.-S. Raducanu, F. Rashid, N. Merino, T. J. Ragan, C. G. Savva, M. S. Zaher, A. Shirbini, F. J. Blanco, S. M. Hamdan, A. De Biasio, Structure of the processive human Pol δ holoenzyme. *Nat. Commun.* **11**, 1109 (2020).

- 11.** H. Davarinejad, Y.-C. Huang, B. Mermaz, C. LeBlanc, A. Poulet, G. Thomson, V. Joly, M. Muñoz, A. Arvanitis-Vigneault, D. Valsakumar, G. Villarino, A. Ross, B. H. Rotstein, E. I. Alarcon, J. S. Brunzelle, P. Voigt, J. Dong, J.-F. Couture, Y. Jacob, The histone H3.1 variant regulates TON-SOKU-mediated DNA repair during replication. *Science* **375**, 1281–1286 (2022).
- 12.** G. Saredi, H. Huang, C. M. Hammond, C. Alabert, S. Bekker-Jensen, I. Forne, N. Reverón-Gómez, B. M. Foster, L. Mlejnkova, T. Bartke, P. Cejka, N. Mailand, A. Imhof, D. J. Patel, A. Groth, H4K20me0 marks post-replicative chromatin and recruits the TONSL–MMS22L DNA repair complex. *Nature* **534**, 714–718 (2016).
- 13.** M. Carraro, I. A. Hendriks, C. M. Hammond, V. Solis-Mezarino, M. Völker-Albert, J. D. Elsborg, M. B. Weissner, C. Spanos, G. Montoya, J. Rappsilber, A. Imhof, M. L. Nielsen, A. Groth, DAXX adds a de novo H3.3K9me3 deposition pathway to the histone chaperone network. *Mol. Cell* **83**, 1075-1092.e9 (2023).
- 14.** T.-H. Huang, F. Fowler, C.-C. Chen, Z.-J. Shen, B. Sleckman, J. K. Tyler, The Histone Chaperones ASF1 and CAF-1 Promote MMS22L-TONSL-Mediated Rad51 Loading onto ssDNA during Homologous Recombination in Human Cells. *Mol. Cell* **69**, 879-892.e5 (2018).
- 15.** J. G. Moggs, P. Grandi, J. P. Quivy, Z. O. Jónsson, U. Hübscher, P. B. Becker, G. Almouzni, A CAF-1-PCNA-mediated chromatin assembly pathway triggered by sensing DNA damage. *Mol. Cell. Biol.* **20**, 1206–1218 (2000).
- 16.** R. Evans, M. O'Neill, A. Pritzel, N. Antropova, A. Senior, T. Green, A. Židek, R. Bates, S. Blackwell, J. Yim, O. Ronneberger, S. Bodenstern, M. Zielinski, A. Bridgland, A. Potapenko, A. Cowie, K. Tunyasuvunakool, R. Jain, E. Clancy, P. Kohli, J. Jumper, D. Hassabis, Protein complex prediction with AlphaFold-Multimer. bioRxiv [Preprint] (2022). <https://doi.org/10.1101/2021.10.04.463034>.
- 17.** M. Mirdita, K. Schütze, Y. Moriwaki, L. Heo, S. Ovchinnikov, M. Steinegger, ColabFold: making protein folding accessible to all. *Nat. Methods* **19**, 679–682 (2022).
- 18.** S. K. Tadi, C. Tellier-Lebègue, C. Nemoz, P. Drevet, S. Audebert, S. Roy, K. Meek, J.-B. Charbonnier, M. Modesti, PAXX Is an Accessory c-NHEJ Factor that Associates with Ku70 and Has Overlapping Functions with XLF. *Cell Rep.* **17**, 541–555 (2016).
- 19.** M. Hoek, M. P. Myers, B. Stillman, An analysis of CAF-1-interacting proteins reveals dynamic and direct interactions with the KU complex and 14-3-3 proteins. *J. Biol. Chem.* **286**, 10876–10887 (2011).
- 20.** V. Tiwari, D. M. Wilson, DNA Damage and Associated DNA Repair Defects in Disease and Premature Aging. *Am. J. Hum. Genet.* **105**, 237–257 (2019).
- 21.** N. Murzina, A. Verreault, E. Laue, B. Stillman, Heterochromatin Dynamics in Mouse Cells: Interaction between Chromatin Assembly Factor 1 and HP1 Proteins. *Mol. Cell* **4**, 529–540 (1999).
- 22.** B. Roelens, M. Clémot, M. Leroux-Coyau, B. Klapholz, N. Dostatni, Maintenance of Heterochromatin by the Large Subunit of the CAF-1 Replication-Coupled Histone Chaperone Requires Its Interaction with HP1a Through a Conserved Motif. *Genetics* **205**, 125–137 (2017).

- 23.** H. Huang, Z. Yu, S. Zhang, X. Liang, J. Chen, C. Li, J. Ma, R. Jiao, Drosophila CAF-1 regulates HP1-mediated epigenetic silencing and pericentric heterochromatin stability. *J. Cell Sci.* **123**, 2853–2861 (2010).
- 24.** R. C. Allshire, H. D. Madhani, Ten principles of heterochromatin formation and function. *Nat. Rev. Mol. Cell Biol.* **19**, 229–244 (2018).
- 25.** E. K. Monson, D. de Bruin, V. A. Zakian, The yeast Cac1 protein is required for the stable inheritance of transcriptionally repressed chromatin at telomeres. *Proc. Natl. Acad. Sci.* **94**, 13081–13086 (1997).
- 26.** C. Ng, M. Aichinger, T. Nguyen, C. Au, T. Najjar, L. Wu, K. R. Mesa, W. Liao, J.-P. Quivy, B. Hubert, G. Almouzni, J. Zuber, D. R. Littman, The histone chaperone CAF-1 cooperates with the DNA methyltransferases to maintain Cd4 silencing in cytotoxic T cells. *Genes Dev.* **33**, 669–683 (2019).
- 27.** P.-O. Estève, H. G. Chin, A. Smallwood, G. R. Feehery, O. Gangisetty, A. R. Karpf, M. F. Carey, S. Pradhan, Direct interaction between DNMT1 and G9a coordinates DNA and histone methylation during replication. *Genes Dev.* **20**, 3089–3103 (2006).
- 28.** Y. Hatanaka, K. Inoue, M. Oikawa, S. Kamimura, N. Ogonuki, E. N. Kodama, Y. Ohkawa, Y. Tsukada, A. Ogura, Histone chaperone CAF-1 mediates repressive histone modifications to protect preimplantation mouse embryos from endogenous retrotransposons. *Proc. Natl. Acad. Sci.* **112**, 14641–14646 (2015).
- 29.** B. Wen, H.-X. Zheng, D.-X. Deng, Z.-D. Zhang, J.-H. Heng, L.-D. Liao, L.-Y. Xu, E.-M. Li, CHAF1A promotes the translesion DNA synthesis pathway in response to DNA replication stress. *bioRxiv [Preprint]* (2023). <https://doi.org/10.1101/2023.04.21.537900>.
- 30.** T. Thakar, W. Leung, C. M. Nicolae, K. E. Clements, B. Shen, A.-K. Bielinsky, G.-L. Moldovan, Ubiquitinated-PCNA protects replication forks from DNA2-mediated degradation by regulating Okazaki fragment maturation and chromatin assembly. *Nat. Commun.* **11**, 2147 (2020).
- 31.** J. R. Becker, C. Pons, H. D. Nguyen, M. Costanzo, C. Boone, C. L. Myers, A.-K. Bielinsky, Genetic Interactions Implicating Postreplicative Repair in Okazaki Fragment Processing. *PLOS Genet.* **11**, e1005659 (2015).
- 32.** J. Mejlvang, Y. Feng, C. Alabert, K. J. Neelsen, Z. Jasencakova, X. Zhao, M. Lees, A. Sandelin, P. Pasero, M. Lopes, A. Groth, New histone supply regulates replication fork speed and PCNA unloading. *J. Cell Biol.* **204**, 29–43 (2013).
- 33.** A. G. Sykaras, A. Pergaris, S. Theocharis, Challenging, Accurate and Feasible: CAF-1 as a Tumour Proliferation Marker of Diagnostic and Prognostic Value. *Cancers* **13**, 2575 (2021).
- 34.** S. E. Polo, S. E. Theocharis, L. Grandin, L. Gambotti, G. Antoni, A. Savignoni, B. Asselain, E. Patsouris, G. Almouzni, Clinical significance and prognostic value of chromatin assembly factor-1 overexpression in human solid tumours. *Histopathology* **57**, 716–724 (2010).
- 35.** S. Staibano, M. Mascolo, F. P. Mancini, A. Kisslinger, G. Salvatore, M. Di Benedetto, P. Chieffi, V. Altieri, D. Prezioso, G. Ilardi, G. De Rosa, D. Tramontano, Overexpression of chromatin assembly factor-1 (CAF-1) p60 is predictive of adverse behaviour of prostatic cancer. *Histopathology* **54**, 580–589 (2009).

- 36.** M. Mascolo, G. Ilardi, M. F. Romano, A. Celetti, M. Siano, S. Romano, C. Luise, F. Merolla, A. Rocco, M. L. Vecchione, G. De Rosa, S. Staibano, Overexpression of chromatin assembly factor-1 p60, poly(ADP-ribose) polymerase 1 and nestin predicts metastasizing behaviour of oral cancer. *Histopathology* **61**, 1089–1105 (2012).
- 37.** M. Mascolo, M. L. Vecchione, G. Ilardi, M. Scalvenzi, G. Molea, M. Di Benedetto, L. Nugnes, M. Siano, G. De Rosa, S. Staibano, Overexpression of Chromatin Assembly Factor-1/p60 helps to predict the prognosis of melanoma patients. *BMC Cancer* **10**, 63 (2010).
- 38.** M. Mesoilella, B. Iorio, M. Landi, M. Cimmino, G. Ilardi, M. Iengo, M. Mascolo, Overexpression of chromatin assembly factor-1/p60 predicts biological behaviour of laryngeal carcinomas. *Acta Otorhinolaryngol. Ital. Organo Uff. Della Soc. Ital. Otorinolaringol. E Chir. Cerv.-facc.* **37**, 17–24 (2017).
- 39.** M. Mascolo, G. Ilardi, F. Merolla, D. Russo, M. L. Vecchione, G. De Rosa, S. Staibano, Tissue Microarray-Based Evaluation of Chromatin Assembly Factor-1 (CAF-1)/p60 as Tumour Prognostic Marker. *Int. J. Mol. Sci.* **13**, 11044–11062 (2012).
- 40.** S. Yang, Q. Long, M. Chen, X. Liu, H. Zhou, CAF-1/p150 promotes cell proliferation, migration, invasion and predicts a poor prognosis in patients with cervical cancer. *Oncol. Lett.* **20**, 2338–2346 (2020).
- 41.** E. Barbieri, K. De Preter, M. Capasso, Z. Chen, D. M. Hsu, G. P. Tonini, S. Lefever, J. Hicks, R. Versteeg, A. Pession, F. Speleman, E. S. Kim, J. M. Shohet, Histone Chaperone CHAF1A Inhibits Differentiation and Promotes Aggressive Neuroblastoma. *Cancer Res.* **74**, 765–774 (2014).
- 42.** A. Volk, K. Liang, P. Suraneni, X. Li, J. Zhao, M. Bulic, S. Marshall, K. Pulakanti, S. Malinge, J. Taub, Y. Ge, S. Rao, E. Bartom, A. Shilatifard, J. D. Crispino, A CHAF1B-Dependent Molecular Switch in Hematopoiesis and Leukemia Pathogenesis. *Cancer Cell* **34**, 707-723.e7 (2018).
- 43.** F. F. Chan, C. M. Wong, PP039 Inhibition of CAF-1 histone chaperone complex triggers cytosolic DNA and dsRNA sensing pathways and induces intrinsic immunity of hepatocellular carcinoma. *ESMO Open* **7** (2022).



7

Addendums

Curriculum Vitae
English Summary
Dutch Summary
French Summary
Acknowledgments

Curriculum Vitae

Clément Rouillon, born on March 14th, 1994, in Bouxières-aux-Bois, France, embarked on his academic journey with a focus on biology at Lycée Louis Lapique in Épinal. His early exposure to the field during a summer job in a pathology laboratory, working alongside his mother, ignited his passion for biomedical studies. Clément then moved to Nancy where he studied Molecular Biology and Biochemistry in his bachelor while concurrently undertaking training in engineering and biotechnologies. During his bachelor's internship in Xavier Mannival's laboratory in the Biopôle in Nancy, he uses Nuclear Magnetic Resonance to study the 3D structure of a snoRNP domain, a crucial element of the ribosomal RNA modification machinery. Graduating with honors in 2016, Clément continued his academic journey with a Master in Biophysics and Structural Biology in Nancy. In 2017, he performed an internship at Birkbeck College in London, working in Elena Orlova's group, where he uses Cryo Electron Microscopy to investigate the 3D structure of a bacteriophage. Early in 2018, he joined Francesca Mattioli and her newly established laboratory at the Hubrecht Institute in Utrecht. Here, his research delved into understanding the packaging of DNA molecules following their duplication that precedes cell division. Graduating with honors from both his Master and a Cursus Master Ingénierie in 2018, Clément's passion for chromatin studies and biochemistry led him to start a Ph.D. in Francesca Mattioli's group, contributing to the results presented in this thesis. As of February 2024, Clément will pursue his academic career with a Postdoc in Benjamin Rowland's laboratory at the NKI in Amsterdam.

English Summary

Genomic DNA is packaged inside the cell as chromatin, a structure that encodes genetic and epigenetic information. The accurate transmission of the genetic and epigenetic information during cell division is critical for maintaining cell identity. This transmission occurs during S phase of the cell cycle, when DNA and its chromatin organization are replicated. Several dozens of proteins coordinate DNA and chromatin replication mechanisms. Histone chaperones are responsible for copying chromatin by binding and depositing histones onto newly-replicated DNA. A key histone chaperone is Chromatin Assembly Factor 1 (CAF-1). CAF-1 is recruited at sites of DNA replication by the DNA replication factor Proliferating Cell Nuclear Antigen (PCNA). Serving as a central hub in several cellular processes, PCNA orchestrates a variety of activities during DNA replication, where it promotes DNA synthesis and genome stability. How PCNA precisely coordinates CAF-1 recruitment with these different functions remains unclear.

This thesis studies the PCNA-CAF-1 interaction and its function in chromatin replication using *in vitro* biochemistry, to understand how chromatin assembly, DNA synthesis and epigenome stability are coordinated at the molecular level.

Chapter 1 provides a brief overview of chromatin biology. We reviewed how histones post-translational modifications (PTMs) and variants impacts chromatin structure and function, and we took a specific view on the role of histone chaperones in controlling chromatin dynamics. We delved into how histone chaperones take part into DNA replication, and how they promote epigenetic inheritance across cell division, with a focus on the CAF-1 complex. We summarized the current knowledge on CAF-1 function, and more particularly how its activity is regulated by PCNA at DNA replication forks.

In **Chapter 2**, we employed a multidisciplinary approach to bring an in-depth understanding of how CAF-1 and PCNA coordinate chromatin replication. We developed biochemical reconstitutions using yeast proteins that recapitulate the dependency of CAF-1 for PCNA during chromatin assembly. We found that the CAF-1-PCNA interaction strongly depends on CAF-1 ability to bind DNA. In this context, two CAF-1 complexes bind PCNA simultaneously, which enables CAF-1 function. Using genomic-based assay, we showed that CAF-1 is equally active on both leading and lagging strands of DNA replication forks. Yet, we found that CAF-1 function is physically uncoupled from DNA synthesis on leading strands, as CAF-1 and Pole compete on PCNA. Our findings suggest that a more complex mechanism controls simultaneous DNA synthesis and chromatin assembly on the leading strand.

Our findings in Chapter 2 highlighted the complexity of reactions occurring on DNA-loaded PCNA. We realized that the use of bulk studies limits our understanding of how a single PCNA entity drives multiple interactions with its binding partners. In **Chapter 3**, we set out to develop a single molecule-based assay to visualize individual PCNA molecules loaded on DNA with high temporal resolution. To enable this assay, we prepared fluorescently labeled PCNA, and we found that published labeling strategies affect PCNA stability on DNA. Instead, using a sortase-based approach for the labelling of PCNA preserved its functionality on DNA. In collaboration with the group of Nynke Dekker at the TU Delft, we developed a single molecule-based assay that allows to visualize distinct PCNA loaded onto DNA, which can now be used to study its interactions at higher resolution. This work paves the way for a better understanding of how PCNA regulates its multiple interactions on DNA.

Our investigation in Chapter 2 provided significant insights into the chromatin assembly mediated by CAF-1 and PCNA. However, the structural basis of this interaction remains unknown. In **Chapter 4**, we used AlphaFold and biochemical reconstitutions to describe how CAF-1 and PCNA interact. Biochemically, we found that both PCNA Interacting Peptides (PIPs) in CAF-1 contribute to its recruitment to PCNA, while only one is essential for the PCNA-dependent activity of CAF-1. AlphaFold predictions identified a potential new binding interface between the two complexes, offering valuable insights for ongoing structural studies using Cryo Electron Microscopy on the CAF-1-PCNA-DNA complex.

Throughout this thesis, we employed yeast proteins to unravel the mechanism by which CAF-1 and PCNA coordinate chromatin assembly with new histones. Given the acknowledged role of CAF-1 in health and diseases, especially cancer, the relevance of our work required an exploration of this mechanism using human proteins. In **Chapter 5**, we found that the PCNA-CAF-1 interaction and the chromatin assembly mechanism is largely conserved from yeast to human. Moreover, we investigated the regulation of CAF-1 function by PTMs found on histones or PCNA. CAF-1 displayed low specificity for histones and their PTMs or variants, suggesting that these factors alone do not confer binding specificity for the appropriate histone cargo. Consequently, additional cellular regulations must exist to ensure the accurate deposition of the correct histones onto DNA. Furthermore, we found that PCNA modified by ubiquitin efficiently recruits CAF-1, enabling its chromatin assembly activity. These findings indicate that, similarly to histones, bulky PTMs on PCNA do not affect CAF-1. This research brought a better understanding of the regulation of CAF-1 activity in humans and its interplay with genome stability mechanisms.

In **Chapter 6**, we discussed the implications of our work and the remaining questions in understanding the actions of CAF-1 and PCNA at DNA replication forks. We explored new directions for further research on CAF-1 function within cells, considering the broader implications for cellular processes. Additionally, we discussed the role of CAF-1 in cancer and tumorigenesis, evaluating its potential as a biomarker for cancer diagnosis and therapy.

Nederlandse samenvatting

In onze cellen, zit het genomisch DNA verpakt in de vorm van chromatine, een structuur die genetische en epigenetische informatie bevat. Voor het behoud van de identiteit van cellen is de nauwkeurige overdracht van zowel de genetische als de epigenetische informatie van cruciaal belang. Dit vindt plaats tijdens de S-fase van de celcyclus, waarin zowel het DNA en de chromatineorganisatie worden verdubbeld, een proces dat replicatie genoemd wordt. Enkele tientallen eiwitten coördineren de replicatiemechanismen van DNA en chromatine. Histon-chaperones organiseren het kopiëren van chromatine door de histonen te binden en te plaatsen op nieuw geproduceerd DNA. Een belangrijk histon-chaperone is Chromatin Assembly Factor 1 (CAF-1). CAF-1 wordt door DNA-replicatiefactor Proliferating Cell Nuclear Antigen (PCNA) naar de plaats van DNA-replicatie gebracht. PCNA speelt een centrale rol in verschillende cellulaire processen en organiseert verschillende facetten van de DNA-replicatie, waarbij het de DNA-synthese en genoomstabiliteit bevordert. Hoe PCNA de plaatsing van CAF-1 precies coördineert is tot op heden onbekend.

In dit proefschrift wordt de PCNA-CAF-1 interactie bestudeerd en onderzocht wat de functie hiervan is tijdens chromatinereplicatie met behulp van *in vitro* biochemische experimenten. Hierdoor hebben we inzicht verkregen in hoe de chromatine samenstelling, DNA-synthese en epigenetische stabiliteit op moleculair niveau worden gereguleerd.

Hoofdstuk 1 is een kort overzicht van de chromatinebiologie. We beschrijven hoe post-translationele modificaties (PTM's) en varianten van histonen de structuur en functie van chromatine beïnvloeden. We hebben specifiek ingezoomd op de rol van histon-chaperones bij het coördineren van de dynamiek van chromatine. We hebben ons verdiept in de manier waarop histon-chaperones deelnemen aan DNA-replicatie en hoe ze epigenetische overerving tijdens celdeling bevorderen, waarbij de focus ligt op het CAF-1-complex. We hebben de huidige kennis over de functie van CAF-1 en hoe zijn activiteit bij DNA-replicatievorken wordt gereguleerd door PCNA samengevat.

In **Hoofdstuk 2** hebben we een multidisciplinaire aanpak gebruikt om een beter beeld te krijgen van hoe CAF-1 en PCNA de replicatie van chromatine coördineren. We hebben biochemische reconstitutie experimenten ontwikkeld met behulp van gisteiwitten die de afhankelijkheid van CAF-1 voor PCNA tijdens de samenstelling van chromatine nabootsen. We hebben ontdekt dat de interactie tussen CAF-1 en PCNA sterk afhankelijk is van het vermogen van CAF-1 om DNA te binden. We laten zien dat twee CAF-1-complexen tegelijkertijd PCNA kunnen binden, wat correcte functie van CAF-1 mogelijk maakt. Hoewel we met behulp van genom-brede analyses hebben aangetoond dat CAF-1 even actief is op zowel de "leading", als de "lagging" strengen van DNA-replicatievorken, hebben we ontdekt dat de functie van CAF-1 niet fysiek gekoppeld is aan de DNA-synthese op "leading" strengen omdat CAF-1 en Polε concurreren voor binding aan PCNA. Onze bevindingen suggereren dat een complexer mechanisme de gelijktijdige DNA-synthese en chromatine-samenstelling op de leidende streng regelt.

Onze bevindingen in Hoofdstuk 2 benadrukken de complexiteit van reacties die plaatsvinden op PCNA dat zich op het DNA bevindt. We realiseerden ons dat het gebruik van bulkstudies het niet mogelijk maakt om te onderzoeken hoe één PCNA de verschillende interacties met zijn bindingspartners coördineert. Daarom hebben we in **Hoofdstuk 3** een test ontwikkeld die gebaseerd is op één molecuul. Hierdoor kunnen individuele PCNA-moleculen met hoge

temporele resolutie gevisualiseerd worden terwijl ze op DNA gebonden zijn. Om dit mogelijk te maken, hebben we fluorescent gelabeld PCNA gemaakt, maar kwamen erachter dat deze gepubliceerde labelingsstrategieën de PCNA-stabiliteit op DNA beïnvloeden. Daarom zijn wij overgestapt naar een op sortase gebaseerde benadering voor de labeling van PCNA, waardoor deze de functionaliteit op DNA wel behield. In samenwerking met de groep van Nynke Dekker aan de TU Delft hebben we een test ontwikkeld die op één molecuul gebaseerd is, en waarmee verschillende PCNA-eiwitten afzonderlijk op DNA kunnen worden geladen. Met deze methode kunnen de interacties van PCNA met een hogere resolutie bestudeerd worden. Dit werk maakt het mogelijk om een beter begrip te krijgen op hoe PCNA zijn meerdere interacties op DNA reguleert.

Ons onderzoek in Hoofdstuk 2 heeft waardevolle inzichten verschaft in hoe CAF-1 en PCNA betrokken zijn bij de samenstelling van chromatine. Desondanks is de structurele basis van deze interactie nog onbekend. In **Hoofdstuk 4** hebben we gebruik gemaakt van AlphaFold en biochemische reconstitutie experimenten om te beschrijven hoe CAF-1 en PCNA met elkaar samenwerken. Biochemisch onderzoek toonde aan dat beide "PCNA Interacting Peptides" (PIPs) in CAF-1 bijdragen aan de binding van CAF-1 aan PCNA, maar slechts één van deze PIPs essentieel is voor de PCNA-afhankelijke CAF-1 activiteit. De voorspellingen van AlphaFold identificeerden een potentieel nieuw bindingsgebied tussen de twee complexen. Deze bevindingen leverde waardevolle nieuwe inzichten op voor lopende studies naar de structuur van het CAF-1-PCNA-DNA-complex met behulp van Cryo-elektronenmicroscopie.

Gedurende dit proefschrift hebben we gebruik gemaakt van gisteiwitten om het mechanisme te onderzoeken waarmee CAF-1 en PCNA samen werken om nieuwe histonen in chromatine te plaatsen. Aangezien CAF-1 een belangrijke rol heeft bij fysiologische als pathologische processen (met name kanker), vonden wij het belangrijk om dit mechanisme ook met humane eiwitten te bestuderen. In **Hoofdstuk 5** hebben we ontdekt dat de PCNA-CAF-1 interactie en de manier waarop chromatine wordt samengesteld grotendeels gelijk zijn in de gist en in de humane situatie. Daarnaast onderzochten we hoe de functie CAF-1 wordt beïnvloed door PTM's gevonden op histonen of PCNA. We ontdekten dat CAF-1 geen specifieke voorkeur heeft voor de verschillende histon PTM's of varianten. Dit suggereert dat deze factoren op zich niet voldoende en dat er aanvullende cellulaire processen plaats moeten vinden om de nauwkeurige plaatsing van de juiste histonen op DNA te garanderen. Bovendien hebben we ontdekt dat PCNA dat is gemodificeerd met ubiquitine efficiënt CAF-1 rekruteert, en dus de productie van chromatine door CAF-1 toelaat. Deze bevindingen geven aan dat lijvige PTM's op PCNA, net als op histonen, geen invloed hebben op de werking van CAF-1. Dit onderzoek geeft ons een beter inzicht van de regulatie van CAF-1-activiteit bij mensen en de wisselwerking van CAF-1 met mechanismen die de stabiliteit van het genoom waarborgen.

In **Hoofdstuk 6** bespreken we de implicaties van ons onderzoek en de nog onbeantwoorde vragen met betrekking tot de functie CAF-1 en PCNA bij DNA-replicatievorken. We hebben nieuwe richtingen verkend voor verder onderzoek naar de functie van CAF-1 in cellen, waar we rekening hebben gehouden met de bredere implicaties voor cellulaire processen. Daarnaast bespreken we de rol van CAF-1 in kanker en bij de ontwikkeling van tumoren en evalueren we de potentie van CAF-1 als biomarker voor zowel de diagnose als behandeling van kanker.

Résumé

L'ADN génomique, qui gouverne la vie cellulaire, réside au sein du noyau de chaque cellule humaine. À l'intérieur de chaque noyau se trouve environ deux mètres d'ADN, posant ainsi un défi significatif, équivalent à compacter 20 km de fil dans une balle de tennis. Pour résoudre cette complexité, l'ADN est emballé en s'enroulant autour de protéines appelées histones, formant des structures connues sous le nom de nucléosomes. Cette succession de nucléosomes crée une organisation semblable à des perles sur une chaîne, communément appelée chromatine. Les histones ne servent pas uniquement de cadre structurel à la chromatine ; elles régulent également son accessibilité en portant des modifications chimiques (méthylation, acétylation) qui impactent directement des processus cellulaires vitaux, tels que l'expression génique dans l'ADN.

La préservation de ces informations de la chromatine, également désignée sous le nom d'information épigénétique, est cruciale pour assurer la survie de chaque cellule et, par extension, celle de l'organisme. Tout au long de la vie, de nombreux organismes subissent des divisions cellulaires, un processus observé chez les humains pendant le développement embryonnaire et quotidiennement chez les adultes. Cependant, avant toute division cellulaire, la cellule doit répliquer son contenu génétique afin de fournir une copie intacte du génome aux cellules filles à venir. Ce processus est connu sous le nom de réplication de l'ADN. Parallèlement à la réplication de l'ADN, l'information épigénétique sur les histones est minutieusement reconstitué sur le nouvel ADN synthétisé, un processus appelé réplication de la chromatine. Ce mécanisme implique la déposition d'histones sur l'ADN, afin qu'il s'y enroule et forme un nucléosome. Pour assurer le bon déroulement de cette opération, les histones, réputées pour leur instabilité et leur propension à l'agrégation, nécessitent une manipulation méticuleuse. Les chaperonnes d'histones, une classe de protéines, prennent en charge la protection des histones, garantissant leur trafic contrôlé et facilitant leur déposition sur l'ADN.

Dans le contexte de la réplication de la chromatine, la chaperonne d'histones Chromatin Assembly Factor 1 (CAF-1) joue un rôle central en déposant directement des histones sur le nouvel ADN synthétisé. CAF-1 est précisément ciblé vers les sites de synthèse de l'ADN par une interaction directe avec PCNA. PCNA est un acteur clé de la synthèse de l'ADN qui active les polymérases d'ADN, les enzymes responsables de la copie de l'ADN. Le travail présenté dans cette thèse explore la coordination complexe entre CAF-1 et PCNA dans la réplication de la chromatine, en examinant la dynamique de leur interaction pendant la synthèse de l'ADN. De plus, nous examinons également comment CAF-1 dépose des histones sur l'ADN fraîchement répliqué formant ainsi des nucléosomes.

Acknowledgments

I'd like to give a very special mention to my headphones and the various artists who helped me run my experiments. It may sound trivial, but that made all the difference for me.

I apologize in advance if I forget anyone, but don't hesitate to tell me if I did and I will redeem myself!

I first wish to thank the committee members for accepting to take the time to assess my work.

Francesca, thanks for giving me the chance to join your lab, and for trusting me from the start. Thanks for the continuous support, for taking care of my mental health and well-being at work when I was not able to, for finding ways to always keep me happy and motivated when the PhD brought difficult moments. You invested a lot of time in training and teaching me things I will take with me for my postdoc and I am very grateful for this. You also made sure to keep a good atmosphere in the group and it was a pleasure to be part of it. I often said it, this is not so common to have such a well-rounded supervisor in every aspect of the job. Thanks again for all these things that made my PhD a great experience!

Roxanne and Anne, I think the earliest I can remember "These friendships are for the long run" was this night at WAS, heading there under the snow and just spending an incredible night we all more or less remember... This truly turned into an amazing friendship, to a point where we would always be seen together and people in the institute would be very confused when one of us was missing! Our friendship has been such a great support during my PhD, just getting these few minutes every day to sit on the couch of the second floor and complain about our lives. We brought it at the borrels every Friday, at all balcony parties, all mid-week drinks at Olympos etc. Our friendship sent us several times on holidays together, including 3 incredible weeks in Brazil. I hope the future sends us just as far and brings amazing new moments together.

The **Mattioli lab, Imke, Giulia, Jolijn, Charlotte and Anders**, a big Thanks to all of you, for your support during these 5 years. Working alongside each of you was an amazing experience and I wish it did not have to end. A special mention for **Bruna and Jan**, we started this together, and it was such a blast to work by your side through high and low! We spent the first few years figuring out, together, what the hell we were doing, and it was awesome to do that with both of you. I am leaving with many memories, especially us wandering at the CHAINS meetings! Another specific mention goes to **Inge**, even though you stole my desk... You are a fantastic technician, you bring a considerable support to us all, working harder than everyone else, while becoming the protein purification queen. Keep up the amazing work, and don't forget to put yourself first.

A big Thank You to the students I supervised and who contributed to the work in this thesis, **Christina, Georgiana, Charlotte and Rosanne**. You really helped a lot with this work, and you also kindle in me the interest of teaching/training. I'm really grateful and lucky that I got to be your supervisor.

Among the few people I collaborated with, I want to give a big Thanks to **Juliette**, we spent several late Friday nights at the microscope, hoping to see a complex which, as we expected, turned out to be quite complicated to get... The best of luck starting your group now! I also want

to thank the member of the Dekker lab at the TU Delft, especially **Theo, Humberto** and **Kaley** who were a huge help in my work in our shared project, and all the people who worked with me.

To the **Knipscheer** lab, we shared many meetings and discussions that helped me polish my work. Thanks to all, with a special mention for **Koichi**, you were always willing to help and found time for me when I had questions. The best of luck for the future, go get all those Nature papers!

One of the best things I found during my PhD is the PV 2019, **Reinier, Joris, Wouter.T, Wouter.B, Anne, Roxanne and Jorik**. I still think we had the best PV I've ever seen, it was so much fun organizing all these events for the institute with you, and I am thrilled that our group is still thriving years after! To more of that, Cheers guys.

Ardennes crowd, there are dozens of names I could add here, what a group! I shared so much awesome moments in those weekends, thanks so much to all of you for them, and I hope others will now rise to the occasion to perpetuate this tradition.

Juri, how many borrels, balcony sessions, drinks, masterclass & PhD retreats I can remember! Even the finale of the world cup to watch France take the win! I will carry all those memories of such amazing times, good luck and have fun in Canada.

I still cannot believe how many amazing people from all across the world I had the chance to meet. Our encounters may have been brief for some, but I have great memories with every single one of you. **Job**, thank God your labwork skills are better than your bouldering ones...good luck for the few years to come, and take care of yourself! **Dennis** thanks for opening your door (and Kinan's) to the balcony sessions nearly every Friday, during which I met most people mentioned here, including you. **Erik**, I loved organizing the Ardennes together, I hope that tradition goes on now. **Sonja and Max**, we started together as baby master students and here we are! Good luck to both of you, you're nearly there. **Erica** singing together at the Karaoke borrel, **Stijn, Juliette, Anabelle, Wessel, Joe, Silke, Kim, Joana, Spiros, Ajit, Kim, Bas, SuJi, Micha**, and of course my dear **Sunshine**.

Litha, thank you for your kindness and patience to help me navigate the last months of the PhD. I also want to thank all the **Hubrecht Staff** that make our PhD life easier. Most institute do not have so much help and I am aware of it, so thanks for your work.

Gaby and Thomas and TOSAM studios, you were very patient and willing to accommodate my wishes for this thesis, best of luck with your company, I strongly recommend it to those reading this who will soon need to defend!

My dear **Buffoons**... God you are such buffoons.

Miguel, my dad can't believe I have a Spanish friend either... you prick! But we've grown really close friends and I couldn't be more grateful for it. To more of that, more beers, more Star Wars, more buffoonery. Let's now shake off the NKI and turn the next couple of years in more amazing memories.

Pagona mou, hopefully, me writing this down means that we will understand each other's English for once. If not, we'll ask Miguel to translate! I have the sweetest memories of our friendship all throughout my PhD, coming to the second floor to find you for coffee breaks every

day, all the borrels together, buffoons' nights and more. I am patiently waiting until you come back to Utrecht, hurry up!

Iliana, when are you coming back? This "learning Dutch while living in Greece" nonsense has to stop now! You are another one of those buffoons that I got to know at the institute first, and I am so happy it happened. If you come back, I promise to cook for you every weekend (If that doesn't get you back... I don't know what will). We all miss you and we need our dearest buffoon back.

Alex, it has been quite the 5 years together, sharing so many beers, borrels and of course... drinking at Olympos in random days of the week. Now you're our last baby PhD student, so don't give up and go get it, and we will become "a bunch of doctors*".

Kinan, we have grown very close through the years and you have had such a positive influence on me. You've welcomed us all in your place every balcony party after the borrels, you've welcomed us many times more and I am very happy I got to be a part of it. I have incredible memories from those nights at Salamancapad. We then went on to build other memories, from Paris to Sint Marteen back to Utrecht. Let's go places to build some more now!

Jamie, everyone think you are my boyfriend.... I can't blame them for it, they are not entirely wrong after all. If I could have a 3rd paranymp you'll surely be in the team. Our friendship brought much laugh and unforgettable moments during my PhD, and that made all the differences to finish this marathon in the last years. I hope you'll stay around with us, in the NL, for much longer (no need to go back to the UK, we all agree on that).

Tuti, A very special mention for you, for our friendship has become one of the best I found in my whole life. Mostly forged through our loves for fashion, Metallica, sanity, and all the other crazy things we have in common. You definitely have been and remain one of the biggest supporters throughout my PhD, and I am very thankful for it. I am looking forward to whatever comes next as long as I count you as one my friends.

Themis, our friendship grew in the last 2 years of my PhD, and it certainly made the experience way better. I feel very lucky it happened, all these "gay nights" at Kalff every week are a treat! I'm looking forward to more holidays with you and those snakes we call friends, and to more drinks at the gay bars every week. Good luck finishing your own PhD, we don't doubt you will nail it, and we will be here to support you through it.

Un très gros merci à vous les copains de la **Languette**, pour votre soutien à chaque fois que je rentre dans les Vosges, avec un petit clin d'œil particulier pour **Manon** et nos appels intercontinentaux pendant lesquels tu m'écoutes me plaindre du boulot, et à **Laurie** et nos petits weekends à Paris qui ont toujours été un super moyen d'oublier les problèmes du doctorat.

Un très gros Merci à **Isa** et **Bruno** pour votre générosité et votre confiance, et pour m'avoir aidé à débiter ce doctorat.

Un merci également pour **Fanny** qui m'a trouvé ce job et **Florent** et tout ce groupe du Biopôle avec qui j'ai adoré passer des soirées mémorables ! Vous m'avez donné l'envie et la confiance de me lancer dans un doctorat, merci à vous tous, j'espère vous revoir bientôt !

Maman et Papa et Marine, Merci pour votre soutien depuis toutes ces années, et m'avoir permis d'aller à Londres, puis à Utrecht pour poursuivre mes études et faire ce que j'avais envie. Et grâce à vous je continue maintenant, vers de nouvelles aventures !

"You step onto the road, and if you don't keep your feet, there's no knowing where you might be swept off to"

J.R.R Tolkien

